CRANFIELD UNIVERSITY

PRASETYO EDI

INVESTIGATION OF THE APPLICATION OF HYBRID LAMINAR FLOW CONTROL AND VARIABLE CAMBER WING DESIGN FOR REGIONAL AIRCRAFT

COLLEGE OF AERONAUTICS

PhD THESIS

CRANFIELD UNIVERSITY

COLLEGE OF AERONAUTICS

PhD THESIS

Academic Years 1995 - 1998

PRASETYO EDI

INVESTIGATION OF THE APPLICATION OF HYBRID LAMINAR FLOW CONTROL AND VARIABLE CAMBER WING DESIGN FOR REGIONAL AIRCRAFT

Supervisor : Prof. J. P. Fielding

October 1998

SUMMARY

Approximately 65% of the world's commercial jet fleet consists of narrow-body, single-aisle aircraft with a capacity of 70 to 170 seats. The trend since deregulation in the US has been towards hub-and-spoke networks and a reduction in average aircraft size. The liberalization of the European market could exacerbate this trend. Because of congestion and the competitive environment the airlines are forced to buy technology and competitive aircrafts at low cost and to ask to the manufacturers to provide more operational flexibility, without drastic performance losses.

In the feasibility phase of an Advanced Technology Regional Aircraft (ATRA) family, a combined HLFC-VCW (Hybrid Laminar Flow Control – Variable Camber Wing) concept was investigated to improve the overall efficiency, flexibility and reduce weight as the weight-growth factor is a critical issue.

A methodology of a conceptual design and wing design incorporating a combined HLFC-VCW concept for regional transport aircraft was developed. For the purpose of this study, SWEPTDES was used to initially design the aerofoil sections for ATRA's wing. RAMPANT was used to analyse ATRA wing aerodynamic performance in the transonic speed regime for both turbulent and laminar flows.

A simple transition prediction method was used, based on assumptions that extended regions of favourable pressure gradient would correspond to extended regions of laminar flow. The boundary layer transition is expected to be just in the front of the recovery point.

To identify the drag reductions by the applications of combined HLFC-VCW system, a simple drag prediction method was used, to show an initial comparison with a turbulent datum design.

Relative to a baseline aircraft, with current state-of-the-art technology, a cruise drag improvement potential of more than 10 % was identified. This drag reduction leads to MTOW reductions up to 4 % or increased range by more than 7 %.

Variable camber (VC) offers an opportunity to achieve considerable improvements in operational flexibility, buffet boundaries and performance and enable the use of one wing for a regional aircraft family. Although in this work the design lift requirement was not achieved, but the results showed that using VCW the wing lift could be increased or decreased and could be optimized to produce the desired lift range. The introduction of VC could set off a new generation of intelligent airliners which will optimize their camber schedule automatically throughout the entire mission. Variable Camber is a prerequisite for HLFC wing to control the pressure gradients and the off-design behaviour.

Before HLFC and VCW technology can be applied to the transport aircraft, a large multidisciplinary research effort is needed in order to master the technology and demonstrate it on flying test-beds and in-service operational tests.

ACKNOWLEDGEMENTS

The author express sincere gratitude to the many people who have aided in the completion of this thesis.

The author would like to acknowledge the personal contributions of Prof. J. P. Fielding for his supervision and guidance throughout the research, Prof. A. J. Bocci (DRA Bedford) for acting as aerodynamics consultant.

Other College Staff who have made significant contributions include Dr. R. I. Jones and Dr. Ning Qin.

Without the enduring support and encouragement from my wife Arum Lukitaningsih and understanding of my lovely children : Diatri Anisa Zahrani, Arditra Luqman Amin and Andita Aisya Rabbani, this research would have seemed interminable and I would like to dedicate this work to them.

LIST OF CONTENTS

LIST OF FIGURES

CHAPTER 2

CHAPTER 3

CHAPTER 4

CHAPTER 5

CHAPTER 6

CHAPTER 7

CHAPTER 8

APPENDIX A

APPENDIX B

APPENDIX C

LIST OF TABLES

ABBREVIATIONS

A.L.T.	Attachment Line Transition
A (AR)	Aspect Ratio
ATRA	Advanced Technology Regional Aircraft
b	Span
CFD	Computational Fluid Dynamic
C.F.I.	Cross Flow Instability
DLM	Direct Lift Mode
DOC	Direct Operating Cost
DR&O	Design Requirements and Objectives
FAR	Federal Aviation Regulation
GCS	Geometric Constraint Surface
GLA	Gust load alleviation
HLFC	Hybrid Laminar Flow Control
HT	Horizontal tail
L/D	Lift/Drag ratio
LEFT	Leading Edge Flight Test
LFC	Laminar Flow Control
PSE	Parabolized Stability Equation
M	Mach number
MAC	Mean Aerodynamic Chord
MAW	Mission Adaptive Wing
MLC	Manoeuvre Load Control
N	Ultimate acceleration factor
NLF	Natural Laminar Flow
OEW	Operating Empty Weight
R	Reynolds number/Range
S	Wing surface area
SOB	Side of Body
TOGW	Take-Off Gross Weight
T.S.I.	Tollmien-Schlichting Instability
T/W	Thrust/Weight ratio
t/c	Thickness/chord ratio
V	Speed
VC	Variable Camber
VCW	Variable Camber Wing
VT	Vertical Tail
W/S	Wing loading
α	Alpha (angle of incidence)
λ	Taper ratio
Λ	Sweep

CHAPTER ONE

GENERAL INTRODUCTION

1.1 RESEARCH BACKGROUND

Approximately 65% of the world's commercial jet fleet consists of narrow-body, single-aisle aircraft with a capacity of 70 to 170 seats. The trend since deregulation in the US has been towards hub-and-spoke networks and a reduction in average aircraft size. The liberalization of the European market could exacerbate this trend. Because of congestion and the competitive environment the airlines are forced to buy technology and competitive aircrafts at low cost and to ask to the manufacturers to provide more operational flexibility, without drastic performance losses.

Referred to a baseline aircraft with state-of-the-art technology, with the application of a combine HLFC-VCW, an aircraft drag improvement potential during cruise, climb and descent could be expected. This drag reduction should lead to MTOW reductions or increased payload-range performance.

Variable camber (VC) is offers an opportunity to achieve considerable improvements in operational flexibility, buffet boundaries and performance and enable the use of one geometric wing for a regional aircraft family. The introduction of VC could start a new generation of intelligent airliners which will optimize their camber schedule automatically throughout the entire mission. Variable Camber is a prerequisite for HLFC wing to control the pressure gradients and the off-design behaviour.

1.2 RESEARCH OBJECTIVES

The objective of this research were :

a) to investigate a conceptual design and a simple wing aerodynamic design methodology, suitable for conventional and HLFC/VCW configuration.

b) to demonstrate the feasibility of a Hybrid Laminar Flow Control (HLFC) and Variable Camber Wing (VCW) system to the regional transport aircraft family.

c) to introduce the combined HLFC-VCW into the initial aircraft sizing and wing design processes for a regional transport aircraft family.

1.3 RATIONALE

Current trends in the design of transport aircraft have shown that in order to be economically viable and competitive it is necessary to investigate technologies which may give an improvement in performance and operational flexibility. It is believed that the application of a Hybrid Laminar Flow Control (HLFC) and Variable Camber (VC) to a wing would assist in achieving such a goal, but must be shown to be cost-effective.

1.4 RESEARCH STRUCTURE AND OUTLINE OF WORK PERFORMED

In order to investigate the feasibility of Hybrid Laminar Flow Control (HLFC) and Variable Camber Wing (VCW) systems to regional transport aircraft family, it is necessary to determine the various benefits and drawbacks associated with the changes that are made.

Therefore, the size and performance of the baseline aircraft with state-of-the-art technology was required, as well as the size and performance of the new combined HLFC-VCW derivative. The errors and approximations associated with the various analysis methods will apply equally to the work performed on both variants. This should hopefully result in as true a comparison as possible, because the effects of common errors would be eliminated.

The investigations of the feasibility of Hybrid Laminar Flow Control (HLFC) and Variable Camber Wing (VCW) system to the regional transport aircraft family was conducted in the following manner :

1. Drawing up of the specification of baseline ATRA family and performing the initial aircraft sizing required for subsequent analysis (see Chapter 2).
2. Scheming of combined HLFC-VCW system for the derivative aircraft (see Chapter 5).
3. Investigation of theoretical and practical backgrounds of laminar flow and VCW (see Chapter 3, 4 and 6).
4. Initial aerodynamic wing design for the derivative aircraft (see Chapter 7).
5. Aerodynamic performance and laminar analysis for the derivative aircraft (see Chapter 8).
6. The benefits and drawbacks of combined HLFC-VCW system affects to the derivative aircraft sizing (see Chapter 9).
7. Discussion of practical considerations (see Chapter 10).
8. Conclusions and recommendations of improved schemes (see Chapter 11).

The work was performed in this sequence, although there was a considerable overlap between some of the stages. The contents of this thesis are arranged largely in the above order, and amplified by appendices.

CHAPTER TWO

AIRCRAFT INITIAL BASELINE DESIGN

2.1 INTRODUCTION

Approximately 65% of the world's commercial jet fleet consists of narrow-body, single-aisle aircraft with a capacity of 70 to 170 seats. These are deployed on routes of 1,300 nautical miles or less. This sector also dominates the current order-book. More than 60% of aircraft on order are in the short-haul narrowbody category. The trend since deregulation in the US has been towards hub-and-spoke networks and a reduction in average aircraft size. The liberalization of the European market could exacerbate this trend (Reference 2.1).

There are several forecasts for demand for the above type aircraft in the next 20 years. Bombardier believes that there is a demand for a little over 3,000 aircraft in the 60- to 90-seat class (Reference 2.2). According to a DASA market forecast, published in June 1995, excluding the commonwealth of Independent States, 2,350 71-130-seat aircraft will be delivered to regional carriers (Reference 2.3). IPTN (Indonesian Aircraft Industry) is forecasting demand for 2,757 passenger aircraft in the 80- to 130-seat class (Reference 2.4). McDonnell Douglas predicts requirements for 1,700 in that class of aircraft (Reference 2.5). Figure 2.1 (Reference 2.6) gives more details about the above figures.

To fulfil the above demand the regional-jet manufacturers are trying to attract the airline carriers with their own designs. Aircraft already in the market are McDonnell Douglas MD-87, Fokker-70/-100, Airbus A319, Boeing 737-500/-600 and BAe-146/Avro RJ-70/-85/-100/-115. The regional-jet manufacturers which still waiting to go ahead with their plan or their aircraft still under development are Boeing-MD-95-20/-30/-50, IPTN's N-2130, Fairchild Dornier's 728JET and Bombardier's Canadair Regional Jet (CRJ) Series 700 programme (see Appendix A).

Only three models of the above aircrafts are smaller than 120-seats-the Avro RJ-70/-85/-100/-115, the Fokker-70/-100 and the Boeing 737-500/-600. The Avro RJ and the Boeing 737 family are 6 abreast seating, while the Fokker family is 5 abreast seating.

The Fokker-70/-100 has one of the lowest noise footprints of any commercial jet aircraft and already beats the proposed Chapter IV European noise limits. It has also recently received certification to operate at London City Airport. The Fokker-70/-100s can land on runways as short as 4,330 ft at sea level with maximum payload. Together with its noise performance, this gives the aircraft access to smaller airports, thereby facilitating the expansion of hub-and-spoke networks to destinations previously served only by turboprops. Seat-mile costs were significantly lower that those of its competitors. Direct operating costs per aircraft-mile approach those of the lowest capacity commercial jet aircraft. As a result, the Fokker 100 can be deployed on the thinnest routes requiring jet aircraft, and can be the most economical jet aircraft for

developing new short-haul routes. Category 3 autoland capability gives the Fokker-70/-100 improved on-time performance and reduces operating costs by increasing utilization through greater schedule reliability. In other respects, the Fokker-70/-100 may be seen as a complementary family rather than a competitor to the other narrowbodies. It fills a niche between mainbody jets and turboprops (Reference 2.1).

Despite its performance superiority, the Fokker-70/-100 is not an all-new design. It was developed from F28 Mk 4000 and it has a maximum operating Mach number 0.77. The Fokker-70/-100 are not in production any more.

The following section is a brief design methodology for conceptual sizing of aircraft based on References 2.5 - 2.38, and the author's experience when he worked as an aircraft configurator in IPTN (Indonesian Aircraft Industry). For a more extensive discussion of aircraft sizing, the reader is referred to References 2.5 - 2.38. Due to the limitations of time, the design process is concentrates on the fuselage, wing and wing-engine integration only.

2.2 AIRCRAFT COMPETITOR ASSESSMENT

The competitor assessment section provides engineering data on existing and potential competitor products. This includes configuration descriptive characteristics, technical features, standardised weights, and standardised performance parameters based on Reference 2.5, 2.8 - 2.10 and 2.38 (see Appendix A), which is to give the information as a data for comparison in aircraft initial sizing (see Chapter 2.4).

2.3 AIRCRAFT DESIGN REQUIREMENTS AND OBJECTIVES

In developing an Aircraft Design Requirements and Objectives (DR&O) several important points need emphasis. For example, no design can satisfy the real wants of Airline customers unless adequate requirements are provided to the configuration designer/design team as input to the Aircraft Configuration Design Subprocess. Marketing and engineering must collaborate to provide the highest quality requirements. Both Aircraft Operational & Economic Analysis and Aircraft Configuration Design have to take active roles to ensure that requirements are correctly specified, complete, potentially realisable and economically rational. Through both feed-forward and feedback loops the marketing department becomes both a customer and a supplier. The "documented requirements" also define the technical requirements of various engineering disciplines also and of the regulatory agencies (Reference 2.7).

Definitions :

1. Design Requirements (R). Design requirements are items that must be satisfied by the designer, without deviation, to meet government/regulatory bodies, aircraft manufacturer, and customer standards of design, performance and safety. Design requirements are subject to change as the design progresses through formal change

procedures and with engineering management approval. Generally these changes will be responsive to increases in technical knowledge and customer requirements.

2. Design Objectives (O). Design objectives are items which are desirable to achieve an improved product. These items must be satisfied by the designer, without deviation unless there are undue penalties in cost and/or performance. Design objectives are subject to change as the design progresses through formal change procedures and with engineering management approval. Generally these changes will be responsive to trade-off study results on each specific item.

It is beyond this work to make a complete DR&O, as described above. The following are DR&O for the baseline aircraft configuration (ATRA-100), based on Reference 2.11. The values of DR&O for the ATRA-100 are taken as an average or an improvement of the data of the competitors (see Appendix A).

A. Aircraft designation : ATRA (Advanced Technology Regional Aircraft)-100

B. Interior layout

Capacity (R)

Design payload : 108 mixed-class passengers with 100 tourists at 32 inch pitch and 8 first class at 36 inch pitch. Passenger and baggage shall be equal to 95.5 kg/passenger.

Comfort standards shall be at least as good as those of the Fokker F-100. 18 inch minimum aisle width with adequate spacing at galley and costrooms to allow ease of access and service.

Three attendants seats with sufficient galley space for 108 hot meals, 3 toilets, and specified stowage space.

The flight deck shall be designed for a two-man crew.

Cargo (R)

Baggage space should be determined by assuming 2 ft^3 per seat minimum. Cargo space should be 7 ft^3 per seat minimum.

C. Performance

Range (R) with the design payload shall be approximately 2,250 nm (4,125 km) with FAR reserves.

The maximum design cruise speed (O) will be approximately Mach 0.85 with minimum cost cruise (O) at Mach 0.8. Maximum approach speed (O) will be 127 knots.

Maximum cruise altitude (O) should be around 39,000 ft with initial cruise altitude at 31,000 ft (R).

The dry FAR landing field length (O) at maximum landing weight should not exceed 4,921 ft (1,500 m).

The dry FAR take-off field length (O) at maximum take-off weight should not exceed 6,562 ft (2,000 m).

Runway loading (O) should not exceed that of a Fokker F-100 at maximum take-off weight 101,000 lb.

Exterior noise (R) levels should be lower than FAR 36 stage 3.

D. Regulations : FAR parts 25, 36 and 121.

2.4 INITIAL SIZING

As was stated in Section 2.3, requirements definition comes before the aircraft definition process begins; however, once the aircraft definition process begins, one of the first steps is initial sizing.

Conceptual design is a "chicken or egg" problem. The configuration designer cannot draw the aircraft until he develops some information about the aircraft, such as takeoff gross weight (TOGW), wing loading, etc. The performance analyst needs to know about the geometry of the aircraft before he can determine the drag, and hence find aircraft payload-range capability, and hence takeoff gross weight. "Initial Sizing" usually refers to the initial estimation of takeoff gross weight to achieve a specified mission, and the estimation of thrust/weight (T/W) ratio and wing loading (W/S) to meet specified performance constraints. This estimation is normally done with either no knowledge or very little knowledge of the geometry of the aircraft. The data in Section 2.2 can be used as an initial value or for comparison.

The equations which define compliance with performance constraints in terms of T/W and W/S do not in general contain a term for aircraft weight, although they do contain terms for the ratio of aircraft weight at a given operating condition versus take-off gross weight. Thus the initial calculation for TOGW and estimation of T/W and W/S can be performed independently (Reference 2.7).

The following section is a brief design methodology for estimating take-off gross weight, finding wing loading and thrust/weight ratio, and initial aeroelastic check based on Reference 2.7, 2.12 and 2.13.

2.4.1 Mission Definition

To calculate the required Take-Off Gross Weight (TOGW), the payload (passengers, baggage and cargo) and range over which the payload will be carried must be defined. In addition the mission profile (i.e. the schedule of engine start and warm-up, taxi, take-off, climb, cruise, descent and landing, taxi and shut-down) must be defined. For the purpose of this work, a simplified mission profile definition is used and it is shown in Figure 2.2. The design payload-range for ATRA Family and it's competitors are shown in Figure 2.3.

2.4.2 Estimating Take-off Gross Weight

TOGW is estimated by matching the empty weight required from structural considerations to the empty weight available when the aircraft is analytically "flown" on the mission. For an assumed value of TOGW, mission fuel fraction is calculated assuming that fuel burned on engine start and warm-up, taxi, take-off, climb, descent and landing, taxi and shut-down segments of the flight are proportional to TOGW (and suggested segment fuel fractions are given), and that cruise fuel burn can be calculated from the Breguet range equation.

For initial estimation of TOGW it's can be assumed that the aircraft flies at near-optimum lift/drag (L/D) and specific fuel consumption (SFC), therefore a value of 0.97 L/D_{max} would be used. The L/D_{max} can be estimated based on ratio of fuselage cross-sectional area to wing area and fuselage fineness ratio.

Operating Empty Weight (W_{OEW}) available is then calculated from :

$$W_{TO} = W_{OEW} + W_{PAYLOAD} + W_{FUEL} \qquad (2.1)$$

where :

W_{TO} = assumed value of TOGW
W_{OEW} = $W_{EW} + W_{CREW}$
W_{EW} = empty weight
W_{CREW} = crew weight
$W_{PAYLOAD}$ = payload weight
W_{FUEL} = mission fuel weight
= $W_{FU} + W_{RES} + W_{TFO}$
W_{FU} = fuel actually used during the mission
W_{RES} = fuel reserves required for the mission
= 0.25 * W_{FUEL}
W_{TFO} = weight of trapped fuel and oil

The procedure is repeated for different values of assumed value of TOGW until empty weight available matches empty weight required.

If the initial geometry of the aircraft is undefined, the relationship between required empty weight and TOGW is based on historical data for other aircraft in the same class (e.g. transport jets, regional turbo-propeller, business jets, etc.). If the geometry is defined, required empty weight may be determined from component weight build up. The equations defining the component weight are given in Reference 2.13.

For the ATRA-100 Family the weight breakdown are contained on Section B.5 of Appendix B. The empty weight versus maximum take-off weight for ATRA Family and it's competitors are shown in Figure 2.4.

2.4.3 Finding Wing Loading and Thrust/Weight ratio

A convenient way of defining the quasi-nondimensional forces on an aircraft is to divide the thrust and lift forces by the aircraft weight. The local thrust/weight is the

thrust at a given operating condition divided by the weight at that condition. Logically, lift/weight could be the nondimensional lift parameter; however, instantaneous lift is somewhat harder to define, and so wing area (which is proportional to maximum lift for a given maximum lift coefficient) is used. To complicate matters, instead of using wing area/weight (to be consistent with thrust/weight), the parameter of weight/wing area (W/S) is used. The two parameters of T/W and W/S show up in almost all equations defining aircraft performance (such as take-off field length, climb rate, ceiling, and landing distance).

For given performance requirements, T/W may be defined in terms of W/S and plotted in the form of Figure 2.5. The equations defining the constraint curves are given in Reference 2.13. In this figure, T/W refers to the reference thrust/weight ratio which is the maximum installed sea level static thrust of all engines divided by the maximum take-off gross weight. The values of thrust and weight at the conditions at which the constraints apply (e.g. climb or cruise) will be different from the reference conditions, so the values of thrust/weight at these conditions must be factored accordingly.

Contours of constant take-off gross weight of aircraft that achieve the required mission may be superimposed on this graph. To construct contours of constant TOGW, a carpet plot of TOGW versus T/W and W/S must first be constructed. From this carpet plot, interpolated values of T/W and W/S can be found for which TOGW is constant.

From Figure 2.5 can be drawn some important conclusions, e.g. :

- Too high thrust to weight ratio it's means engine too large (too much engine weight and high fuel burn)
- Too low thrust to weight ratio it's means engine too small (too much afterburner, if applicable)
- Too high wing loading it's means wing too small (high induced drag)
- Too low wing loading it's means wing too large (high profile drag and too heavy)

So for a good lightweight design and for a certain performance constraints we need to maximise wing loading and minimise thrust to weight ratio as far as possible.

Contour defining other objective functions to be minimised, such as direct operating cost, block fuel, or empty weight, could equally well have been plotted and the configuration found that met all the performance constraint requirements for the minimum value of objective function (Reference 2.7).

2.4.4 Arrival at the Match Point

For the ATRA-100 Baseline as shown in the Figure 2.5, the cruise constraints and the constant TOGW curves are calculated for four different wing aspect ratio (e.g. AR = 8, 9.5, 10 and 11). While the FAR 25 climb and the initial cruise altitude constraints are not drawn (and for this case those two constraints are not critical) for the reason of having a clear plot

Based on the above figure the minimum TOGW configuration is on the point which represent the intersection between cruise constraint curve and landing constraint line. The values of T/W and W/S for wing aspect ratio = 9.5 are as follows :

T/W = 0.2911 and W/S = 510.491 KG/M^2 = 104.544 LB/FT^2

ATRA-100 Baseline with TOGW = 56,260.4 KG = 124,032 LB (see Section B.5 of Appendix B, so the values of wing area (S) and thrust (T) are as follows :

Wing area (S) = 110.209 M^2 = 1,187.83 FT^2

Thrust (T)/engine = 8,188.7 KG = 18,052.7 LB

2.4.5 Initial Aeroelastic Check

Reference 2.7 states that flutter is an aeroelastic phenomenon associated with unsteady aerodynamics and structural dynamic interaction. The structural motion of a wing or empennage in torsion or bending (resulting in a pitching or plunging the lifting surface) introduces a momentary change in the local angle of attack. The lag in build-up of circulatory lift resulting from this momentary change produces unsteady airloads which can be detrimental to the structural stability of the airframe.

Control surfaces complicate this problem by adding additional degrees of freedom in the structural dynamics problem. Usually control surfaces are dynamically balanced with a slightly nose heavy condition about the hinge line. Another option, is to rely on the damping introduced by the hydraulic actuators to introduce enough phase and gain margin to overcome the destabilising effects of the unbalanced surface.

A key thing to remember in the concept development or early preliminary design phase is the issue of placement of large lumped masses (such as engines) relative to the elastic axis of wing or other lifting surfaces. On a podded twin-engines-on-the-wing configuration the inboard position does not generally have as much effect on wing mode shapes because of the high stiffness characteristics nearer the wing root. However, whenever outboard wing locations are considered (such as the A340 and the B747) much more attention is required in the placement of engine pylons relative to structural vibration node lines of those modes associated with the flutter phenomenon.

The following section is a brief design methodology for an initial aeroelastic check based on Reference 2.14.

2.4.5.1 Torsion

For subsonic aircraft with wing-podded jet engines the requirement for wing torsional stiffness :

$$(AR)^{3/2} / ((t/c)_{SOB})^2 < (3 * 10^8) / ((V_D)^2 * (\cos \Lambda_{c/4}) \qquad (2.2)$$

where :

AR = wing aspect ratio

$(t/c)_{SOB}$ = wing thickness chord ratio at side of body

V_D = diving speed (knots)
$\Lambda_{c/4}$ = a quater sweep angle (degre)

JAR 25:335 states that there should be a M = 0.05 margin between $M_{max\ cruise}$ and M_D.

2.4.5.2 Bending Stiffness

For subsonic aircraft with wing-podded jet engines the requirement for wing bending stiffness :

$$(AR)^{3/2} * \sec \Lambda_{c/4} / (t/c)_{SOB} < (3 * 10^8) / (850 / N) \qquad (2.3)$$

where :

N = ultimate acceleration factor

Figure 2.6 shows the boundary of the above requirements for the conditions : $M_{max\ cruise}$ = 0.82, $\Lambda_{c/4}$ = 25 degree and N = 2.5 * 1.5 = 3.75. Also the values of an existing aircraft are added (just based on the values of AR and $(t/c)_{SOB}$)). Any combinations of wing aspect ratio and wing thickness chord ratio at side of body which lay under the boundary curve are safe from the structural point of view. Based on Figure 2.6 for ATRA's wing which it's have an aspect ratio = 9.5, should have $(t/c)_{SOB}$) greater than 14.9 %.

2.5 GENERAL ARRANGEMENT

Designing an aircraft can be an overwhelming task for a new configurator. The configurator must determine where the wing goes, how big to make the fuselage, and how to put all the pieces together.

The task of the commercial aircraft configurator is to make the following decisions (Reference 2.17) :

a. Selection of the overall configuration :

- Tail aft (T-tail, mid/low tail) or canard
- High wing or low wing
- Engines mounted on the wing or fuselage
- Landing gear attachment and stowage

b. Selection of the fuselage layout :

- Cockpit layout
- Cabin layout (seating for attendants and passengers, galley, lavatory, stowage, wardrobe, overhead stowage bin)
- Cargo
- Door, window and emergency exit layout

c. Selection of planform design parameters for the wing and the empennage :

- Size (i.e. area)
- Aspect ratio, Taper ratio, Sweep angle

- Airfoil type and thickness ratio distribution
- Twist, dihedral angle
- Control surface size and disposition

d. Selection of type, size and disposition of high lift devices :

- Leading edge devices
- Trailing edge devices

e. Selection of powerplant type and the number of engines :

- Turbofan
- Propfan, unducted fan (UDF)

f. Selection of landing gear type and arrangement :

- Tricycle type
- Landing gear location/footprint
- Number of struts and tires
- Wheel location up and down
- Landing gear attachment, stowage and retraction feasibility.

Based on an existing aircraft (see Appendix A.2) there are two main types of general arrangement for a regional passenger jet transport aircrafts, i.e. :

1. Boeing, Airbus, IPTN type : low-wing, low/fuselage-tail, engine mounted on the wing and tricycle landing gear attached on the wing and stowage on the wing-fuselage fairing (see Figure A.6-7, A.11-13 and A.15).

2. Douglas, Fokker, Canadair type : low-wing, T-tail, engine mounted on the rear fuselage and tricycle landing gear attached on the wing and stowage on the wing-fuselage fairing (see Figure A.8-10, A.3-5 and A.14).

There are several advantages and disadvantages between the above two types of general arrangement, e.g. :

Consideration	Type 1	Type 2
a. aerodynamic cleanliness wings	bad	good
b. bending relief	yes	no
c. cabin noise levels	better	bad
d. aircraft c.g. management	easy	difficult
e. one angine out trim	difficult	easy
f. engine rotor burst	critical	good
g. engine ground clearance	critical	good
h. engine accessability	good	difficult
i. fuel system	lighter	heavier

A sound choice of the general arrangement of a new aircraft design should be based on a proper investigation into and interpretation of the transport function and a translation of the most pertinent requirements into a suitable positioning of the major parts in relation to each other. No clear-cut design procedure can be followed and the task of devising the configuration is therefore a highly challenging one to the resourceful designer (Reference 2.15).

The study of possible configurations should result in one or more sketches of feasible layouts. They serve as a basis for more detailed design efforts, and they can therefore be regarded as a first design phase.

Usually trade studies between several possible configurations will be required before the choice of the best configuration is made. The engine mounted on the wing configuration is typical transport aircraft and the most common for most airliner. It is beyond this work to make a trade study, as described above. For this study, general arrangement type number 1 is selected for the ATRA-100 baseline configuration, ATRA-80 and ATRA-130 (see Figure B.1 of Appendix B).

2.6 FUSELAGE DESIGN

The fuselage in commercial aircraft carries the crew, the payload (passenger and cargo) and many of the systems needed for the operation of an aircraft to a certain distance at a specified speed. It must permit rapid loading before the flight and rapid unloading after it. The fuselage structure also offers protection against climatic factors (cold, low pressure, a very high wind velocity) and against external noise. The fuselage (usually the nose) normally also houses the cockpit (or flight deck).

The fuselage interior design reflects a compromise between level of creature comforts and the weights and sizes required to create the creature comforts. In commercial operations the problems associated with servicing and maintenance dictate where access must be designed into the fuselage. Design for good access, maintenance and inspectability usually conflicts directly with design for low structural weight, low complexity and low drag.

2.6.1 Payloads

Payload is one of the first considerations in designing an aircraft. Satisfying the passenger and/or cargo requirements will effect every aspect of the aircraft. Comfort may have more influence on the sale of an aircraft than esoteric items like drag performance. Number of seats and cargo volume directly relate to the economical attractiveness of the aircraft. All of these items are addressed when designing an aircraft for payload (Reference 2.7).

2.6.1.1 Cabin cross-section parameters

Creating a cross-section is one of the first steps in laying out commercial aircraft. Based on Reference 2.7, design considerations include the following :

- Payload : Total number of passengers, seat pitch, number passengers to seat abreast, and cargo volume requirements.
- Mission definition : Is the proposed mission short range which may require less comfortable seating ?

- Cruise altitude : Is the aircraft pressurised ?
- Customer requirements : As specified by Marketing (seat width, pitch, bin volume, etc.)

In developing a Lay-out Accommodation, the aircraft cross-section must be determined.

2.6.1.2 Design considerations of a cabin cross-section

Cabin cross-sections, for commercial aircraft are the result of compromises between weight, drag, systems and comfort considerations. Comfort is mainly dependent on the following factors (Reference 2.15) :

- The design and arrangement of the seats.
- The general aesthetic impression created by the interior.
- Sidewall clearance.
- The room available for the passenger to move about in the cabin.
- The climate in the cabin : temperature, moisture, air quality, pressure.
- Noise in the cabin, or more specifically Speech Interference Level (SIL) and the presence of resonances.
- Acceleration, mainly normal to the flight path but also in the direction of roll during braking.
- The aircraft's attitude during climb and descent.
- The duration of the trip.
- The number and accessibility of lavatories, washrooms, lounges (if provided) and such amenities.
- Stewardess service, in-flight entertainment, meal service, snacks, etc.

The shape of the passenger cabin is determined by the combination of the diameter (if pressurised) desired for seating and the curvature required to ensure passenger/sidewall clearances. On commercial passenger aircraft, the width of the cross-section is determined by the selection of seat width, aisle width, number of seats, and number of aisles. Clearances at the head, shoulder, armrest, and feet determine the location of the radius centre.

The sales appeal of the projected aircraft may be far more dependent on choosing the proper seating arrangement than in achieving a high aerodynamic efficiency for the design. The geometric requirements for the seats, aisles, etc. are established by customer/marketing requirements.

Cargo deck diameter and radius requirements for cargo containers can be generated using the same method as the one used for the upper lobe.

In most passenger aircraft baggage and cargo is carried in "standard" containers. From a competitive viewpoint it is important to be able to carry as many different types of containers as possible. This represents a very difficult design problem. The problem needs to be solved as part of the overall cross section and fuselage layout process.

The location of the wing on the fuselage as well as the amount of space needed for landing gear retraction can help dictate the amount of cargo containers that can be carried in a given volume. If from a competitive viewpoint it becomes desirable to carry one or two more containers, the fuselage length, the cross section or the wing location on the fuselage may have to be reexamined. In passenger transports it is undesirable to interrupt the fuselage cross-section locally by a wing torque box. This can be a real problem in the case of high wing transports.

For pressurised aircraft the most efficient cross-section from a structural viewpoint is the circle (Reference 2.17). However, for small aircraft a circular cross-section is wasteful in terms of volume. To solve this problem, usually a cabin cross-section for small aircraft consists of two or more circular arch. From a manufacturing viewpoint a flat sided fuselage is the cheapest to build.

Sizing the passenger cabin

The dimensions of the human body dictate the minimum cabin size that will "fit around" the occupant(s) after a decision has been made whether the cabin cross-section allows for "stand-up" room or for "crawl-to-your-seat" room.

After the above decision, the first step is to decide upon the number of seats to be placed abreast in a cross-section. This is a critical choice in passenger transports. The fewer seats abreast, the longer the fuselage and the more difficult "growing" the aircraft becomes. The more seats abreast, the shorter the fuselage and the easier it becomes to "grow" the aircraft, but the fuselage may have poor aerodynamic characteristics.

The passenger cabin is first sized for the tourist section since that class usually determines the passenger cabin width (Reference 2.7).

The minimum allowable width of aisles between seats is dictated by emergency evacuation considerations. Figure 2.7 (Reference 2.17) summarizes the allowable dimensions based on FAR 25.815.

Although the preliminary design will be based on a certain type of seat, due allowance should be made for the fact that airlines tend to lay down their own specifications for the cabin furnishings. The passenger seats on which data are given in Figure 2.8 (Reference 2.15) can be used as an initial value. FAR 25.817 states that on each side of an aisle, no more than three seats may be placed abreast.

For transport aircraft, a check on the total cabin width and the length can be made with the statistical data in Figure 2.9 (Reference 2.15).

Sizing the cargo hold

The cargo hold geometry and size are determined by the cargo-carrying requirements. The industry has developed a range of so-called standard containers and

pallets as shown in Figure 2.10 (Reference 2.17). LD-3 containers tend to be the most prevalent, but they are sized for larger aircraft. Selection of cargo containers must satisfy mission, cargo, fuselage diameter, section perimeters, and area requirements.

Fuselage width versus perimeter

If cargo and baggage containers are not required, then fuselage widths, diameter, and perimeter are set by the number of seats abreast chosen by the designer. Perimeter must be emphasized here because once cargo containers are used, fuselage width does not properly indicate the wetted area and aircraft efficiency that may result (Reference 2.7).

Appendix A.3 shows the cabin cross-section of the competitors.

2.6.1.3 Sizing the interior

Once the cross section has been developed, the next step is laying out an aircraft interior. This means determining the location of the seats, galleys, lavatories, closets, attendant seats, doors, etc. Parameters which should be known prior to this task are (Reference 2.7) :

- Approximate cabin length.
- Diameter and radius control points.
- Wing type and location.
- Number of engines and location.
- Passenger split and approximate location of class divider.
- Door locations.
- Galley locations.
- Lavatory locations
- Closet requirements

The passenger cabin should be laid out so that in cruise flight the cabin floor is level. If this criterion is not satisfied, cabin service and moving about in the cabin are made much more difficult. The level cabin floor requirement is linked directly to the choice of wing incidence.

The actual cabin arrangement for a commercial aircraft is determined more by marketing than by regulations. The dimensions of interest are include : seat pitch, seat width, headroom, aisle width, passengers per cabin staff, passengers per lavatory, galley volume per passenger. Typical seat pitch are classified based on Reference 2.15 :

- De luxe type : seat pitch 37 - 42 inches.
- Normal type : seat pitch 32 - 36 inches.
- Economy type : seat pitch 28 - 31 inches.

When arranging the seats, congestion should be avoided. Seats should not be located adjacent to galley or lavatory doors if possible. Seats should be kept against

sidewall (windows) when galleys can be positioned on aircraft centreline. Rows should be positioned to maximize window use.

The minimum number of flight attendants is specified by the airworthiness regulations (e.g. FAR 91.215); the actual number of cabin staff/passenger is fixed by the company. The average number of cabin staff/passenger are as follow (based on Reference 2.15) :

	first class	mixed	tourist class
International scheduled flights	16	21	31
U.S.A. domestic flights	20	29	36
Other domestic flights	21	-	39

At least one folding chair is placed at each exit for members of the cabin staff. This should permit a good view into the passenger cabin and be as safe as possible in crash landings.

The number and dimensions of the galleys, lavatories and wardrobe facilities are shown in Table 2.1 (Reference 2.15). It is advisable to locate those facilities at the forward and/or rearward end of the cabin, thus allowing for different cabin layouts. For aesthetic reasons toilets should preferably be located so that they are not directly visible from the galley. They should be easily accessible, and when the cabin arrangement includes a separate first-class section it is desirable to provide toilet facilities in that part too.

For passenger aircraft, to be certificated according to FAR 25 and JAR 25, Figure 2.11 (Reference 2.15) shows the classification of emergency exits and the minimum number of passenger emergency exits according to the FAR Part 25 requirements. In addition, according Reference 2.39, for emergency exit Type III, a seat space at least 13 inches should be available for improvements in the times taken by passengers to operate the Type III exit to be achieved.

For a maximum of up to 70 or 80 passengers, one passenger door per side is generally sufficient, while two doors can be used for up to about 200 passengers. Passengers doors are located to port while service doors are fitted to starboard. Wide-body jets are an exception as these can be boarded from both sides. Doors should preferably be 6 ft high and 3 ft width (Reference 2.15).

Consideration should be given to galley servicing and lower cargo loading requirements, as well as maintaining adequate clearance from engines, wings, etc., for escape slides (see also Figure 2.17). Passenger exits and service doors should not be aligned with cargo doors to ensure structural strength. To ensure efficient use of cargo storage space, cargo doors must be aligned with the cargo containers or pallets.

The window pitch is not always decided by the seat pitch, but frequently by the optimum distance between the fuselage formers. An average figure is 20 inches (0.5 m) for the former and window pitch. The top of the window is roughly at the passenger's eye level (Reference 2.15).

The designer must allow for a viable slide escape from emergency exits with the aircraft in unusual positions such as nose gear collapse. Space in the interior must also be reserved for the slide pack (Reference 2.7).

2.6.2 Aerodynamic Design Considerations

The fuselage is responsible for a large precentage of the overall drag of most airplanes : 25 - 50 percent. Since it is desirable to have as little drag as possible, the fuselage should be sized and shaped accordingly. Fuselages generate the following types of drag : friction drag, profile drag, base drag, compressibility drag and induced drag. For more detailed data on the relationship between fuselage drag and fuselage shape the reader should consult References 2.21 and 2.22.

2.6.3 Integration

Once the interior of the fuselage has been defined, the fuselage design must be developed and integrated with the rest of the aircraft. Wing position (high, mid, or low), engine location (wing or fuselage), and landing gear location (wing or fuselage) will all affect fuselage configuration. Also, future growth should be allowed for, bearing in mind the limits set on fuselage length and aircraft performance by ground clearance. Moreover, in the final analysis, factors in addition to weight, drag, and cost become important. Passenger evacuation, compatibility with existing terminals, and likely passenger preference must also be considered.

2.6.4 Fuselage design for the ATRA-Family

The objective of designing the fuselage of ATRA-100 Baseline are :

- To guarantee the passengers to have comfort standards at least as good as those of the Fokker F-100
- The passengers feeling should not change too much when they move from big jumbo jet to the ATRA-100 Baseline aircraft
- To have the capability of aircraft growth
- Easy and rapid loading and unloading the aircraft, as well as good servicing capabilities
- To have good access, for maintenance and inspectability
- Could accommodate LD3 container on main deck on future cargo version

2.6.4.1 Passenger requirements

- Number of passenger : 108 mixed-class passengers with 100 tourists at 32 inch pitch and 8 first class at 36 inch pitch, see Figure B.7.
- Comfort standards shall be at least as good as those of the Fokker F-100.

- Aisle minimum width : 18 inch.

2.6.4.2 Cargo requirements

- Baggage space : 2 ft^3 per seat minimum
- Cargo space : 7 ft^3 per seat minimum

see Figure B.2.

2.6.4.3 Service requirements

- Cabin staff : 3 attendants.
- Galley : 108 hot meals.
- Lavatory : one (for first class) and two (for tourist class).
- Wardrobe : two

2.6.4.4 Fuselage cross-section

From seat abreast trade-off study, its was found that fuselage with 6 abreast is too short for ATRA-80 and fuselage with 4 abreast is too long for ATRA-130. The comparison of fuselages with 4 and 6 abreast are shown in Figure B.6 of Appendix B.

For the number of passenger ranging from 83 (ATRA-80 two classes cabin layout) until 140 (ATRA-130 all tourist class cabin layout), a single aisle aircraft with 5 abreast tourist and four abreast first class seating was decided for the ATRA-Family fuselage cross-section, see Figure B.2 and B.7. The selection are based on the following considerations :

- Fuselage growth potential
- Fuselage fineness ratio
- Tail arm availability

It was futher decided to use a circular cross section as this is the lightest solution for a pressurised cabin and is easy to manufacture. The fuselage cross-section for ATRA-Family is shown in Figure B.2 of Appendix B. While the comparison of ATRA-Family fuselage cross-section with the competitors and with the larger aircraft are shown in Figure B.3, B4 and B5 of Appendix B respectively.

2.6.4.5 Interior layout

The interior layout for the ATRA-100 (Baseline), the ATRA-80 (Shortened Version) and the ATRA-130 (Stretched Version) are shown in Figure B.7 of Appendix B.

Figure B.16 shows accessibility/serviceability of ATRA-100 Baseline.

2.7 INITIAL WING DESIGN

Designing the wing is one of the most complicated aspects of aicraft design. The wing must satisfy infrastructure requirements, mission/performance requirements, and design requirements.

The mid to low wing mounted configuration is typical transport aircraft. For ATRA family, low wing mounted configuration was chosen. For more detailed design methodology on the initial wing design and initial wing design for ATRA-100 Baseline the reader should see Chapter 7 of this thesis.

2.8 SELECTION AND INTEGRATION OF THE PROPULSION SYSTEM

The propulsion system serves many purposes. It provides :

- thrust to propel the aircraft in flight and on the ground
- hydraulic, electrical, mechanical power output
- compressed air for environmental control system, anti-ice and engine start

Selection and integration of the propulsion system involves the following three decisions (Reference 2.17) :

1. Selection of the propulsion system type or types.
2. Determination of the number of engines to be used and the power (or thrust) level of each.
3. Disposition of these engines, i.e. integration of these engines into the configuration.

The following section is a brief design methodology for selection and integration of the propulsion system based on References 2.6, 2.17, 2.23 - 2.33.

2.8.1 Choice of the number of engines and the engine type

The following factors play a role in selecting the type of propulsion system to be used (Reference 2.17) :

1. Required cruise speed and/or maximum speed
2. Required maximum operating altitude
3. Required range and range economy
4. FAR 36 noise regulations
5. Installed weight
6. Reliability and maintainability
7. Fuel amount needed
8. Fuel cost
9. Fuel availability
10. Specific customer or market demands
11. Timely certification
12. Engine cost

13. Aircraft layout clearances

Overall fuel efficiency and installed weight often dominate the arguments pro and con a certain type of propulsion system. The energy crisis in the late 70's has set off a considerable effort in the engine industry which were concentrated on either turbofans with very high by-pass ratio (superfan) or the open rotor concept called propfan or unducted fan (UDF). The common key to better SFC is driving the by-pass ratio to extreme values and thus increasing the propulsive efficiency while maintaining the cruise speed of current turbofan. The common message is that only at fuel prices exceeding $ 1.5/gallon this technology would efficient (Reference 2.40), see also section 2.8.4. Most engine manufacturers have returned to a turbofan engines for high subsonic transports.

There are two engine-development possibilities for a decision on the number of engines :

1. A new engine will be developed for the proposed design. In this case, the engine(s) can be tailored to the existing design. If a candidate engine is still in the conceptual design stage, the engine manufacturer may give the option of allowing the engine reference thrust to be scaled up or down from the "scale 1" reference thrust (rubber engines). The "scale 1" reference thrust is the reference thrust corresponding to the engine performance deck, weights and dimensions supplied by the manufacturer. The designer must be aware of the fact that the development and certification of a new powerplant is expensive and takes a long lead time. For new jet engines a typical lead time is 7 - 10 years.

2. An existing engine must be used. Reference 2.5 provides data on existing aircraft engines. Because the power or thrust level of existing engines is basically "frozen", the number of engines is determined by dividing the required take-off power or thrust level by an integer : usually 1, 2, 3 or 4. With today's turbofan engine technology for aircraft up to the B777's size use usually the twin-engine configuration, see also Reference 2.23. The consensus today is that more engines lead more maintenance, rigging and cost.

Although the modern turbine engine is very reliable, the possibility of an engine malfunction must never be ignored. Although only 50 % of the thrust will be available after failure of one engine out of two, the aircraft must be designed to provide an acceptable level of safety.

2.8.2 Engine integration into the configuration

Propulsion system integration is one of the more interesting and challenging aspects of aircraft design. To achieve success requires a multi-disciplined approach involving aerodynamics, structures, loads, noise, weights, propulsion, flutter, and ECS. A clear understanding is required of design requirements, and a more open, "working-together" relationship is needed with the engine companies and the airlines to obtain a design with the best balance between performance (drag/TSFC), weight, noise, maintainability, producibility, and cost. Traditional rules, emphasizing aircraft design mainly for best fuel economy, does not apply in today's environment since both fuel

costs and cost of ownership are major portions of airline operating expenses (Reference 2.24).

Historical nacelle placement relative to the wing for several aircraft/engine combinations is shown in Figure 2.12, while Figure 2.13 gives guidlines for nacelle placement for minimum interference drag for turbofan engines (Reference 2.25). Aerodynamically, history has shown that forward engine placement is generally beneficial for minimizing installed drag. The conventional wing/nacelle installation boundary delineates close-coupled configurations which usually present challenges to aerodynamicists, with highly tailored configurations often required (Reference 2.26).

2.8.2.1 Aerodynamic and non-aerodynamic design considerations for wing-mounted twin-engined aircraft.

The design of the powerplant installation involves careful consideration of many factors both aerodynamic and non-aerodynamic (Reference 2.25).

A. Aerodynamic factors include (Figure 2.14) :

- Overall shape and orientation of the nacelle affects nacelle and wing profile, wave, and induced drag at cruise and engine-inoperative conditions.
- The fore/aft, up/down, and spanwise positioning affect interference drag, wing span loading and induced drag. Spanwise location also influences vertical tail sizing for engine-inoperative control.
- The inlet external contours must provide minimum drag at cruise conditions while satisfying engine-inoperative requirements of separation free flow and minimum spillage drag.
- The inlet internal geometry should be designed to provide distortion-free air to the engine at all operating conditions such as take-off and climb (high airflow, high angle of attack), while maximizing inlet recovery at cruise conditions.
- The strut contours must clear all hardpoints, such as engine mounts and wing attachment fittings, while minimizing adverse flow interactions with the nacelle and wing flow.
- The exhaust system and jet have a strong influence on the installation drag for under-wing mounted engines. Careful design of this component of the nacelle insures a successful design with trades often required between exhaust system, TSFC and installed drag.

B. Non-aerodynamic factors include (Figure 2.15 - 2.21) :

- Engine size and bypass ratio should be determined to meet the aircraft thrust requirements for take-off, climb, cruise, and engine-inoperative conditions while providing efficient cruise operation. The size, location and orientation of the engine has a strong influence on the overall design of the aircraft.

- Ground, runway and taxi light clearances, allowable wing shear, manufacturing capability, installed drag, and airport gate compatibility (200" passenger entry door sill height limit) influences the maximum engine sized allowed.
- Sufficient aircraft roll clearance should be maintained to allow for abnormal conditions such as severe crosswind landings or flat tires.
- The engine spanwise location should be chosen to satisfy passenger door escape slide, loading ramp and engine inlet flow hazard zone (suction) clearance requirements.
- Ground clearance criteria also allows sufficient clearance for critical engine components in the event of a collapsed nose gear, although this is an extremely rare event for modern transports.
- Turbine disk burst zones should be identified and wing dry bays should be provided to avoid hazardous conditions in the event of a turbine disk burst. Location of critical aircraft control systems in this region should be avoided. Shielding of the turbine it's not practical due to the extremely high energy of a turbine disk burst.
- Spanwise position of the engine should be established outside a 22 degree cone to be free of nose or main gear water spray ingestion zones (based on statistical data) to ensure stable engine operation during take-off or landing.
- Engine weight provides relief in wing root bending moments resulting from air loads, the further out the better.
- The relationship between engine location and wing flutter is complex. On the one hand a pylon-mounted engine moves the section c.g. forward of the flexural axis and thus tends to reduce the flutter. On the other hand, placement of the pylon at a spanwise anti-node of bending or torsion increases the effective mass of the system.
- Engine-out yawing moment must be balanced by a moment from the vertical tail. Increased vertical tail volume coefficient is required as the engines are moved outboard.
- Both the airframe and engine contribute to the total noise of the aircraft, with the dominant component dependent on the flight condition examined. At take-off conditions, engine noise dominates while during approach at low power and high flap deflections, airframe noise may dominate. It is important to consider noise during the development of the engine installation and flap design. Powered model testing is often used to understand the trades involved in minimizing noise due to jet/flap interaction.

  Engine noise reduction requires the use of acoustic materials inside the inlet, fan nozzle, and core exhaust (Figure 2.21). Requirements often dictate that the length of the inlet and fan nozzle extend beyond optimum for minimum aerodynamic drag. Engine efficiency also suffers due to acoustic material surface roughness and leakage losses.

  To reduce noise, full-length duct mixed flow exhaust systems are in use on several commercial aircraft at the present. The concept uses pre-mixing of the fan and core

flows prior to exiting the nozzle in order to reduce the jet velocity and associated mixing, but is generally offset by higher installed nacelle drag and weight.

2.8.2.2 Nacelle design philosophy

The aerodynamic design of the inlet and cowling involves compromises between satisfying criteria for take-off, climb, cruise, descent, and engine-inoperative conditions. For twin-engine aircraft, engine-inoperative requirements at take-off conditions are more stringent than for 3 or 4 engine aircraft. Additionally, to provide airlines with operational flexibility, modern twin engined transports strive for Extended Twin-Jet Operations (ETOPS) which imposes additional engine-inoperative design requirements for cruising with a failed engine at high speed for extended times (Reference 2.23). Each engine-inoperative flight regime imposes different design challenges since the inlet is exposed to a variety of flow, speed, and angle of attack conditions, Figure 2.22. The successful design is achieved by satisfying design requirement at these conditions while maintaining good cruise performance (Reference 2.26).

The external nacelle flow environment varies widely depending on engine airflow, speed, and angle of attack, Figure 2.23. At normal take-off power conditions the inlet captured streamtube is large and the stagnation point is near the lip producing low external velocities on the cowl. As power is reduced the stagnation streamline move inside the lip requiring the uncaptured flow to accelerate around the lip. At engine-inoperative conditions the inlet flow is low, causing high velocities and gradients on the external lip. If the gradients are sufficiently steep, flow separation occurs and external drag increase rapidly (Reference 2.26).

2.8.3 Future turbofan engine developments

Future engine developments are heading toward larger, higher bypass ratio engines with higher thrust capability due mainly to the economics of twin-engined aircraft.

Different engine manufacturers offer different solutions to this challenge (Reference 2.28), Figure 2.24, with direct drive fan engines up to Bypass ratio (BPR) 9, geared fans to BPR 15 - 25, unducted ultra-high-bypass-ratio propfans, and counter-rotating fan concepts being studied.

While engine TSFC is improved for the higher bypass ratios, the aerodynamic challenge is to install these engine with minimal offsetting drag increases (Reference 2.6) which could reduce the optimum bypass ratio, hence, efficiency, achievable, Figure 2.25.

2.8.4 Potential powerplants for the ATRA-100 Family

Propfan technology (i.e. the open rotor concept) offers an unmatched fuel saving at moderate jet speeds (M < 0.75) at the expense of 10% weight increase along with a much higher engine price. The common wisdom in 1989 was that a propfan aircraft would be viable only at fuel prices beyond $1.5/gal. In addition a flying tesbed like the McDonnell Douglas demonstrator (Reference 2.29) would have been inevitable in order to reduce the development risk and obtain sufficient data.

Since the propfan technology is not economically viable at this time, an underwing mounted turbofan with a bypass ratio of 4.9 - 6 was chosen comprising a long duct nacelle with internal mixing (confluent or forced mixer) to reduced the engine noise and to improved engine's thrust and engine's SFC.

In the required thrust classes of 16,000 to 23,000 LB a total of four candidate engine projects are studied and pursued by manufacturer groupings :

- BMW Rolls Royce : BR 710 (14,970 LB thrust), BR 715 (22,000 LB thrust)
- MTU/Pratt & Whitney: MTFE (15,000-24,000 LB thrust)
- CFM International : CFM 88 (15,000-20,000 LB thrust)
- Allison : GMA 3014 (14,000-19,000 LB thrust)

They all base their designs on some existing, proven HP core hardware, propose very similar by-pass and overall pressure ratios and aim for a basic thrust class at the upper end of what Regional Airliner currently requires. They will feature a fan diameter of 52-58 in, a built-in growth potential of 30% with a common core and nacelle, and an average SFC improvement of 13% with respect to the RR Tay (Reference 2.5, 2.6, 2.30). Thus ATRA-80 at the lower end will get a down rated version. This is beneficial in terms of reliability especially for short range operation, but causes weight and some first cost penalties.

The concept of internal mixing of the cold bypass air and hot core stream before their acceleration in the thrust nozzle has recently regained attraction as it offers a thrust gain in the order of 1%, a slight SFC improvement and a significant noise reduction of 2-5 dB. The secondary nozzle is replaced by the mixed flow nozzle and the mixer replaces the primary nozzle (Figure 2.26, from Reference 2.31). This concept is already used on the PW300 engine and on the CFM56-5C2 for the Airbus A340. A predecessor concept, confluent mixing, is used on the IAE V2500 engine. This has no mechanical mixer, and a mixing efficiency of 20%. An increased mixing efficiency would either require a very long mixing chamber (6-8 diameters) or a mechanical device known as a lobed mixer. The optimisation of the installed engine configuration taking into account the adverse trend in installation drag and weight were covered in joint trade-off studies between aircraft configurator and the engine manufacturer. The engine locations for Airbus family are shown in Figure 2.27 (Reference 2.6).

The engine uses in this study is BMW Rolls Royce BR 715, engine data's are taken from Reference 2.32. For engine data and installation see Appendix B.

2.9 UNDERCARRIAGE LAYOUT

It was decided to use a conventional hydraulically retracable tricycle undercarriage, with twin wheels and oleo-pneumatic shock-absorbers on each unit. Main units, retract inward into wing/fuselage fairing; nosewheels retract forward.

The positions of the units were chosen using the method of Reference 2.34. The nosewheel static loads were in the allowable 8 - 14% range at various C.G. positions.

The requirements call for a Load Classification Number (L.C.N.) of less than 65. The tyres size chosen were the standard H40x14-19 type (inflation pressure 120 psi) for mainwheel and 24x7.7-10 type (inflation pressure 100 psi) for nosewheel and using the method of Reference 2.15 the mainwheel Load Classification Number was calculated to be 62.

2.10 EMPENNAGE SIZING

The empennage section describes the horizontal and vertical tails. Additional general information on empennage surfaces, including the qualitative effects of dorsal extensions and control surface mass balancing, may be found in Chapters 11 and 12 of Reference 2.19 and Chapter 8 of Reference 2.20.

For the empennage initial sizing, the so-called V'-method is often used. The tail volume (V') coefficients are defined as follows (Reference 2.17) :

$$V'_{HT} = (l_{HT}/MAC)*S_{HT}/S \qquad (2.2)$$

$$V'_{VT} = (l_{VT}/b)*(S_{VT}/S) \qquad (2.3)$$

where :

l_{HT} = horizontal tail arm
l_{VT} = vertical tail arm
S_{HT} = horizontal tail area
S_{VT} = vertical tail area
S = wing area
MAC = wing mean aerodynamic chord
b = wing span

2.10.1 Horizontal tail

The horizontal tail provides longitudinal stability and control. Tail reference area is the trapezoidal area; for a wide-body aircraft with small horizontal tail, the exposed area may be of the order of 30% less than the reference area. Since tail effectiveness depends on exposed area, great care should be taken in evaluating the capability of a horizontal tail based on reference area (Reference 2.36).

2.10.1.1 Sizing the horizontal tail

For preliminary tail sizing and location, see Part II, Chapter 8 in Reference 2.17 or Section 4.5 in Reference 2.16. Table 8.7 in Reference 2.17 and Table 9.2 in Reference 2.15 lists horizontal tail design data for existing aircraft. For a more detailed analysis of horizontal tail sizing criteria, see Chapter 9 in reference 2.15; this reference contains a description of the horizontal tail sizing chart.

Horizontal tail geometry (aspect ratio, thickness/chord ratio, taper ratio, etc.) requires weight and performance trade studies for the design options. Note that the tail normally experiences a download, so that the airfoil section may be cambered with the concave side upward; many horizontal stabilizers have uncambered airfoil sections (Reference 2.36).

2.10.1.2 Positioning the horizontal tail

The horizontal tail should be kept out of the wing wake at cruise (this may require significant tail dihedral). However, a high tail should be carefully evaluated because tail effectiveness at the stall may become inadequate (see Figure 2.28, from Reference 2.18), resulting in pitch-up, and/or the possibility of a "deep stall". In a deep stall, the horizontal tail is immersed in separated flow from the wing, so that there is insufficient longitudinal control power to get out of the stall (Reference 2.36).

The pitch-up characteristics of the aircraft are as follows (Figure 2.28) :

Region A Pitch-up at high lift generally preceded by warning
Region B Pitch-up without warning, avoid
Region C Generally no pitch up at subcritical speeds
Region D Generally no pitch-up

Additional information on tail location may be found on Part III, Chapter 5 in Reference 2.17.

2.10.1.3 Horizontal tail for the ATRA-100 Baseline

The individual component centres of gravity were determined and used to determine the overall aircraft centre of gravity. The method shown in Reference 2.35 was used and the results summarised in Section B.5 of Appendix B.

Comparisons with other fuselage(low)-tail airliners suggested a tail volume of 1.2. Therefore :

$$1.2 = (l_{HT}/MAC)*S_{HT}/S$$

A typical value of S_{HT}/S, AR_{HT}, λ_{HT}, Λ_{HT} are 0.243, 4.43, 0.295 and 30 deg. respectively; S is 110.21 M^2 and and MAC is 3.44 M. Therefore :
$S_{HT} = 26.814\ M^2$ and $l_{HT} = 16.909$ M

2.10.2 Vertical tail

The vertical tail provides directional (or weathercock) stability and control. The definition of vertical tail reference area depends on the configuration, but the most common definition is defined as the trapezoidal area whose root is taken as the horizontal line which intersects the intersection of the 50% chord line and the crown fuselage skin line (Reference 2.36).

If directional stability at high angles of attack is inadequate, a ventral fin (or fins) may be required. The dorsal fin is often used as a design modification to provide additional directional control with minimum structural change.

2.10.2.1 Sizing the vertical tail

For preliminary tail sizing and location, see Part II, Chapter 8 in Reference 2.17 or Section 4.5 in Reference 2.16. Table 8.7 in Reference 2.17 and Table 9.3 in Reference 2.15 lists vertical tail design data for existing aircraft.

The vertical tail is sized to the following criteria :

1. ensuring that the minimum control speed with one engine inoperative $(V_{MC})_{OEI}$ does not exceed 1.2 stall speed (V_S), meeting the criteria of FAR Part 25.149
2. meeting the crosswind landing requirements of FAR Part 25.237
3. ensuring that C_{n_φ} (weathercock stability) is positive (FAR Part 25.177)

Normally the one-engine-inoperative requirement sizes the vertical tail for a twin engined aircraft with wing-mounted engines (Reference 2.36).

For a more detailed analysis of empennage sizing criteria, see Chapter 9 in Reference 2.15 which contains a description of vertical stabilizer sizing for engine-out and cross-wind landing. Part VI, Chapter 10 in Reference 2.17 contains an empirical method for calculating C_{n_φ}; this method is extracted from Reference 2.37

2.10.2.2 Vertical tail for the ATRA-100 Baseline

Empirical studies for fuselage(low)-tail airliners suggested a fin volume of 0.081. Therefore :

$$0.081 = (l_{VT}/b)*(S_{VT}/S)$$

A typical value of S_{VT}/S, AR_{VT}, λ_{VT}, Λ_{VT} are 0.16, 1.6, 0.34 and 35 deg. respectively ; S is 110.21 M^2 and b is 32.357 M. Therefore :
$S_{VT} = 17.6543\ M^2$ and $l_{VT} = 16.314$ M

2.11 AIRCRAFT FAMILY CONCEPT

Many Aircraft manufacturers , i.e. : Airbus, Boeing, McDonnell Douglas, Fokker, British Aerospace, IPTN, etc., develop their aircraft family based on one wing and one fuselage cross section to reduce development costs. For one fuselage cross section aircraft family , alternatives for Regional Airliner family are :

1. Fixed wing geometry on mid-size, then DOC penalties for off-optimum.
2. Fixed wing geometry on mid-size, modification of wing extension/reduction, then development costs
3. Variable Camber Wing (VCW) which could be optimum for all family, but will have increased development costs

The ATRA family will use the third of the above concepts. The Variable Camber Wing concept is describes in Chapter 5.

The ATRA-100 has maximum design commonality with the ATRA-80 and ATRA-130. The level of commonality between the members of the ATRA standard-body aircraft family is such that the ATRA-80, ATRA-100 and ATRA-130 can essentially be operated as one aircraft type with positive effects on crew training, maintenance and aircraft scheduling. In addition, a mixed fleet of ATRA-100 aircraft combined with other aircraft in the ATRA family will allow airlines to better match capacity to demand whilst reducing operating costs, increasing crew productivity and simplifying ground handling.

Being the reduced/increased size development of the ATRA-100 the ATRA-80/ATRA-130 key changes are primarily related to size and capacity as all aircraft share similar systems and the same flight deck. Key changes include : derated/uprated engines, adapted systems and two fuselage plugs removed/added. Figure 2.29 shows The ATRA Family concept.

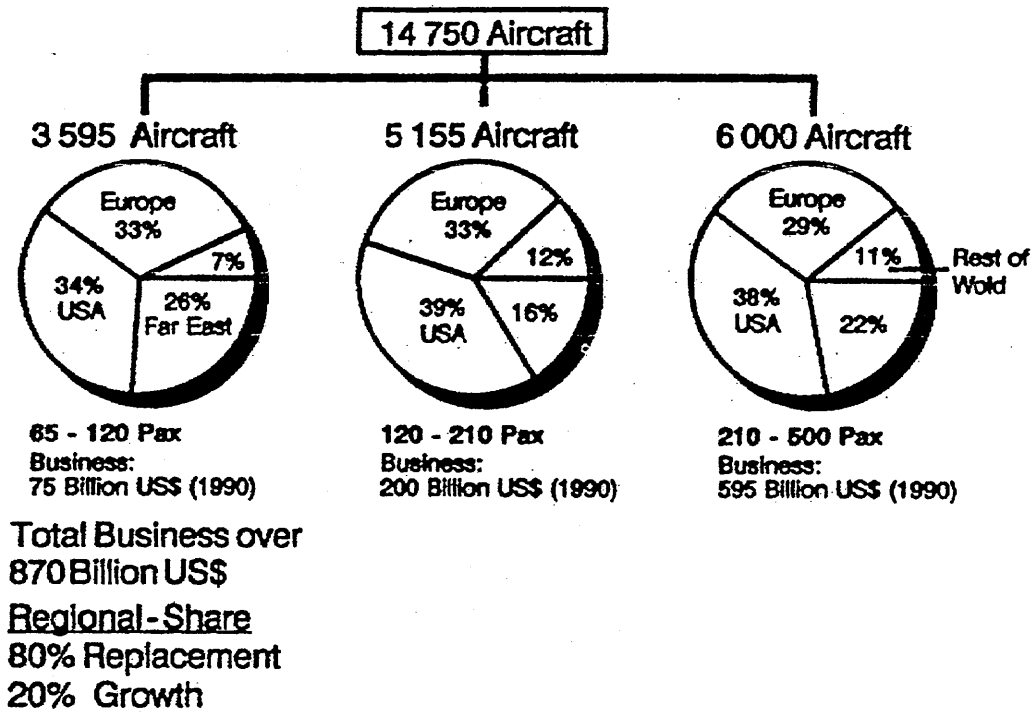

Figure 2.1 Market potential for transport aircraft, Ref. 2.6

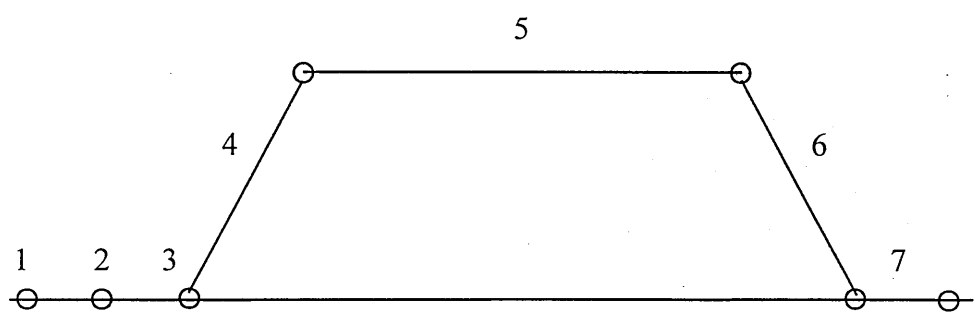

Phase 1 : Engine start and warm-up
Phase 2 : Taxi
Phase 3 : Take-off
Phase 4 : Climb to cruise altitude and accelerate to cruise speed
Phase 5 : Cruise
Phase 6 : Descent
Phase 7 : Landing, taxi and shut-down

Figure 2.2 Simplified mission profile.

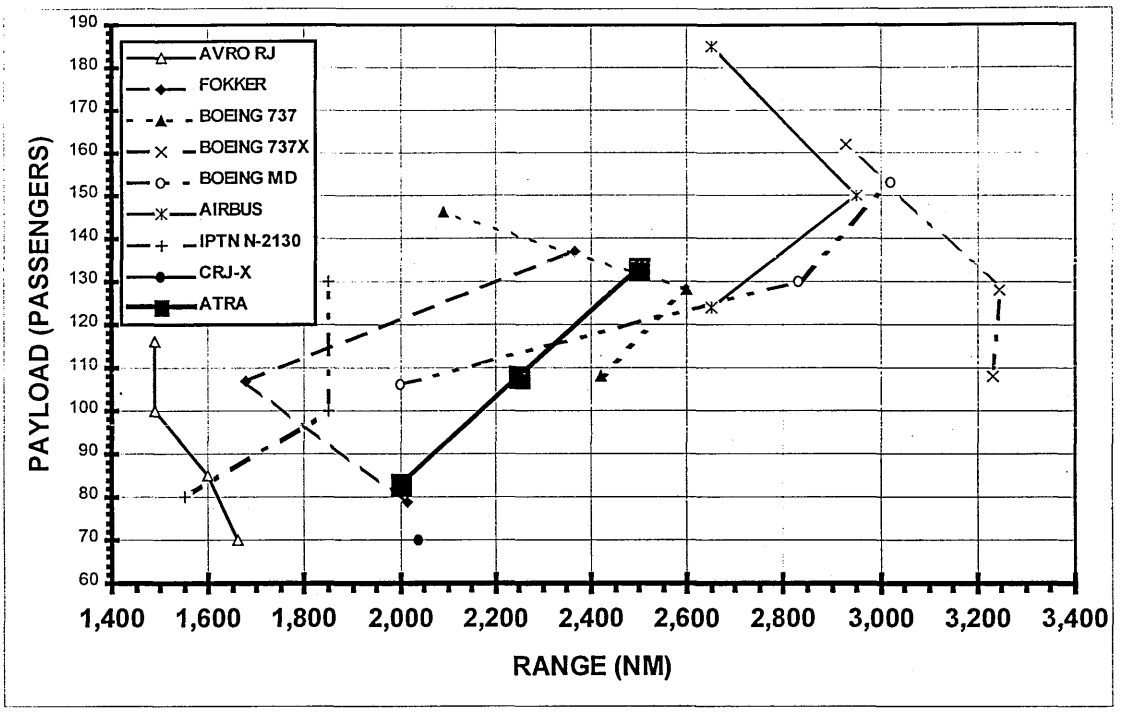

Figure 2.3 The design payload-range for ATRA Family and it's competitors

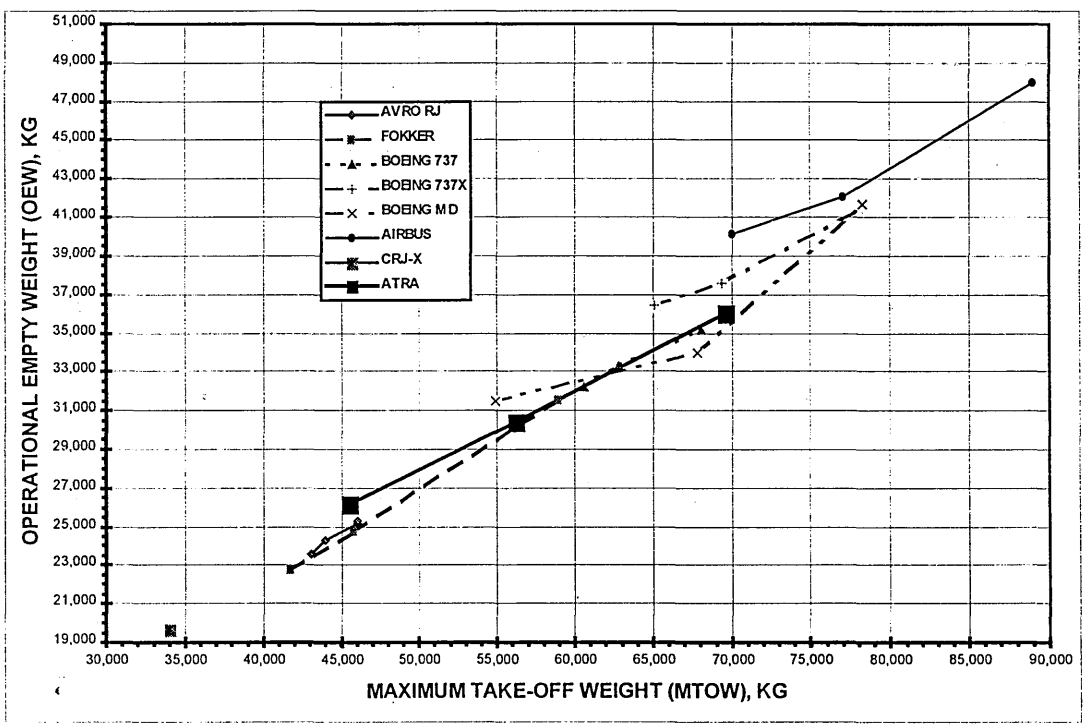

Figure 2.4 The empty weight versus maximum take-off weight for ATRA Family and it's competitors

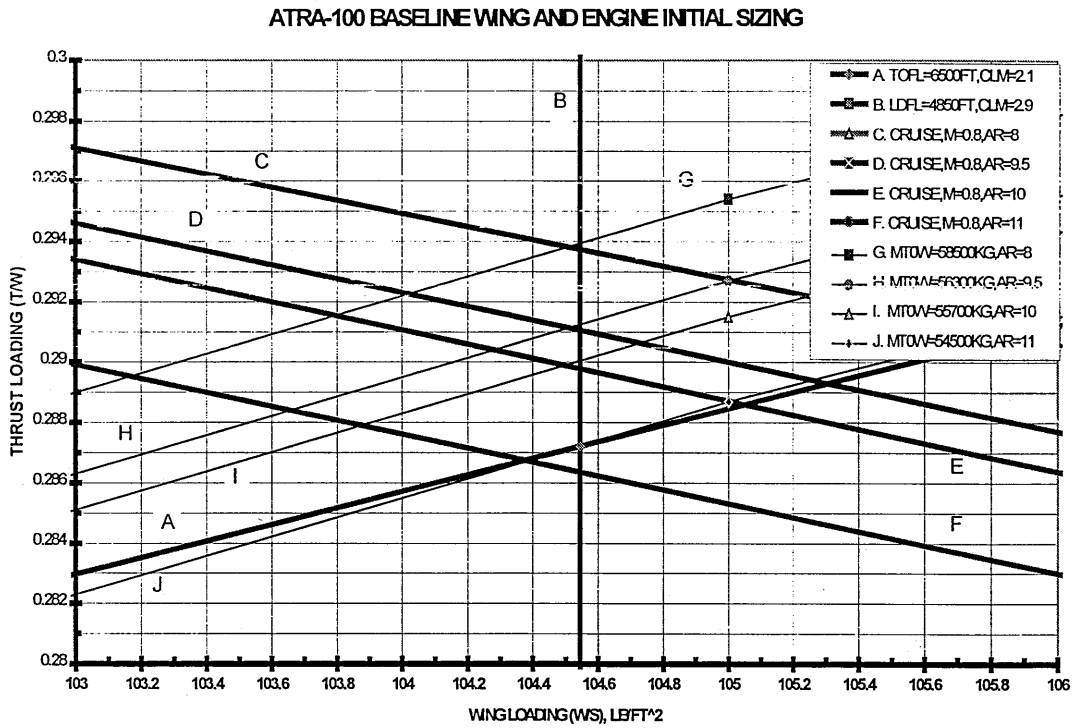

Figure 2.5 ATRA-100 Baseline wing and engine initial sizing

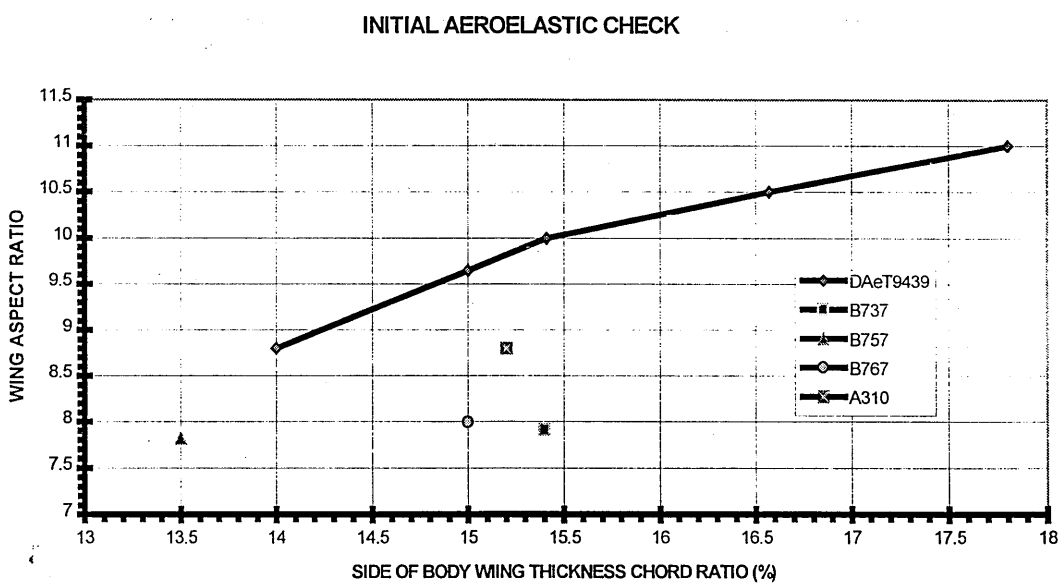

Figure 2.6 Initial aeroelastic check

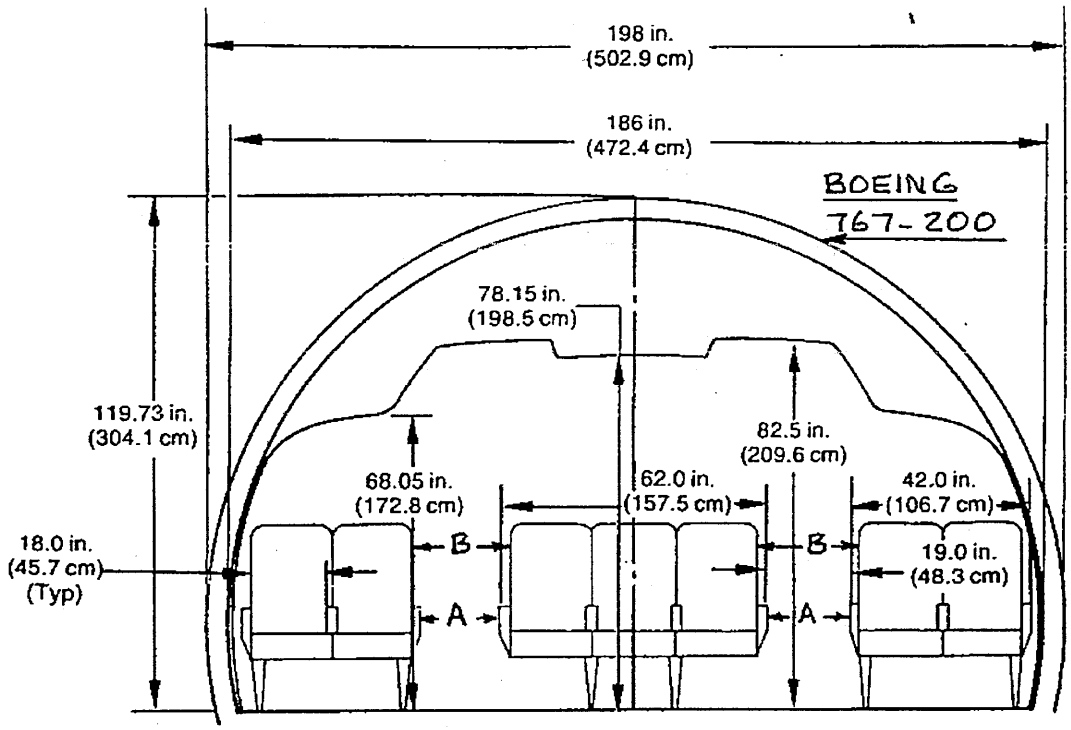

Number of Seats	Minimum Value of A	Minimum Value of B
10 or less	12 inches	15 inches
11 - 19	12 inches	20 inches
20 or more	15 inches	20 inches

Figure 2.7 Minimum aisle width requirements (Ref. 2.17)

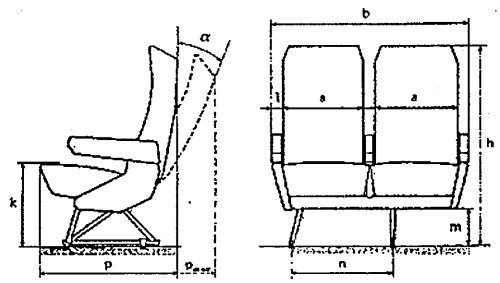

SYMBOL*	UNIT	SEAT CLASSIFICATION: DE LUXE	NORMAL	ECONOMY
a	inch	20(18½-21)	17(16½-17½)	16.5(16-17)
	cm	50(47-53)	43,5(42,5-45)	42(40,5-43,5)
b_2^{**}	inch	47(46-48½)	40(39-41)	39(38-40)
	cm	120(117-123)	102(100-105)	99(97-102)
b_3^{**}	inch	-	60(59-63)	57
	cm	-	152(150-160)	145
l	inch	2½	2½	2
	cm	7	5.5	5
h	inch	42(41-44)	42(41-44)	39(36-41)
	cm	107(104-112)	107(104-112)	99(92-104)
k	inch	17	17½	17½
	cm	43	45	45
m	inch	7½	8½	8½
	cm	20	22	22
n	inch	usually 32	(24-34)	
	cm	usually 81	(61-86)	
p/p_{max}	inch	28/40	27/37½	26/35½
	cm	71/102	69/95	66/90
α/α_{max}	deg	15/45	15/38	15/38

Figure 2.8 Definitions of seat dimensions (Ref. 2.15)

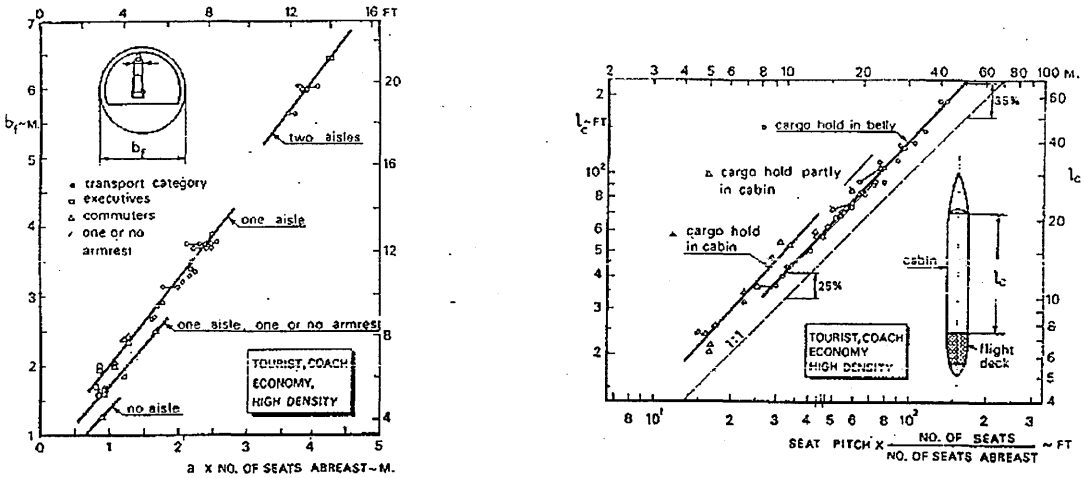

Figure 2.9 Statistical data of fuselage width and cabin length (Ref. 2.15)

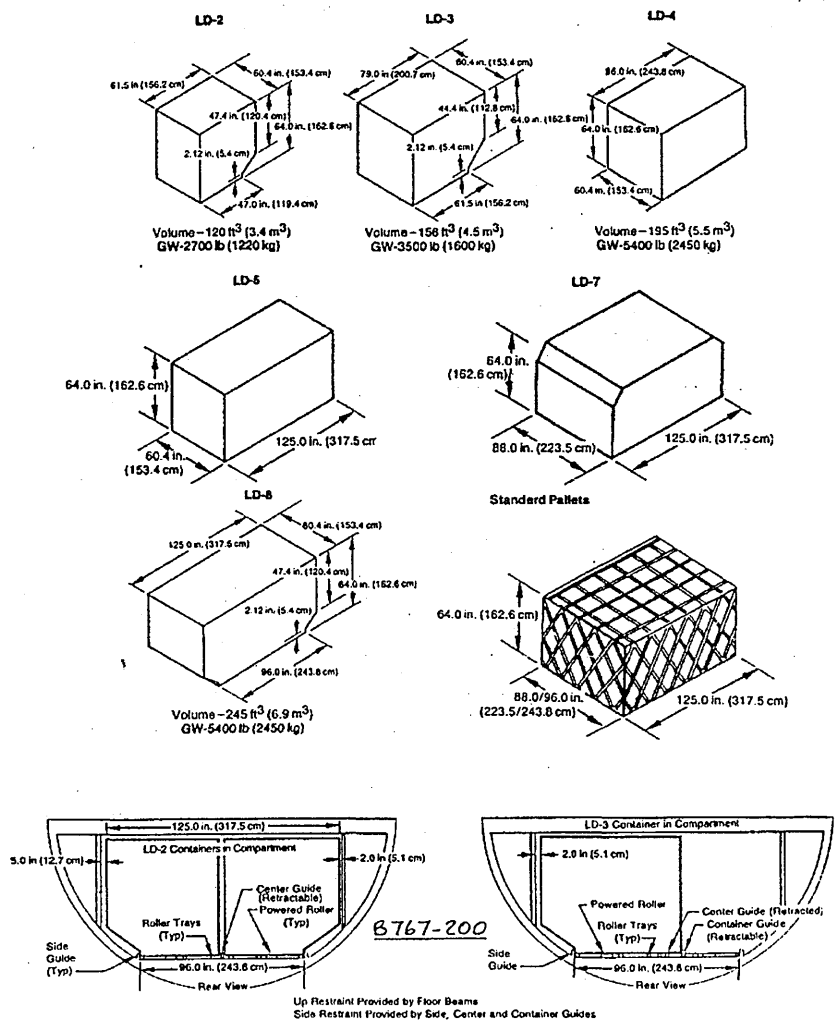

Figure 2.10 Typical pallet and container size (Ref. 2.17)

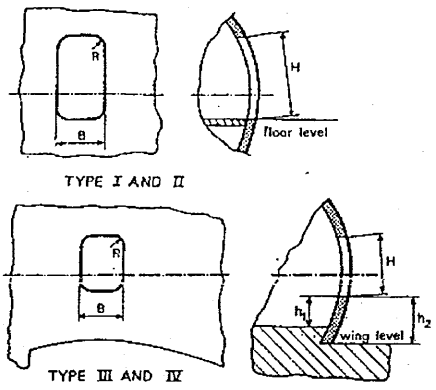

SEATING CAPACITY (EXCL. CABIN STAFF)	NUMBER OF EXITS REQUIRED ON EACH SIDE OF THE FUSELAGE			
	TYPE I	TYPE II	TYPE III	TYPE IV
1 through 10	-	-	-	1
11 through 19	-	-	1	-
20 through 39	-	1	-	1
40 through 59	1	-	-	1
60 through 79	1	-	1	-
80 through 109	1	-	1	1
110 through 139	2	-	1	-
140 through 179	2	-	2	-

NOTE

1. BCAR requirements are slightly different for 1-10 passengers; for this case an emergency exit of type III is required on both sides of the fuselage. Two exits of type I and II are required for a seating capacity of 180 up to 219.
2. The relevant rules should be consulted where passenger seats exceed this number and for special regulations.
3. Exits need not be at locations diametrically opposite each other. They should be located in accordance with the passenger seating distribution.
4. Two exits of type IV may be used instead of each type III exit.

EMERGENCY EXIT CLASSIFICATION AND LOCATION		B (min) inches (mm)	W (min) inches (mm)	R (max) inches (mm)	MAX. HEIGHT OF STEP: inside (h_1) inches (mm)	MAX. HEIGHT OF STEP: outside (h_2) inches (mm)
I	FLOOR LEVEL	24 (610)	48 (1219)	$\frac{1}{3}$ B	-	-
II	FLOOR LEVEL	20 (508)	44 (1118)	$\frac{1}{3}$ B	-	-
	ABOVE WING				10 (254)	17 (432)
III	ABOVE WING	20 (508)	36 (915)	$\frac{1}{3}$ B	20 (508)	27 (686)
IV	ABOVE WING	19 (483)	26 (661)	$\frac{1}{3}$ B	29 (737)	36 (914)

Figure 2.11 Classification and minimum number of passenger emergency exits according to the FAR Part 25 requirements (Ref. 2.15)

Aircraft type:	N_{pass} -	Range N M	galleys: number	galleys: l x b (inch)	toilets: number	toilets: l x b (inch)	toilets: pass/toilet	wardrobes: number	wardrobes: l x b (inch)
Aérospatiale N-262 Frégate	29	400	1	23 x 20	1	41 x 28	29	1	40 x 24
Grumman Gulfstream I	19	2100	1	34 x 25	1	67 x 37	19	1	36 x 32
Hawker Siddeley 748 srs 200	44	1000	1	37 x 14	1	53 x 35	44	-	
Fokker-VFW F.27 Friendship srs 200	48	1100	1	43 x 35	1	47 x 46	48	1	31 x 16
De Havilland Canada DHC-7	44	800	1	26 x 24	1	46 x 30	44	1	26 x 24
Lockheed L-188 Electra	95	2300	2	46 x 26	4	46 x 41	24	2	46 x 34
MFB 320 Hansajet	7	1000	1	24 x 24	1	30 x 26	7	1	24 x 15
Hawker Siddeley HS-125 srs 400	8	1450	-		1	35 x 28	8	1	24 x 12
Dassault Falcon 20.F	10	1500	1	27 x 18	1	44 x 30	10	1	31 x 25
Dassault Falcon 30/Hystère 40	34	750	-		1	41 x 31	34	-	
VFW-Fokker 614	40	700	1	35 x 28	1	53 x 32	40		65 x 40
Fokker VFW-F.28 Mk 1000	60	1025	1	44 x 25	1	58 x 25	60	1	25 x 21
BAC-111 srs 200/400	74	900	2	49 x 22	2	65 x 35	37	1	49 x 22
Mc Donnell Douglas DC-9 srs 10/20	80	1100	1	48 x 33	2	48 x 48	40	2	48 x 21
Boeing 737 srs 200	115	1800	1	55 x 43	2	43 x 34	58	1	55 x 43
Aérospatiale Caravelle 12	118	1000	1	51 x 43	2	55 x 43	59	2	24 x 17
Dassault Mercure	140	800	-		2	47 x 34	70	2	49 x 16
Boeing 727 series 200	163	1150	2	51 x 32	3	43 x 39	55	-	
Europlane	191	1400	3	42 x 42	4	42 x 42	48	1	52 x 26
A-300 B/4	295	1600	3	-	5	59 x 35	59	-	
Lockheed L-1011	330	2700	1	20 x 13.5 ft^2	7	45 x 36	47	-	head racks
Mc Donnell Douglas DC-10	380	3000	1	under floor galley	9	40 x 40	42	2	6.3 x 1.8 ft^2
BAC-VC-10	135	4200	1	49 x 32	5	47 x 47	27	2	42 x 24
Boeing 707-320 B	189	5000	2	79 x 47	4	40 x 37	48	1	79 x 43
Mc Donnell Douglas DC-8 srs 63	251	4000	2	48 x 34	5	42 x 42	50	4	34 x 20
Boeing 747	490	5000	4	6.6 x 2.1 ft^2	12	40 x 40	41	2	5.9 x 2.3 ft^2

NOTES:

N_{pass} = maximum number of passengers, tourist class, approx. 34" seat pitch

Range at about N_{pass} x 205 lb payload and including normal fuel reserves

Dimensions are approximate average length x width; toilets are not always rectangular.

Table 2.1 Number and dimensions of the galleys, lavatories and wardrobes of some airliners (Ref. 2.15)

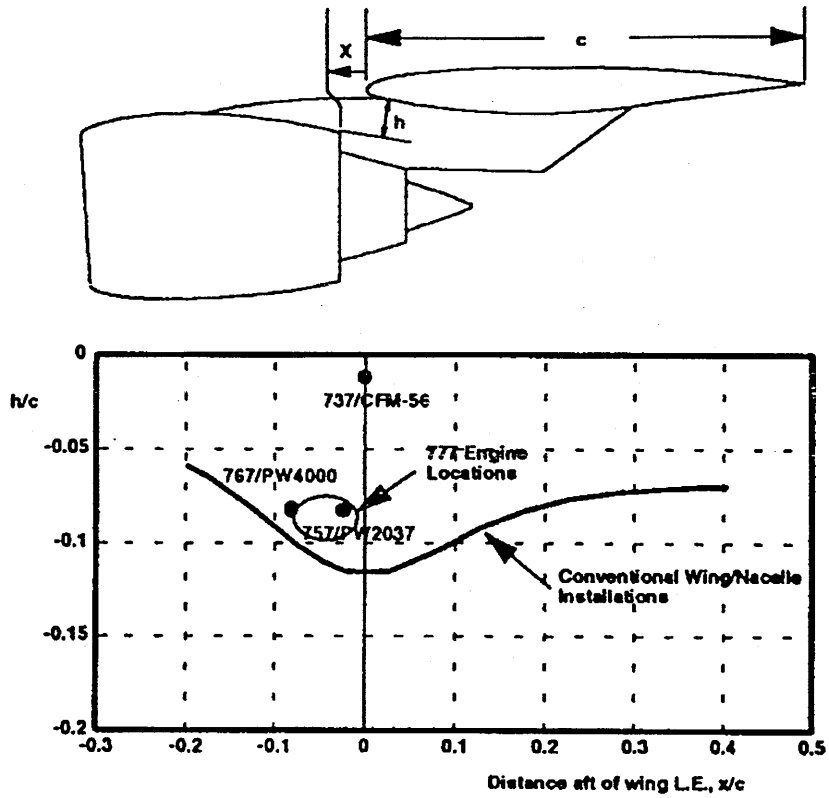

Figure 2.12 Nacelle/wing installation location

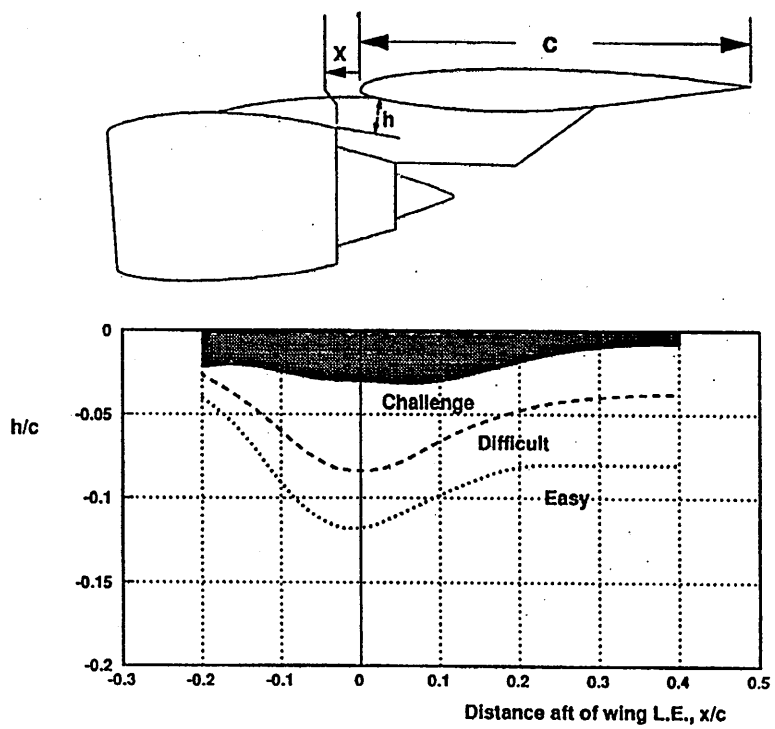

Figure 2.13 Guidelines for nacelle placement for minimum interference drag

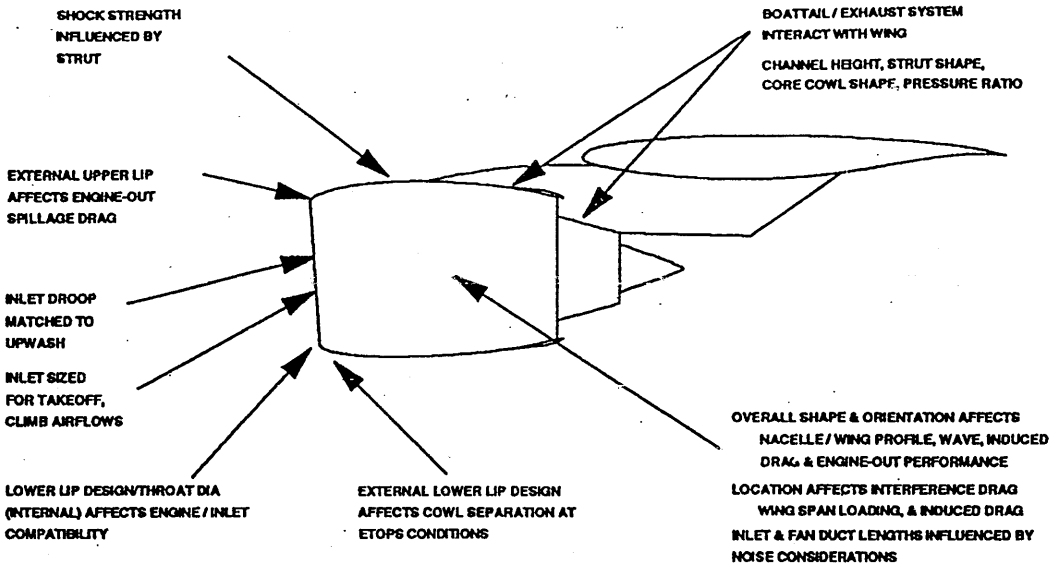

Figure 2.14 Factors influencing nacelle installation design

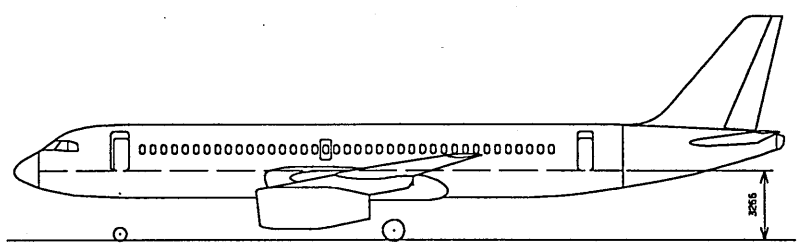

Figure 2.15 Passenger/loading door sill height consideration

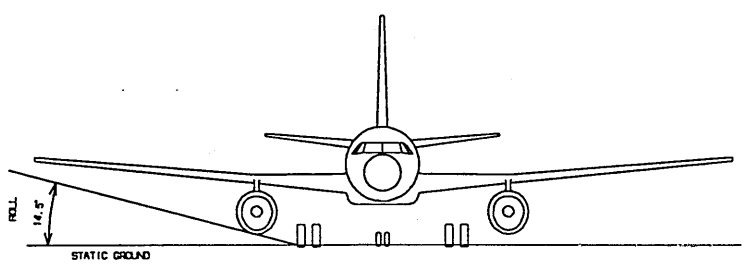

Figure 2.16 Roll clearance

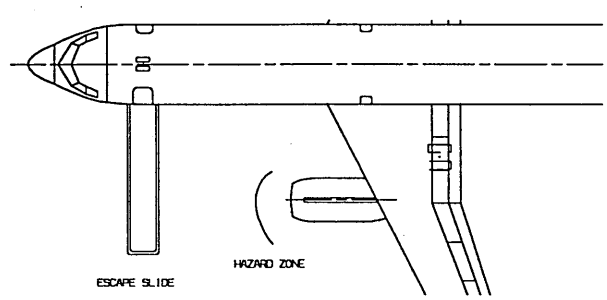

Figure 2.17 Escape slide, loading ramp & inlet hazard zone consideration

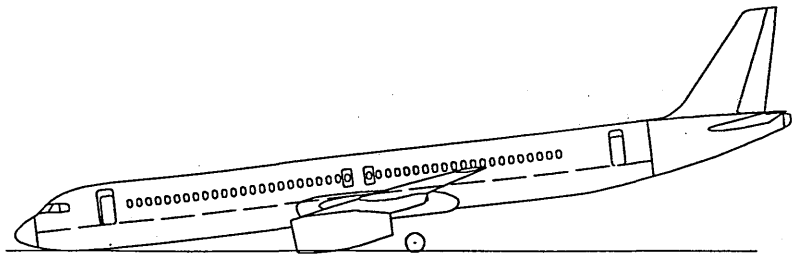

Figure 2.18 Collapsed nose gear

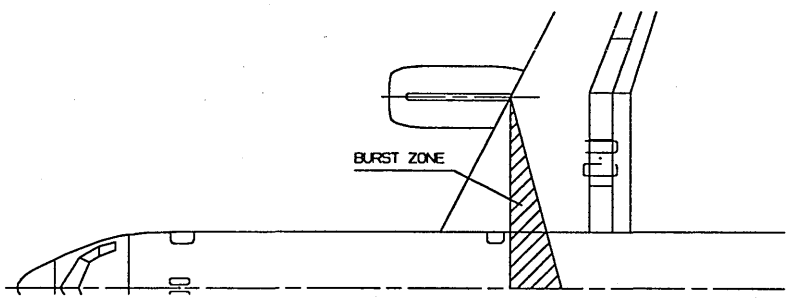

Figure 2.19 Turbine disk burst zone consideration

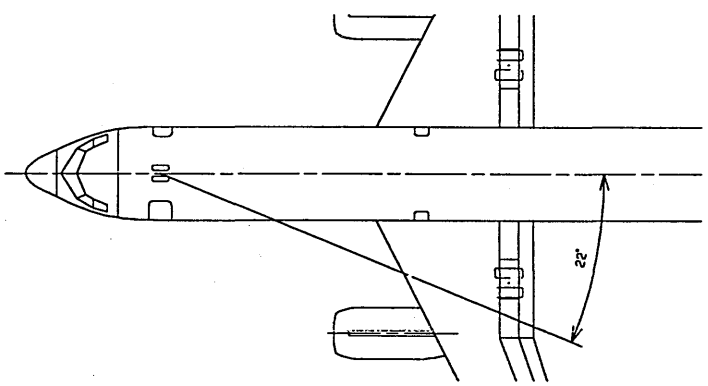

Figure 2.20 Nose gear water spray clearance

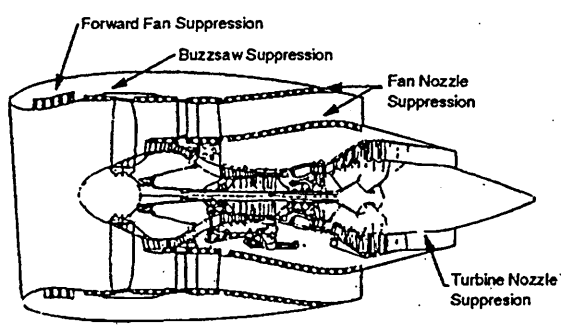

Figure 2.21 Engine noise treatment

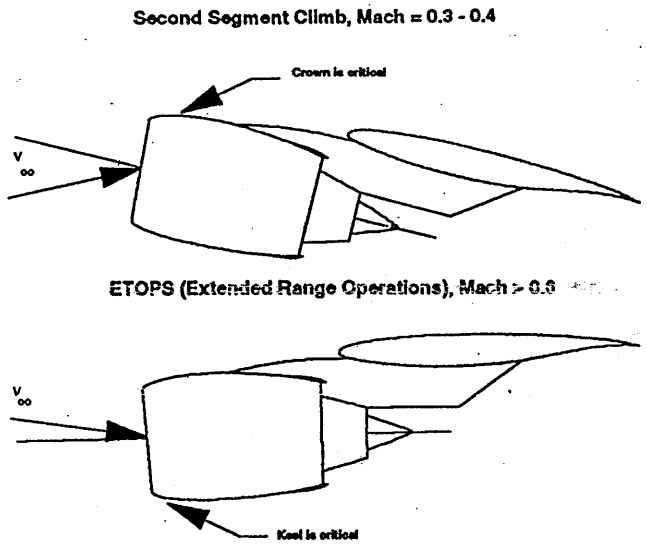

Figure 2.22 Inlet design conditions for engine inoperative operation

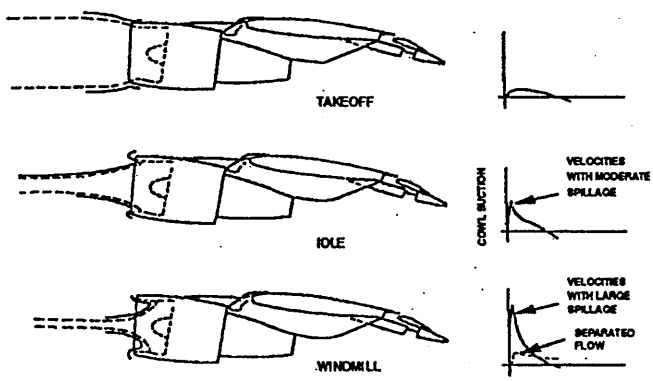

Figure 2.23 Nacelle inlet external flow environment

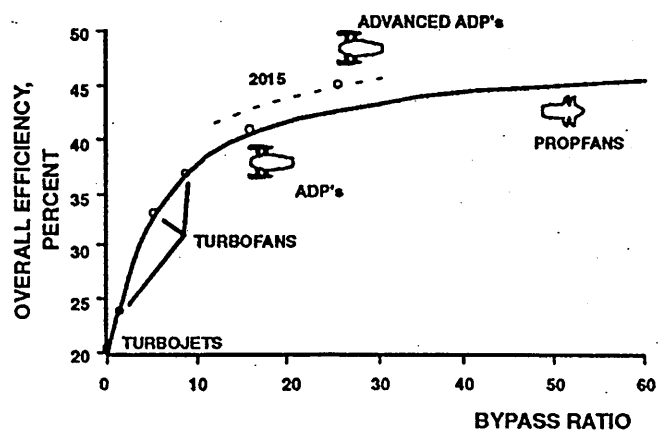

Figure 2.24 Advanced engine efficiencies

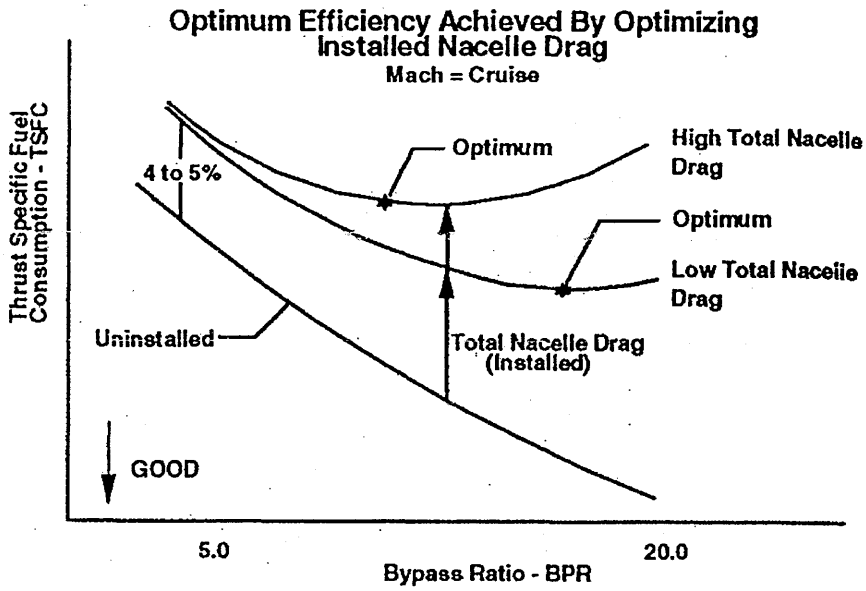

Figure 2.25 Optimizing installed engine efficiency (Ref. 2.6)

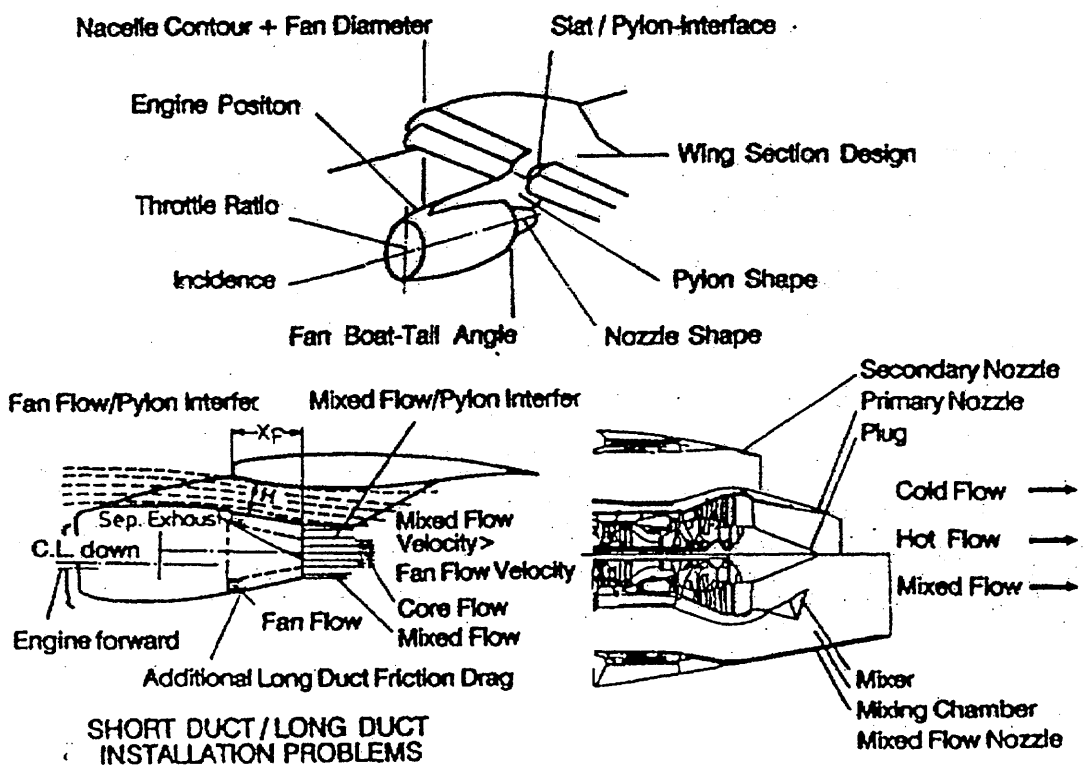

Figure 2.26 Parameters influencing wing-engine interference (Ref. 2.31)

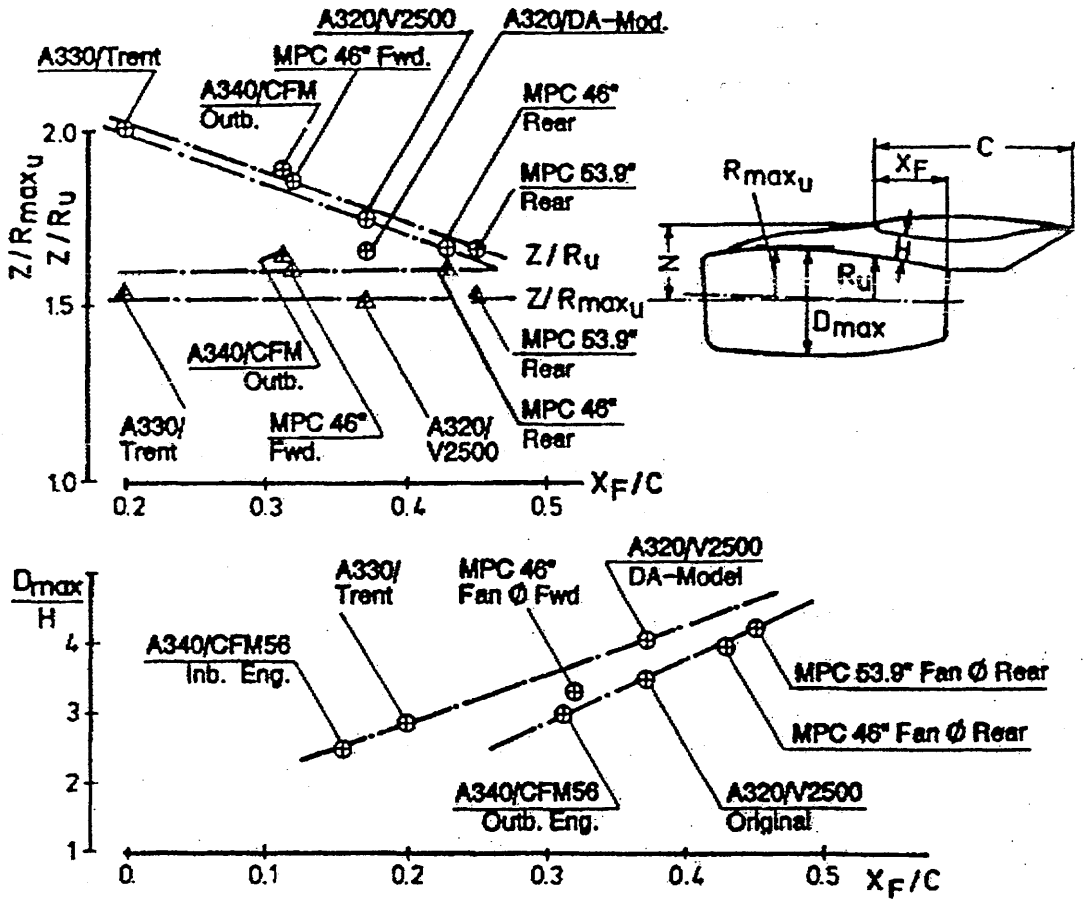

Figure 2.27 Long cowl positions for Airbus family (Ref. 2.6)

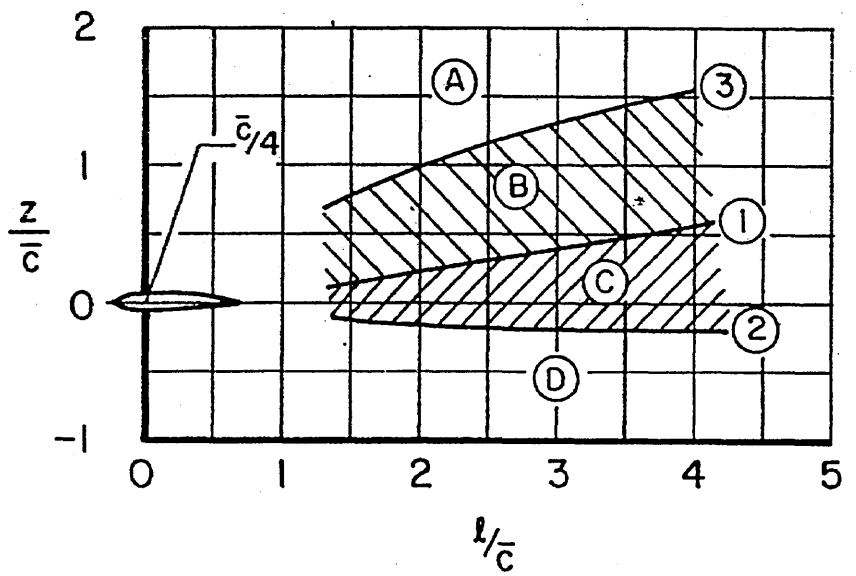

Figure 2.28 Effect of horizontal tail location on pitch-up (Ref. 2.18)

Payload-range concept

trio regional airliner

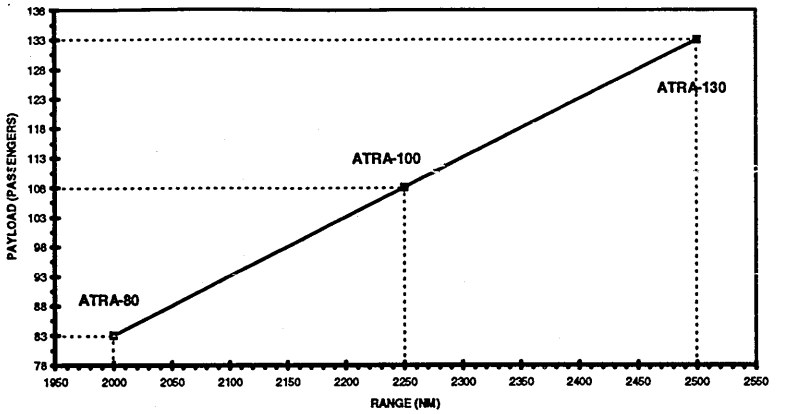

System concept

adapted systems

Fuselage concept

two fuselage plugs removed/added

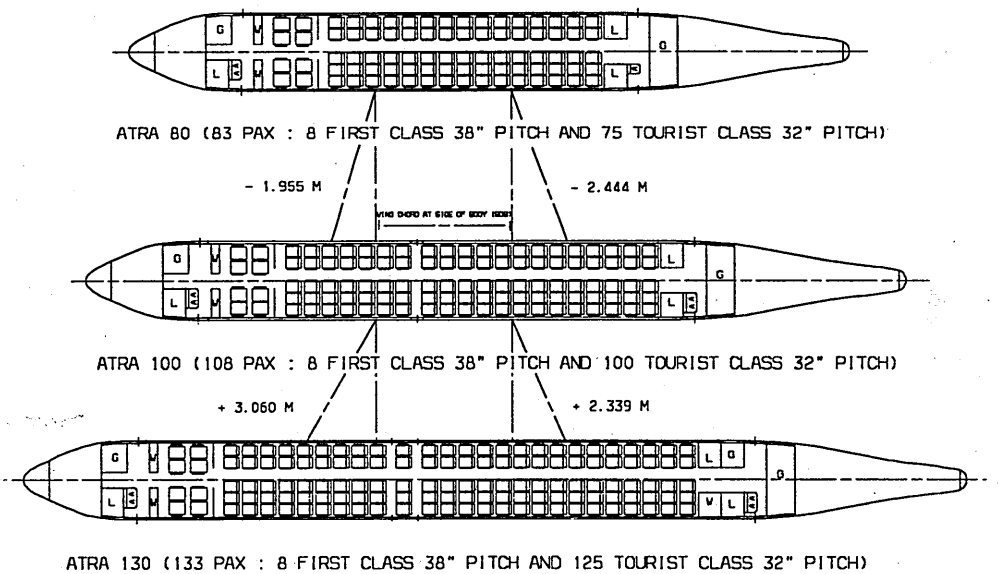

Variable camber wing concept

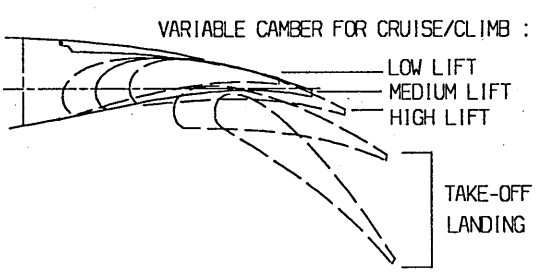

optimum cruise/climb management
constant altitude cruise management

Powerplant concept

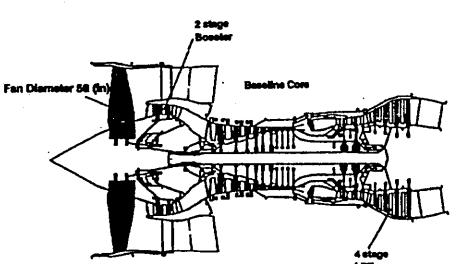

derated/uprated engines

Figure 2.29 The ATRA Family concept

CHAPTER THREE

OVERVIEW OF HYBRID LAMINAR FLOW CONTROL TECHNOLOGY

3.1 INTRODUCTION

This Chapter presents an overview of design activities devoted to advancing the state-of-the-art and reducing the risk associated with the application of Hybrid Laminar Flow Control (HLFC) technology to commercial transports.

HLFC seems to be the most promising drag reduction technique for the next generation of transport aircraft. This new technology will have a large impact on many of the current standards of the industry.

Drag reduction in the form of HLFC applied to future, advanced commercial transports across the speed regime offers breakthrough opportunities in terms of reductions in take-off gross weight (TOGW), operating empty weight (OEW), block fuel for a given mission, and significant improvements in cruise lift to drag ratio (L/D).

3.2 HYBRID LAMINAR FLOW CONTROL (HLFC)

Laminar flow flight research in the 1950's and 1960's demonstrated that manufacturing techniques needed to obtain the stringent surface smoothness and waviness criteria required for laminar flow aircraft presented a major challenge. Today, it is recoqnized that conventional production aircraft wing surfaces can be built to meet these design constraints (Reference 3.1).

Three concepts have been pursued for obtaining significant percentages of laminar flow on the wings of subsonic transport aircraft. Laminarization through wing shaping (Natural Laminar Flow, NLF) is attractive for small-to-moderate size subsonic transport wings having relatively low sweep. However, for larger, higher-speed subsonic transports with higher sweep, laminar flow on the wing can only be achieved by the use of suction. Early LFC (Laminar Flow Control) studies for large aircraft had suction covering a significant portion of the wing chord, but this approach had some major drawbacks in that it required integration of the suction system with the load-carrying surfaces of the wing (Reference 3.2).

Boundaries for laminarization for Boeing and Airbus transport aircraft wings are shown in Figure 3.1 (Reference 3.3) and Figure 3.2 (References 3.4 and 3.6) respectively, which is a diagram of Reynolds number versus a quarter chord/leading-edge sweep angle. Iso-transition location lines are computed assuming infinite swept wing conditions, taking both cross-flow and Tollmien-Schlichting instabilities into account.

The most significant advance made in the development of the laminar flow technology is the concept of Hybrid Laminar Flow Control (HLFC), an idea which integrates the concepts of NLF and LFC. It avoids the undesirable characteristics of

both, see Figure 3.3 (References 3.1 and 3.3). NLF is sweep limited and full-chord LFC is very complex. The key features of HLFC are (a) conventional spar box construction techniques are utilized, (b) boundary-layer suction is required only in the leading edge, (c) natural laminar flow is obtained over the wing box through appropriate tailoring of the geometry, and (d) the HLFC wing design has good performance in the turbulent mode. Typical aircraft drag reductions of around 10% - 11% are expected for this approach (Reference 3.2 and 3.3).

The Leading Edge Flight Test (LEFT) on the NASA Jetstar aircraft addressed HLFC leading-edge system integration and reliability questions and set the stage for a commercial transport demonstration of HLFC as shown in Figure 3.4 and 3.5 (Reference 3.5).

NASA initiated a cooperative HLFC flight experiment program with the U.S. Air Force Wright Laboratory and the Boeing Commercial Airplane Group on a Boeing 757 transport aircraft in 1987. During the conduct of the flight test, it was shown that the HLFC concept was extremely effective in delaying boundary-layer transition.

3.2.1 HLFC on Empennage

An extensive programme aimed at the demonstration of laminar flow technology on an aircraft was set up by Airbus Industrie in 1987. This programme started with a theoretical investigation of the possibility of achieving significant laminar flow over Airbus aircraft components. These studies allowed the selection of the A320 fin as a demonstrator. This was suitable due to an easily removable leading edge, the absence of any de-icing system, minimized costs, and most importantly, the possibility of large scale wind-tunnel testing at flight Reynolds numbers. Detailed studies shows that with suction applied ahead of the front spar of the actual fin about 50 % of the wetted surface can be laminarized providing a fin drag reduction of 40 % and an aircraft drag reduction of 1.3 %. These values will be checked during a wind tunnel test on a half scale model in the ONERA S1MA wind tunnel at the flight Reynolds and Mach number (see Figure 3.6). This test planned in 1992 will be the first industrial wind tunnel test for laminar flow application in Europe and will provide vital inputs for the application of laminar flow technology to new aircraft. After this test the progamme will be oriented towards the preparation and the carrying out of flight test in 1994. This programme will allow Airbus Industrie to make a major step towards the application of laminar flow technology on commercial aircraft (Reference 3.7).

3.2.2 HLFC on Engine Nacelle

The friction drag associated with modern, turbofan nacelles may be as large as 4 to 5 % of the total aircraft drag for a typical commercial transport aircraft, and NASA and Industry studies indicate potential specific fuel consumption reductions on the order of 1-1.5 % (Reference 3.8) or 2 % (Reference 3.9) for advanced necelles designed to achieve laminar boundary layer flow.

Building upon the success of the B757 HLFC Flight Experiment, General Electric Aircraft Engines initiated a project in 1991 with Rohr, Industries, Inc., Allied Signal Aerospace, and NASA directed toward the aerodynamic flight demonstration of the HLFC concept applied to the external surface of large, turbofan engine nacelles. A production GEAE CF6-50C2 engine nacelle installed in the number two (on the starboard wing) position of a Airbus A300/B2 commercial transport aircraft was modified to incorporate two HLFC panels, one inboard, and one outboard (see Figure 3.7). The HLFC concept was extremely effective over the range of cruise altitudes and Mach numbers tested, resulting in laminar flow to 43 % of the nacelle length (the design objective) independent of altitude. Without suction, significant laminar flow was achieved; however, the extent of laminar flow decreased as altitude decreased (unit Reynolds number increased) for the case of no suction (Reference 3.8).

The laminar nacelle studies carried out by Rolls-Royce, Snecma, Hispano-Suiza, ONERA and DLR for the European programmes ELFIN (European Laminar Flow Investigation) II and LARA (Laminar Flow Research Action) have highlighted the potential of HLFC nacelles. The reduction in drag resulting from laminar flow reached 57 % of the drag compared with a fully turbulent nacelle (Reference 3.9).

3.3 THE CRANFIELD LAMINAR FLOW RESEARCH PROGRAM

The College of Aeronautics at Cranfield has an ongoing research program involved with the study of laminar flow. The published work to date, in chronological order, includes :

1. **D. I. A. Poll**. Theoretical and experimental study of the transition behaviour of the boundary layer which is formed along infinite swept attachment line has been made by Poll (see References 6.3, 6.4, 6.11, 6.27, and 6.29-6.31). The attachment line transition criterion used in this work is referred to the above references (see Chapter 6).

2. **R. A. L. Wilson**. A methodology has been developed by Wilson (see References 7.4 and 7.93) to model the direct consequences of laminar flow technology on wing, empennage and nacelle surfaces. In particular natural laminar flow (NLF) and hybrid laminar flow control concepts were considered. The methodology was introduced into an existing numerical design synthesis for commercial transport aircraft. This permitted the impact of laminar flow technology on the optimum aircraft configuration and direct operating costs (DOC) to be assessed. Some benefits and drawbacks associated with laminar technology from the above study were used in this work (see Chapter 9).

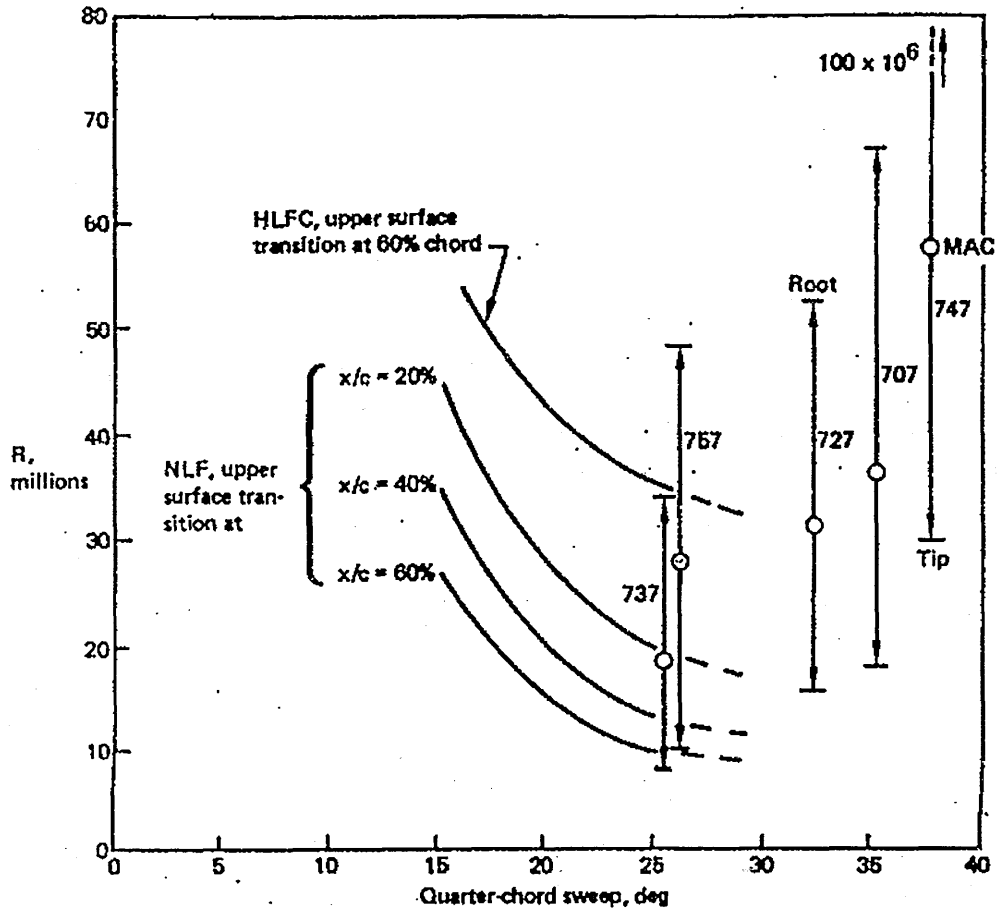

Figure 3.1 Boundaries for laminarization (Boeing aircraft), Ref. 3.3

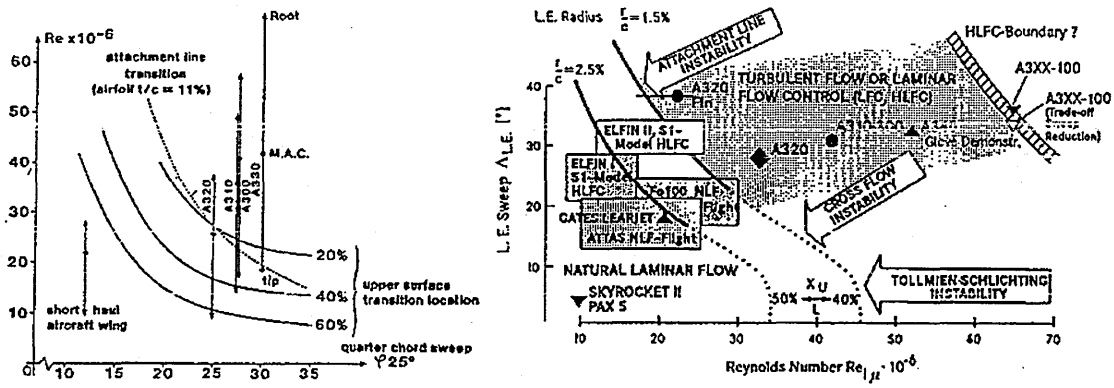

Figure 3.2 Boundaries for laminarization (Airbus aircraft), Ref. 3.4 & 3.6

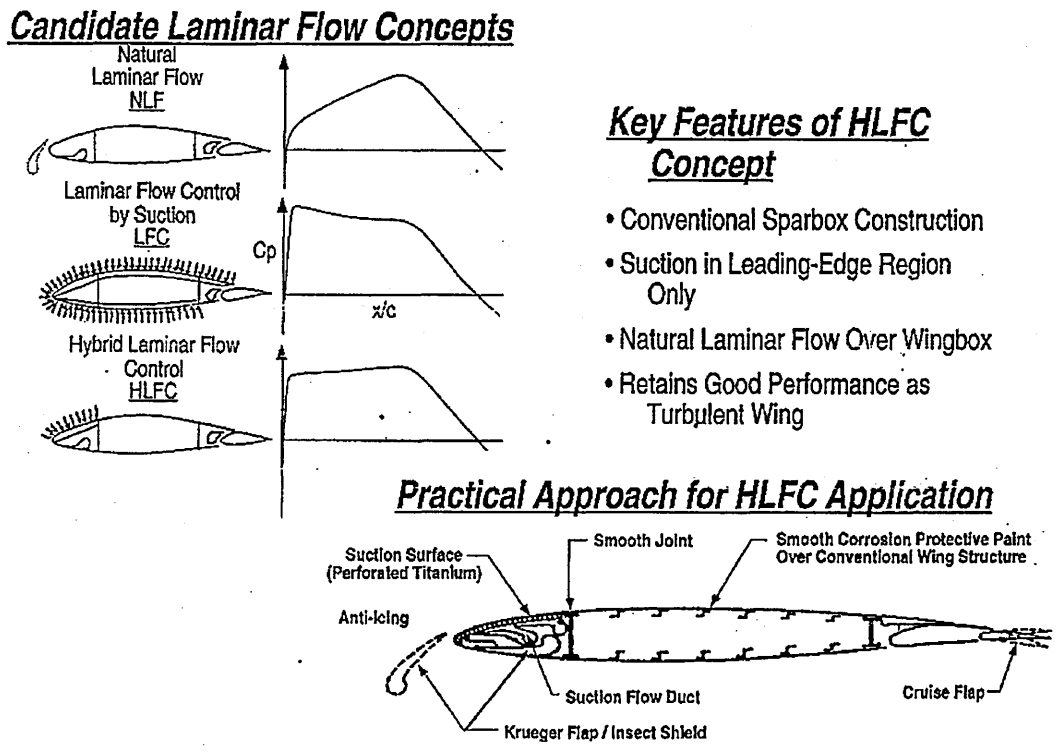

Figure 3.3 Candidate laminar flow and schematic of the HLFC concept (Ref. 1.1)

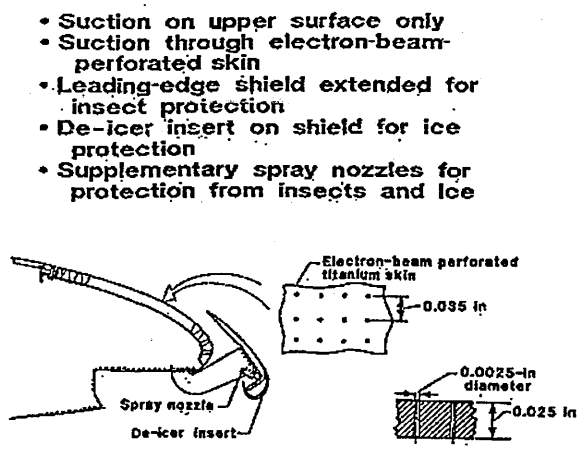

Figure 3.4 Cross section of the perforated test article by Douglas (Ref. 3.5)

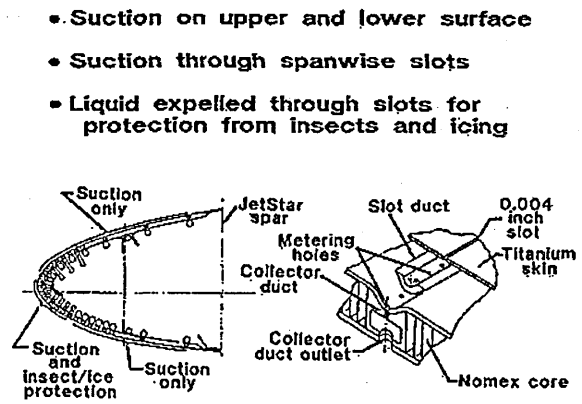

Figure 3.5 Cross section of the slotted test article by Lockheed (Ref. 3.5)

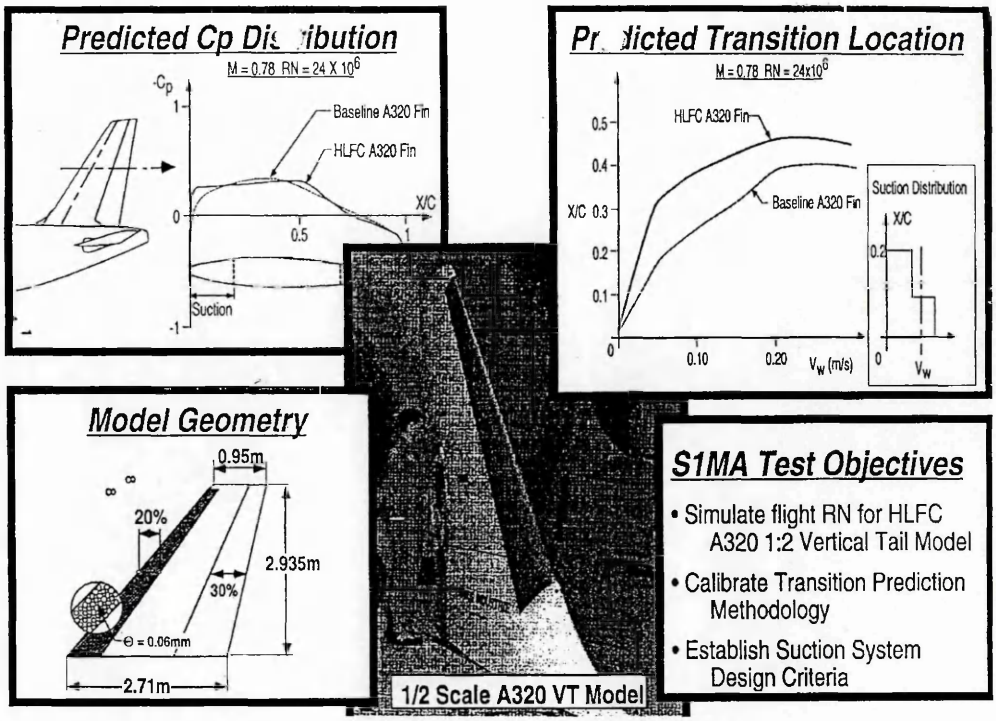

Figure 3.6 A320 HLFC vertical fin analysis and test in ONERA S1MA Ref. 3.7

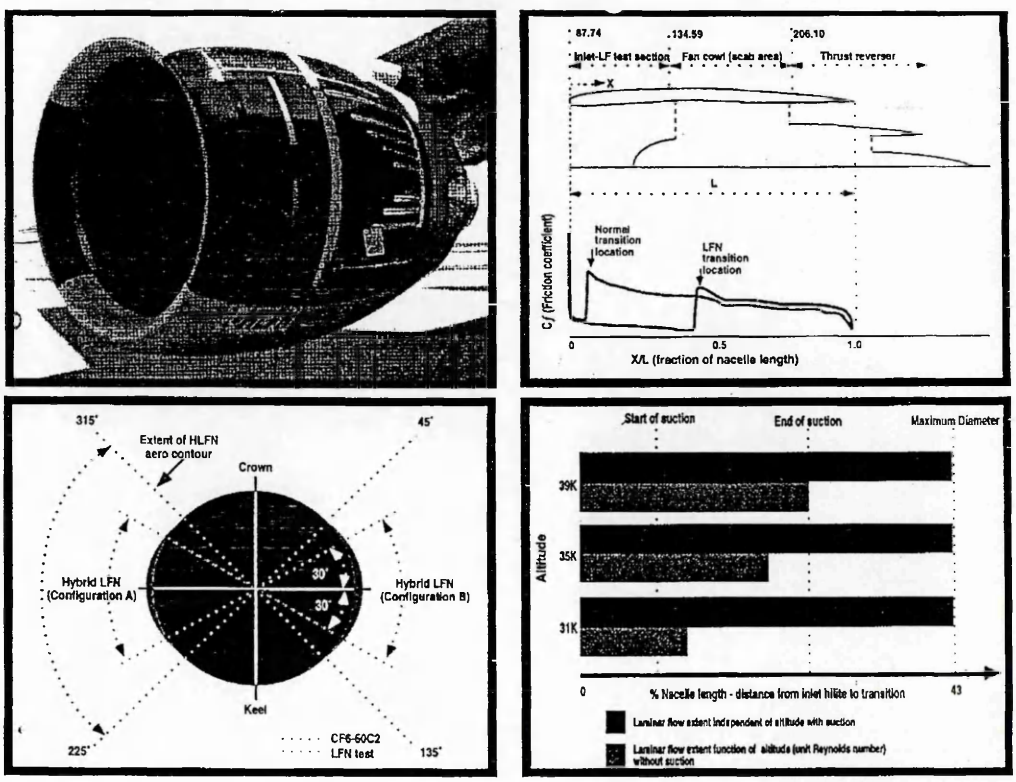

Figure 3.7 General Electric hybrid laminar flow nacelle program Ref. 3.8.

CHAPTER FOUR

OVERVIEW OF VARIABLE CAMBER WING TECHNOLOGY

4.1 INTRODUCTION.

A deliberate product srategy is usually aimed at creating a transport aircraft family on the basis of a common wing by stretching the fuselage. Due to this policy of high fleet commonality the costs for development, manufacture and maintenance can be reduced. On the other hand the wing designer has to choose an appropriate wing area for the maximum stretched version and try to find the best trade-off between design and off-design conditions.

A high subsonic wing however shows optimum performance at high loadings which are not achieved at entry into service with such a conventional fixed geometry wing. Variable camber (VC) is offering an opportunity to achieve considerable improvements in operational flexibility, buffet boundaries and performance which allow a reduction in optimum wing size (Reference 4.1).

Significant drag reductions and increases of the buffet boundary were found from research work. This work led to the current concept where the leading edge camber devices, trailing edge flaps and ailerons are used to modify the wing camber in cruise according to the lift demand.

Variable camber will contribute an average reduction of 3 to 6% in fuel burn and enable the use of one wing for a family transport aircraft (Reference 4.1). The introduction of VC will launch a new generation of intelligent airliners which will optimise their camber schedule throughout the entire mission.

However, the main issue in transport aircraft application of new technologies is the ability to employ them at low cost.

2.2. THE VARIABLE CAMBER WING CONCEPTS

From the beginning of aeronautics aircrafts used wing camber and twist variation to alter lift characteristics and achieve lateral control. Most aircraft today mechanically change their low-camber, high cruise speed wings into high camber, low-speed wings for take-off, landing, and other operations. To date, the methods used are characterized by leading-edge and trailing-edge slat and flap systems that, in general, move in large increments with associated undesirable steps and gaps in both the high-camber and low-camber positions. The result is an airfoil that is never quite optimum for every flight condition and an axcrescence drag that is appreciable under all conditions.

A remarkable job of engineering has provided today's highly efficient civil transports with high ranges of speed and flight conditions. However, the spiraling cost of fuel requires renewed efforts to absolutely minimize the fuel consumed by these civil

transports. In the area of camber-changing devices, structural and mechanical technology has advanced to where practical systems may be possible for changing the shape of an airfoil continuously and smoothly such that it is more nearly optimum for all flight conditions. In the following section are an examples of this technology.

2.2.1 Leading-Edge Variable-Camber Krueger Flap

The 747 leading-edge variable-camber Krueger flap system (see Figure 4.1), wherein the camber of the flap changes from a flat surface when stowed to a curved airfoil when the flap is extended (Reference 4.2).

2.2.2 Airbus Variable Camber.

In order to ease development and certification costs a camber variation in transport aircraft by using the traditional high lift devices was proposed and investigated under the sponsorship of the German Ministry of Research and Technology (Reference 4.1)

A scheme of the system solution is given in Figure 4.2. The camber variation is achieved by a small fowler motion, where the wheels of the flap carriage are guided by two individual tracks in such a way that the flap body slides underneath the spoiler trailing edge. The control track and the flap upper surface have to be shaped such that camber variation is performed with minor discontinuities in surface curvature.

From the most deflected camber position the flap proceeds on its normal track into the high lift positions. No mechanical additives besides the second track nor additional drives related to VC are needed. The basic positive effects of a trailing edge camber flap on the aerodynamic forces of a transonic wing are :

A significant drag reduction with increasing camber at higher lifts is combined with increased lift capability,

The shift in buffet boundary is a powerfull tool to increase operational flexibility and in consequence to design smaller wing areas for a given mission,

A futher drag benefit at lower lifts by means of a camber reduction.

A negative effect, an increase in pitching moment (nose down), is recognised it is interesting to note, however, that the trim drag penalty is one order of magnitude less than the gain in total drag.

Two different research programmes on camber modifications of existing wings were investigated. They were directed towards a payload increase of the Airbus A300 and A310. One camber modification has successfully been applied to the Airbus A300-600 resulting in 10% more payload and 15% more range (Reference 4.1).

2.2.3 Boeing Variable Camber.

Variable camber concepts available from Boeing earlier studies, were examined for conformance to the design objectives established for Boeing study and listed below (Reference 4.2) :

- smooth, continuous airfoil surfaces for lower cruise drag
- a mechanism capable of deflections adequate to meet approach high-lift requirements.
- lightweight structure and mechanisms
- adequate fuel volume in wing box
- high reliablity and low maintenance

Leading edge concept.

An extremely efficient mechanism, an A-frame lying horizontally (Figure 4.3), was developed as the basic linkage for the leading edge variable concept. The upper leg is attached near the spar, and the lower leg is driven up and down with a rotary actuator arm located near the front spar. The upper and lower skins and the leading edge radius are attached to the mechanism by spanwise stringers and short links. As the leading edges moves down, the upper surface becomes longer, forward and aft, while the lower surface becomes shorter. The overall length of the skin surface forward of the front spar remains the same without breaks or overlaps. The upper and lower surfaces are fiberglass, but the leading edge radius is stainless steel or titanium for flexibility and erosion resistance. The lower surface contains a removable panel for inspection and maintenace, and a clearance hole is located in the mechanism supports for a hot-air anti-icing duct.

Trailing edge concept.

The trailing edge concept, shown in Figure 4.4, uses a basic mechanism of a four bar linkage driven by a rotary actuator. The upper and lower fiberglass skins are attached to the four-bar linkages with spanwise stringers and short links. The trailing edge wedge segment beyond the mechanism is honeycomb, and the upper surface is continuous. The lower surface has overlapping sealed surfaces to allow articulation of the mechanism. The lower panels are removable for inspection and maintenance.

The above variable concept was found to have insufficient lift capability to meet the approach speed requirement unless the wing area is increased. Consequently, to avoid increasing the wing area, a second trailing edge variable camber concept was studied with double slotted, trailing edge flaps to obtain higher approach C_L levels.

To attain the potential high-speed aerodynamic benefits of variable camber, the trailing edge must have variable camber with the double-slotted flaps retracted. To achieve variable camber capability, the main flap (and nested aft flap) rotates about a pivot attached to the flap extension mechanism. The spoiler then follows both upward and downward deflections to provide a smooth upper surface.

Drive mechanisms

Two sets of mechanisms drive each flap segment with spanwise shafts connecting both mechanisms. All pivot points are self-aligning teflon-lined bearings to provide maintenace-free, lifetime durability and a close tolerance fit.

During normal high-speed operation, the flaps are nested, and the spoiler is locked down by its actuation mechanism. The airfoil camber then is varied with an electromechanical actuator (section A-A, Figure 4.5) inside the main flap. Rotating the flap up forcibly deflects the spoiler (the base of the spoiler is held rigid by a spoiler mechanism), giving smoothly contoured airfoil with decreasing camber. The spoiler and main flap mountings are designed so the maximum airfoil camber position is fixed rest position with no pressure between the main flap and spoiler. Shown here with double-slotted flaps, this concept is also applicable to single-slotted or triple-slotted flaps.

2.2.4 General Dynamics Mission Adaptive Wing (MAW).

A "mission adaptive wing" is defined as a wing having the ability to actively modify airfoil camber, spanwise camber distribution, and wing sweep in flight, while maintaining a smooth and continuous airfoil surface. This ability produces a near-optimum wing configuration for the entire flight spectrum as well as providing control function performance (Reference 4.3).

Features of a MAW include :

1. Variable camber : L/D optimization (decamber supercritical airfoil for efficient supersonic flight)
2. Roll control : integral aileron action
3. Manoeuvre load control (MLC) : spanwise control of the aerodynamic center for wing root moment reduction at high load factors.
4. Direct lift mode (DLM) : increase lift without increased angle of attack.
5. Gust load alleviation (GLA) : quick response camber variation to avoid gust impulse loads.

The flight envelope of Figure 4.6 illustrates several of these MAW features.

Benefits

Aerodynamic benefits afforded by the supercritical airfoil mission adaptive wing include improveed drag polar shapes and increased $C_{L_{MAX}}$ resulting in significant performance gains (139% F-111 high-altitude supersonic mission radius increase is predicted at constant penetration distance). However, a particular benefit of great impact to the hardware design is the effect of Manoeuvre load control (MLC). The ability to shift the aerodynamic center inboard during pull-up Manoeuvres results in an increased load factor capabilty approaching 1 g while maintaining a constant maximum wing root moment. The MAW accomplishes this by automatically decreasing airload at the tip (decamber) and simultaneously increasing airload inboard (increased camber).

Many other improvements are availeble from the MAW features :

1. Terrain following and weapon delivery : vertical maneuvering can be accomplished without change of pitch attitude by direct lift mode.
2. Radar cross section : smooth, continuous contours are desirable for reducing radar cross section.
3. Parasite drag improvement : the presence of slots, gaps, fixed geometry shapes, and misallignment of components generates aerodynamic drag. Maintenance of a smooth continuous contour increases overall aerodynamic efficiency.

The variable camber leading edge concept

The variable camber leading edge concept is shown in Figure 4.7. The leading edge system incorporates seven linkages per wing half span and is driven by one linear actuator per side. Each control linkage consits of a main drive bellcrank driven by actuator push roads and connected to two control links. One of the control links is connected to and controls the forward bay of the linkage, and the other control link is connected to and controls the aft bay of the linkage. The two bay linkage system supports a rigid aluminium nose cap and upper and lower flexible skins. The fiberglass skins are designed to permit smooth contour deflection of leading edge from the supersinic cruise position to the fully deflected high lift position. No sliding joints or gaps exist on the leading edge nose or upper surface. A faired sliding joint exist on the lower surface at the front spar in a region of positives pressures and minimum velocities. All movable joints and wear surfaces are designed to have permanent lube type surfaces. With this system, the completed leading edge assembly is capable of a production fighter airplane without requiring routine lubrication or maintenance.

The variable camber trailing edge concept

The variable camber trailing edge concept is shown in Figure 4.8. Seven mechanisms per wing halfspan are required for the MAW wing. Each mechanism may be driven by its own integrated servo actuator utilizing tandem hidraulic motors and a planetary gear reduction. All 14 actuators (full span) are independently controlled by the flight control computer. Each mechanism is a three-bay variable geometry truss. Each of the three truss bays consists of triangular-shaped upper and lower truss members joined at the centroid of the truss by means of a triple-thread acme screw and nut combined with a slide arrangement. The forward ends of the forward truss bay upper and lower chord members are pivoted off of the rear spar and interconnected to the others bays at pivots adjacent to the skins. Acme screws in each bay of the truss are connected in series. The forward end of the drivelines are connected to the actuators. Screw and nut lead varies in each bay of the truss to produce the desired deflected airfoil camber.

The upper and lower skins are continuous (root to tip) glass-reinforced plastic with no sliding joints on the upper or lower contour. A slip joint is provided at the trailing edge. The skins are supported on spanwise-oriented beams. The ends of the skin support beams are supported at each mechanism control station by means of a slide block and ball joint arrangement. This skin support system allows the skins to pick up only normal air load and local bending (transferring that air load to the spanwise support

beams). All movable joints and wear surfaces in the trailing edge mechanism are designed to have permanent lube-type surfaces.

2.2.5 Cranfield Variable Camber.

Spillman (Reference 4.4) pioneered a novel method of camber variation by means of rotation and translation of leading edge (LE) and trailing edge (TE) elements. The top surface was kept smooth and continuous to generate a family of cambered airfoil sections. Aerodynamic investigations suggest that the predicted airfoil performance improvements can best be achieved if the upper surface curvature is kept smooth and continuous (Reference 4.5).

A supercritical aerofoil of 14% thickness to chord ratio (t/c.max) was designed with generous section thickness between 50% and 70% chord and significant TE thickness. This was perceived to assist in accommodating the camber actuation equipment.

The details of the change in section profile are depicted in Figure 4.9. The position of maximum curvature on the upper surface lies at 64.5% chord and so was chosen as the junction between the centre body and the TE element. The origin of this curvature was selected as the centre of rotation and the camber angle, δ, was pescribed as the angle of rotation of the TE element in a circular arc about this origin. A flexible upper surface plate joins the centre body and TE element to permit extension yet maintain curvature. The lower surface was a simpler system in which a rigid closing plate is hinged from the centre body at 60% chord and held by spring loads to the TE element. This geometry maintains a smooth top surface when deployed.

The purpose of LE deployment is to control the LE suction pressure peak caused by variations in circulation due to camber changes. Deployment of the LE element on a circular arc presented insurmountable design problems. These are overcome (see Figure 4.9) by simple drooping the LE element without extension, similar to the RAEVAM system.

The practical size of the upper surface skin restrics the range of deflection to either 0° to +10° or -3.5° to +7°. The position of the wing rear spar for the former range is 64.5% while for the later it is placed at 54%. The negative deflection was required for the flap to contribute to the roll control and wing root bending moment control.

Spanwise variation in camber is possible by dividing the control devices (LE and TE) into several segments similar to high lift devices of conventional wings. Figure 4.10 illustrates the planform arrangement of a typical transport aircraft wing, with the TE split in to six segments. The three inboard segments are deployed through positive angles only, while the three outboard segments have both positive and negative deflections.

The research program of the above variable camber scheme has continued to date under the auspices of Prof. J. P. Fielding (see also References 7.75, 7.24, 7.26 and 7.25).

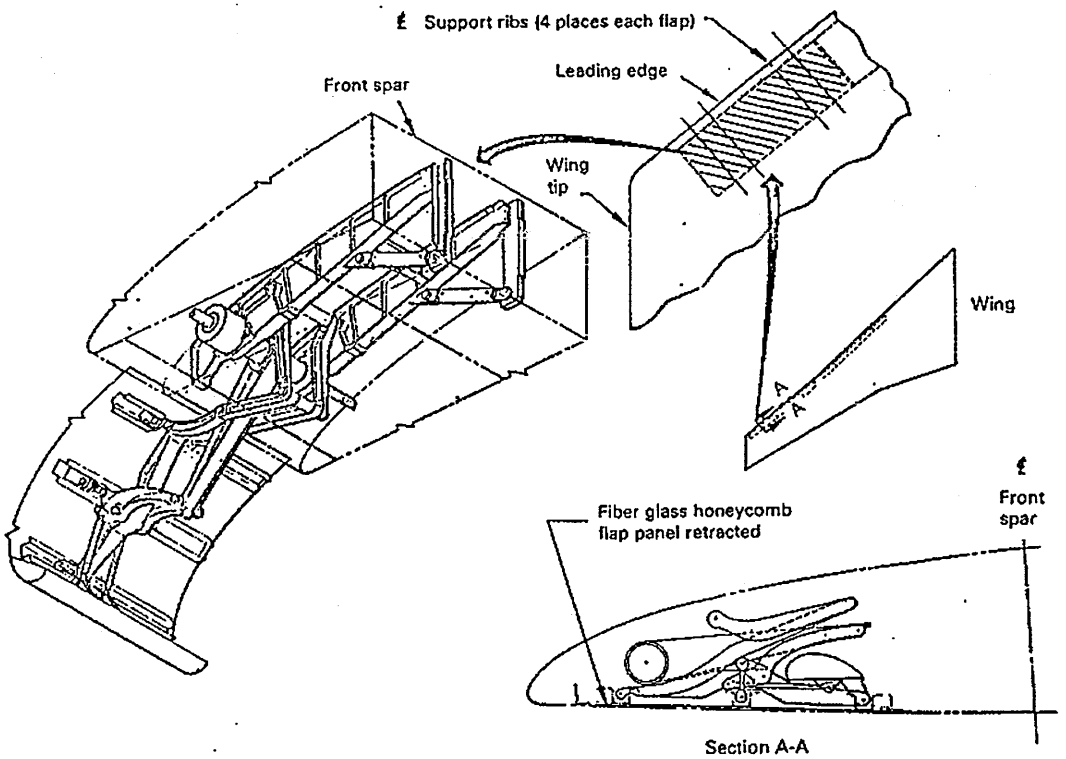

Figure 4.1. Variable camber Kruger flap - B747 (Ref. 4.2).

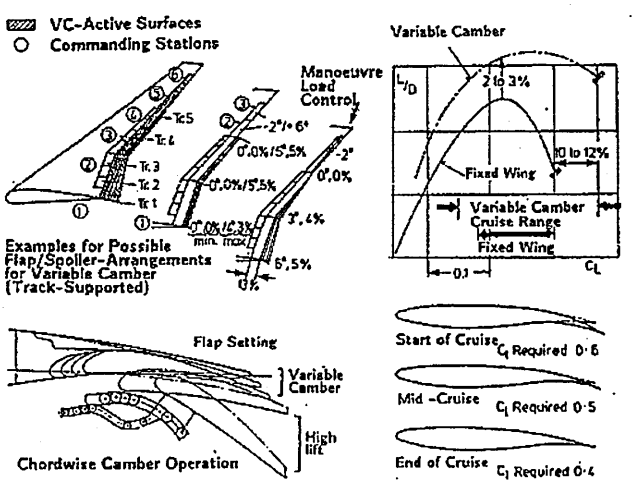

Figure 4.2. Principle of variable camber operation (Airbus), Ref. 4.1.

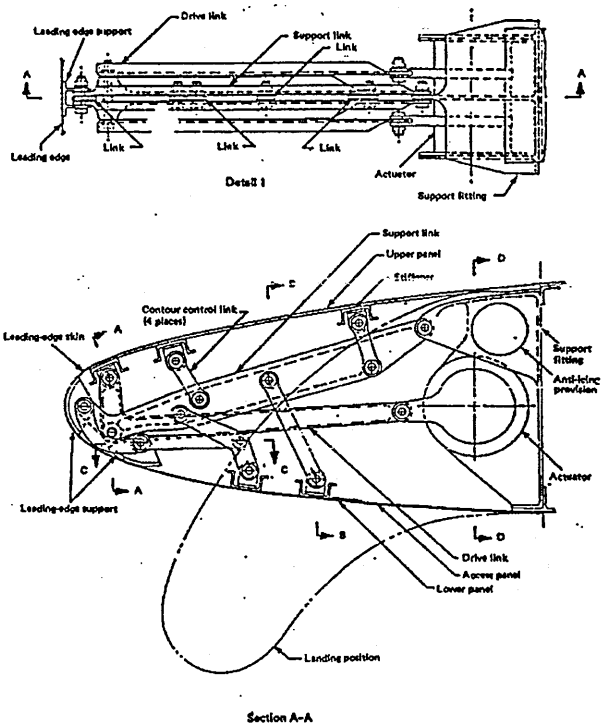

Figure 4.3 Variable camber leading edge concept (Boeing), Ref. 4.2.

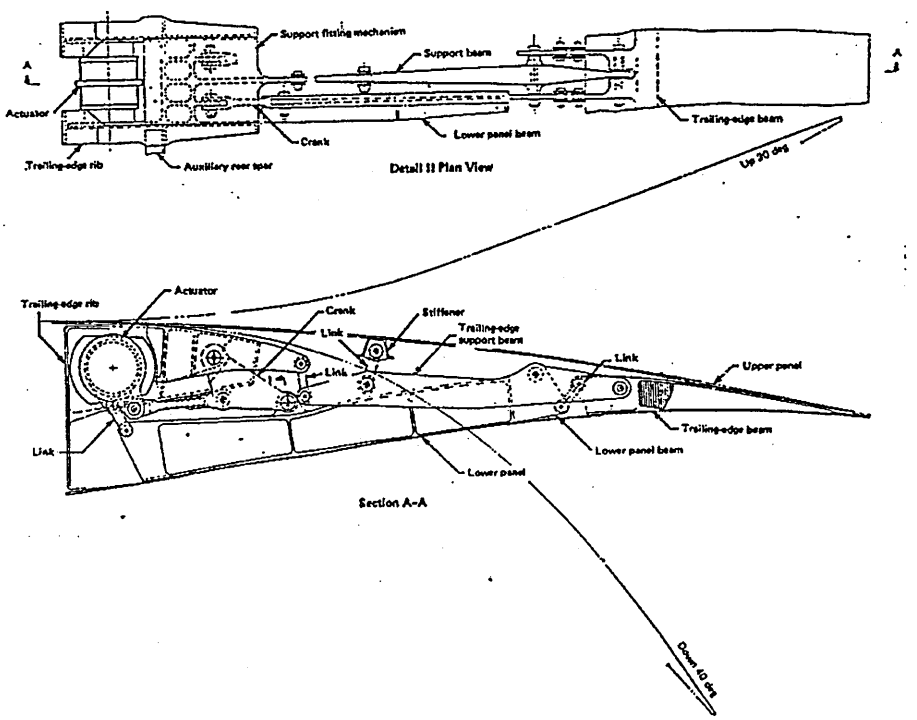

Figure 4.4 Variable camber trailing edge concept (Boeing), Ref. 4.2.

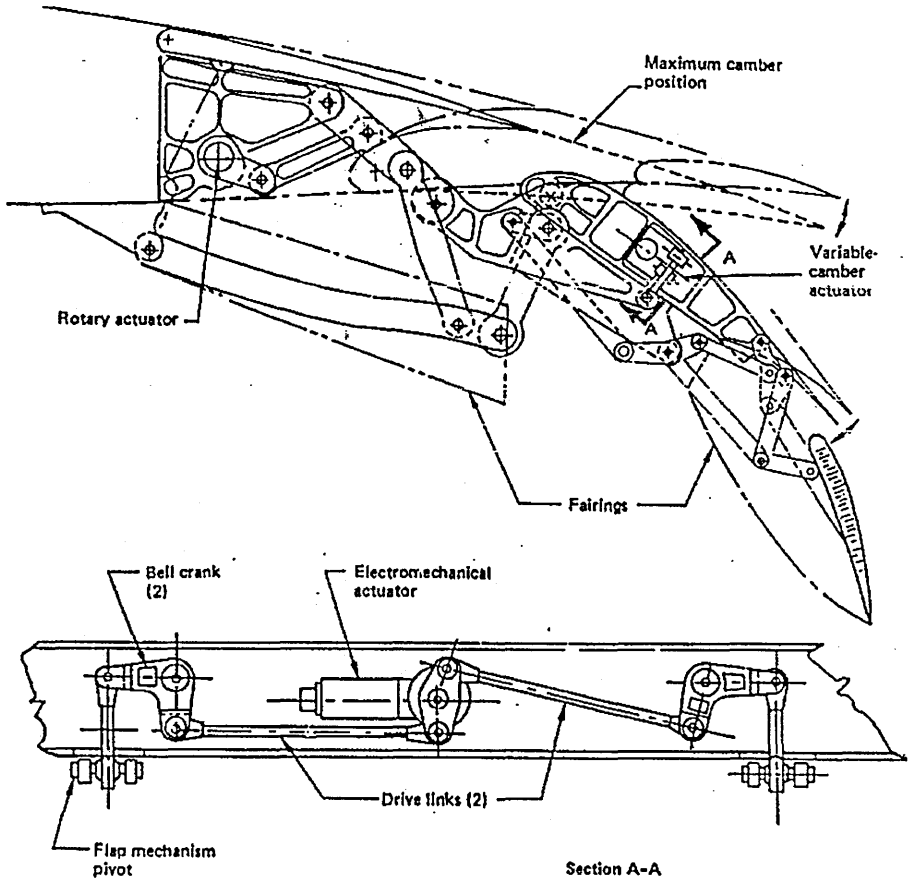

Figure 4.5 Double slotted variable camber flap (Boeing), Ref. 4.2.

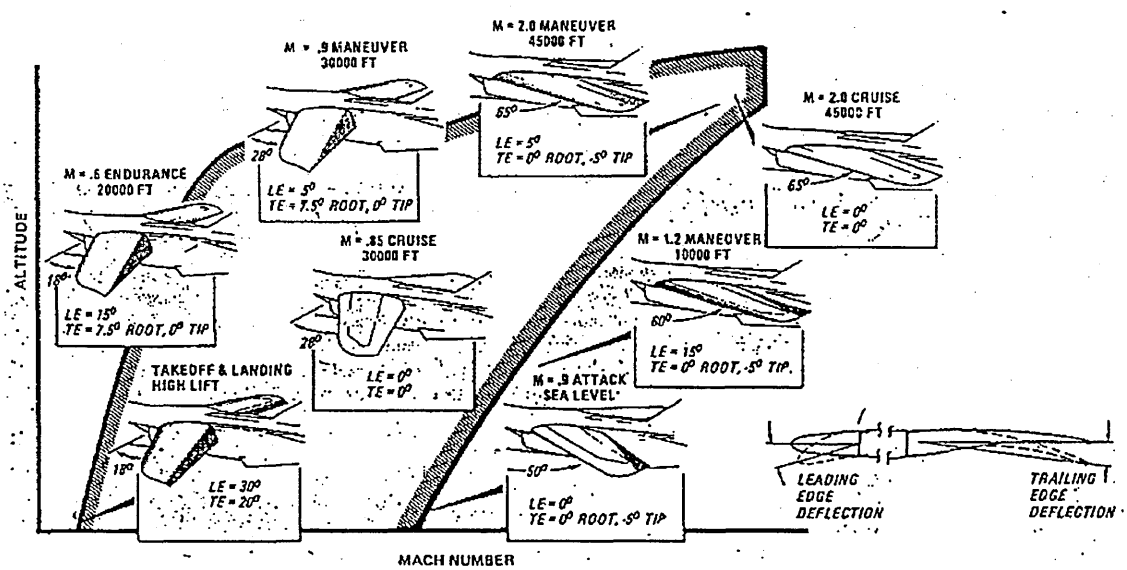

Figure 4.6 Mission adaptive wing improves full envelope performance (Ref. 4.3).

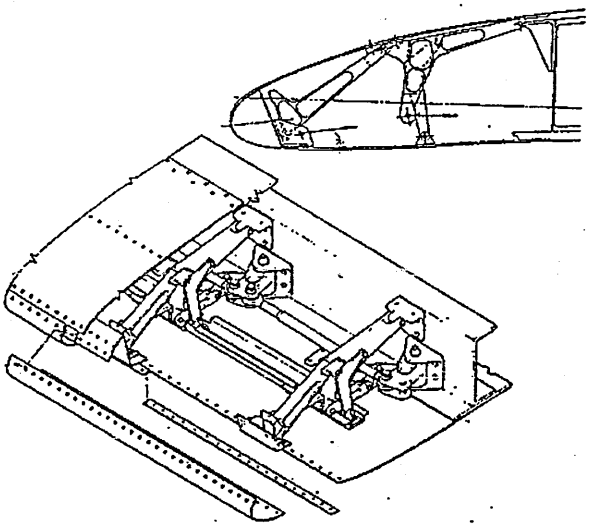

Figure 4.7 Leading edge mechanisms concept (MAW), Ref. 4.3.

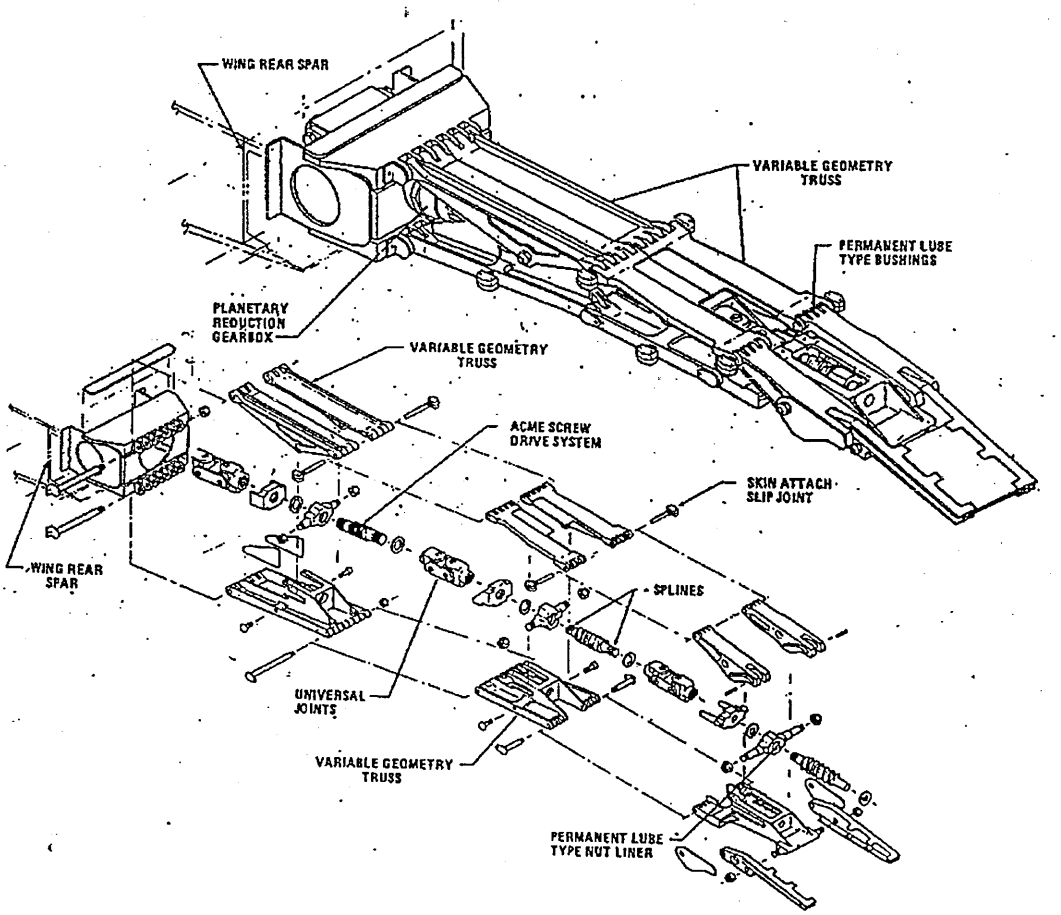

Figure 4.8 Trailing edge mechanisms concept (MAW), Ref. 4.3.

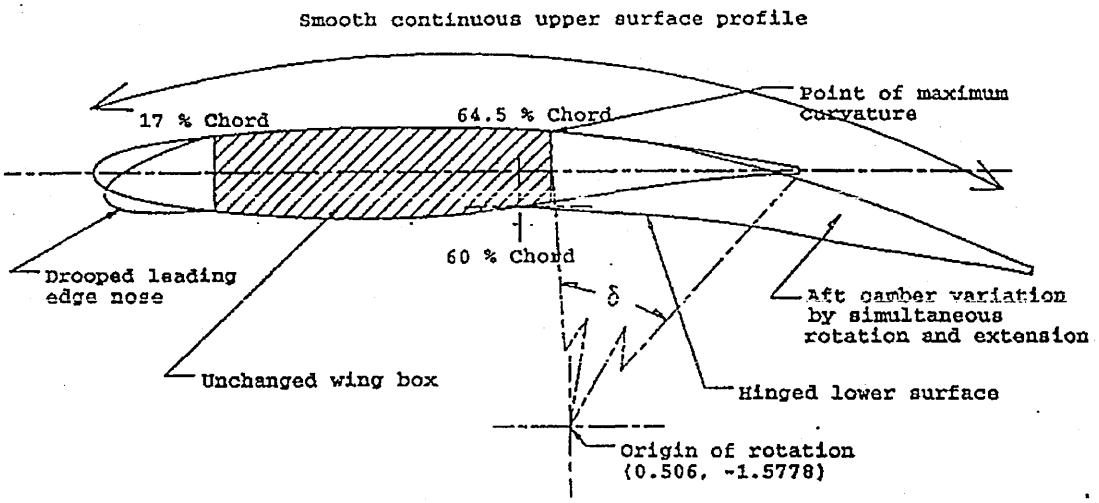

Figure 4.9 Aerofoil section indicating proposed camber variation scheme (Ref. 4.5).

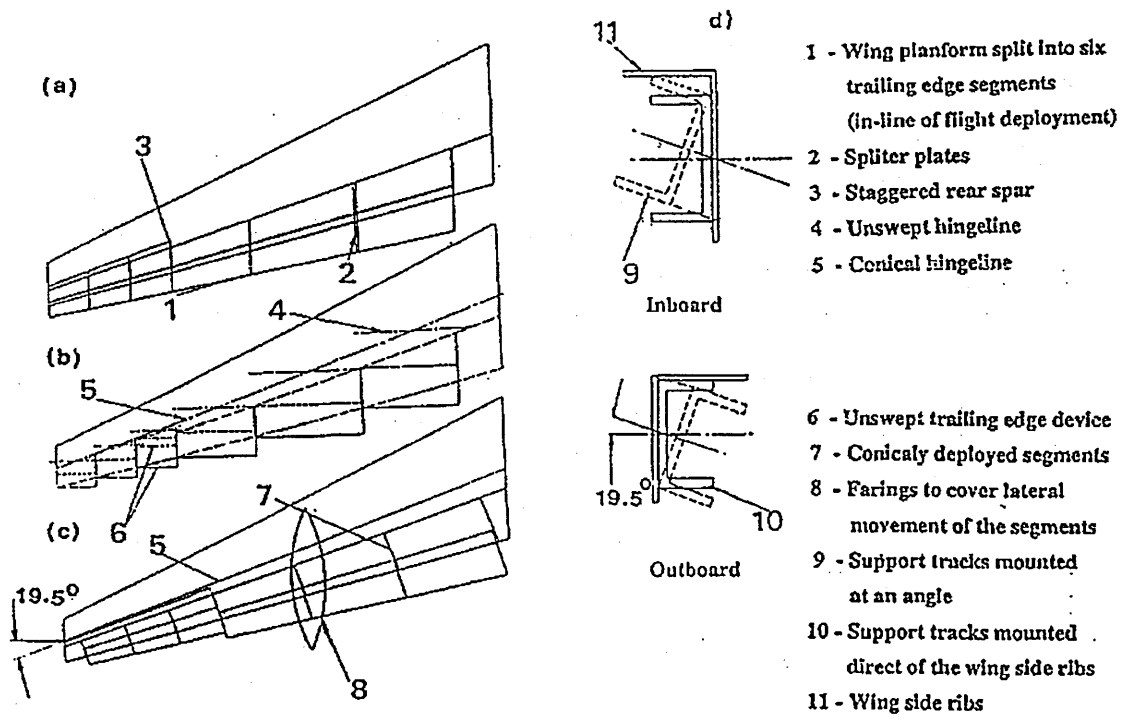

Figure 4.10 Three dimensional geometric implication of spanwise camber variation on a typical transport aircraft wing (Ref. 4.5)

CHAPTER FIVE

COMBINED LAMINAR FLOW-VARIABLE CAMBER CONFIGURATION

5.1 INTRODUCTION

The main issue in the application of new technologies in transport aircraft is the ability to employ them at low cost without reduction of their benefits. This cost is reflected in the following shares of Direct Operating Costs (DOC) : fuel, ownership and maintenance. Laminar flow-variable camber technology will only produce acceptable DOC if the penalties due to additional weight and the complexity of the system do not exceed those of the fuel savings. Hence the most important objective in realizing advanced laminar flow-variable camber technology is to reduce their additional system costs, weight and minimise maintainability and reliability costs.

The concept of combined laminar flow-variable camber sections is examined in the following sections.

5.2 LAMINAR FLOW - VARIABLE CAMBER WING TECHNIQUES FOR FLOW CONTROL ON WINGS

Practical use of HLFC requires that laminar flow be maintained through a range of cruise lift coefficients and Mach numbers. Variations in lift coefficient and Mach number will change the wing pressure distributions from the optimum and may result in some loss of laminar flow. Therefore, it was decided to investigate a HLFC wing together VC-flap. Deflection of the VC-flap permits controlling the pressure distribution over the forward part of the airfoil, keeping it similar to the design pressure distribution, even when the lift coefficient and Mach number differ considerably from the design values (Reference 5.1). With careful design of VC-flap, it can be used to reduce the wave drag penalty, and to sustain attached flow in turbulent mode (Reference 5.2), and also see Section 7.3.2.3. Flow control on such a wing, is shown schematically in Figure 5.1.

5.3 CANDIDATE LAMINAR FLOW - VARIABLE CAMBER SECTION CONFIGURATIONS

Section views of the two wing configurations considered in this study are shown in figure 5.2. Configuration I has both upper and lower surface suction, from the front spar forward with leading edge systems as proposed by Lockheed (see Figure 3.5). Because it has no leading-edge device, it requires double-slotted fowler flaps to achieve $C_{L_{max}}$ requirements. Configuration II replaces the lower surface suction with full-span Krueger flaps, which, combined with single-slotted fowler flaps, provide equivalent high lift capability, see Section 7.3.2.2. The Krueger flaps also shield the fixed leading edge from insect accumulation and provide a mounting for the anti icing system. Only the upper surface, however, has suction panels. The leading edge system used on

configuration II is similar to leading edge systems as proposed by Douglas (see Figure 3.4). A summary of the advantages, risks, and disadvantages are :

- Configuration I : the advantages are (1) a simple system with no leading edge device and (2) upper and lower surface laminar flow for least drag. The disadvantages and risks are (1) more potential for insect contamination on the suction device (see Figure 7.55) which may cause boundary-layer transition, (2) high approach speeds and landing field lengths and/or a more complex trailing-edge high lift system, (3) longer take-off field lengths, particularly for hot, high-altitude conditions, and (4) a trim penalty due to higher rear loading (when the flaps are deployed).
- Configuration II : the advantages are (1) less potential insect contamination on the suction device (see Figure 7.55), hence laminar boundary layer will be more stable, (2) simpler trailing-edge high lift devices, (3) lower approach speeds and shorter take-off and landing field lengths, and (4) less a trim penalty (when the flaps are deployed). The disadvantages and risks are (1) less drag reduction due to laminar flow only on the upper surface and (2) a more complex leading-edge system.

Preliminary estimates (Reference 5.1) indicated cruise drag reductions of about 11% for HLFC having laminar flow on the upper and lower surface, while the reduction for HLFC having laminar flow only on the upper surface was only 7%. The deficiencies noted for configuration I are related to low speed performance and insect contamination problems. The potential exists for high lift performance improvements if wings were specifically designed for the HLFC task. Although it has an inherently lower drag reduction, configuration II is more likely to provide a stable laminar boundary-layer due to a lower likelihood of being contaminated by insects. Taking into account the above considerations, configuration II was selected, for this study.

5.4 HYBRID LAMINAR FLOW - VARIABLE CAMBER SECTION BASELINE CONFIGURATION

The HLFC-VC section baseline configuration for use on the ATRA-100's wing is shown in Figure 5.3. For more detail about the leading edge system design for the configuration, see Section 7.9. While the variable camber concept is described in the following paragraphs, see also Section 7.8.

Ideally the change in section profile aft of the rear spar should not cause separation of airflow, which would otherwise give rise to higher profile drag (Reference 5.3; see also section 7.3.2). To overcome the problem of separation, the radii of local curvature must be greater than half the chord (Reference 5.4), but not too high, as the section will have a higher pitching moment, and hence higher trim drag, which then will reduce the benefit of variable camber it self. The radii should be optimized between these two constraints. The radius is inherent to the trailing-edge upper surface of the aerofoil, so when the aerofoil is used for a VC concept, the aerofoil should be designed with taking into account the above considerations from the beginning (see also Figure 7.10 of this thesis).

The concept of variable camber used for the ATRA-100's wing is quite similar to traditional high lift devices. The camber variation is achieved by small rotation motions (in two directions for positive and negative deflections). In VC-operation the flap body slides between the spoiler trailing edge and the deflector door.

The radius of flap rotation is picked-up from the radius of curvature of the aerofoil trailing edge upper surface at about 90% chord. Camber variation is therefore performed with continuity in surface curvature at all camber settings. During this process the spoiler position is unchanged.

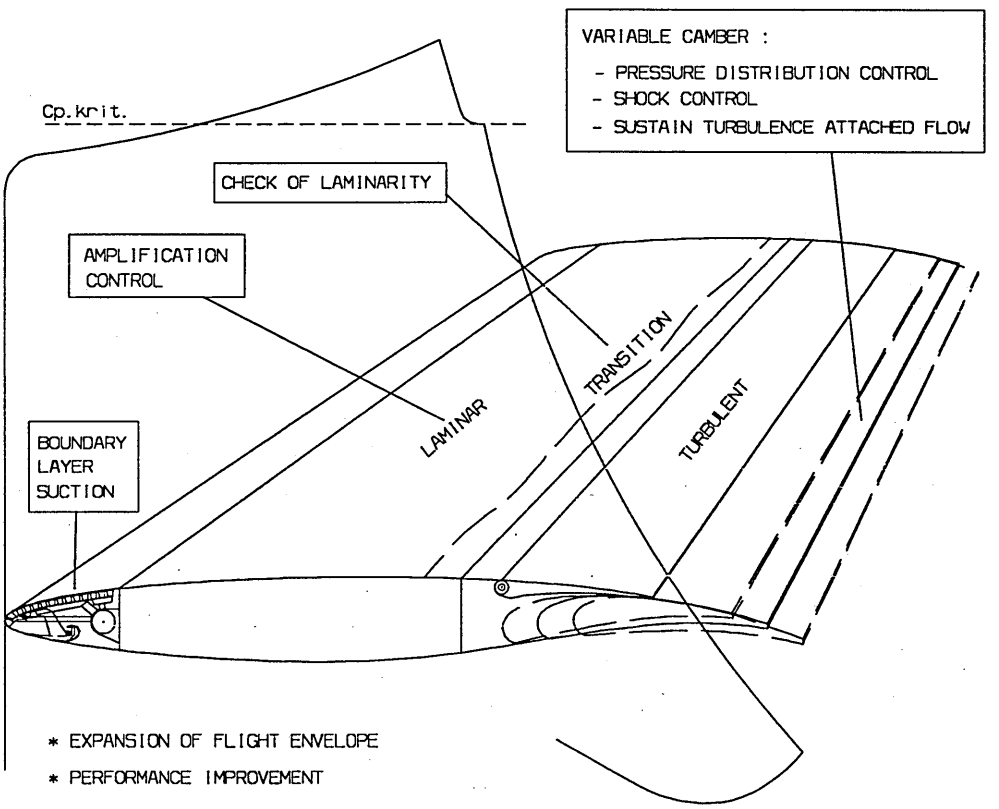

Figure 5.1 Flow control on the wing

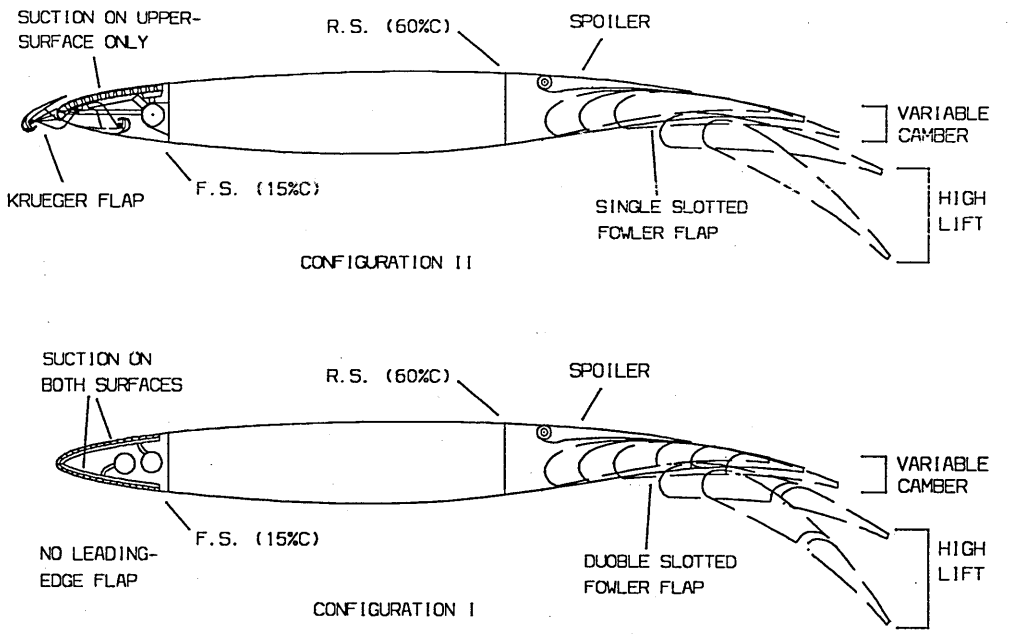

Figure 5.2 Cross sections of candidate combine HLFC-VCW configurations

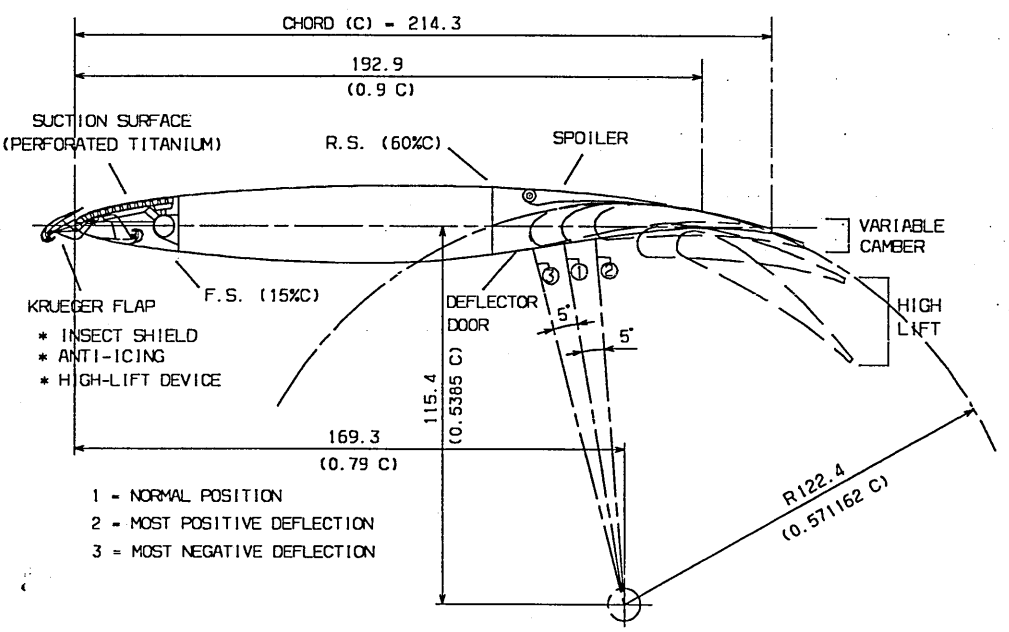

Figure 5.3 HLFC-VC section baseline configuration

CHAPTER SIX

OVERVIEW OF LAMINAR FLOW WING ANALYTICAL STUDIES

6.1 INTRODUCTION

The process of transition from laminar to turbulent flow remains one of the most important unsolved problems in fluid mechanics and aerodynamics. Transition of boundary layers from laminar to turbulent flow is a consequence of the non-linear response of that very complicated oscillator, the laminar boundary layer, due to forcing disturbances. These disturbances are part of the environment in which the laminar flow develops. Transitional flows are characterized by increased skin friction and heat transfer, and the accurate determination of heating rates and drag critically depends on the ability to predict the onset and extent of transition. However, no mathematical model exists that can accurately predict the location of transition under a wide range of conditions. Design engineers resort to methods that are based on empirical correlations, linear stability theory, non-linear parabolized stability equations (PSE) and a two-equation model similar to that employed in turbulent calculations.

This chapter describes the analytical study of transition from laminar to turbulent boundary layers on swept wings, and provides an assessment of the suitability of methods for predicting accurately the instability characteristics of a complicated three-dimensional boundary layer flow. See also Chapter 3.

6.2 TRANSITION FROM LAMINAR TO TURBULENT BOUNDARY LAYERS ON SWEPT WINGS

Studies of economical operations of transport aircraft show that a high value of cruise speed times lift/drag ratio is necessary, see also section 7.2.3 of this thesis. As the lift/drag ratio of transport aircraft is nearly independent of the cruise speed, (as long as no undesirable transonic effects occur), the highest velocity possible is the basis for a good economic operation. This leads to swept wing planforms for transonic transport aircraft.

Due to the sweep angle, the boundary layer on swept wings becomes highly three-dimensional, and additional effects can cause boundary layer transition. Figure 6.1 gives an overview of the flowfield in the boundary layer of a swept wing (Reference 6.1). In the simple case of an infinite swept wing, the incoming flow can be split up into a spanwise component and a normal component. The flow component in the spanwise direction remains constant over the wing, forming an attachment line at the leading edge with a finite velocity. The streamlines of potential flow over the wing are highly curved in the planform plane at the leading edge region as a result of pressure gradients acting transversely to the local flow direction. Due to the presence of a boundary layer with zero velocity at the wing surface, the curvature of the wall streamlines is different from that of the potential flow, as indicated in Figure 6.1 by the full and dotted lines. This behaviour leads to skewed velocity profiles in the

boundary layer, where the flow direction changes as distance to the wall increases, from the direction of the wall streamline to the direction of the potential flow streamline. Splitting up these velocity profiles, in the direction of outer flow and perpendicular to it, yields the two velocity profiles given in Figures 6.1c and 6.1d. The first profile, in the direction of the outer flow, is very similar to that of a two dimensional boundary layer, whereas the second one shows a different shape. This so called crossflow distribution is characterized by a maximum near the surface, decreasing to zero velocity at the surface and at the outer edge of the boundary layer, including always a point of inflection.

These complicated flow patterns in the boundary layer, especially in the leading edge region, considerably influence the transition of the laminar boundary layer on swept wings. There are four basic transition mechanisms on a swept wing (References 6.1 - 6.3). These are : viscous or Tollmien-Schlichting Instability (T.S.I.), inflectional or Cross Flow Instability (C.F.I.), Taylor-Goertler Instability (T.G.I.), and leading-edge Attachment Line Transition (A.L.T.).

T-S instability (as known from the two dimensional case) depends on the action of viscosity to transfer energy from the mean boundary layer flow to the disturbance. Its direction of propagation is close to the local freestream direction. Amplification of T-S disturbances is small in regions of negative pressure gradient and large in regions of positive pressure gradient. (For severe positive gradients such as shocks, transition will occur immediately at any practical Reynolds number).

C-F instability propagates in a direction nearly perpendicular to the local freestream. It is referred to as an inviscid instability because it results from the presence of an inflection point in the C-F velocity profile. C-F in the boundary layer results from the combination of sweep and pressure gradient and is, therefore, most severe in the leading edge and the trailing edge regions where the pressure gradients are the largest.

Taylor-Goertler instability is a centrifugal instability that occurs in viscous flow over concave surfaces. Because the HLFC airfoil which is used in this study does not has concave surfaces in the region designed to have laminar flow, this type of instability was not considered in this analysis.

Leading edge attachment line transition differs fundamentally from the first three transition mechanisms that begin as infinitesimal disturbances that are amplified until they cause transition or are damped out. It arises at the leading edge of sweptback wings, where the local flow is outward along the attachment line rather than across the wing. This flow develops its own boundary layer, which is also susceptible to transition. Leading edge attachment line transition, however, refers to the spanwise spread along the wing leading edge attachment (or stagnation) line of turbulence originating from such sources as leading edge roughness elements or fuselage boundary layer. Under some conditions, turbulence can propagate along the wing attachment line and trigger turbulent flow over the entire wing.

The external streamline pattern for the flow close to a swept attachment line is shown schematically in Figure 6.2 (Reference 6.4). There are two particular features which should be noted. Firstly the attachment line, A-A, has a boundary layer type of flow in the spanwise direction which may be either laminar or turbulent and,

secondly, at stations off the attachment line the curvature of the streamlines generates pressure gradients which produce cross flow within the boundary layer. This cross flow introduces at least one point of inflection into the three-dimensional velocity profile and, consequently, instability to small disturbances is expected to occur at relatively low Reynolds numbers.

As shown in Figure 6.1 the boundary-layer profile in the direction of the outer flow is very similar to that of a two dimensional boundary layer and, therefore, Tollmien-Schlichting waves (Reference 6.5) can occur which lead, through a complicated process, to transition into a turbulent boundary layer. The main parameters which influence the occurrence of unstable oscillations are pressure distribution and Reynolds number (Reference 6.1).

Early experiments on swept wings (References 6.6 - 6.8) showed a premature transition near the leading edge on smooth swept wings, and detailed investigations indicated that the instability of the crossflow velocity profiles caused boundary layer transition. As these velocity profiles always have an inflection point, one can show from stability analysis considerations that the instability of such types of profiles is larger than usual (Reference 6.9). The main parameters which influence the crossflow instability are sweep angle, Reynolds number, and pressure distribution.

Within the boundary layer of the attachment line flow, spanwise turbulent contamination can occur (References 6.10 and 6.11), induced by an inherent instability of the boundary layer or by leading edge roughness. This behaviour results in a fully turbulent boundary layer over the whole wing surface. Moreover, at high sweep, the disturbances coming from the fuselage boundary layer can propagate along the attachment line and cause transition (Reference 6.12). Attachment line transition is dependent on sweep angle, Reynolds number, and acceleration of the flow in the attachment line region. Criteria for avoiding this kind of transition have been reported (Reference 6.10 and 6.11). Crossflow instability and attachment line transition are highly important, and special attention has to be paid to these phenomena when designing laminar airfoils for swept wings (Reference 6.1).

As a result of the above considerations, for a laminar wing the gradients must be optimized taking into account T.S.I. and C.F.I. and the natural laminar flow concept can only be applied to the following configurations :

- Low sweep and moderate Reynolds number;
- High sweep and small Reynolds number.

For high sweep and high Reynolds numbers encountered on a large transport aircraft, it is necessary to maintain laminar flow by suction of the boundary layer over the entire wing surface (Laminar Flow Control, LFC) or near the leading edge only (Hybrid Laminar Flow Control, HLFC), see section 5.2 of this thesis.

6.3 ANALYSIS METHODS FOR TRANSONIC WINGS

The design of a laminar flow system for the wing of a transonic aircraft requires the ability to compute accurately the instability characteristics of a

complicated three-dimensional boundary layer flow described above. The methods can be classified in increasing order of complexity as (References 6.1 and 6.12) :

- Empirical criteria;
- Database methods;
- Mathematical modelling.

For low Reynolds numbers (Re ~ $3x10^6$) and zero sweep angles, very efficient empirical relationships have been derived (References 6.24 and 6.25) from a large data base of experiments. For higher Reynolds numbers, only a few experiments exist to prove these criteria. For attachment line transition, empirical relations (References 6.10, 6.11 and 6.27) also seem to work satisfactorily. Empirical relations for determining transition due to crossflow instability have been established (References 6.23 and 6.26).

The experimental database for high Reynolds number swept wings is very small. The above relationships seem to be inadequate to serve as realistic tools in the design of high Reynolds number swept wings (Reference 6.1). It is therefore necessary to use the following analytical methods.

6.3.1 Attachment Line Contamination

For swept wings, the attachment line can be contaminated by the turbulent structures originating from the fuselage. It is very well known that leading-edge transition depends on the attachment line boundary layer momentum thickness Reynolds number ($R_{\theta al}$) and on the magnitude of disturbance present. For a wing section the values of $R_{\theta al}$ are strongly dependent on the initial pressure gradients (geometry) in the leading-edge region.

This gross attachment line contamination is likely to occur when the attachment line Reynolds number (R_{ALT}) exceeds a value of around 245 (Reference 6.27). Where :

$$R_{ALT} = W \times e \times \eta / \upsilon \quad \text{with} \quad \eta = (\upsilon/k)^{0.5} \quad \text{and} \quad k = dUe/dX \qquad (6.1)$$

where : υ = kinematic viscosity
dUe/dX = velocity gradient at boundary layer edge
$R_{ALT} = (1/0.404)\, R_{\theta al}$ (Reference 6.11).

Boeing (Reference 6.2) gave more details about the above figures. For very low disturbance levels, $R_{\theta al}$ can be as large as 200 or higher, but if disturbances are present, $R_{\theta al}$ must be 100 or less to maintain laminar attachment line flow. Figure 6.3 (Reference 6.2) shows how $R_{\theta al}$ is defined and gives an approximate formula based on section geometry that can be used if the normal velocity gradient, dUe/ds, is not known.

Although the attachment line gross contamination problem may be resolved by devices such as a Gaster bump or a fence (see section 7.9.1 of this thesis), the attachment line boundary layer is also susceptible to Tollmien-Schlichting disturbances (Reference 6.28). Poll (Reference 6.27) has shown that these waves first appear when R_{ALT} reaches a value of approximately 580. If R_{ALT} exceeds 580 then the

waves amplify as they travel along the attachment line and ultimately reach some threshold condition beyond which the waves break down to form localised turbulent spots. The greater the value of R_{ALT} the more rapid the amplification of the disturbances and the shorter the distance to breakdown. If the local value of R_{ALT} drops below 580 then the wave will be damped and eventually die out. This critical value of R_{ALT}, $R_{ALT.crit}$, is strongly dependent on surface roughness and reduces rapidly with increasing chord Reynolds number (Reference 6.28), see also section 7.9.3 of this thesis. However, Hall et al (Reference 6.29) have shown that the attachment line $R_{ALT.crit}$ can be increased effectively by suction. This is illustrated by the results shown by Figure 6.4 taken from Reference 6.29.

6.3.2 Crossflow and Tollmien-Schlichting Instability

The methods of predicting boundary layer transition based on linear boundary layer stability theory is presented in References 6.9 and 6.15, where a stability analysis based on temporal stability theory for boundary layers on swept wings has been described. The basic idea is the investigation of the amplification of disturbances in the form of waves within the boundary layer. The governing three dimensional disturbance equations (Reference 6.16) derived from the Navier Stokes equations can be reduced to a single quasi two dimensional disturbance equation in the direction of the disturbance wave front, which in the three dimensional case is normally not in the direction of the local flow. This equation, known as the Orr Sommerfeld equation (Reference 6.5), was derived in Reference 6.16 for the direction normal to the wave front. It can be applied (Reference 6.16) to the three-dimensional stability problem by solving a series of two-dimensional problems with various propagation wave angles. Solutions of this equation are obtained by solving an eigenvalue problem and are described in Reference 6.9 for incompressible, three-dimensional parallel flow.

The amplification ratio A/A_0 can be expressed by an exponential function e^N, where N is the amplification exponent, or N factor. It describes the growth of the oscillations and will be related to the transition condition. The N factor is dependant on the turbulence level and has to be specified (Reference 6.12). This procedure must be carried out for those oscillation frequencies, wave lengths, and wave propagation directions, where the amplification exponent N becomes a maximum across all oscillations.

The e^N method generally requires the following steps (Reference 6.32).

1) Mean flow must be precalculated at a large number of streamwise locations along the body of interest.
2) At each streamwise station, a local linear stability analysis is performed. By assumptions of the linear theory, the unsteady disturbances are decomposed into separate normal modes of different frequency. The stability equations are solved for the spatial amplification rate of each unstable frequency.
3) An amplitude ratio for each frequency is then calculated by integrating the spatial amplification rate in the streamwise direction on the body, i.e.,

$$\ln\left(\frac{A}{A_0}\right) = \int_{x_0}^{x} \alpha_i dx \qquad (6.2)$$

4) The N factor is then determined by taking the maximum of the just calculated quantity at each streamwise location.

The usual way to proceed from these stability analysis results to the transition location is to determine the calculated N factors at the experimental transition locations, thus establishing a limiting N value (Reference 6.1). Various linear stability methods have been calibrated against wind tunnel and flight test data (References 6.1, 6.2, 6. 9, 6.17 - 6.20). Reference 6.21 provides an excellent summary of previous natural laminar flow and laminar flow control studies.

When analyzing the boundary layer of swept wing pressure distributions, it turns out that two principal wave front propagation directions are important. The first one is related to wing regions with weak pressure gradients, where the disturbances are propagating nearly in the direction of the outer flow, corresponding to the two-dimensional type of Tollmien-Schlichting Instability. The second one is related to the wing region with strong pressure gradients near the leading edge, where the disturbances of maximum amplifications are propagating in the crossflow direction, corresponding to the crossflow instability (Reference 6.1) which are due to the inflection point in the crossflow mean velocity profile (Reference 6.28).

The crossflow transition criterion has been derived by Poll (Reference 6.30) based on a correlation of the crossflow Reynolds number (χ) and the boundary layer shape factor (H) for incompressible flow. The results from Reference 6.28 indicate that an increase in leading-edge pressure gradient reduces the crossflow instability (by reduction in the value of χ). Atkin and Poll (Reference 6.31) have correlated an N factor of 14.5 for crossflow transition using Poll's swept cylinder experimental data (It should be noted that Poll's crossflow transition criterion was derived for flows without suction). Further work in this area may lead to the provision of an empirical modification to the correlation for flows with suction, which could be supported by experimental data. For flow with suction, Reference 6.28 recommended an N factor for crossflow transition of about 10 - 12. Figure 6.5 (Reference 6.28) could be used for an indication of the suction quantities required to suppress crossflow for a range of wing section leading-edge geometries and aircraft operating conditions. Figure 6.6 (Reference 6.28) shows the sensitivity of the N factor to suction quantity for various conditions.

For Tollmien-Schlichting Instability induced transition, the criterion due to Granville could be used. Reference 6.28 recommends an N factor for this instability of about 9 for flow with suction. Results from Reference 6.28 indicate that for a steeper leading-edge pressure gradient, transition is more forward (this is probably due to the neutral stability point being further forward for the steeper leading-edge pressure gradient cases). This study also indicates that suction may be more effective for delaying transition at higher Reynolds numbers than at lower Reynolds numbers and it is much more effective to employ moderate suction over longer chordwise extents than to increase suction levels closer to the leading edge. It is also clear from the above study that the simple criterion, while being useful for predicting transition for cases without suction in the unstable T-S region, is unable to predict the correct

trends when suction is present. It would be valuable to derive a modified version of the compressible Granville criterion to take account of suction.

Comparing the various N factors for transition from different publications and experiments does not show a clear picture. From References 6.17 - 6.19, it seems reasonable that T.S.I. transition is likely to occur at $N_{TSI} = 11$ in low turbulence wind tunnels and $N_{TSI} = 18$ in flight experiments. The crossflow N values in wind tunnels reach values of $N_{CFI} = 9 - 11$ (References 6.9 and 6.17) and no real flight data are available. Based on Reference 6.1, $N_{TSI} = 18$ and $N_{CFI} = 12$ have been assumed. Boeing studies (Reference 6.2) recommended transition amplification factors for T.S.I. ranging from 9 to 15 and for C.F.I. ranging from about 6 to 12.

None of the studies assessed the reduction in transition amplification factors that may be caused by the mutual interaction of C.F. and T.S. disturbances. Reference 6.2 recommended transition criterion for combined Tollmien Schlichting and Cross Flow Instability as shown in Figure 6.7.

The major problem with the e^N method is that the N factor does not represent the amplitude of a disturbance in the boundary layer but rather an amplification factor from an unknown amplitude A_0. The amplitude A_0.represents the amplitude of a disturbance of specified frequency at its neutral stability point. Its value is related to the external disturbance environment through some generally unknown receptivity process. As a consequence, the value of N that determines transition onset must be correlated to available experimental data (Reference 6.13). Additionally, the e^N method requires the use of several computational tools such as a boundary-layer or Navier-Stokes flow solver to calculate the mean flow and the linear stability solver to determine the amplification rates (Reference 6.33).

Methods based on the nonlinear parabolized equations (PSE, Reference 6.34) are being use to determine transition onset but they have not received the wide acceptance enjoyed by the e^N method. Methods based on the PSE also require precalculation of the mean flow and specification of initial conditions such as frequency and disturbance eigenfunctions. Methods based on linear stability theory only provide an estimation of the location of transition and can provide no information about the subsequent transitional and turbulent flow (Reference 6.32).

In Reference 6.32, a different approach has been developed, which does not require precalculation of the mean flow or the specification of frequencies. It determines the transition onset and calculates the laminar, transitional, and turbulent regions in a single computation. The approach employs a two-equation model similar to that employed in turbulent calculations. It is based on the premise that, if a flow quantity can be written as the sum of a mean and a fluctuating quantity, then the exact equations that govern the fluctuations and their averages are identical irrespective of the nature of the oscillation, i.e., laminar, transitional, or turbulent. Moreover, if it is possible to model the equations governing the mean energy of the fluctuations and their rate of decay (or other equations) in such a way that one does not appeal to their nature, then the resulting model equations will be formally identical. However, the parameters that appear in the modelled equations will depend on the nature of the fluctuations.

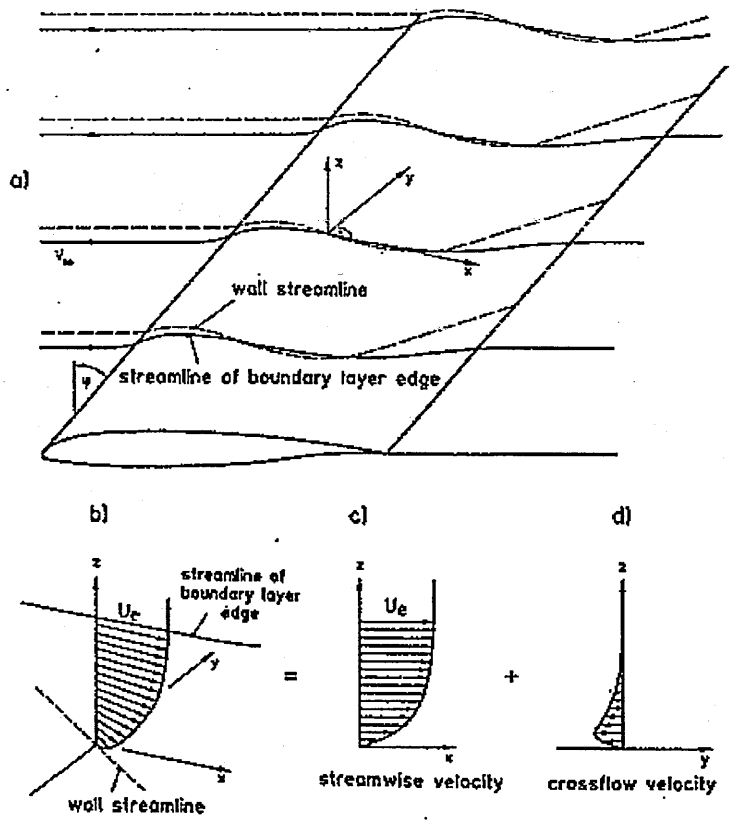

Figure 6.1 Flow pattern and boundary-layer velocity distribution on an infinite swept wing : (a) flow pattern; (b) 3 dimensional velocity profile; (c) streamwise velocity profile; (d) crossflow velocity profile (Reference 6.1)

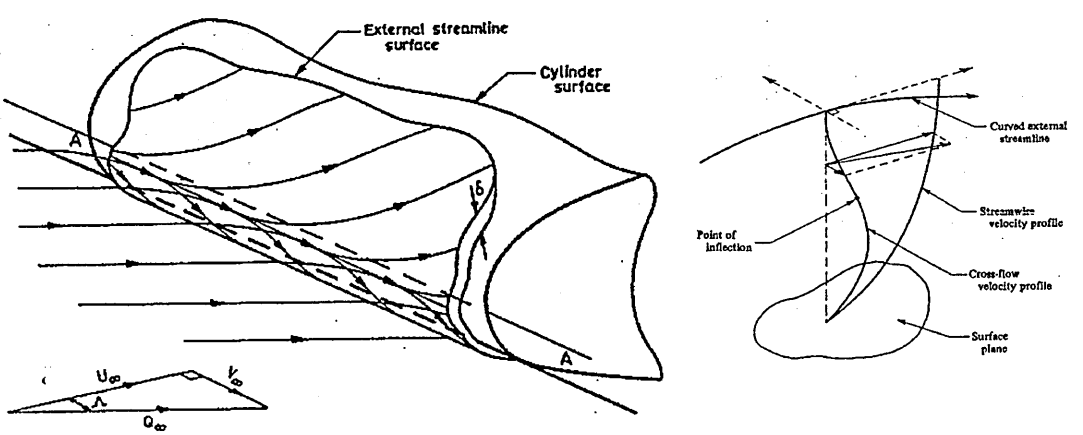

Figure 6.2 Flow near the leading edge of a swept wing (Reference 6.4)

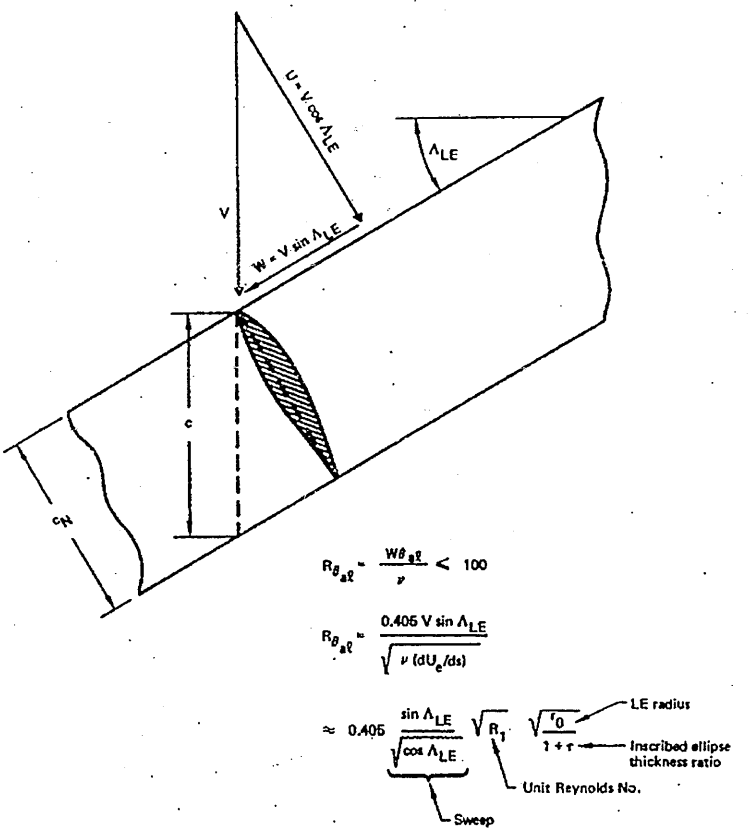

Figure 6.3 Attachment line transition criterion (Reference 6.2)

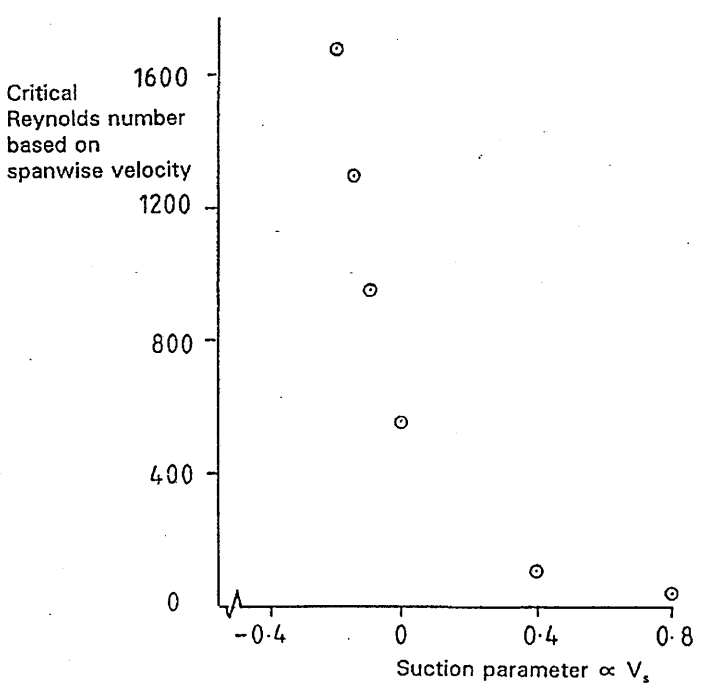

Figure 6.4 Effect of suction on critical attachment line Reynolds number (Ref. 6.28)

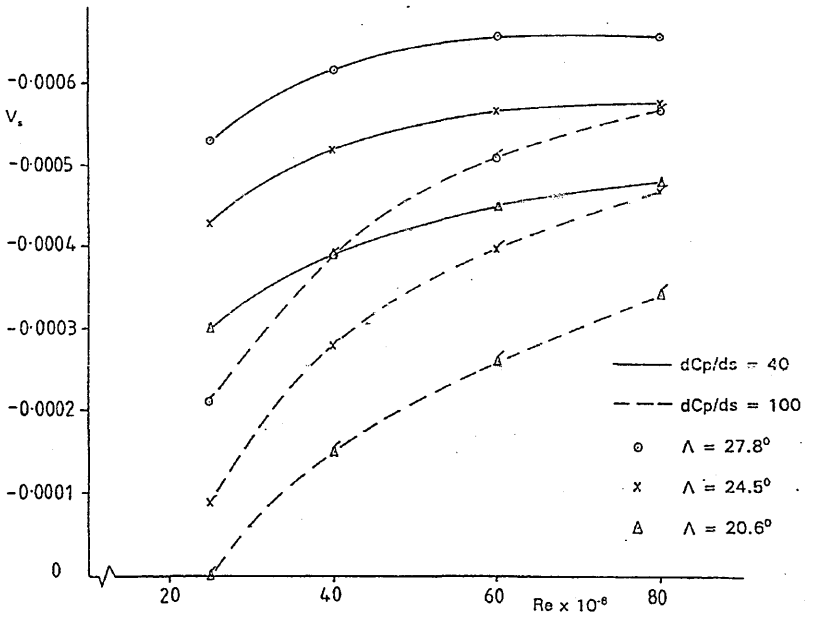

Figure 6.5 Variation of minimum suction quantity (Reference 6.28)

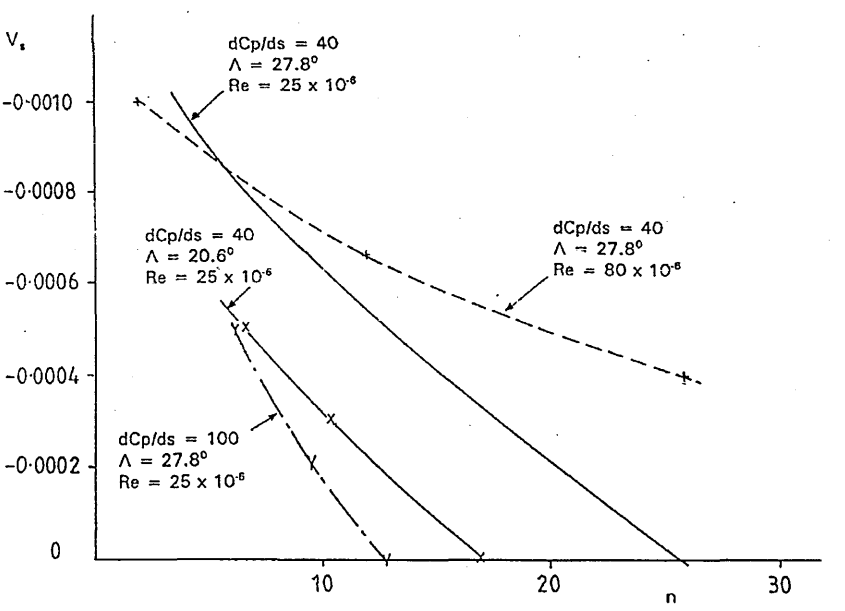

Figure 6.6 Sensitifity of N factor to suction quantity (Reference 6.28)

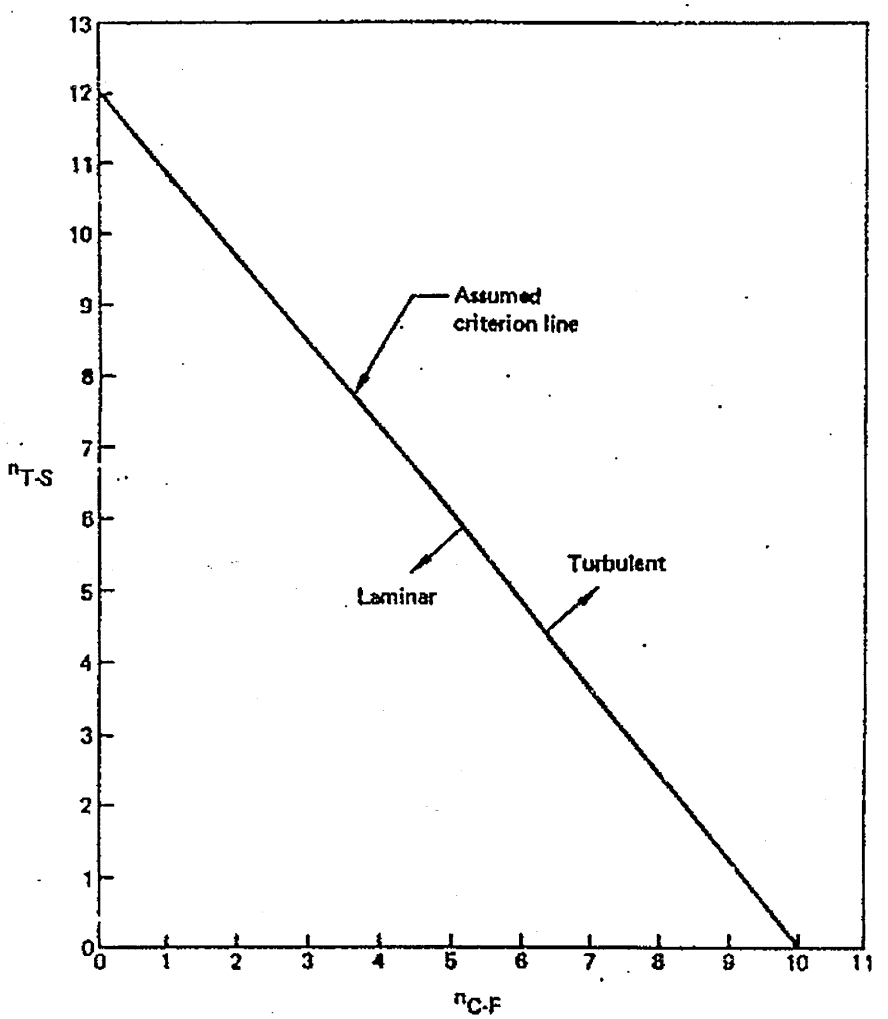

Figure 6.7 Transition criterion for combined Tollmien-Schlichting and Crossflow Instability (Reference 6.2)

CHAPTER SEVEN

ATRA-100 BASELINE : INITIAL WING DESIGN

7.1 INTRODUCTION

Wing design is of key interest to the aerodynamicist because of its dominant influence on aircraft performance. Early jet transport wing designs were based almost entirely on previous military flight experience and considerable wind tunnel testing. Computational aerodynamics is changing the design process so that more highly refined configurations are possible.

This section describes the initial design of wing for ATRA-100 baseline configuration. This wing design is unique, because it incorporates hybrid laminar flow control and variable camber wing technology.

A detailed examination of the very complex wing design is outside the scope of this work, but it is considered appropriate to mention some of the measures which may be taken, although not all of them are required for each design.

7.2 GENERAL REQUIREMENTS

Wing design is a highly integrated process involving not only the aerodynamicists but also all other engineering disciplines, marketing, sales, manufacturing, and design groups. Basic requirements that must be achieved for a successful wing design include (Reference 7.1, 7.2., 7.3, 7.50 and 7.63) :

a) The configuration must satisfy the performance goals in the design specifications while achieving good economic return.

b) Flight characteristics, handling qualities, and aircraft operation must be satisfactory and safe over the entire flight envelope for all aircraft configurations (high speed, low speed, flap settings, gear positions, power settings, ground handling).

c) Design of a structure must be possible within the defined external shape that meets the strength, torsion, fatigue, flutter, weight, life cycle, maintainability, accessibility and engine requirements and the development and manufacturing costs.

d) Sufficient space must be provided for fuel for the design range, for retraction of the main landing gear, and for the aircraft systems (flaps, ailerons, spoilers, fuel, gear, etc.) where appropriate.

Meeting all these requirements simultaneously is difficult and will most likely require compromise for a satisfactory configuration to be achieved.

Performance requirements will typically include the aircraft manufacturer company management's perception of the airline requirements for the design payload, cargo, range and speed. Objectives will vary from specific requirements, such as sea level and high altitude field performance and span limitations, to constraints such as approach speed and initial cruise altitude capability. Compatibility with current flight operations (speed and altitude) must be considered. Design Mach number and lift coefficient will be based on either average cruise performance or on climb and descent conditions. Short range aircraft, which spend a majority of their flight time relatively in high speed, flaps up, climb and descent, should consider average climb and descent speeds, weights and altitudes for design conditions. Economic return is a direct function of aircraft purchase price, direct operating costs (DOC), and fuel efficiency and will significantly influence aircraft sales.

Flight characteristics and handling qualities influence wing design primarily in stall speeds and handling characteristics prior to and during stall, in initial buffet boundaries, and in longitudinal and lateral-directional stabilities.

The aircraft's structural design will impact the wing design primarily in its influence on aeroelasticity wing span limitations and landing gear storage. Structural efficiency for minimum wing weight is defined by not only span and chord but also by spar depth. Requirements for fuel volume, flap and control systems and actuator sizes all influence the spar depth and thus weight.

Parameters affecting wing design are presented in Figure 7.1.

It is convenient to separate wing area and wing shape effects in the design process. Wing area and the high lift flaps are closely related to aircraft performance. Wing shape parameters such as planform, sweep, taper, twist, and airfoil sections will typically influence stall and buffet characteristics. This is complicated by span and aspect ratio which are planform parameters that affect performance. Wing area and planform affects wing design as well as performance objective are discussed separately.

7.2.1 Wing Area

A convenient plot identifying the aircraft weight, wing area and engine size trades that satisfy the design payload, range and cruise Mach number requirements is presented in Figure 2.5. This plot represents a matrix of point design aircraft solutions that meet the design requirements for a fixed aircraft configuration concept. Wing, engine and empennage size and weight are scaled to meet the fixed payload and range requirements. The dependent aircraft performance and maximum take-off weight (MTOW) are shown as lines of constant value on the plot of thrust loading (T/W) versus wing loading (W/S).

The above chart (Figure 2.5) is an optimisation plot that allows selection of wing area and engine thrust while minimising or constraining various parameters. Contour of constant MTOW are shown in Figure 2.5. The minimum of this parameter represents a "valley" of goodness. Additional contours that could be included on this plot would be contours of constant block fuel or DOC. Lines of constant aircraft

performance are also presented along with the performance objectives that define limiting boundaries. Aircraft performance will typically include lines of constant landing field length, take-off field length, cruise speed Mach number, initial cruise altitude capability and engine out altitude capability.

For the unconstrained configuration of Figure 2.5, the minimum MTOW occurs at a high wing loading and represents a small aircraft size (small wing area and low thrust). When performance objectives are considered, the region of acceptable design points is significantly reduced. The constraint of cruise speed and landing field length create limiting boundaries in this case. The initial cruise altitude capability and engine out altitude capability (both are not shown on the figure) are greater than the requirements and therefore are not limiting constraints on the design.

The design point will typically represent the "best" wing area that meets the design mission requirements and performance objectives for the smallest penalties in MTOW, fuel burn and DOC. If the wing area is too small the aircraft L/D is too small (high induced drag) and so fuel volume, while if the wing area is too large the aircraft weight is too high and therefore costs are excessive.

With increasing lift/drag ratio by the application of laminar flow and variable camber wing concepts, fuel burn could be reduced and hence MTOW and wing area (see Section 7.2.3 and also Reference 7.4 and 7.5).

7.2.2 Planform Selection

The planform of the wing is defined as the shape of the wing when viewed from directly above, as shown in Figure B.8 of this thesis. Planform is directly related to aspect ratio and taper. The main aerodynamic characteristics influenced by planform are the induced drag coefficient and the stalling characteristics (Reference 7.15).

Wing planform selection is based on a combination of criteria that require constant review during the design phase. Planform span, aspect ratio, sweep, and taper will be revised based on the trades studies taking place during the design. As sweep increases, the MTOW, operating empty weight (OEW), mission fuel and engine size increase for a constant aspect ratio and wing loading. As aspect ratio increases, OEW and MTOW increase while engine size and fuel burn decrease (Reference 7.1 and 7.6).

A detailed trade off study of planform parameters is outside the scope of this work. For ATRA-100 Baseline, sweep and taper ratio are taken from comparison with existing aircraft data (see Appendix A), while aspect ratio is taken from the "sizing chart" (see Figure 2.5) i.e. :

- A quarter chord sweep ($\wedge_{c/4}$) = 25 deg.
- Taper ratio (λ) = 0.274
- Aspect ratio (AR) = 9.5

Reference 7.7 suggests a new regional aircraft could have an aspect ratio as high as 11. As with wing area, by the application of laminar flow and variable camber wing concepts, the wing sweep also could be reduced (see Section 7.3.3). Studies

supported by wind tunnel results showed the feasibility of a lower sweep/high aspect ratio wing with similar aeroelastic distortion, but better cruise and field performance than the higher sweep/low aspect ratio (Reference 7.89).

The application of laminar flow on swept wings is effectively limited at high Reynolds numbers by a high sweep angle, as crossflow instability and attachment line transition lead to fully turbulent boundary layers on the wing. Theoretical and experimental investigations on finite swept wings show, because of three-dimensional displacement effects, an effective increase of wing sweep for backward swept wings and an effective decrease of wing sweep for forward swept wings compared to the geometrical sweep. For a laminar flow wing, the reduction in sweep in the case of a forward swept wing leads to a more stable laminar boundary layer concerning transition because of crossflow instability and attachment line transition. Thus, with this concept, a laminar forward swept wing can be realized more easily than a comparable swept back wing (Reference 7.9). An example of a forward swept laminar wing aircraft has been proposed by Airbus (Reference 7.10) as shown on Figure 7.2. The main problem for the forward swept wings is flutter (see also section 7.3.1).

Based on the results from the "sizing chart", the wing planform area is selected (see Chapter 2.4). Wing sweep, aspect ratio, airfoil section and thickness distribution are interrelated and are determined to meet the design Mach number and lift coefficient requirements. These parameters are discussed in greater detail in the Aerodynamic Design Consideration section. For ATRA-100 Baseline wing planform see Figure B.8 of Appendix B.

7.2.3 Performance Objectives

For a typical jet aircraft, the equation for cruise range (R) can be expressed as (Reference 7.11) :

$$R = \left(\frac{a_0\sqrt{\Theta}}{TSFC}\right)\left(\frac{M\,L}{D}\right)\ln\left(\frac{W_{initial}}{W_{final}}\right) \qquad (7.1)$$

where : a_0 = speed of sound

Θ = temperature ratio, T/T_0

The equation states that if the thrust specific fuel consumption, TSFC, is considered to be nearly constant (which it usually is in the cruise region), a jet aircraft will get the most range for the fuel burned between wieghts $W_{initial}$ and W_{final} by making the quantity (Mach number)(Lift/Drag), M(L/D), a maximum. The basic aerodynamic performance objective is, therefore, to achieve the highest value of $M(L/D)_{max}$ at the cruise Mach number. Climb and descent performance, especially for short range missions, is also important and may suggest the "cruise" design conditions be compromised.

The aerodynamic advantages of the combined laminar flow - variable camber wing stem from two considerations (see also section 7.7.2.5) :

a. Laminar-flow is potential means of reducing viscous drag in cruise, by up to 15 - 20%. Aircraft components such as wings, fin, tailplane, engine nacelle are candidates for laminar flow treatment (see Chapter 3 and Reference 7.12 - 7.23).

b. Variable-camber is potential means of increasing lift/drag ratio in cruise and climb, by up to 4% (cruise) due to cruise and climb always at optimum lift coefficient (see Chapter 4 and Reference 7.5, 7.24 - 7.26). Theoretically the aerodynamic advantages of variable camber wing stem from four considerations :

1. A reduction in profile drag, resulting from the obtaining of lift by the use of an optimum amount of section camber.
2. Operation with the minimum of induced drag, due to the achievement of an elliptical lift distribution at all lift coefficients.
3. A reduction in wing/fuselage interference drag and fuselage drag, stemming from operation at a near constant angle of attack over a wide range of lift coefficients.
4. A higher buffet onset Mach number, resulting from minimal wing twist and minimal wing camber at high speeds/modest lift coefficients. This creates the potential for a higher maximum cruise and limit Mach numbers.

However, a point design that neglects the off-design considerations must be avoided. The off-design characteristics should show no drop in lift or $(L/D)_{max}$ at Mach numbers below cruise. The variation of L/D with lift at cruise Mach number should provide at least 95 % of $(L/D)_{max}$ for a (+/-) 0.1 variation in lift about cruise (Reference 7.1).

7.3 AERODYNAMIC DESIGN CONSIDERATIONS

This section will discuss the aerodynamic considerations in the selection of the wing/fuselage configuration. Selection of wing planform characteristics such as sweep, section, aspect ratio, spanload and taper is discussed. This is followed by discussion of the wing placement and fuselage influence on the configuration aerodynamics.

7.3.1 Wing Sweep Selection

The primary effect of wing sweep is to increase the Mach number capability of an unswept wing with the same airfoil section. Swept wing aerodynamics are based on the simple sweep theory outlined in Figure 7.3 (Reference 7.1, 7.12 and 7.31). Simple sweep theory is based on the concept of an inviscid infinite yawed wing and does not account for the effects of a finite wing, taper, a fuselage, a nacelle, or boundary layer flow.

Wing sweep has several other important aerodynamic effects which are listed below. Beneficial effects of increased sweep are :

a. To increase the Mach number at which drag rise occurs.

b. To decrease the wing lift curve slope and therefore reduce the aircraft response to gust inputs. The result is an improvement in passenger ride comfort and a reduction or elimination of the gust design weight penalty.

c. To increase the flutter speed at a constant structural aspect ratio. (Flutter speed increases at a rate slightly greater than 1/cos $\wedge$ up to 50 or 60 degrees where it begins to decline rapidly with futher increases in sweep, Reference 7.1).

The adverse effects of wing sweep are :

a. To reduce the aerodynamic aspect ratio and increase the airplane induced drag for a constant structural aspect ratio. (Increasing sweep reduces the aerodynamic span).

b. To reduce the maximum lift coefficient and low Mach high lift buffet boundary.

c. To introduce nonlinear stability and control effects.

Forward swept wings have not received much attention until just recently when fighter concepts have been configured and wind tunnel tested. Forward swept wings on conventional transport aircraft have some advantages and some disadvantages. The following are comparison between a forward and aft swept wing (Reference 7.1 and 7.27, also see Figure 7.12 for sweep definitions) :

A. Aft sweep :

- Washout with increasing load (see also Figure 7.4), lower wing weight. Swept back wings have two disadvantages at increased angles of attack and reduced speeds (Reference 7.27):
  1. Wing boundary layers tend to drift outboard (in separated boundary layer condition), assisted by the spanwise component of flow in Figure 7.5, which causes them to thicken and separate prematurely at the tips.
  2. Sweep staggers the vortices shed across the span, so that those shed inboard are ahead of those shed further out. This causes increased upwash ahead of the tip, with a corresponding increase in tip angle of attack, accompanied by premature peaking of the lift coefficient (Figure 7.4).

  The overall result is that swept back wing tips stall before the root, while the root (which is ahead of the centre of gravity) continues to lift. Pitch-up follows, forcing a full stall, a rapid drag rise, and possible pitch-roll-yaw divergence. There may also be degradation of control effectiveness, perhaps even control reversal in some cases.
- Better trailing edge flap effectiveness.
- Higher maximum lift.
- Conventional looking.
- Additional directional (C_{n_β}) and lateral stability (C_{l_β}), see also Figure 7.6.

B. Forward sweep :

- Washin with increasing load (see also Figure 7.4), higher wing weight. Forward sweep avoids premature tip stall, because the root stalls first. Ailerons tend to remain effective, but pitch-up still occurs. However, forward sweep has an adverse effect upon directional stability, and larger fin area is needed than with sweepback.
- More aft C.G. limit, better trim.
- Improved gear stowage.
- More effective shock sweep.

- No tip stall.
- Better leading edge flap effectiveness

For forward swept wings the major technical disadvantages of a further outboard centre of lift could possibly be overcome in the future when active load alleviation and/or composites are designed to reduce bending and minimize centre of pressure movement. There is little to choose between forwards/aft swept wings in terms of nacelle integration. Stability and control characteristics of forwards swept wings are not well understood. The main problem of forward swept wings is natural divergence stall and can lead to a flutter.

7.3.2 Aerofoil Design

Selection/design of the outboard wing sweep and outboard aerofoil section are made at the same time. Usually for most swept wings, the outboard aerofoil section defines the wing Mach number capability. This is a result of the higher outboard wing section loading compared to the inboard wing. The lower inboard wing lift is due to wing taper and the lower lift curve slopes near the side of fuselage. The outboard wing aerofoil is selected/designed based not only on the design Mach number but also on the aerofoil off-design characteristics. Good low Mach number lift capability is required for climb performance and for aircraft gross weight growth capability. High Mach number characteristics should exhibit low drag creep (see Figure 7.7) below cruise Mach number and still maintain gentle stall buffet characteristics. Shock position should remain fairly stable with small changes in Mach number or angle of attack to maintain good ride quality and handling characteristics (Reference 7.1).

7.3.2.1 HLFC-VCW Aerofoil Design Criteria

The introduction of laminar flow represents an additional design criterion that must be satisfied along with all existing considerations. The issues raised for NLF section design are also relevant to HLFC sections although leading edge suction reduces the severity of the constraints imposed for NLF. Typically transonic HLFC aerofoil sections have been designed with pressure distributions having a small peak close to the leading edge, followed by a region of increasing pressure (an adverse pressure gradient) over the suction region, after which the 'roof-top' has a mildly favourable pressure gradient . Such a pressure distribution has been found to maximise the extent of laminar flow (References 7.28, 7.30 and 7.93).

Development of an aerofoil is concerned mainly with the selection of the desired pressure distribution. Once this is done, the shape can be computed by a mathematical procedure. However, not all pressure distributions correspond to physically meaningful airfoil shapes; real flow constrains the pressure distribution to have a leading edge stagnation point, low pressure forward, and gradually rising pressure aft, ending somewhat above ambient at the trailing edge. Within these constraints, details must be tailored to meet the specific requirements of HLFC and of

low drag rise due to compressibility. The following points should be observed (Reference 7.28, 7.29 and 7.30).:

- A steep initial gradient (rapidly falling pressure) is helpful in preventing attachment line transition on a wing having substantial leading-edge-sweepback. The initial pressure gradients for an Airbus type and a Pfenninger type airfoil are shown in Figure 7.8 (Reference 7.30).
- The midchord pressure distribution affects susceptibility to the two other principal transition mechanisms. Falling pressure tends to suppress the growth of Tollmien-Schlichting disturbances, and rising pressure will generally promote their rapid amplification. Hence, a negative gradient (falling pressure) is often called "favourable", and a positive gradient (rising pressure) is termed "adverse". However, substantial gradients of either sign will combine with sweepback to produce boundary layer crossflow, which tends to amplify disturbances and to promote transition. The favourable pressure gradient should not be so great to avoid excessive loss of lift for a given shock strength compared to the turbulent design.

  The fundamental technical strategy of HLFC is to confine the unavoidable large negative gradients to the region ahead of the front spar and to use boundary layer suction to suppress disturbance amplification due to crossflow there. Downstream of the front spar, gradients are kept in the weakly favorable to zero range.
- The minimum pressure level on the upper surface must correspond to a slightly supersonic velocity on an efficient high-speed wing. To limit wave drag, the local Mach number has to be restricted to a value less than Mach 1.2. The shock strength at the return to subsonic flow must not be so great as to cause excessive wave drag or separation of the turbulent boundary layer.
- Reference 7.29 assumed that extended regions of favourable pressure gradient would correspond to extended regions of laminar flow. Therefore, it was required that the pressure gradients be favourable as far aft as the design transition points.
- To ensure attached flow, the maximum slope of the aft pressure gradient, $dC_p/d(x/c)_{max}$, was to be less than 3.0.
- The pressure level on the lower surface is determined by the desired lift coefficient and airfoil thickness ratio. The flow will normally remain subsonic and therefore shock-free. A recovery region having an adverse pressure gradient and turbulent flow must occupy the aftmost portion.
- Variable Camber is a prerequisite for HLFC wing to control the pressure gradients and the off-design behaviour (see section 7.7.2.5).

These design criteria are summarized in Figure 7.9.

However, aerofoils described above are often prone to increased shock growth which result in earlier occurrence of drag rise conditions, relative to an aerofoil with an adverse 'roof-top' pressure gradient. In fundamental wing design terms this implies increased sweep, reduced thickness/chord ratio, and/or reduced wing loading, all of which reduce the aerodynamic and/or structural efficiency of the wing for a specified design condition. An alternate approach may be to use an aerofoil with a mildly adverse 'roof-top' pressure gradient to improve wave drag and lift capabilities, although with a

reduced extent of laminar flow. Careful consideration would be required to select/design an aerofoil section to achieve maximum aircraft efficiency and minimum operating economics with laminar flow and a suitable off-design performance. In addition, it is necessary to ensure adequate efficiency and economics with turbulent boundary layers (References 7.28, 7.30 and 7.93).

7.3.2.2 Low Speed Design

Low speed design considerations will typically involve only the leading edge region. The typical design sequence is to first design the best high speed section that meets the design requirements (lift, Mach number and off-design) and then review the low speed lift capability. The process is iterated until little or no loss in high speed performance is obtained. If the low speed performance cannot be achieved with the compromised aerofoil then the flap concept is typically modified. Wings with no leading edge device will typically require more compromise between the high and low speed aerofoil design. A more rounded nose (larger radius) is usually necessary to reduce the maximum velocities on the airfoil in the high lift condition. The angle of attack capability for this design will be significantly reduced compared to a wing with a conventional leading edge device (Reference 1). Therefore, the maximum lift capability will be reduced. Significant differences in airfoil shapes between the high and low speed sections will require either a high speed performance penalty, a different flap concept, or a larger wing or flap area. Table 7.2 of Reference 7.31 can be used as a guideline for an initial estimate of $C_{L_{max}}$ for several commonly used high lift configurations. For a more extensive discussion of high lift systems design, the reader is referred to References 7.32-7.38.

In the case of a laminar aerofoil, due to its specific geometry (high curvature of the leading edge, rearward maximum cross section, etc.....) and absence of leading edge slats, special attention is required in high-lift conditions, mainly concerning prediction of leading edge stall. The main feature for the flapped laminar airfoil is the dramatic loss in α_{max} occurring when the flaps are deflected. This loss in α_{max} is probably a consequence of the leading edge type of stall, as expected from the small leading edge radius. For a more extensive discussion of the stalling properties of airfoil sections, the reader is referred to Section 7.3.3 of Reference 7.31. To increase α_{max} capability, two alternatives can be considered (Reference 7.39 and 7.40).:

1. Compromise between low-speed and cruise may lead to greater value of leading edge radius (can increase attachment line contamination possibility), compatible with acceptable value for α_{max}.
2. A leading edge high-lift device (kruger flap) may be used, but this will make the laminarization of the lower surface more difficult.

7.3.2.3 Aerofoil Design Sequence and Procedure

The design an aerofoil is an iterative procedure. The design procedure for

the HLFC-VC aerofoil to achieve the design goals described in the previous section is depicted in Figure 7.10 (clearly dominated by off-design constraints and VC implementation). The basic design starts with an optimization with respect to TSI at constant suction level as there is a minimum N-factor with increasing suction for TSI. Then follows an optimization of suction for cross-flow and ALT, which requires an increase towards the nose. In this context it may be necessary to modify the nose shape also to achieve a sufficiently low level in NCFI at the nose and damping downstream. Once this basic design is established, off-design calculations including a variation of VC flap geometry have to be carried out in order to reduce the wave drag penalty, and to sustain attached flow in turbulent mode. If no additional means of wave drag reduction, as for example passive ventilation or a surface bump, are considered (References 7.89 and 7.90). Figure 7.11 shows several laminar aerofoil from References 7.44, 7.8, 7.88 and 7.29, see also Reference 7.45.

It is beyond the scope of this work to design an aerofoil with a procedure such as that described above. For aerofoil development on the ATRA wing see section 7.7.

7.3.3 Sweep/Thickness/Mach Number Trades-offs

Several methods are available to estimate the airfoil section design lift coefficient as a function of wing design lift coefficient and wing sweep. For a more extensive discussion of those subjects, the reader is referred to References 7.31, 7.46 and Reference 7.47. The basic methods described in References 7.31, 7.46 and Reference 7.47 outlines a process for estimating 3D aerodynamic characteristics based on 2D aerofoil performance data. The result of those methods is an estimate of the sweep required to achieve the required Mach number and lift coefficient for a constant aerofoil technology and wing thickness. Figure 7.12 (Reference 7.27) can be used as a guideline for an initial estimate of a combination of airfoil section thickness and wing sweep for a certain critical Mach number. The airfoil design lift coefficient is defined as the lift coefficient at the intersection of the Mach drag divergence curve and the C_l at $(C_l/C_d)_{max}$ versus Mach number curve (Reference 7.1).

The concept of a sweep efficiency factor, $\eta_s = (M_{3D}/M_{2D})*\cos\Lambda$, is the fundamental difference between simple sweep theory and the actual aircraft wing. Well defined wings will achieve sweep efficiency factors ranging from 0.93 to 0.98 (Reference 7.1). The primary reasons why an aircraft wing cannot achieve the Mach capability of the infinitely yawed wing of constant section include :

1. The presence of the fuselage induces a flow field of greater velocity than freestream.
2. For a tapered wing, the shock or effective sweep at drag divergence is usually aft of the quarter chord and therefore has less sweep.
3. The inboard wing may cause unsweeping of the outboard shock.
4. The inboard wing may cause early drag rise.
5. The wing tip may cause unsweeping of the shock which results in early drag rise.

By the application of VCW, C_L buffet onset is enhanced (which is due to the relaxed off-design constraints for the VC-wing, see section 7.2.3 and Reference 7.42), producing higher Mach critical lift, hence allowing the aircraft to fly to a higher Mach number, and/or can have lower sweep, or higher thickness to chord ratio for the same flight Mach number. Both phenomena i.e. higher Mach critical drag, and Mach critical lift help VCW aircraft to be designed and optimised for higher thickness to chord ratio and/or alternatively lower sweep angle. Wing with lower sweep angle is preferred for HLFC application to reduce the possibility of attachment line contamination and cross flow instability. Wings with HLFC tend to have lower thickness to chord ratio for the same flight Mach number compared to the turbulent wings, but this phenomenon may be eliminated or reduced by the application of VCW concept (see also section 7.3.2.1).

7.3.4 Span and Aspect ratio Selection

With the wing area previously chosen and the sweep now selected, the wing span can be picked based on trade studies. Considerations include airport "gate" requirements for ground handling and wing weight changes with increased span. Airline "gate" requirements are somewhat flexible and usually cycle several times in the design phase. Trade studies of increased wing structural weight with increased wing span or reduced induced drag will be required before the choice of wing span is made. Once wing span is selected the wing aspect ratio is a fall-out. Once the planform of a wing is fixed the induced drag depends upon span loading (L/b) and not aspect ratio. The longer the span the lower the span loading and the faster an aircraft climbs and cruises. Span loading arises from the average pressure difference between the upper and lower surfaces. The lower the span loading, the smaller the pressure difference, and the further away the wing operates from those conditions where separation becomes critical (Reference 7.27). Once area is picked, then induced drag can be related to aspect ratio and this is usually how trades are presented. Induced drag, D_i, is :

$$D_i = (1/(\pi * q * e)) * (L/b)^2 \qquad (7.2)$$

For the given area picked and with dynamic pressure, q, fixed for the design speed and altitude; therefore,

$$C_{D_i} = D_i/(q*S) = (S/(\pi * q^2 * S^2 * e)) * (L/b)^2 = C_L^2/(\pi * A * e) \qquad (7.3)$$

Aspect ratio (A) allows the designer a better picture of the wing geometry since it relates the average chord to span. Aspect ratio affects directly the slope of the lift curve, $dC_L/d\alpha$. The larger the aspect ratio, the more closely does the lift slope approachs the theoretical maximum for an infinitely long wing i.e. :

$$\text{ideal lift slope, } dC_L/d\alpha = 2\pi \text{ /radian } (0.11/\text{deg}) \qquad (7.4)$$

But as aspect ratio is reduced, lift slope decreases by a factor A/(A+2), so that for aspect ratios less than infinity (Reference 7.27).:

$$dC_L/d\alpha = 2\pi * A/(A+2)/\text{radian} \qquad (7.5)$$

Inherent with an increase in aspect ratio is an increase in wing design lift coefficient and a decrease in the average wing chord. With increasing aspect ratio the drag polar "opens

up" and thus the maximum Lift/Drag, L/D, occurs at a higher lift. To realize the full benefit of increasing aspect ratio will require increasing the design lift coefficient.

7.3.5 Spanload and Taper Ratio Selection

Choice of the wing spanload distribution is an important decision in the wing design process. Ideally, an elliptic distribution is desirable at the cruise condition because of the implied minimum induced drag. However, several factors make a slightly triangular distribution very desirable. First, an elliptic loading at cruise will tend to overload the wing tip at the design load condition. This implies a more outboard center of pressure and associated increased wing structural weight. Also associated with the further outboard loading is the tendency for increased tip stall and its influence on pitch-up and handling qualities. Trade studies of increased drag and reduced wing weight for more triangular spanload distributions must be made.

With the wing incorporating variable camber concept, the wing spanload distribution can be matched to the prevailing conditions by varying the camber along the span, thus ensuring that during cruise/climb the wing always possesses an optimum lift distribution.

The influence of horizontal tail spanload on the selection of the wing spanload distribution is not well understood. Usually with a typically downloaded tail the horizontal load distribution suppresses the wing spanloading. Therefore, with a slightly triangular wing spanload the resultant aircraft spanwise load distribution will be more elliptical (Reference 7.1). This is schematically presented in Figure 7.13.

For practical structural reasons will require that the wing be tapered ($C_{root} > C_{tip}$). An estimate of the taper can be made from the selected spanload distribution and the chosen wing area, span and lift coefficient. The procedure is straightforward and is outlined in Figure 7.14.

Selection of the wing section lift distribution (C_l versus η) is usually made such that the outboard wing section lift is a constant. A constant section lift distribution is desired so that shock development and eventually separation will occur uniformly (progressive stall from the trailing-edge). The actual distribution of section lift will be dependent upon the wing taper and chosen spanload ($CC_l/C_{ave}C_L$). Typical outboard loadings vary from 1.1 to 1.2 times the wing design lift coefficient to account for the finite span and fuselage effects. It is expected that the maximum wing section lift coefficient will be less than the airfoil section design lift coefficient times the cosine squared of the quarter chord sweep angle. If not, then an airfoil section must be found that meets this criterion or the wing loading must be reduced/increased chord (Reference 7.1).

Section loading where the root or tip are highly loaded must be approached with caution. A highly loaded root will typically result in significant shock unsweeping, premature drag rise and poor critical Mach Number. A highly loaded tip is undesirable because the outboard wing is working too hard and premature drag rise and severe pitch-up will occur (aft swept wing).

Figure 7.15 (Reference 7.27) shows (for a given wing lift) the way in which taper causes section lift coefficient to peak towards an early stall. The point at which the C_l curve comes closest to the $C_{l_{max}}$ line shows where the stall is most likely to start. A rectangular wing stalls first at the root. The more tapered or sweep back a wing becomes, the more the C_l curves becomes humped outboard, and the stall occurs first towards the tip. This is dangerous, because slight sideslip and asymmetries between each wing can cause one wing to stall before the other. A violent wing drop and roll may be result of a stall, which can be exaggerated by use of corrective aileron. A spin might follow.

Taper has a dominant effect on the wing weight and therefore, may be selected based on the weight trade while the spanload is achieved by a combination of twisting the wing and varying the camber In principle as a whole design, taper and spanload are selected dependently. Wing twist (ε) is the angle of incidence of a wing section, measured in a plane parallel to the XOZ plane (Figure 7.16 from Reference 7.31). Positive twist : nose rotated upwards, WASH-IN. Negative twist : nose rotated downwards, WASH-OUT. The combination of twist and taper will allow the desired 1-g spanload to be achieved. Usually, the wing 1-g spanload distribution and corresponding twist is selected by aerodynamicists and is given to structural engineers to determine the "jig" twist for manufacturing.

Jig Loft is defined as the shape of the wing as it is manufactured in the jig. Since a wing will bend and twist in flight, the wing is intended to be manufactured such that its loaded shape at cruise has the optimum lift distribution. Bending does not greatly affect the lift distribution, but twist does. Thus, the jig loft accounts for twist but not for bending. The Jig Loft also accounts for the shear and dihedral. Shear is the gull-shaped vertical displacement of airfoil sections relative to the WRP (wing reference plane) normally used to provide engine ground clearance. Figure 7.17 shows the shear definition.

The jig twist is defined as follows :

- The Aerodynamics group supplies the desired twist distribution of a loaded wing in the 1-g mid-cruise condition.
- The Structures group provides the aeroelastic twist that results when this 1-g cruise load is applied to an unloaded wing.
- The Configurations group adds the twist of the cruise condition to the twist due to aeroelastic effects to define the Jig Loft which is the twist used in manufacturing a wing.

7.3.6 Fuselage Influence

The shape of the aircraft fuselage can have a dominant effect on the wing aerodynamic characteristics. The flow field of a wing-fuselage system at subsonic velocity in symmetric incident flow (angle of sideslip $\beta = 0$) is illustrated in Figure 7.18 (Reference 7.48).

There are four main effects on the flow along the junction between a wing and a fuselage, all equally important in practice (Reference 7.49) :

(1) Displacement effects, arising from the thickness of the wing and the curved intersection lines.
(2) Lift effects, arising from the circulatory flows around wing and fuselage.
(3) Effects of asymmetry, associated with the shape of the cross-section of the fuselage or with the position of the wing on the fuselage (mid, high, or low position).
(4) Effects of viscosity over and above those present on the bodies in isolation, arising from the viscous flow along the corner formed by two walls.

For the typical transport aircraft with the wing located on the fuselage constant section and with a fuselage diameter to wing span ratio of 0.1, the fuselage influence is small. As the fuselage diameter (D) increases in relation to the wing span (b), the wing will effectively lose more lift. This result is graphically illustrated in Figure 7.19, while Figure 7.20 shows effect of fuselage representation on wing root calculated transonic pressure distribution (Reference 7.62), both curves are based on the gross-wing area. The total wing/fuselage lift ($C_{L_{WB}}$) can be approximated based on the exposed wing lift ($C_{L_{W.exp.}}$) and ratio of fuselage diameter to wing span as follows (References 7.1 and 7.11) :

$$C_{L_{WB}} = C_{L_{W.exp.}} * (1 + D/b)^2 \qquad (7.6)$$

According to Reference 7.1, the fuselage has an influence on the induced drag of the configuration. Downstream of the wing and fuselage, the trailing vortices and downwash will have come to equilibrium in a plane perpendicular to the flow direction and the effective span will have been reduced by

$$b^2_{effective} = (1 - D^2/b^2) * b^2 \qquad (7.7)$$

Since the induced drag is a function of $1/b^2$ (see equation 7.2), the result will be an increase in induced drag.

7.3.7 Wing Placement

Vertical placement of the wing on the fuselage must be considered. Transport aircraft typically have a "low" mounted wing to provide aircraft flotation and improved crashworthiness. Certain aircraft have "high" mounted wing configurations to reduce engine foreign object damage for rough or minimally prepared runways and for cargo loading considerations. Low wing mounted configurations provide a place for landing gear storage while gear pods or a fixed gear would be necessary for a high wing configuration.

An exposed high mounted wing configuration allows the flow to expand over the wing upper surface inboard to the aircraft centerline. Because of symmetry, the isobars at the centerline must be perpendicular to the fuselage axis and thus a strong unswept shock is likely. Therefore, it is desirable to sweep the shock forward as much as possible and then unload the wing center section and keep the suction below critical

value. This should eliminate any formation of a "normal" shock near the aircraft centerline, see Figure 7.21 (Reference 7.49) and 7.22 (Reference 7.1).

Low wing mounted configurations where the wing lower surface is exposed are highly undesirable. Because the flow on the lower surface is allowed to expand and cause a loss in lift. Fairings, to cover up the lower surface help but a loss in lift will still occur. Fairings on the upper surface are required to provide a perpendicular reflection plane instead of a canted plane which would aggravate the inboard wing upper surface pressures, see Figure 7.22 (Reference 7.1).

Subsonic area rule techniques may be useful in the design of the wing-to-fuselage fairings or in the tailoring of the wing and/or fuselage at the intersection. For a more extensive discussion of area ruling techniques, the reader is referred to Reference 7.11.

The mid to low wing configuration is typical of many transport aircraft, where the wing upper surface provides an upward load and the lower surface a much smaller downward load. The net result is an upward lift force that blends with the fuselage lift with no discontinuities in the spanload distribution. Discontinuities in the spanload distribution for either the "high" or "low" wing configurations are not desirable because of the potentially unfavourable effect on the induced drag. Care should be exercised in completely understanding the spanload distribution if a discontinuous type of spanload configuration is chosen.

7.4 PROJECT CONSTRAINTS

Wing designers must recognize the constraints and requirements of the other technology staffs and project groups. Trade-offs and compromises between the various groups are necessary to realize the most competitive and economical design. Typical trade-offs include : wing weight versus spanload and spar depth; landing gear stowage versus root tailoring; fuselage contouring versus wing location, payload requirements, and aerodynamic fairings, and spanwise and chordwise curvature versus wing shear.

7.4.1 Spanload

The wing weight and spanload trade was summarized in the Aerodynamic Design Considerations section, see section 7.3.5 of this thesis.

7.4.2 Thickness

The wing weight versus thickness or spar depth trade should be optimized at the same time. The thicker wing implies increased profile drag for a reduction in weight. The outboard wing spar depth is easily changed by varying in the maximum thickness. The change in maximum thickness not only affects drag but also affects drag divergence Mach number and therefore cruise Mach. A change in spar depth by a modification of

the aerofoil section is possible; however, the process is more difficult and some change in drag and Mach number will probably result.

Usually, the inboard wing can be significantly thicker compared to the outboard wing while still maintaining the required performance. Typical root-to-outboard section thickness ratios vary from 1.3 to 1.5 (see Appendix A of this thesis). A thicker inboard wing is desirable to minimize wing weight, to increase the wing fuel volume, to provide for better nacelle attachment, to provide space for retraction of the main landing gear, and for the aircraft systems (flaps, spoilers, fuel, gear, etc.). Aerodynamically, a higher thickness to chord ratio (t/c) inboard wing is possible because of the reduced section loads and the lower lift curve slopes. The reduced loads are a result of the increased chord due to taper and possibly a Yehudi and/or a leading edge glove (see Figure 7.23). The smaller lift curve slopes are a result of the aft swept wing.

Where did the term "Yehudi" come from? In 1941 a B-29 aerodynamic test was conducted at the Cal Tech wind tunnel. The objective was to obtain a high L/D to maximize aircraft range. The wing and body (WB) were tested together first and a drag polar was plotted showing a nice high L/D. Next the nacelles were added (WBN) and the drag coefficient increased which decreased the L/D as expected. At this point, George Schairer, Chief Aerodynamicist, received a call from the Chief of Structures who said the airloads were further outboard than expected. Could Schairer do something to move the loads inboard and avoid an overweight wing? Schairer recommended adding a short trailing edge extension between the side of body (SOB) and the outboard nacelles. Inexplicably (at the time), when this configuration (WBNY) was tested, the L/D increased to nearly the original value. The trailing edge extension was dubbed a "Yehudi" after a song popularized by Kaye Kayser called, "Who's Yehudi". The song probably reffered to Yehudi Menuhin who played the violin so "unbelievably" well. Despite a later department memo which stated "Thou shall not refer to trailing edge extensions as Yehudi's", the name caught on and is used to this day (Reference 7.1).

The inboard root thickness may be constrained by requirements to locate the wing box between the floor beam and the keel line while allowing for wing root incidence.

7.4.3 Planform

Wing gloves or leading edge extensions are usually added to a wing design as a remedy for some problem. Fuel volume requirements may force the addition of a glove which is beneficial because of the increased effective sweep. However, a glove may lead to problems with increased wing pitch-up. Typical planform geometry is described in Figure 7.23.

Project constraints on the wing tip design are almost always ignored during the high speed design process. Considerations for leading edge flap deployment, tip lights, and antennas have negligible influence on the wing performance. Planform, airfoil section and twist modifications must be considered in the design process (Reference 7.1).

Wing location on the fuselage impacts the wing aerodynamics, as described in the Fuselage Influence section. The longitudinal location is chosen for balance, loadability and stability of the aircraft. The vertical location is usually either below the floor or above the ceiling and is chosen primarily for passenger comfort and to maximize payload (see Figure 7.24).

7.4.4 Weight/Drag Trades

The change in wing weight is usually traded against a change in aircraft drag. The weight/drag trade factor, usually given in terms of pounds OEW per drag count (1 drag count = 0.0001), is determined by several methods. The traditional approach to determine the weight/drag trade uses the range equation from the General Requirements section and assumes that the gross takeoff weight is constant. This implies that the aircraft takeoff characteristics are the same. For a constant engine, speed, and range, the change in drag (L/D) can be directly equated to a change in weight ratio ($W_{initial}/W_{final}$) and operating empty weight (OEW). The second approach uses the range equation but assumes that the fuel burned is constant and lets the gross takeoff weight vary. This method is gaining recognition because of the increased concern for fuel conservation and the dominance that fuel burned has in the direct operating cost (DOC). This would probably require the assistance of the Marketing and performance groups (Reference 7.1).

With a variable camber wing, for the manoeuvre case the wing root bending moment can be reduced (and so also the wing weight) by setting the inboard wing at more camber than the outboard wing. During the weight/drag trades this capability should be considered.

7.4.5 Landing Gear

A poor location for the retracted gear can ruin an otherwise good design concept. A bad choice for the retracted position can chop up the aircraft structure (increasing weight), reduce the internal fuel volume, or create additional aerodynamic drag. Figure 7.25 shows the options for main landing gear retracted positions. Locating the gear in the wing, inside the fuselage, or in the wing-fuselage junction produces the smallest aerodynamic penalty but tends to compromise structural efficiency. Gear stowage the wing reduces the size of the wing box, which increases weight and may reduce fuel volume. Gear in the fuselage or wing-fuselage junction may interfere with fuselage longerons. However, the aerodynamic benefits of these arrangements outweight the drawbacks for higher-speed aircraft. Virtually all civilian jet transports retract the gear into the wing-fuselage junction (Reference 7.51).

For the gear retracted into the wing-fuselage junction, usually, the wing planform has a "Yehudi" shape. All current commercial transports have a Yehudi trailing edge extension to house the landing gear. A Yehudi may be added to provide room to store the landing gear; however, the Yehudi decreases the flap chord to local

chord ratio and thus decreases flap lift. However the Yehudi does provide flap area when the normal flap volume is occupied by the gear and gear beam. The Yehudi can be undesirable because of its influence to unsweep the inboard wing isobars and to increase the tail off nose down pitching moments. Minimizing the Yehudi extension is desired because of the reduced weight and skin friction and trim drag. In the future, aircraft design concepts may have new innovative approaches to the landing gear stowage problem. These landing gear design concepts are allowing wing designs without an inboard wing Yehudi, with a typical planform of a basic trapezoid (Reference 7.1).

7.4.6 Manufacturing

Design and manufacturing are successive phases of a single operation; the ultimate objective of which is the emergence of an acceptable final product. In the aerospace context, achieving such acceptability has several components : market viability, operational efficiency, capacity for further development and structural integrity. Less obviously, but just as importantly, a structure must not be so complex or difficult in concept that its realization will create great difficulties, or increase the cost of the manufacturing process.

Design has always carried with it indeed a degree of prestige; because its effectiveness can be seen in the final product and a successful design can confer something approaching glamour upon those responsible. Production, on the other hand, emerged later as a specialized branch of engineering and is sandwiched between the designer's drawing and the final product. Consequently, its achievement is less apparent and frequently, in the past, it has not been accorded a like degree of consideration or credit. Yet, it is the production phase of the operation that translates the design into hardware (Reference 7.52), see Figure 7.26.

When manufacturing laminar wings, the following aspects should be considered :

1. An HLFC wing will require a smoother surface than a turbulent one in terms of manufacturing tolerances and surface quality. Reference 7.8 suggests that the maximum admissible height for three dimensional protuberances is less than 0.2 mm in the leading edge region.
2. Design criteria for the perforated suction surface. At present, panels with holes are often considered for use as the suction surface because modern electron beam and laser drilling techniques permit economical fabrication and offer structural advantages (Reference 7.8).
3. Perfect sealing of the system between the sheet metal skin and the chambers is an absolute necessity if the system is to be successful and efficient (Reference 7.63).

This implies that a strong development of the technology and the manufacturing techniques is required in order to fulfil the above considerations. Minimising the cost of producing such technology represents a real challenge for the manufacturer.

7.4.7 Fairings

In either high or low wing locations, sealing of the inboard flaps at the sides of the fuselage is required for improved $C_{l_{max}}$ capability. For a low wing configuration, fillets are probably necessary between the fuselage and wing upper surface to prevent vortex formation and boundary layer separation. Lower surface fairings should be minimized to reduce the lift loss on the fuselage. Figure 7.27 shows optimisation of A310 wing root fillets, while Figure 7.28 shows surface flow streamlines over the A310 wing root fillet (Reference 7 .62). Fairings on a high wing configuration should be minimum in size to allow the flow expansion over the center of the wing but should prevent vortex formation at the wing/fuselage intersection (Reference 7.1).

Wing leading edge strakelets can be added to either high or low wing mounted configurations. They provide considerable drag level improvement and increased maximum lift. The wing strakelet relieves the adverse pressure gradients on the fuselage due to the leading edge intersection and thus eliminates any wing/fuselage vortex formation and associated boundary layer separation. The size of the strakelet is typically limited by the span of leading edge devices. Strakelets have tended to be more successful on configurations with relatively large root thickness ratios, i.e. > 14 %. Sealing the leading edge devices at the nacelle strut intersection improves the maximum lift at the expense of a slight drag penalty. The wing design very seldom considers the nacelle flap seal except to assess its drag penalty in a wind tunnel test (Reference 7.1).

7.4.8 Low Speed Considerations

Low speed lift and control requirements have a definite impact on wing design. Because of the necessity for leading edge devices and trailing edge flaps and ailerons, the tip chord of the wing may be constrained. Consideration must be given to the leading edge radius and curvature distribution of the high speed section and how it impacts the low speed performance. Wing trailing edge airfoil section contours are usually not designed for any low speed considerations. For low speed laminar flow airfoil consideration see section 7.3.2.2 of this thesis.

7.5 OFF-DESIGN CHARACTERISTICS

Off-design stability and control characteristics of the aircraft are important in meeting the FAA/JAR certification requirements and aircraft manufacturer criteria for handling characteristics and upset recovery. Off-design criteria include requirements for initial buffet margins, longitudinal and lateral/directional stability, and speed stability.

Buffet is caused by unsteady separated flow at high and low speeds and large angles of attack. It can be caused by shock waves at high speed (References 7.27 and 7.48). With the wing incorporating a variable camber concept, the buffet boundary can be shifted to increase operational flexibility (Reference 7. 5).

Though off-design characteristics are chiefly dependent on aircraft configuration considerations, they are mentioned here since the wing is the major contributor to the aircraft off-design performance. For a more extensive discussion of off-design stability and control characteristics of the aircraft, the reader is referred to References 7.53-7.55.

7.6 NACELLE INSTALLATION CONSIDERATIONS

Historically, wing aerodynamicists often ignored the engine installation during the wing design process. It was up to the Propulsion Integrator to do the best they could with the wing as provided. Today, it is recognized that the engine influence must be accounted for during the design process.

For example, Figure 7.29 shows how the volume of the nacelle increases local velocities on the wing surface. By recognizing this effect during the installation design process, relocating the nacelle to minimize the peak volume, or tailoring the strut/nacelle geometry, velocities can remain below critical resulting in minimal shock and installation losses (Reference 7.56).

Modern design approaches also include inverse design codes which re-optimize the wing/nacelle/strut as an integrated unit, resulting in a considerable savings in design flow time (see References 7.57-7.60).

7.6.1 Location Influences

Wing-mounted engine installation features vary greatly on different aircraft. Designers often seek different solutions to similar installation problems. Aircraft cruise speeds also demand different trades and solutions. Design compromises are often required which do not result in optimum efficiency. In section 2.8 many of both the aerodynamic and non-aerodynamic factors influencing engine installation design were described. Typical engine installations of existing aircraft are shown in Figure 7.30.

One of the first considerations in installing an engine is position relative to the wing. As discussed in section 2.8, flutter, loads, ground clearance, etc. have a strong influence on the final position chosen. Aerodynamically, history has shown that forward engine placement is beneficial for minimizing installed drag. Close-coupled configurations present challenges to aerodynamicists with highly tailored configurations often required. Spanwise location is often determined by factors other than drag as discussed in section 2.8. Aerodynamically, interference with the fuselage, spanloading effects, flap cutouts, and tail sizing for engine-out control all influence the optimum position selection, see Figure 7.31. No generalized trades are possible due to the highly configuration dependant nature of the engine and wing designs. As in designing of other aircraft components, CFD plays an important role in developing a good installation with minimal testing and allows concepts to be studied quickly without the time lag of wind tunnel testing. To be useful, however, CFD codes must be validated by demonstrating that analytical results provide correct trends (Reference 7.56).

7.6.2 Effect of Nacelle Size and Position on $C_{l_{max}}$

Nacelle positioning and size not only influence cruise performance, but can have a significant effect on low speed performance. Nacelle size influences $C_{l_{max}}$ capabilities due to the nacelle lift "hanging on" after the wing has stalled. At larger flap deflections, flap cutouts to accommodate the larger engines reduces $C_{l_{max}}$ available. Aircraft pitch-up is also affected by the nacelle (due to the moments of forward located nacelles) if the wing stalls before the nacelle (References 7.56). For large modern nacelles (such on Boeing 767), to control separated flow at high angle of attack, a devices similar to a 'winglet' is attached on nacelles.

7.6.3 Exhaust System/Strut Aerodynamic Design Considerations

For under-wing mounted engines, the exhaust system and strut design play a key role in the ease of installing the engine for best performance. Several areas are shown which require careful consideration for achieving a successful design, see Figure 7.32. For example, exhaust system/wing flow interactions are minimized by careful tailoring of the design to avoid excessive velocities or shocks which may couple with the wing flowfield. Exhaust systems optimized for best static performance often perform poorly when installed under a wing. Trades between different exhaust system concepts are often required to achieve not just the best drag or engine TSFC, but the best overall installed performance (References 7.56).

The pylon design must not only accommodate the various systems inside the pylon, but provide a non-interfering design when coupled with the wing and nacelle. Aerodynamic design objectives often conflict with other requirements. For example, while it is desired to minimize the length of the heat shield to reduce weight, pylon length is often dictated by closure angles required to avoid flow separation and performance penalties. Pylon /cowl flow interactions can be significant since the cowl flow is usually supersonic at cruise conditions. Tailoring of the pylon leading edge helps to avoid un-necessary drag penalties but sometimes requires an extended leading edge which increases cowl manufacturing and engine removal difficulties (References 7.56).

7.6.4 Power Effects

Power or engine exhaust effects are primarily felt on the nacelle/strut and wing lower surface where the pressures are further reduced (more negative c_p) going from ram to cruise exhaust conditions. The largest effects are felt on the inboard side of the nacelle and strut. These reductions in pressure can lead to a power effect or blowing drag penalty (References 7.1).

The blowing drag is defined as the change in external drag as the jet pressure ratio is increased from ram to cruise conditions. In an underwing mounted engine installation where the wing is lifting, the jets counteracts the natural circulation around the wing, creating a loss in lift. Additional losses are caused by the jet if induced

velocities are sufficiently high to create shocks on the wing or strut. Profile drag increases are also present due to increases in local velocities induced by the jet (scrubbing drag), but are usually minimal unless flow separation occurs (References 7.56). For blowing drag sources, see Figure 7.33.

To reduce the interference drag, a new aerodynamic device, the liplet, has been developed. The Liplet is designed to control the flow in the interference region locally; helping to merge engine outflow with the flow around the wing. Figure 7.34 shows the schematic sketch of the liplet. The liplet is a small wing installed on the pylon just downstream of the upper part of the nacelle fan cowl trailing edge and its shape is smoothly contoured from the nacelle fan cowl (References 7.61).

7.6.5 Spanload

The wing spanload distribution can be significantly affected by the installation of the nacelles (see Figure 7.35). At constant angle of attack, the typical effect is to decrease the overall spanload with the largest decrease occurring outboard of the nacelle. Contouring and locating the nacelle and strut to minimize the effect on the spanload will tend to help in reducing the induced drag of the configuration. The nacelle interference drag is directly related to the nacelle influence on the spanload distribution (References 7.1).

7.7 INITIAL WING DESIGN FOR ATRA-100 BASELINE

The transport wing design procedure is a continually evolving process. The process has evolved from one of only wind tunnel testing mixed with considerable experience to a procedure that includes tunnel testing, experience and analytical computational aerodynamics. With the advent of computational aerodynamics (see also Chapter 8) the process used to achieve a successful wing design has been improved. Both wind tunnel testing and computational aerodynamics techniques are still required so that the wing design process will continue to change and improve with time.

Although many wing design procedures provide a first-cut try at a "good" wing design, the procedure is not substantiated well enough to guarantee a successful design without considerable wind tunnel testing. It should be anticipated that several cycles of wind tunnel testing will be required to achieve a successful wing design. The primary deficiencies in computational aerodynamics include inadequate modelling of separated and vortex flow, no detailed shock/boundary layer interaction scheme, no adequate drag calculations and no body boundary-layer simulation.

It is beyond the scope of this work to undertake a complete wing design, as described above. An inverse code suitable for use as a design tool was not available at Cranfield University. During the course of the study, only a generic analysis code could be utilised (i.e. RAMPANT, offering 2D and 3D, inviscid/viscous and incompressible/compressible capabilities). Taking into account of the wing design

considerations described in the previous Section, a simplified wing design procedure was used for this work and is described in the following Section.

7.7.1 Aerodynamic Design Objectives

The main objectives of the ATRA-100 wing design, which incorporates HLFC and VCW technology are :

1. To obtain a pattern of approximately straight isobar sweep at an angle at least equal to the wing sweepback angle, with the upper surface generally being critical for drag divergence. If this aim is achieved, the flow will be approximately two-dimensional and the drag-divergence will occur at the same Mach number every where along the span.
2. To obtain the greatest possible amount of laminar flow on the wing (3D flow), which will significantly improve wing efficiency (L/D) in cruise flight. The maximum reduction in drag for the wing must be obtained for the cruise C_L corresponding to the design case for the proposed aircraft. To achieve the laminar flow objectives for the design, it also was required that the pressure distributions determined in section 7.3.2 (suitably interpolated over the span) should be realized by the three-dimensional wing.
3. To have a good performance in off-design operation.

7.7.2 Development of Three-Dimensional Geometry

From a structural point of view (i.e. : initial aeroelastic check, see Figure 2.6) the ATRA wing with an aspect ratio of 9.5 should have a root section with thickness chord ratio greater than 14.9%. For an aircraft cruising at Mach 0.8, a typical outboard section thickness chord ratio is about 11% (see Appendix A). The thickness distribution requirement for ATRA's wing is shown in Figure B.10. It will be shown in the following sections, that the above requirement was not achieved by this design because of insufficient sweep for Mach 0.8 (freestream).

To achieve the laminar flow objectives of the design, it was also required that the pressure distributions discussed in the previous section (suitably interpolated over the span) should be realized by the three-dimensional wing.

Use of computer programs capable of designing swept wings to give specified pressure distributions in transonic flow and in the presence of a fuselage and engine nacelle (for wing mounted engine configuration), followed by wind tunnel testing, would be required to develop a final wing design.

Experience shows that it is best to begin with a subcritical design case (Reference 7.28). To get good results from a subcritical design code such as SWEPTDES (Reference 7.64), the target pressure distribution also must be subcritical. Figure 7.36 indicates how the subcritical pressures typically differ from the pressures at the design Mach number. Note that the subcritical upper surface C_p distribution has a

peak near the nose. Despite the simplification afforded by use of a subcritical analysis, it still was necessary to design the wing iteratively.

For purposes of this study, with help of Professor A. J. Bocci (Aerodynamics consultant, formerly based at ARA - Bedford), SWEPTDES was used to design the sections for ATRA-100 wing. Section data taken from Reference 7.28 were used as an initial input. The section co-ordinates were digitized by using CATIA (Reference 7.65), and then the sections curvature smoothness (d^2z_n/dx^2) were checked by the following equations (Reference 7.12) :

$$d^2z_n/dx^2 = ((z_{n+2} - z_{n+1}) - (z_{n+1} - z_n)) / dx^2 \qquad (7.8)$$

where : z_n = section ordinate
dx = absisca interval between z_{n+1} and z_n

Subcritical pressure distributions corresponding to this geometry were then computed by SWEPTDES. These pressure distributions were then adjusted to meet the previously discussed requirements. The aerofoil design process was necessarily iterative. A SWEPTDES aerofoil design computer program was then used to design a set of wing sections plus a twist distribution that gave the required spanwise lift variation. A preliminary transonic analysis was also undertaken using RAMPANT (Reference 7.66). Figure 7.37 shows a simplified HLFC-VC combination wing design process used in this work.

7.7.2.1 Outboard Wing Design

Design of the outboard wing is of primary importance in achieving the performance objective of a high critical Mach number and $M(L/D)_{max}$. Since drag divergence is usually associated with shock development and separation on the outboard wing, care must be taken in tailoring this part of the wing. The outboard wing is arbitrarily defined to be from the first Yehudi break out to approximately 90% semi-span, see Figure 7.38. With the wing planform and 2D aerofoils selected from the Aerodynamic Design considerations section, the objective is to tailor the 3D outboard wing to achieve an equivalent 2D aerofoil performance or better. Usually the outboard wing thickness distribution is constant and therefore, a constant aerofoil section is used in generating the wing geometry. With use of a constant section it is hoped that a constant shock position and strength and constant section lift will be achieved.

Scaling aerofoils to change thickness is typically done about either the aerofoil section chordline or camberline. Transonic similarity rules suggest that scaling should be about the chordline. Correlation of aerofoil section pressure distributions for aerofoils scaled using transonic similarity is given by the following equations (Reference 7.1).:

$$C_{p.s} = C_p((M_\infty^2(\gamma + 1))^{1/3}) / (\tau^{2/3}) \qquad (7.9a)$$

$$(M_\infty^2 - 1) /(M_\infty^2 \tau (\gamma + 1))^{2/3} = -1.578 \qquad (7.9b)$$

where : $C_{p.s}$ = pressure coefficient for scaled aerofoil
C_p = pressure coefficient for original aerofoil

M_∞ = free stream Mach number
γ = ratio of specific heat capacities (taken as 1.4)
τ = scaled airfoil thickness ratio to original aerofoil

Scaling about the aerofoil camberline has not shown good correlation and should not be used. Scaling thickness by keeping the upper surface fixed and modifying the lower surface has not been analyzed in sufficient detail to understand its utility. Scaling techniques are outlined in Figure 7.39 (Reference 7.1).

The aerofoil section design lift coefficient has a dominant effect on airplane drag. A section design lift higher than calculated using the modified simple sweep theory provides better polar shape for a slight penalty in profile drag and drag rise. Design lift coefficients can be calculated by the following equation (Reference 7.1) :

$$C_{l.design} = 1.1(C_{L.design}/\cos^2 \Lambda_s) \qquad (7.10)$$

where : 1.1 (1.2) to account for maximum section lift to wing lift ratio
Λ_s = shock sweep, deg.
$C_{l.design}$ = aerofoil section design lift coefficient
$C_{L.design}$ = wing design lift coefficient

The technique for applying 2D airfoils to 3D swept, tapered wings to achieve the equivalent 2D aerofoil performance is controversial. The process of applying 2D aerofoils either streamwise or perpendicular to some constant percent trapezoidal chordline is the most common. When aerofoils are scaled about the section chordline, the same 3D streamwise aerofoil geometry is obtained whether the sections are placed streamwise or perpendicular.

Wing upper surface isobars (constant Cp's) are the key to the wing performance and achievement of the equivalent 2D aerofoil performance. Usually isobars are defined to be swept along constant percent chordlines on the outboard wing. Constant percent chordline isobars are desirable so that at transonic speeds the shock strength and location and section loading will be constant. This is relatively easy to achieve for a trapezoidal wing with constant thickness. The chordwise values of the isobars are directly a function of the aerofoil pressure distributions and are left to the discretion of the designer.

For an outboard wing with a varying maximum thickness ratio, the objective is to maintain isobars that are swept along constant percent chordlines. To achieve this goal will require camber modifications that will probably result in characteristics equivalent to thicker aerofoil sections (Reference 7.1).

ATRA-100's Outboard aerofoil section design goals were : (1) to sustain laminar flow to 55% chord (or more) on the upper surface with minimum suction quantity and (2) to suffer little or no flow separation or wave drag at Mach 0.8, wing lift coefficient 0.5, and 25 degrees quarter-chord sweepback.

It is beyond the scope of this work to design an airfoil. An aerofoil from Reference 7.28 was used for ATRA-100 wing's outboard section. This aerofoil was designed for a typical outboard section at a normal Mach number (M_N) of 0.744,

reflecting a sweepback angle of 21.5 deg., corresponding approximately to the 50% chord line outboard. The design lift coefficient (C_{l_N}, based on the normal flow) was 0.64 and the airfoil thickness chord ratio (t/c) is 10.3%. Figure 7. 40 shows the pressure distribution and profile of the section.

To facilitate design process, the outboard wing thickness distribution was selected constant and therefore, a constant airfoil section is used in generating the outboard wing geometry (see Figure B.10).

To simplify the modelling in SWEPTDES and RAMPANT, the trailing edge thickness of the above airfoil section is removed by the following equation (Reference 7.12) :

$$(Z_u/C)_{t.te=0} = (Z_u/C) - (X/C)(t.te/C)/2 \qquad (7.11a)$$

$$(Z_l/C)_{t.te=0} = (Z_l/C) + (X/C)(t.te/C)/2 \qquad (7.11b)$$

where :
- $(Z_u/C)_{t.te=0}$ = upper surface section ordinate for aerofoil with t.te/C = 0
- (Z_u/C) = upper surface section ordinate for aerofoil with t.te/C > 0
- $(Z_l/C)_{t.te=0}$ = lower surface section ordinate for aerofoil with t.te/C = 0
- (Z_l/C) = lower surface section ordinate for aerofoil with t.te/C > 0
- (X/C) = section abcisca
- $(t.te/C)$ = trailing edge thickness chord ratio

Figure B.13 shows the profile and coordinate of the ATRA-100's outboard wing aerofoil section (streamwise) and Figure 7.41 shows the subcritical pressure distribution of the ATRA-100's outboard wing aerofoil section obtained from SWEPTDES.

7.7.2.2 Wing Root Design

With the outboard wing geometry defined, the next objective is to tailor the wing root. A well-tailored root is required because of the dominant influence the inboard wing has on the outboard wing performance. A change in upwash at the root affects the entire spanwise upwash distribution on aft swept wings. No precise methods exist to tailor the root sections of a wing. Figure 7.42 illustrates schematically isobar patterns on the upper surface of a typical, thick and lifting sweptback wing (Reference 7.49). It has been recent design philosophy to have the inboard wing subcritical Mach number isobars sweep forward near the fuselage side (Figure 7.42c) compared to extensions of the outboard wing constant percent chordlines (Figure 7.42b). This design technique is intended to eliminate strong "normal" shocks from developing near the side of fuselage and effectively increases the shock sweep allowing the outboard wing to achieve its predicted performance. Wings with Yehudis are more difficult to tailor because of the tendency for the isobars to sweep aft on the inboard wing making the design more challenging. On the other hand, wings with gloves are easier to tailor as the isobars tend to sweep forward. The airfoil section tailoring required to sweep forward the inboard wing isobars, for wings with a Yehudi, will probably require moving the inboard wing maximum thickness forward. A forward movement of 10 to 20 % chord

compared to the outboard aerofoil section is typically required. Tailoring of the inboard wing aerofoil section camber, twist and thickness forms was used to satisfy the spanload and isobar goals. An alternative approach would be a straight line extension of the outboard maximum thickness location to the side of fuselage. This usually requires a larger lower surface modification that may result in undesirable lower surface pressures. Moving the maximum thickness aft on the inboard wing has been found to give unacceptable results. Note that the further aft the maximum thickness is located the larger the rear spar depth and the lower the wing weight (Reference 7.1).

Tailoring of the inboard wing is highly dependent on the wing planform geometry and required thickness distribution. For low-wing designs the pressures tend to be increased at the lower surface. This may be turned to advantage by locally thickening the lower part of the section and bending the nose of the root section slightly upwards. This results in a root section with negative camber which is a few percent thicker than the outboard wing (Reference 7.31). Wash-in of the inboard wing is usually required to increase the lift on the inboard wing as well as to maintain the desired isobar sweep and spanload distribution.

Taking into account all the above considerations, for the ATRA-100's wing root section, a higher thickness ratio was required. To keep the same maximum local Mach number on the upper surface, the pressure on the lower surface has to fall, thus reducing C_{l_N}. Because of the increased chord inboard of the planform break, this was still consistent with smooth and monotonic spanwise loading variation. Another difference was that maintaining isobar sweepback required shifting the upper surface pressure recovery point forward. Figure 7.43 illustrates these differences. The design C_{l_N} was 0.4 (Reference 7.28). Note that the resulting profile will not produce this pressure distribution when located close to the fuselage in a real flow. It is only one step in the design of the three-dimensional wing geometry in this section.

Figure B.11 shows the profile and coordinate of the ATRA-100's root wing airfoil section (streamwise) and Figure 7.44 shows the subcritical pressure distribution of the ATRA-100's root wing aerofoil section from SWEPTDES. In addition to having greater thickness ratio (t/c) and maximum thickness location more forward compared to the outboard wing aerofoil section, it has perceptible inverse camber near the leading edge and a lower surface with reduced aft loading.

7.7.2.3 Wing Inboard Design

The middle (inboard) aerofoil section, illustrates a transition shape in the part of the wing (between side of fuselage and planform break/kink) where thickness chord ratio (t/c) is decreasing. Figure B.12 shows the profile and coordinate of the ATRA-100's inboard wing aerofoil section (streamwise) and Figure 7.45 shows the subcritical pressure distribution of the ATRA-100's inboard wing aerofoil section obtained from SWEPTDES.

7.7.2.4 Wing Tip Design

Varying opinions exist on the wing tip tailoring required to achieve a good wing design. The raked/curved tip is one of several methods used to improve and prolong the outboard wing shock sweep near the tip. By locating the leading edge further aft and reducing the tip chord compared to the trapezoidal wing, the isobars are pulled aft. This effectively keeps the shock swept along constant percent chordlines while not unloading the tip. A disadvantage of the raked tip is that the leading edge protection is not carried to the tip and therefore the possibility exists for a low speed pitch-up problem. Figure 7.46 shows the Kuchemann tip (Reference 7.49).

An alternate approach to tip tailoring to improve the wing shock sweep involves modification of the wing tip airfoil sections. The tip airfoils are tailored compared to the outboard wing sections by moving the maximum thickness aft (maybe 10 % chord) and increasing camber to maintain the section lift. This approach moves the crest of the tip airfoils aft and therefore improves the isobar sweep as the tip load decreases (Reference 7.1). The above approach was also tested and proved to be largely successful by J. Weber (1949).

Wash-out of the wing tip is the third method to improve the wing effective shock sweep. The additional wash-out moves the airfoil crest aft, trapping the shock, and rotating the lift vector forward. Although the section lift is reduced there is the added benefit of delaying tip stall and reducing aircraft pitch-up. Raked/curved tip designs are probably most effective in improving shock sweep; however, a combination of section tailoring and wash-out could be as effective (Reference 7.1).

Since induced drag accounts for about one-third of total aircraft drag in cruising flight and as much as one-half during climb, it is valuable to look more closely at this drag element to highlight the possibilities and limitations for it's reduction. Figure 7.47 shows several wing tip devices concept. For more detail about this subject, see References 7.67-7.70.

Winglets/aerodynamic fences are small vertical mini-wings added to the wing tips, which themselves have planforms with very high leading edge sweep back. Figure 7.48 shows winglets for the Airbus A300-600, A310-300 and Boeing B737-800 (Reference 7.70 and 7.71). It is this distinctive feature that helps give them innocuous qualities over the whole flight envelope. Under conditions when the flow stalls over a straight or low-to-moderate swept back wing, a highly swept planform generates a well-ordered leading edge vortex flow, giving no sudden changes in aircraft handling characteristics. This is also true if premature stalling were to be caused by ice forming on the leading edge of the winglet, the high sweep feature again reducing its effects under conditions when the main wing is protected by a hot air anti-ice system. This design also minimises another undesirable effect. Because winglets tend to maintain the different pressures above and below the main wing, they must increase the lift near the wing tip. Although the effect is not as large as for a span extension , they do affect the bending load on the inner wing. The new design minimises this effect at the manoeuvre conditions that control the strength and hence weight of the wing. With these winglets, it is obviously essential that any effects on wing strength must be kept small to stay within existing structural margins, or to ensure that only minimal further changes to the

main wing were necessary. It is also essential that winglets should stall under similar conditions with the main wing, if not winglets will lead to increased drag, or affect the handling of the aircraft (Reference 7.70).

Taking into account all the above considerations, for the ATRA-100's wing, to improve the shock sweep, a combination of a raked/curved tip and wash-out was selected (see Figure B.8 and B.9). To reduced induced drag, an Airbus winglet type could be implemented on this wing.

7.7.2.5 Off-Design Operation Consideration

Practical use of HLFC requires that laminar flow be maintained through a range of cruise lift coefficients and Mach numbers. Changes in lift coefficient and Mach number will change the wing pressure distributions from the optimum and may result in some loss of laminar flow. Therefore, the ATRA-100's wing incorporates a VC-flap. Deflection of the VC-flap permits control of the pressure distribution over the forward part of the airfoil, keeping it similar to the design pressure distribution even when the lift coefficients and Mach numbers differ considerably from the design values. The desired pressure gradient control can be achieved not only during cruise, but also during a significant portion of climb and descent.

The design concept of the variable camber wing for ATRA-100 is described in Chapter 5 and section 7.8 of this thesis.

7.7.2.6 Spanload Design

Choices of spanwise section loading and taper were discussed previously in the section on Aerodynamics Design Considerations. Outboard wing section loading will typically be constant and the wing taper ratio will be approximately 0.25 to 0.35. If weight/drag trades have not been made, then designing the spanload to an elliptical distribution is probably a good first choice. This will provide the least drag and will be a good point for beginning the design trades (Reference 7.1).

7.8 APPLICATION OF VARIABLE CAMBER FLAP TO THE ATRA-100'S WING

The application of the variable camber concept, described in Chapter 5, to the three-dimensional wing of ATRA-100 is examined in the following Section. The concept of varying the camber of an airfoil in the manner outlined in Chapter 5 appears relatively straightforward, if we restrict ourselves to two-dimensional considerations only. However, for the scheme to be adopted for the ATRA-100, it must be applied to a tapered wing with a kink (Yehudi) and 25 degree of a quarter-chord sweep (as shown in Figure B.8). For a workable scheme to result, it is necessary for the flap configuration to conform to a number of geometrical constraints.

7.8.1 Flap Segmentation

The design objective of most variable camber wings has been the ability to vary the distribution of camber across the span of the wing. The provision of this capability inevitably adds to the complexity of a flap scheme, but it is necessary if the full performance benefits are to be obtained.

Ideally, from aerodynamic considerations, it is desirable to maintain a smooth and continuous wing surface across the whole of the span at all camber settings. However, this would necessitate the use of accurately supported wing skins that possess the ability to stretch, flex and warp. This was considered to be beyond current or immediately foreseeable engineering capabilities.

To control the load distribution across the span of the wing, it is necessary to resort to the application of spanwise variation in camber in a number of discrete spanwise steps or segments. This also prevents incompatibilities developing during wing flexure and enables the provision of roll control. The size of these segments depends on a number of criteria (Reference 7.72) which include :

1. Optimum load distribution characteristics with minimum structural and mechanical component weight.
2. Loss of lift and therefore increased rolling moment due to loss of a segment.
3. Flap flexure and bending moment and track positions (or hinge reaction points)
4. Practical restrictions, i.e. fuel space, engine positions, main wing pick up rib position.

Spillman (Reference 7.73) and Airbus (References 7.5 and 7.74) have proposed the use of about six spanwise segments in a typical subsonic wing semi-span. This figure represents a compromise between aerodynamic efficiency and mechanical complexity considerations. An additional factor is the ability to continue to fly safely with any one flap segment inoperative. In the absence of a detailed investigation, it was decided to use six flap segments per wing for the variable camber ATRA-100.

The objective of flap segmentation is to have spanloading as close as possible to the elliptic loading at any combination of camber settings at all flight regimes. The sizes of the individual flap segments were set to be : two inboard flap segments with the same flap span, three outboard flap segments with the same flap span, and one segment flaperon, as shown in Figure B.8.

7.8.2 Three Dimensional Considerations

Most swept tapered wing subsonic transport aircraft are forced to use flap movements that lie somewhere between a true conical (spanwise constant percentage of the chord) and streamwise motion for the outboard flap and a constant motion for the inboard flap. This is compromise results from the use of wing twist, spanwise variation of aerofoil section and a preference for constant chord inboard flaps in order to leave room for undercarriage stowage (Reference 7.52, 7.24 and 7.26).

The system concept of variable camber used in the ATRA-100's wing is very similar to traditional high lift devices; the flap motion used for the ATRA-100's

variable camber wing is : natural conical motion (spanwise constant percentage of the chord) for the outboard flap and a constant motion for the inboard flap. The above concept was also been proposed by Airbus (Reference 7.5).

7.8.3 System Design

As stated above, the system concept of variable-camber used in the ATRA-100's wing is very similar to the traditional high lift devices. A schematic of the system solution is given in Figure 5.8 and 7.49. The camber variation is achieved by small rotation motions (in two directions for positive and negative deflections), where the wheels of the flap carriage are guided by two individual tracks in such a way, that in VC-operation the flap body slides between the spoiler and deflector door trailing edge. The radius of flap rotation is picked from the radius of curvature of the airfoil trailing edge upper surface at about 90% chord, hence camber variation is performed with continuity in surface curvature at all camber settings. During this process the spoiler position is unchanged. The deflector door is shaped such that the transition from one camber setting to the next is smooth on the lower surface of the VC-flap. Computational investigations showed no aerodynamic effects due to a slight kink appearing at the hinge point of the lower surface of the deflector door (Reference 7.92). The deflector door on the lower side is hinged at the main wing side and spring loaded so that it automatically deflects to follow the movement of the VC-flap and remains continuously attached to the VC-flap.

The natural conical motion (spanwise constant percentage of the chord) of the outboard flap is combined with a constant motion of the inboard flap thus enabling working on a common torque shaft and avoiding the need for additional variable camber drives.

For the inboard flap, the track radius is same across the span. Thus enabling to use the conventional approach. The flap segments are supported by two tracks (inboard and outboard of a flap segment). The flap segment stiffness should be considered, otherwise the flap segment will be bent in the middle during the flap movement. The flap segments are actuated by a dual load path rotary actuators placed at the center of each flap segments.

For the outboard flap, the track radius varies across the span. Thus if the flap segments is made rigid and supported on say two tracks (inboard and outboard of a segment), on actuation the segment will either be reluctant to move or it will tend to ride more on the larger (inboard) track. The later will give an undesirable lateral movement. In order to eliminate this effect the flap segment must be made to flex both across the span and chord. This way the flap segment will effectively have to deploy independently on the two tracks. With a flexible flap segment the system could quite simply be driven by a pair of dual load path rotary actuators placed at the end of each flap segment (in other words, there are two flap actuator on each flap track, one for inboard side flap segment and the other is for outboard side flap segment). Independent input to these actuators would ensure adequate deployment with twisting of the flap segment across the span for parallel motion.

As already described in previous section a spanwise camber variation could be used to redistribute spanwise loading in order to control buffet or minimize drag (Reference 7.5). This would require independent input commands at nine spanwise stations (two actuators for the two inboard flap segments, six actuators for the three outboard flap segments and one actuator for the flaperon) through differential gears thus increasing the complexity of the system and maintenance and reducing the reliability of the mechanical drives. The above system is shown in Figure 7.49.

7.8.4 Effect of Gaps Between Flap Segments

The spanwise split between the segments can cause excess drag due to induced vortices (Reference 7.75) and loss of lift. To reduce or prevent these vortices and lift loss, a plate may be introduced between each segment in order retain the airflow. These "splitter" plate are likely to be twice the depth of the airfoil in order to cover the full VC deflection range (Reference 7.72). The drag of splitter itself must be considered.

An alternate approach to reduce or prevent these vortices and loss of lift involves closing the gap by connecting those adjacent flap segments with a flexible material (i.e. rubber).

7.9 HYBRID LAMINAR FLOW CONTROL DESIGN

The design for HLFC must provide easily removability to permit inspection and repair/replacement of the leading edge structure, a suction surface, a high-lift system, a cleaning system, an anti icing system, cabling and suction ducting. Processes must be developed to ensure that subsequent to maintenance, the surface finish is within the required tolerances for laminar flow.

This section examines how to implement the HLFC design concept described in Chapter 5 on the ATRA-100 aircraft.

7.9.1 Prevention of Attachment Line Transition

In addition to the Tollmien-Schlichting and crossflow instabilities previously discussed, there is a third mechanism that can cause premature boundary layer transition. It arises at the leading edge of sweptback wings, where the local flow is outward along the attachment line rather than across the wing.

As described in Chapter 6, the leading-edge transition depends on the attachment line boundary layer momentum thickness Reynolds number ($R_{\theta al}$) and on the magnitude of disturbance present. Because $R_{\theta al}$ is proportional to the square root of the leading-edges radius, one way to prevent attachment line transition is to use a relatively sharp-nosed airfoil (A related approach would be to use an undercut airfoil shape, which provides a reduced nose-radius and increased the initial velocity gradient,

as proposed by Pfenninger (Reference 7.76) and shown in Figure 7.50). The leading-edge design, however, is constrained by the requirement for operating over a reasonable angle-of-attack range without a pressure peak on either surface. Suction can also be used to thin the attachment-line boundary layer; $R_{\theta al}$ can then be reduced to any desired value independently of the leading-edge radius (Reference 7.28).

Several inboard wing modifications, including a Gaster bump or a fence (with or without suction) near the wing root to isolate the fuselage boundary layer, are effective in preventing contamination of attachment flow and/or excessive disturbance growth leading to premature transition (Reference 7.8, 7.28 and 7.76). Careful consideration is required when locating the bump or fences along the span. The bump or fences should be placed outside the fuselage boundary layer. However, as laminar flow is not possible inboard of the bump or fences, the distance of the bump or fences from the side of fuselage should be minimized. In designing the Gaster bump, the integration with leading-edge high-lift devices and de-icing systems should be considered. Figure 7.51 shows the effectiveness of the Gaster bump for turbulence contamination avoidance along the attachment line (Reference 7.77).

7.9.2 Leading Edge Systems Design

As described in Section 5.4, for ATRA-100 configuration, a leading-edge systems concept proposed by Douglas was selected, as shown in Figure 7.52. Suction is applied only on the upper surface, from just below the attachment line to the wing front spar. It is clear that the position of the front spar is critical, it's position is a compromise between suction requirements, structure requirements and fuel volume requirements. Douglas studies showed the upper surface suction concept to be most cost-effective because of reduced maintenance requirements, less weight and initial cost compared to suction on both surfaces. Elimination of the lower surface suction systems and the stringent smoothness requirements permits the use of a Krueger high lift device (Reference 7.78). The practical advantages of such an approach may more than compensate for the turbulent drag of the lower surface as discussed in Reference 7.79. To isolate the fuselage boundary layer, fences or a Gaster bump could be used.

7.9.2.1 Suction system design

The main part of HLFC application is the suction system. Clearly this must be capable of suppressing any boundary layer disturbances over the forward part of the surface, such that the flow remains laminar for some distance downstream of the suction surface. Air is drawn through the surface into the suction plenum chambers, where in this case it is gathered into a smaller number of collection chambers via metering holes. These chambers are connected by pipes to a main spanwise collector duct which transports the air to the suction unit (compressor). Downstream of the suction unit the air is exhausted to the atmosphere. This suction system is proposed in Reference 7.87 and is adopted to the ATRA-100's laminar wing.

In the present study, panels with holes are often considered for use as the suction surface because the structural design is more straightforward and because modern electron beam and laser drilling techniques permit economical fabrication of sheet metal with large numbers of small, uniform, evenly spaced holes (offering structural advantages). The problem is to establish criteria for suction system design and more specifically for the following parameters : Hole diamater, Hole spacing, Hole pattern and Thickness of the sheet. The velocity in the holes must be small enough to prevent a premature transition due to horseshoe vortices. However, the chosen pattern must create pressure drops across the panel which are sufficiently high to avoid outflow in the compartments due to the external pressure gradients. The optimization of the design parameters is a compromise between these constraints (References 7.28 and 7.8).

To prevent transition due to suction, both the hole size and the hole spacing must be small compared to the boundary layer thickness. According to Reference 7.80, a hole suction surface will function satisfactorily if the suction velocity (u_{hole}/U_e) is kept below the critical value shown in Figure 7.53. Some basic dimensions of the hole-type suction surface are given by Boeing (Reference 7.28). A hole diameter of 0.0635 mm (0.0025 in) and a hole spacing of 0.635 mm (0.025 in) with the holes laid out in a square arrangement gives a porosity of 0.785 % of the surface area. In addition, there is adequate margin to allow up to 50 % of the holes in a given region to be blocked off (if necessary for structural purposes) without violating the criteria. Douglas (Reference 7.78) has proposed the use of a hole diameter of 0.0635 mm (0.0025 in) and a hole spacing of 0.762 mm (0.030 in) on the 0.635 mm (0.025 in) thick titanium panel sheet, and was successfully tested and was reported in Reference 7.81.

In the absence of a detailed investigation, it was decided to use a hole diameter of 0.0635 mm (0.0025 in) and a hole spacing of 0.762 mm (0.030 in) on the 0.635 mm (0.025 in) thick titanium panel sheet for the suction surface of ATRA-100. Panel core and inner face sheet were constructed of fiberglass. The core was corrugated to form flutes for subsurface suction air collection. Bond areas between the perforated surface and the core were impervious to flow; thus, suction on the surface was along spanwise perforated strips.

Reference 7.81 reported that the leading-edge system with the perforated suction surface presented no difficult fabrication problems. So, perforated titanium emerges as suction surface material that can be worked with practical fabrication methods to meet the stringent, laminar flow surface quality requirements.

7.9.2.2 Leading-edge high lift device

The maximum lift coefficient requirement for ATRA-100 is 2.9 (see Chapter 2). From Reference 7.31, the above lift coefficient could be achieved by a combination of a single slotted Fowler flap and leading edge device.

Due to surface quality requirements, conventional leading-edge slats cannot be used on a HLFC wing in low speed conditions and specific studies must be undertaken in order that current values of maximum lift coefficient in landing conditions be maintained. Krueger flaps have been proposed to replace the conventional leading-

edge slats as these overcome many of the difficulties in applying HLFC suction on the upper surface of the wing. For the laminar flow wing, however, Krueger-type leading-edge device have a secondary function to shield the leading edge region from damage and contamination during takeoff and landing.

Taking into account the above design considerations, it was decided to use a combination of Krueger-type leading-edge device and single-slotted trailing-edge device for the ATRA-100's laminar wing.

7.9.2.3 Leading edge insect contamination

Insect remains adhering to the leading edge can constitute roughness elements large enough to cause boundary layer transition. Therefore, a device to shield the wing or a system to prevent the impinging insects from sticking probably must be provided. This device or system must be operable whenever the aircraft is moving at appreciable speed on the ground and in flight at altitudes to 1,500 m (5,000 ft) above the ground level (Reference 7.28).

As described in the previous section, the Krueger high lift device is selected as a protective shield against insect impact. Figure 7.54 shows the Krueger insect shield trajectory analysis and wind tunnel test conducted in the NASA Lewis Icing Research Tunnel (Reference 7.82) to evaluate the effectiveness of a Krueger shield in protecting the leading edge from insect contamination. Insects of representative sizes and number density were injected into the tunnel free stream ahead of the model. These tests (supported by trajectory analysis) demonstrated that the Krueger serves as an effective line-of-sight shield for heavy insects, but suggest that a supplemental spray may be necessary to protect against possible impingement of lighter insects in some areas of the wing. For this reason, the supplemental spray nozzle system was mounted on the Krueger underside. Based on the flight test result from Reference 7.81, as shown in Figure 7.55, it was found that the shield alone was sufficient to protect the leading edge from insect impacts; use of the supplemental spray was then discontinued.

Taking into account the above experiences, for the ATRA-100's laminar wing it was decided to use a Krueger-type leading-edge device to provide the main wing with line-of-sight protection against insect impacts during takeoff and landing and part of climb. The optimization of the position of the Krueger is a compromise between its function as high-lift and shield device.

7.9.2.4 Purging system

A system is provided to purge the wing ducts and perforated surface of any fluids that might be ingested. This is simply a pressurized air source, which produced a positive 0.5 psi pressure differential across the suction surface.

Reference 7.81 reported that the system (described above) for purging the fluids from the air passages operated satisfactorily in flight and on the ground in winter or summer operations.

7.9.2.5 Anti icing system

The Krueger has a glycol fluid anti-icing system, a commercially available system (design by TKS, Ltd., Reference 7.83) which dispenses a freezing point depressant fluid through a porous strip along the Krueger leading edge. The Krueger also has a spanwise row of spray nozzles that dispenses a 60/40 mixture of propylene glycol methyl ether (PGME), a freezing point depressant, and water. These nozzles also provide ice protection for the main wing.

The above anti-icing system concept was succesfully tested and was reported in Reference 7.81.

7.9.3 Wing Surface Smoothness Considerations

An HLFC wing will require a smoother surface than a conventional wing in terms of both manufacturing tolerances and surface quality (i.e. discontinuities and waviness). This implies that a strong development of technology and the manufacturing techniques is required in order to obtain the necessary surface quality.

The admissible height of surface protuberances can be estimated by the roughness criterion, expressed in terms of Reynolds number and defined as (Reference 7.84) :

$$R_k = u_k * k / \upsilon \qquad (7.12)$$

where k is the height of the protuberance, u_k is the local velocity in the boundary layer at height k, and υ is the kinematic viscosity.

For two-dimensional protuberances, such as steps, grooves, or ridges, the critical roughness Reynolds number ranges between from 100 to 300, depending on the shape (Reference 7.85). For three-dimensional protuberances, such as rivet heads, dents, or insect contamination, the Reynolds number varies between from 200 and 600, again depending on the shape (Reference 7.86). Reference 7.28 suggested, mean values of R_k = 200 for two-dimensional protuberances, and R_k = 400 for three-dimensional protuberances.

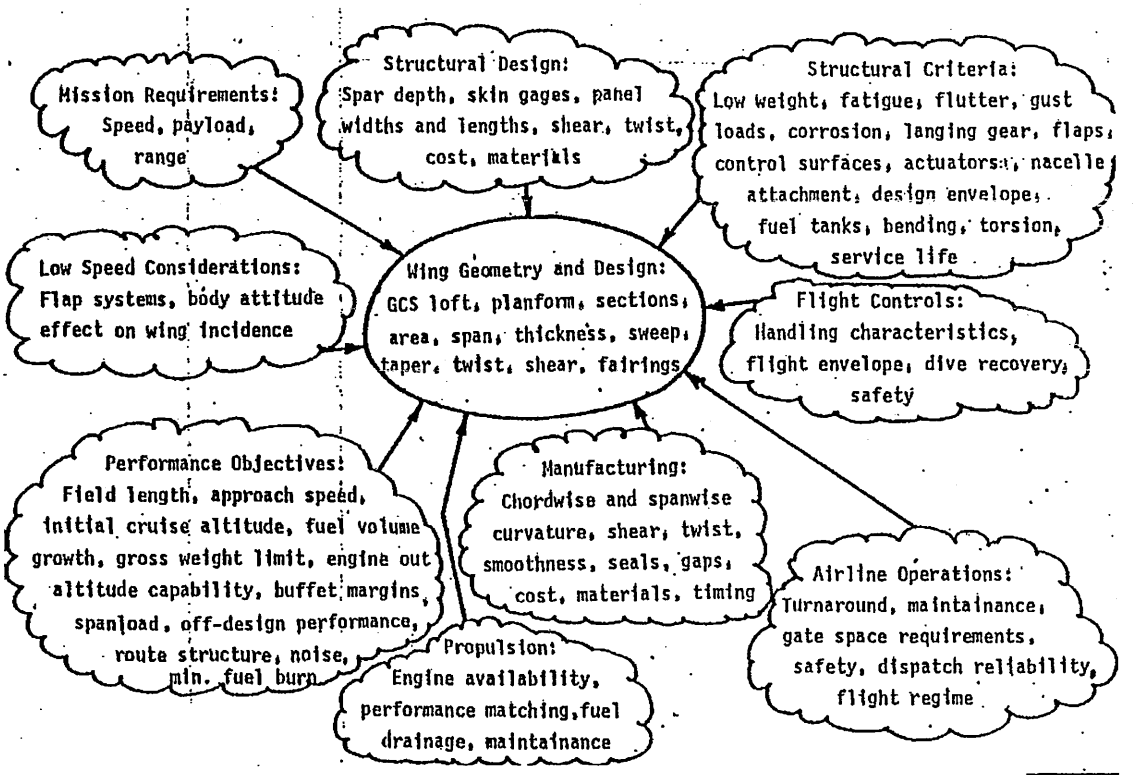

Figure 7.1 Wing design requirements and objectives (Reference 7.1)

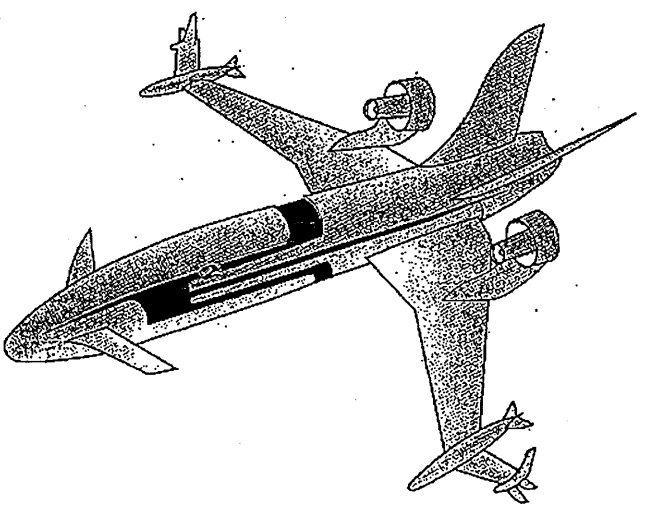

Figure 7.2 Airbus E2 theoretical concept for a medium/long range transport aircraft (Reference 7.10)

1. $M_{SWEPT} = M_{UNSWEPT}/\cos\Lambda$

2. $C_{L_{SWEPT}} \doteq C_{L_{UNSWEPT}} \cos^2\Lambda$

3. $C_{P_{"C"}} = C_{P_{"S"}} \cos^2\Lambda$

4. $(dC_L/d\alpha)_{SWEPT} \doteq 2\pi \left(\frac{AR}{AR+2}\right) \frac{\cos\Lambda}{\sqrt{1 - M^2\cos^2\Lambda}}$ (EMPIRICAL)

5. $D_{INDUCED,SWEPT} = D_{INDUCED,UNSWEPT}/\cos^2\Lambda$

6. $AR_{SWEPT} = AR_{UNSWEPT} \cos^2\Lambda$

7. $t/C_{"C"} = t/C_{"S"} \cos\Lambda$

NOTE: DEFINITIONS FOR CONSTANT STRUCTURAL PLANFORM

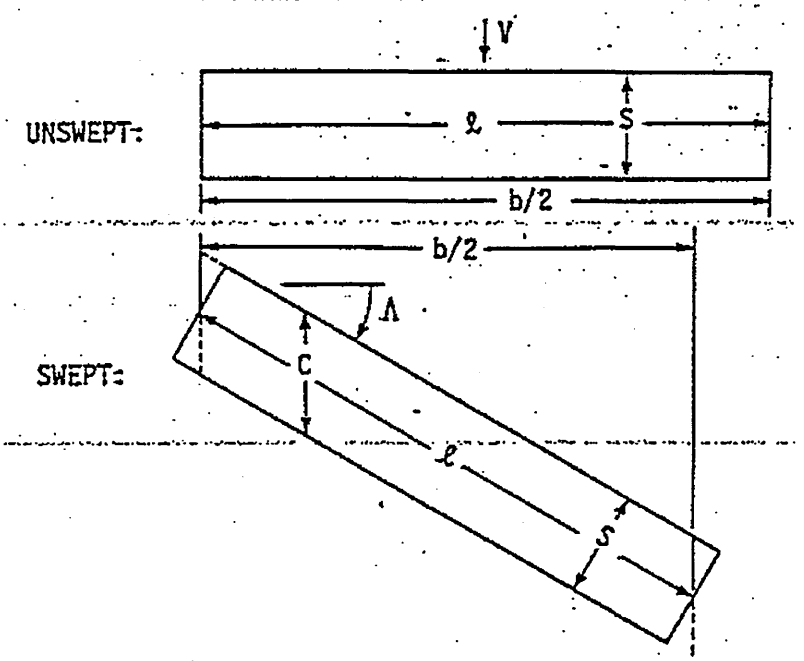

Figure 7.3 The simple wing sweep theory for infinitely long and high aspect ratio wings (Reference 7.1)

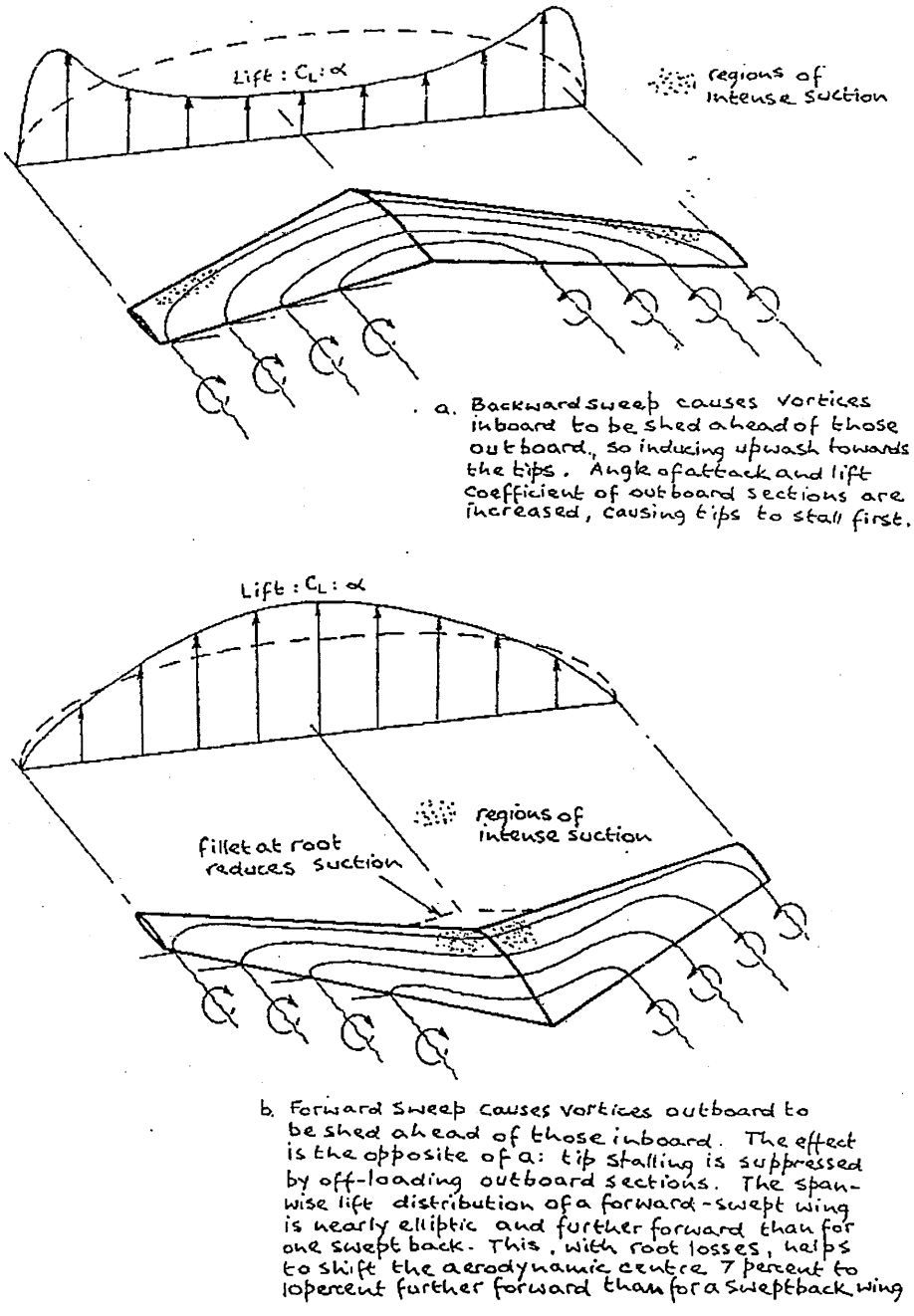

Figure 7.4 Comparison between backward and forward sweep, assuming both wings are rigid and not affected by aero-elasticity (Reference 7.27)

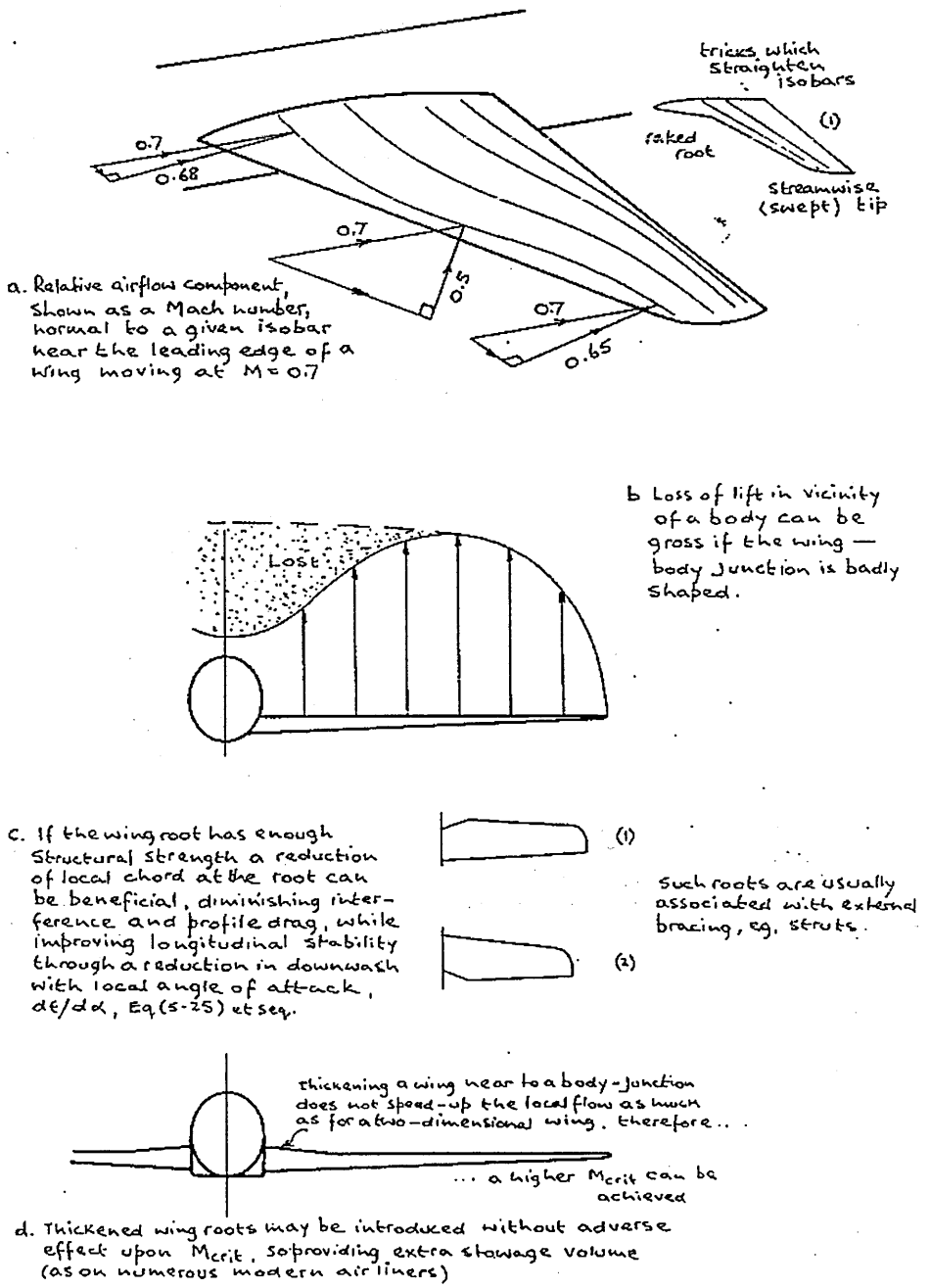

Figure 7.5 The effect of wing ends (roots and tips), from Reference 7.27

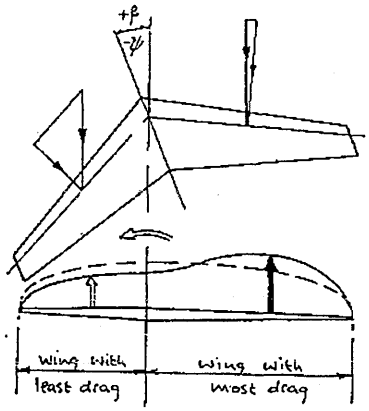

Sideslip increases lift of upwind wing, increasing dihedral effect, L_v, of a backswept wing, while augmenting 'weathercock effect', N_v, due to increased drag of the upwind wing.
A forward swept wing has the opposite effects.

Figure 7.6 Swept back wing in sideslip (Reference 7.27)

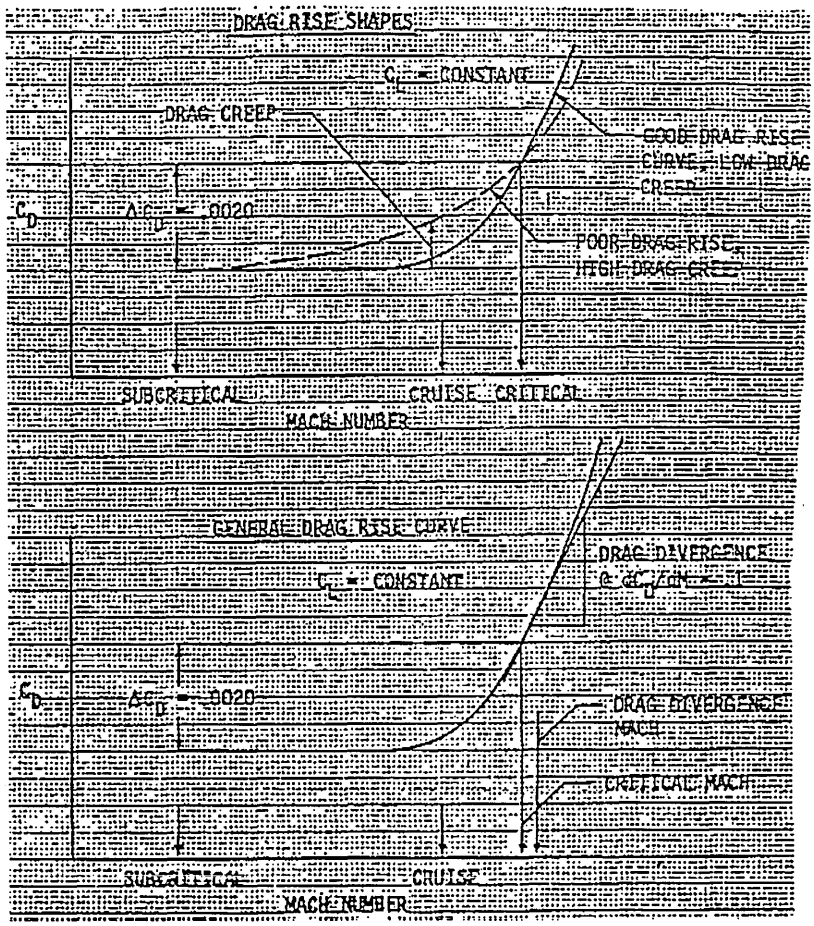

Figure 7.7 Drag rise definitions (Reference 7.1)

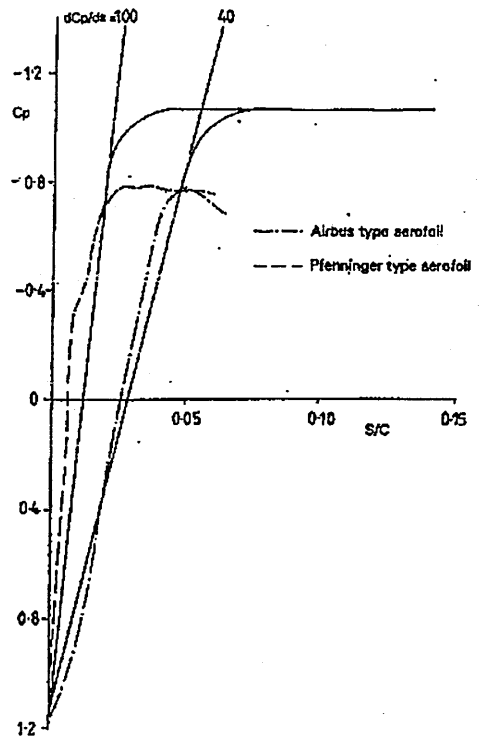

Figure 7.8 Range of practical initial pressure distributions (reference 7.30)

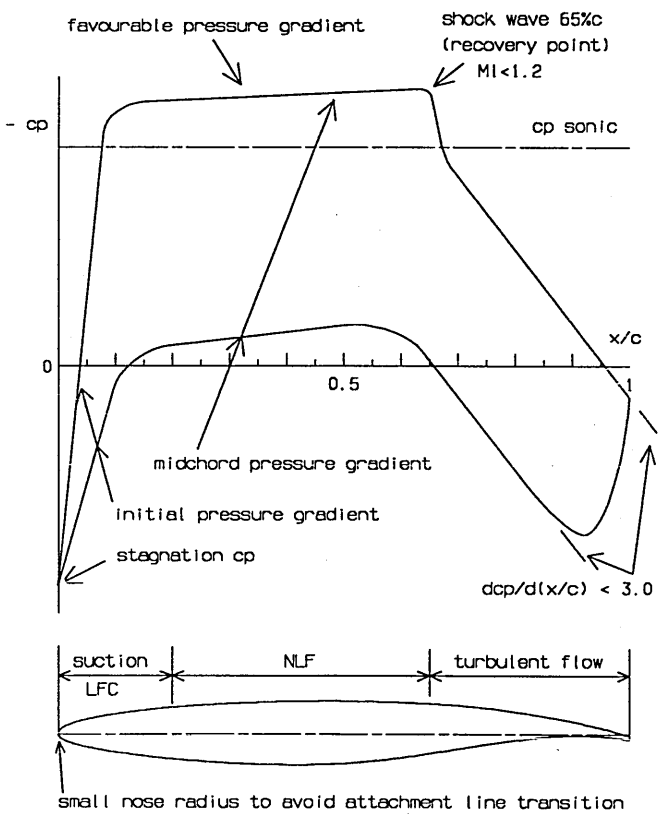

Figure 7.9 HLFC airfoil design criteria

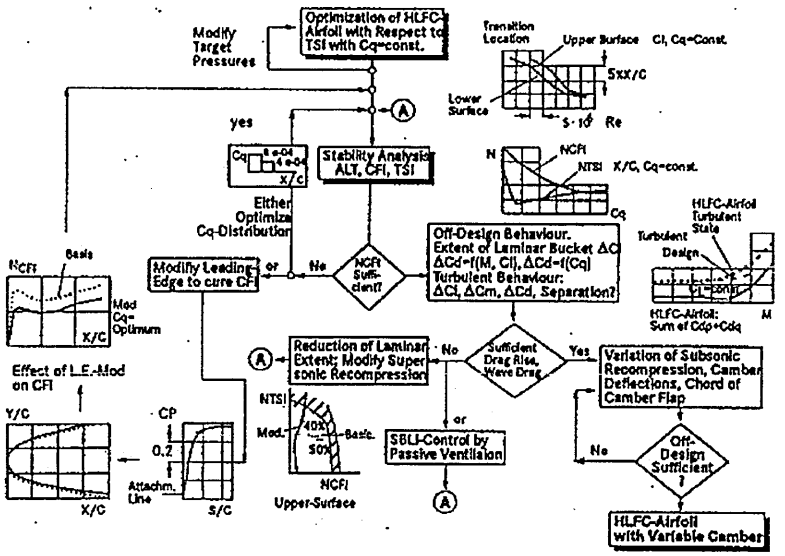

Figure 7.10 Design process of a combine HLFC - VC airfoil (Reference 7.89)

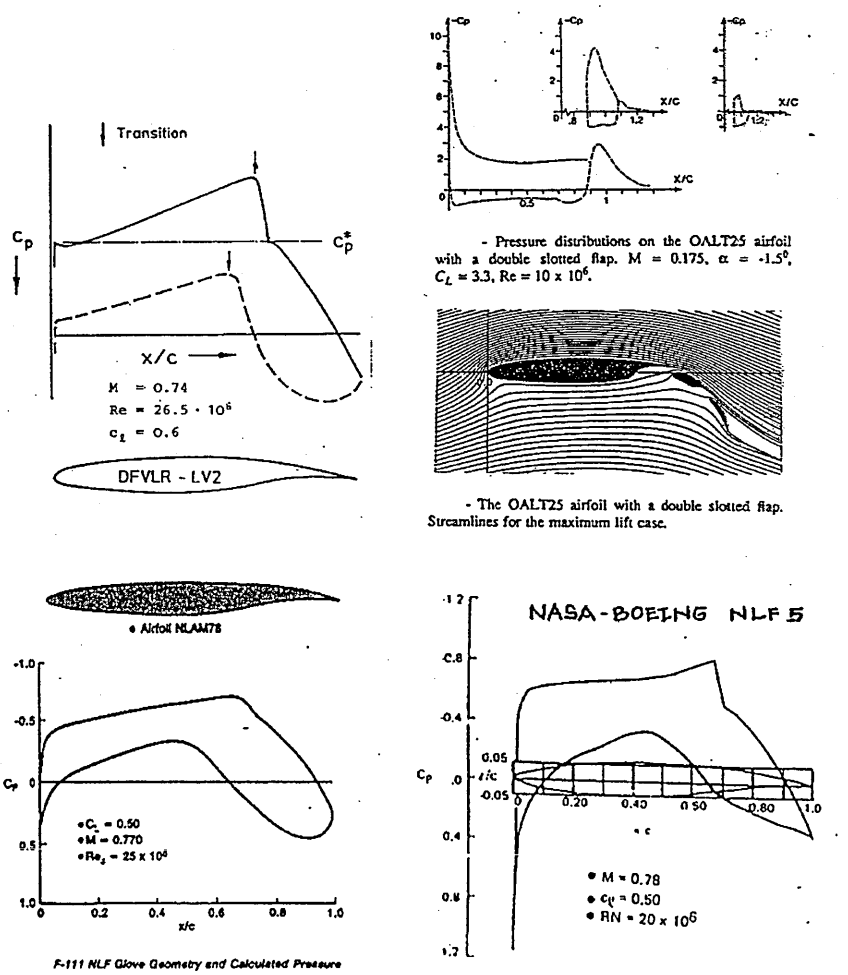

Figure 7.11 Laminar airfoils (Reference 7.44, 7.8, 7.88 and 7.29)

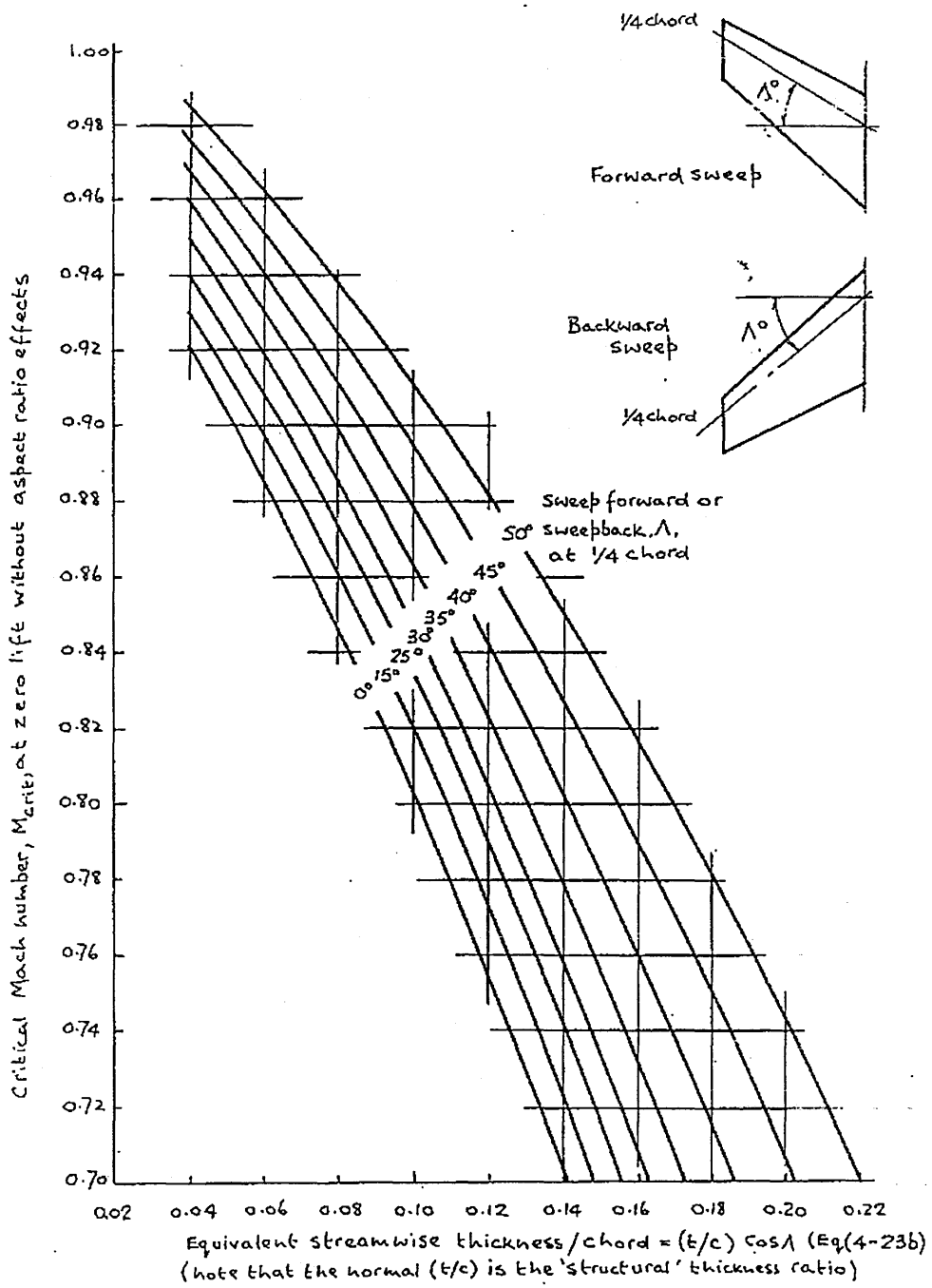

Figure 7.12 The effect of aerofoil sweep at the 0.25 chord upon fineness and, hence, critical Mach number (Reference 7.27)

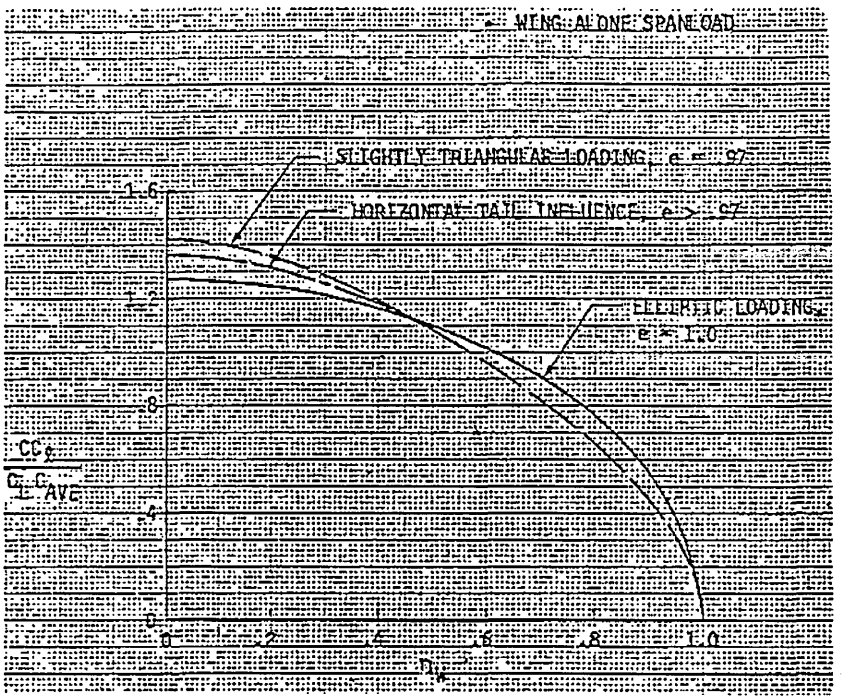

Figure 7.13 Horizontal tail influence on spanloading (Reference 7.1)

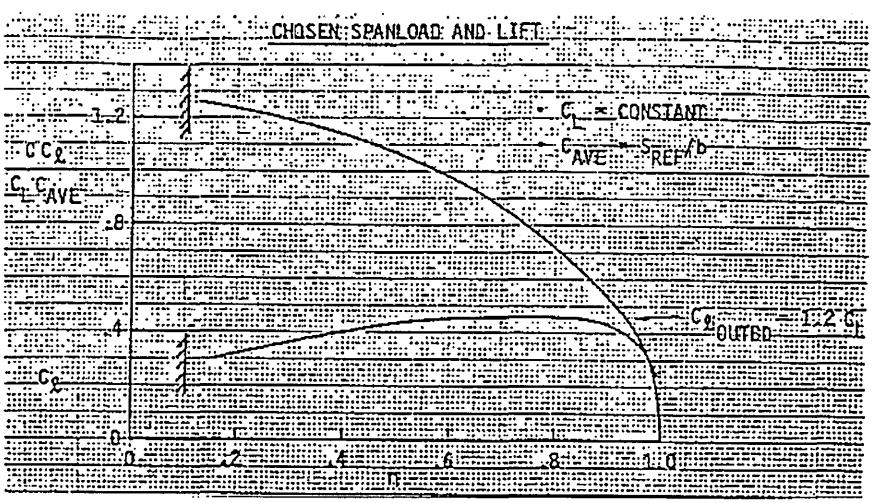

$$C(\eta) = (CC_l / C_L C_{AVE})_\eta (C_L C_{AVE}) / C_l(\eta)$$

Figure 7.14 Taper ratio determination (trapezoidal taper), Reference 7.1

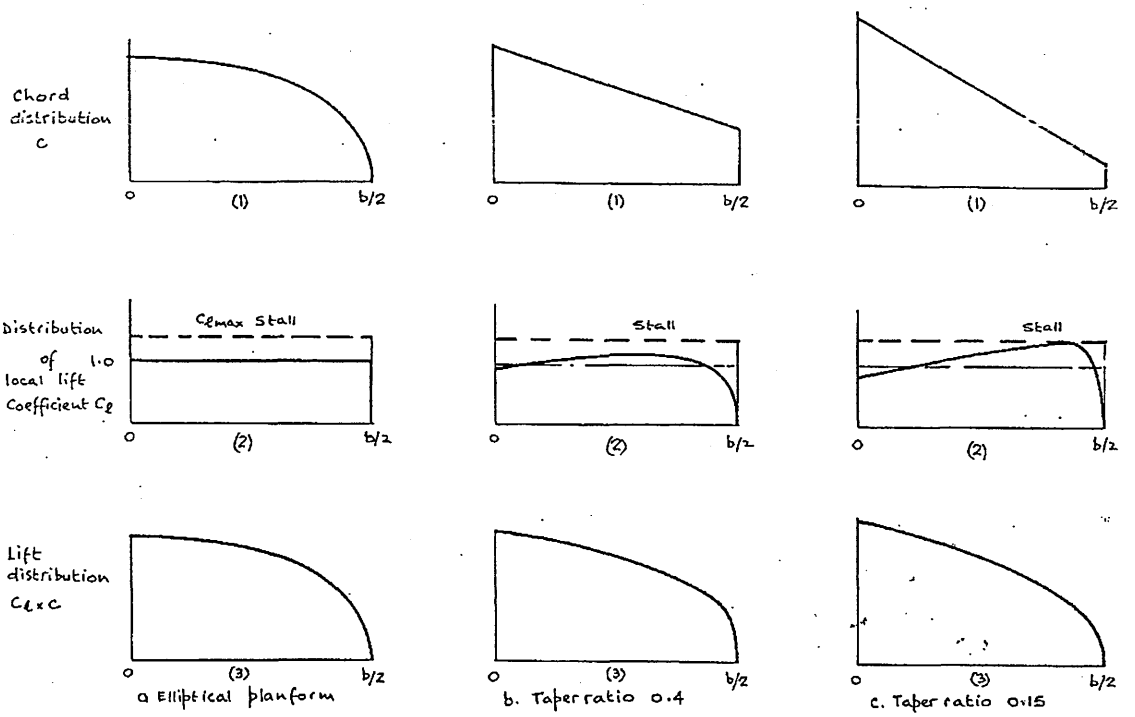

Figure 7.15 (Semi-) spanwise lift distribution for three planforms (Reference 7.27)

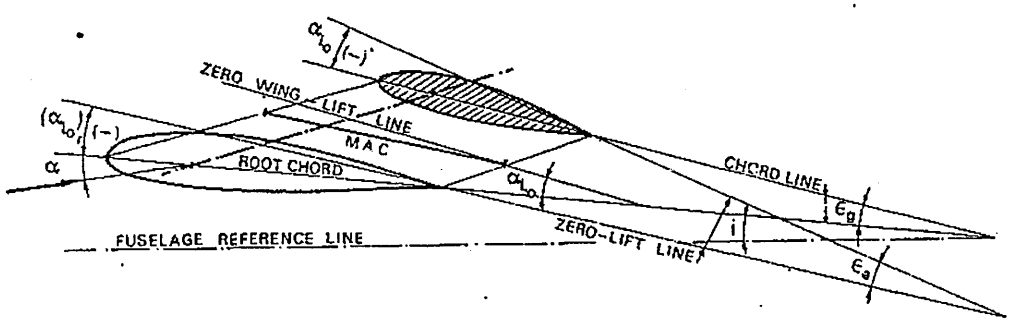

Figure 7.16 Definition of wing twist (Reference 7.31)

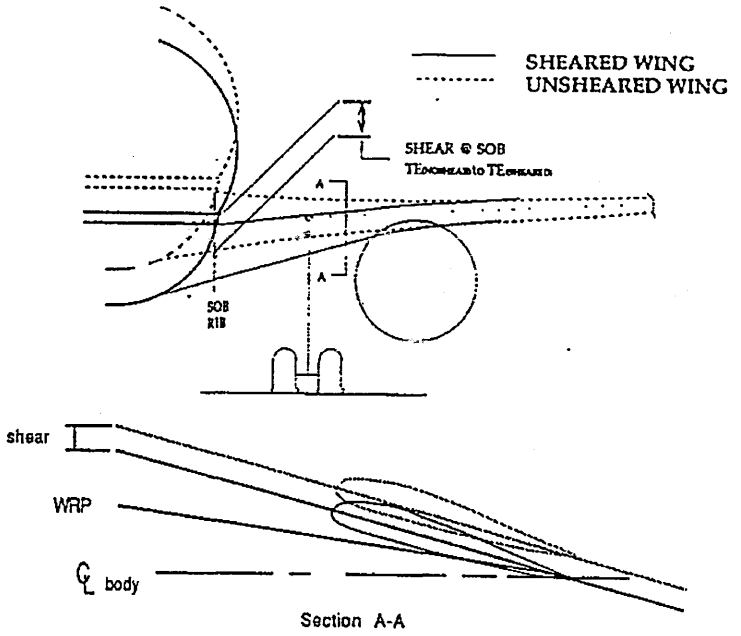

Figure 7.17 Wing shear definition (Reference 7.1)

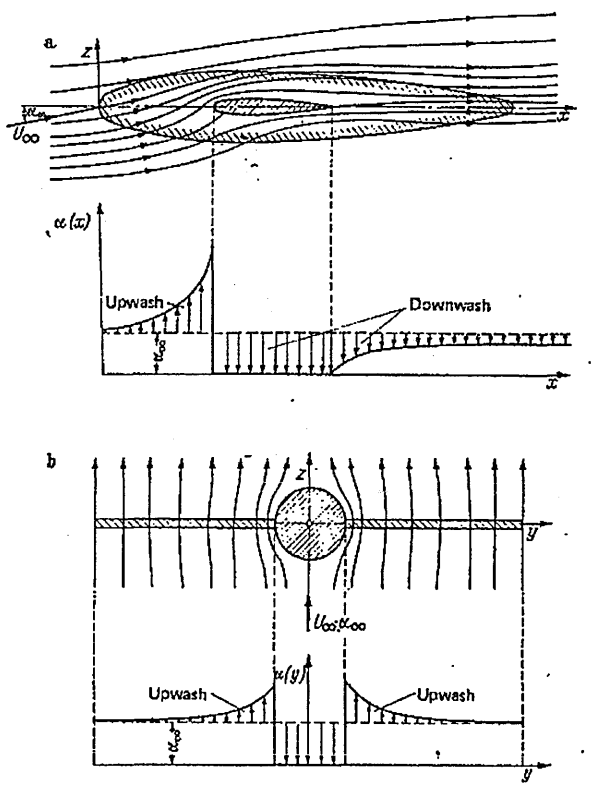

Figure 7.18 Symmetric flow about a wing-fuselage system (schematic), from Reference 7.48

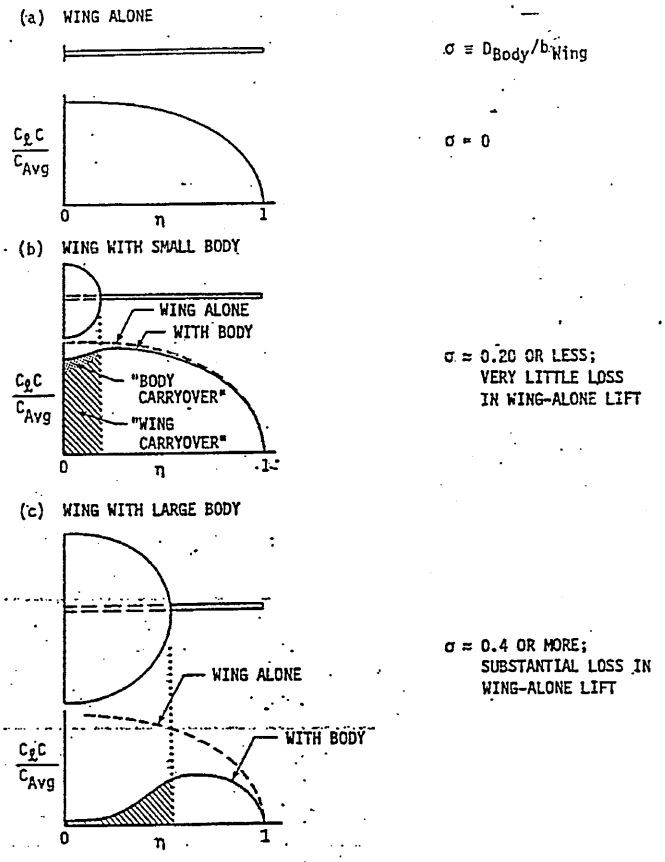

Figure 7.19 Effect of fuselage on wing loading (Reference 7.1)

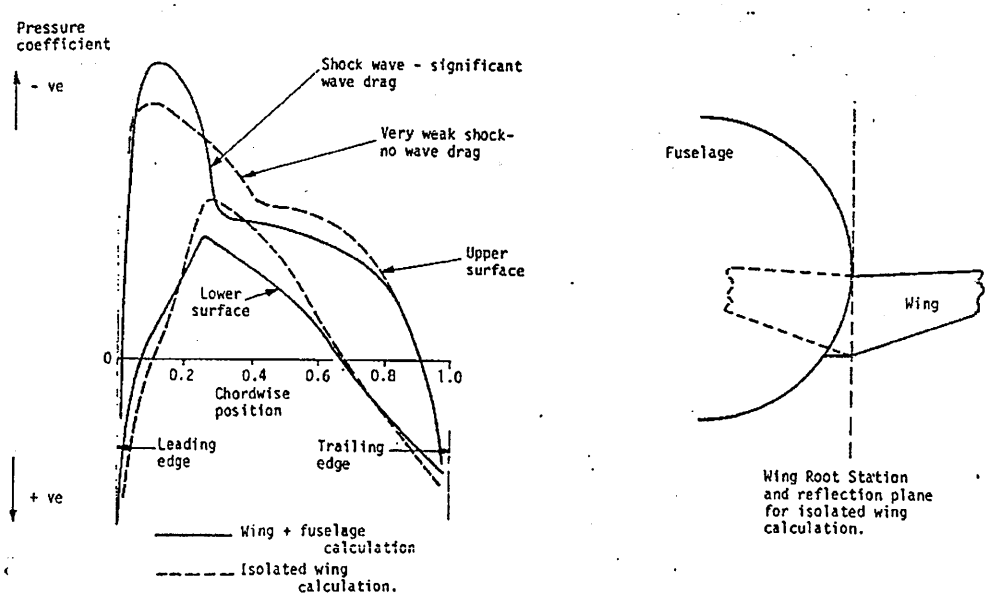

Figure 7.20 Effect of fuselage representation on wing root calculated transonic pressure distribution (Reference 7.62)

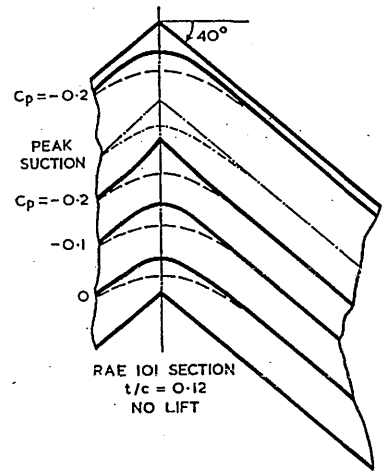

Figure 7.21 Isobar patterns near centre of sweptback wing. Dashed lines : constant section; full lines : modified sections (Reference 7.49)

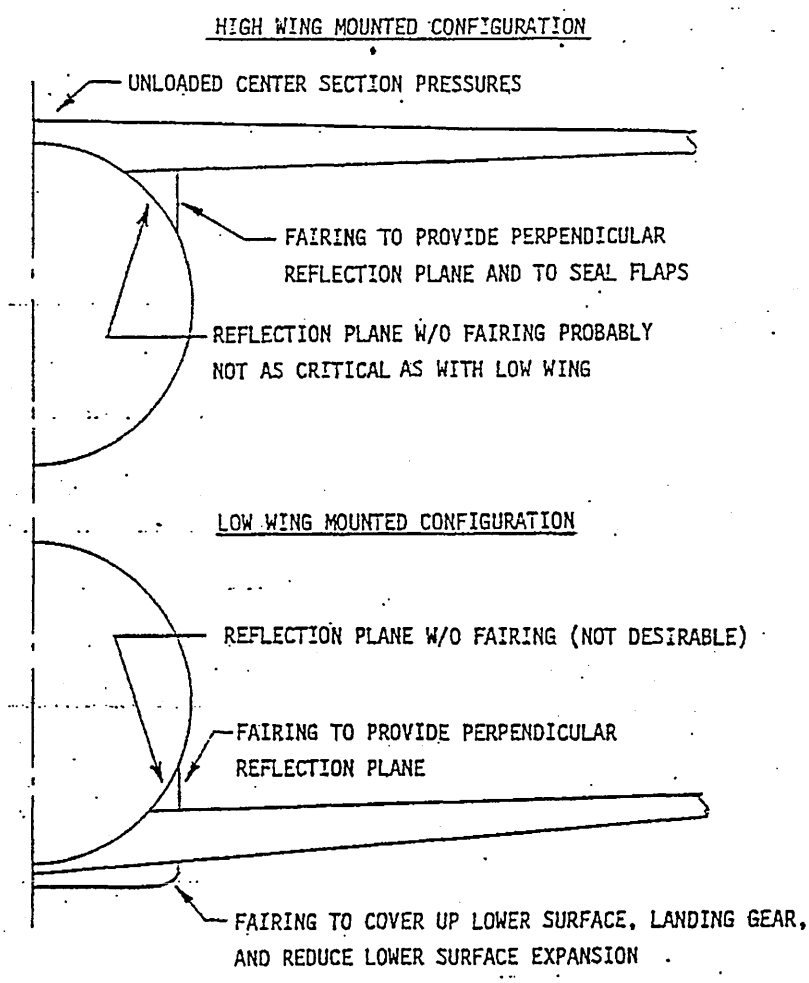

Figure 7.22 Fairing on high and low wing mounted configuration (Reference 7.1)

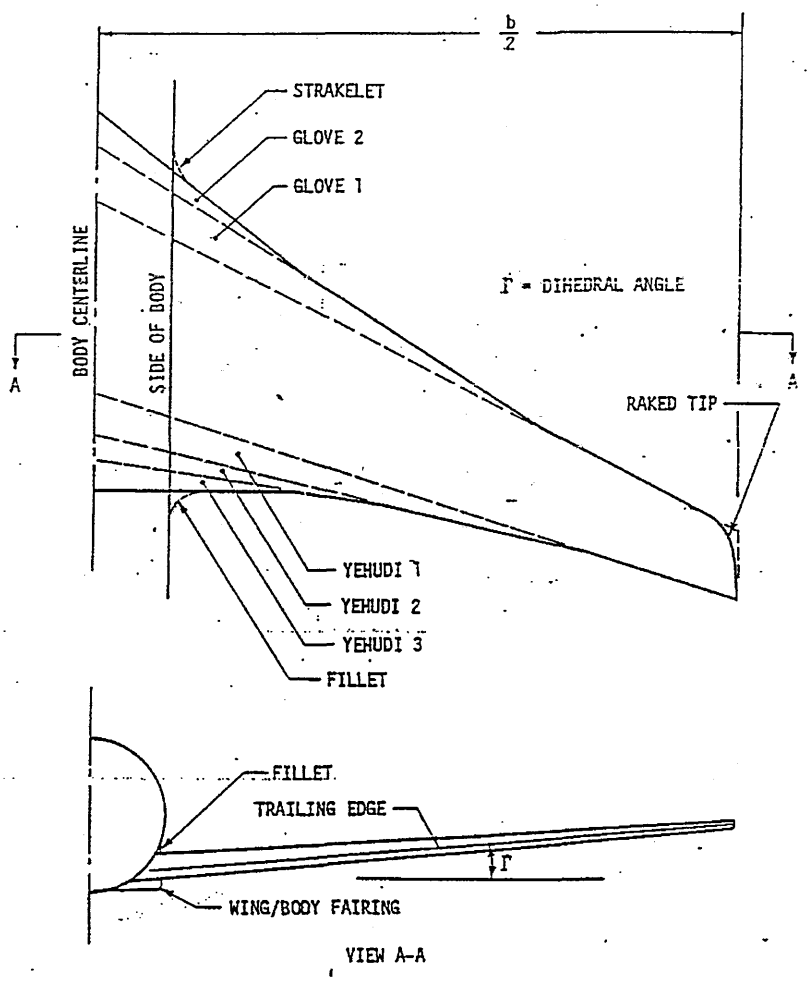

Figure 7.23 Planform geometry definitions (Reference 7.1)

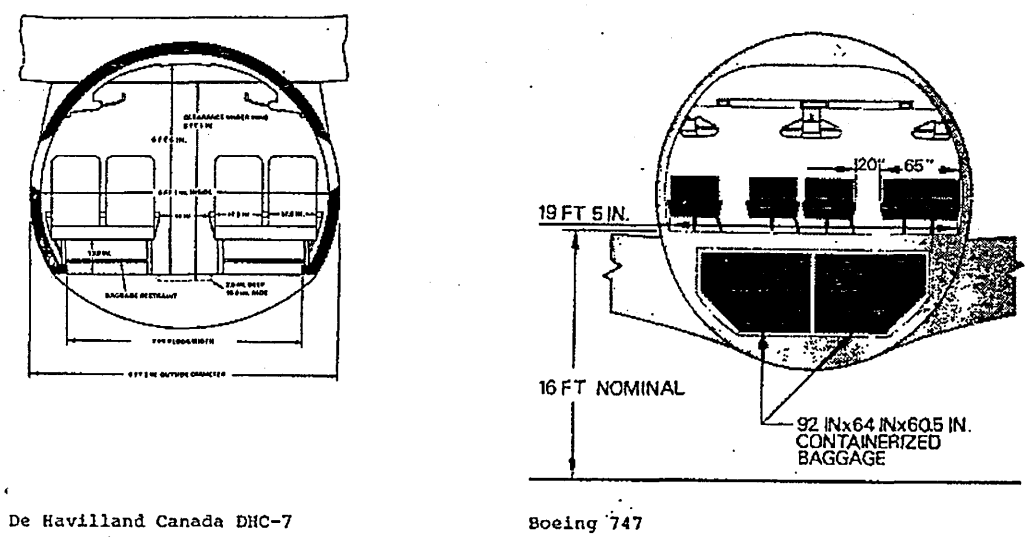

Figure 7.24 Typical wing vertical positions (Reference 7.31)

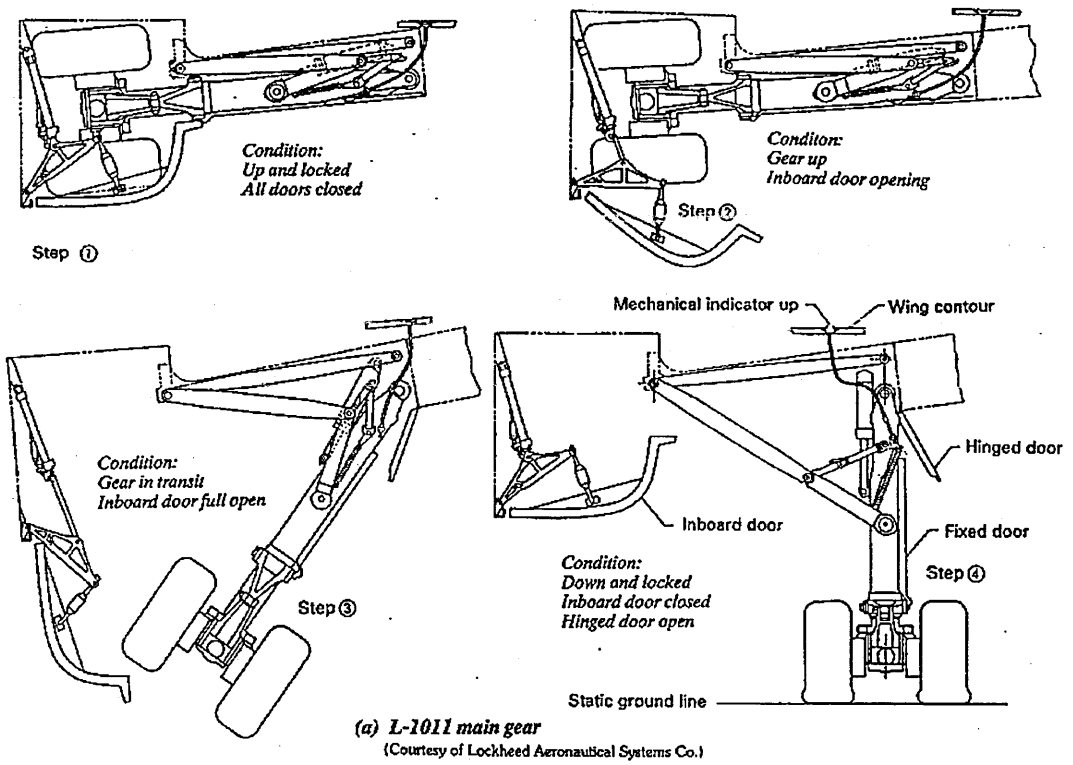

(a) L-1011 main gear
(Courtesy of Lockheed Aeronautical Systems Co.)

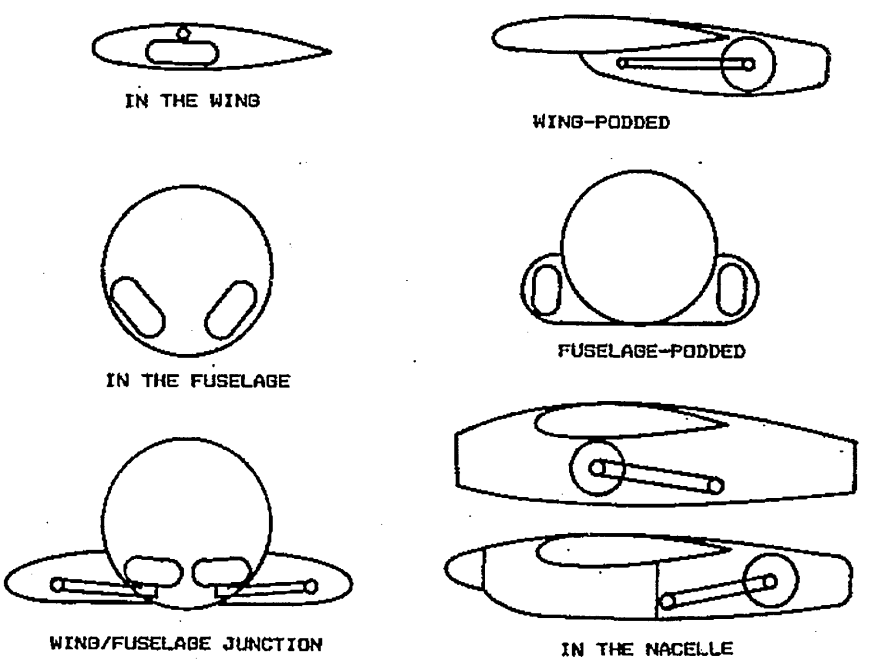

(b) A home for the gear

Figure 7.25 Landing gear stowage considerations (Reference 7.52 and 7.51)

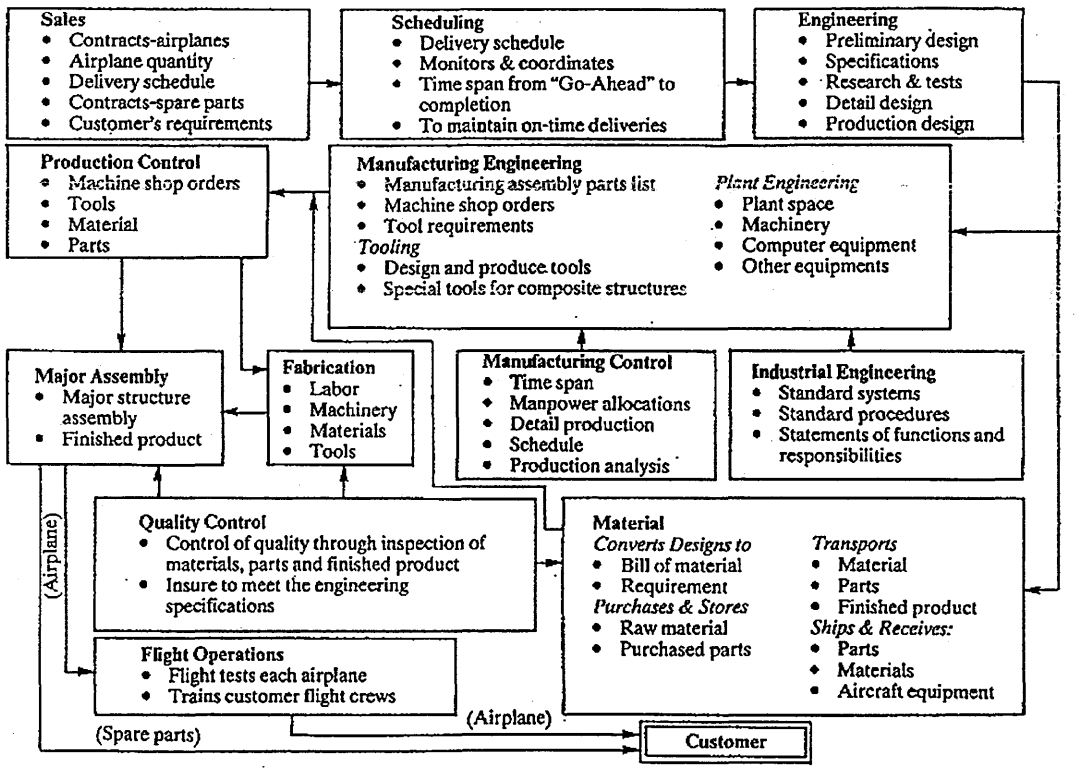

Figure 7.26 How an aircraft is built (Reference 7.52)

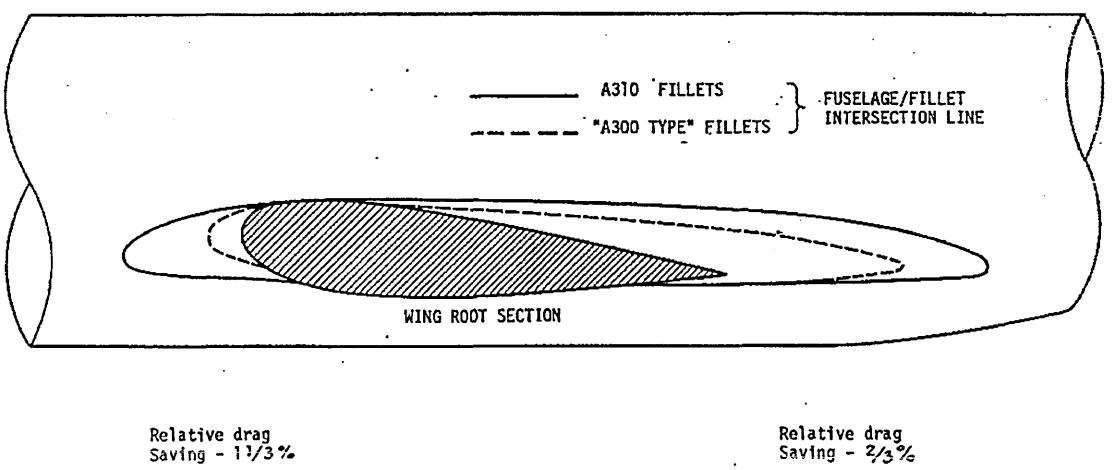

Figure 7.27 Optimisation of A310 wing root (Reference 7.62)

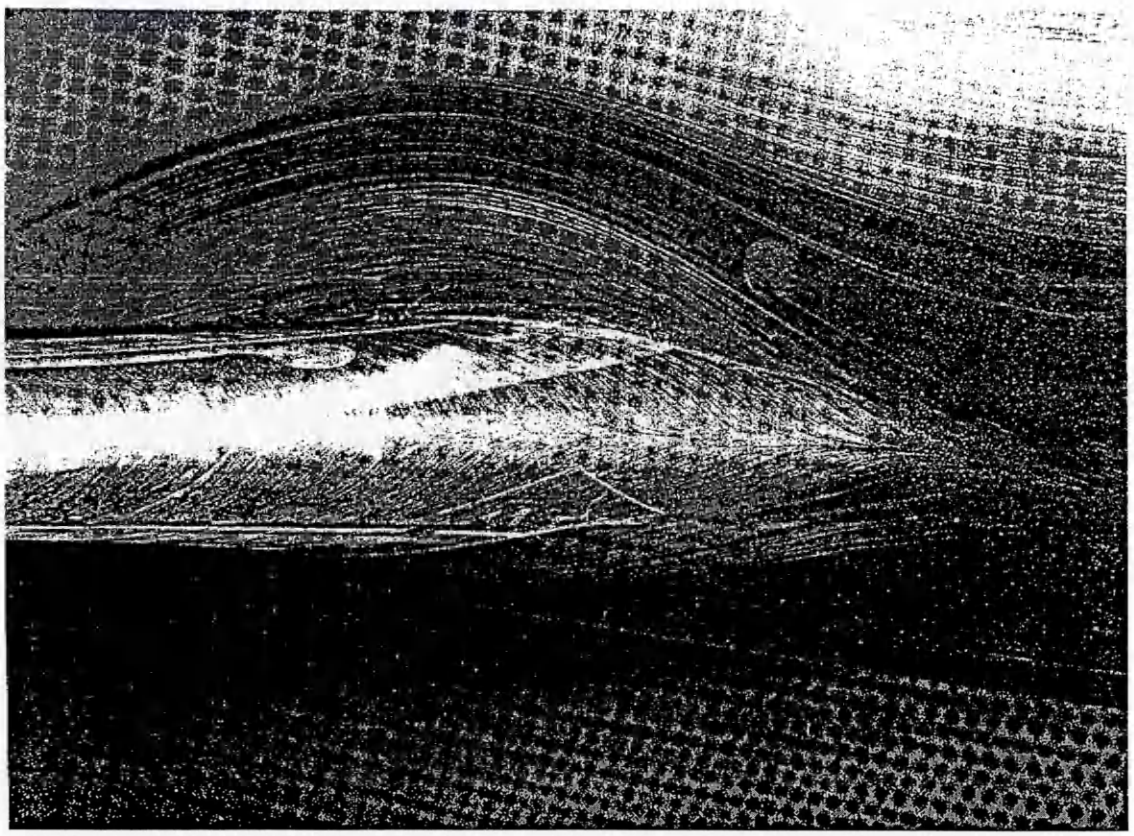

Figure 7.28 Surface flow streamlines over the A310 wing root fillet (Reference 7.62)

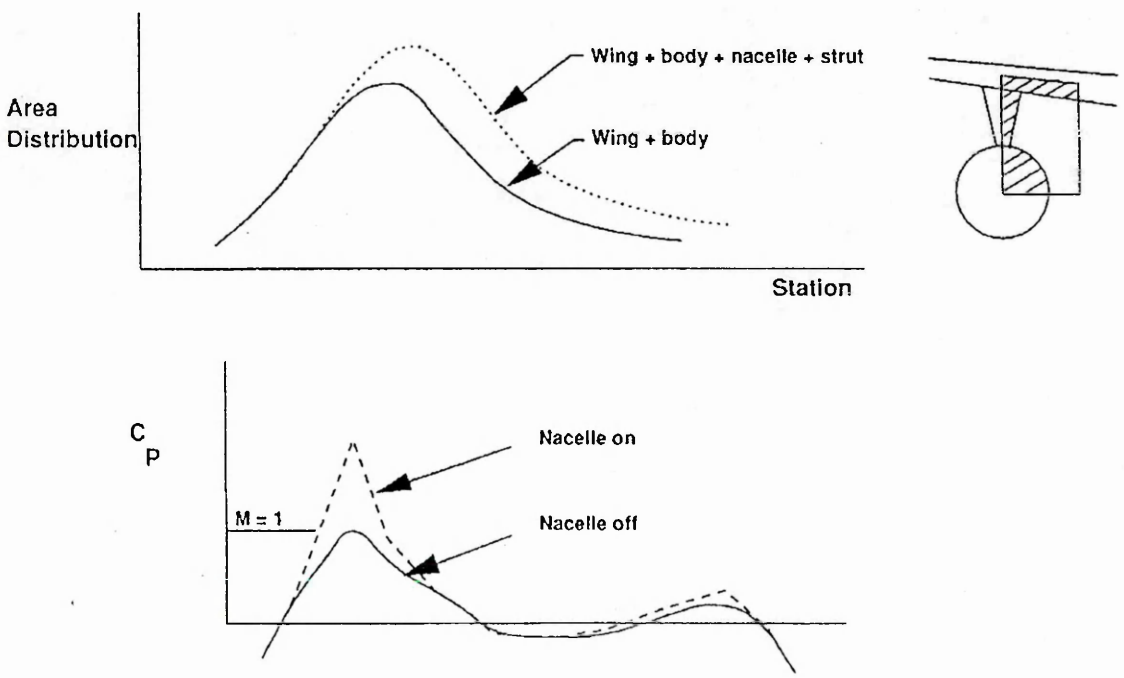

Figure 7.29 Nacelle installation effect on wing lower surface pressures (Ref. 7.56)

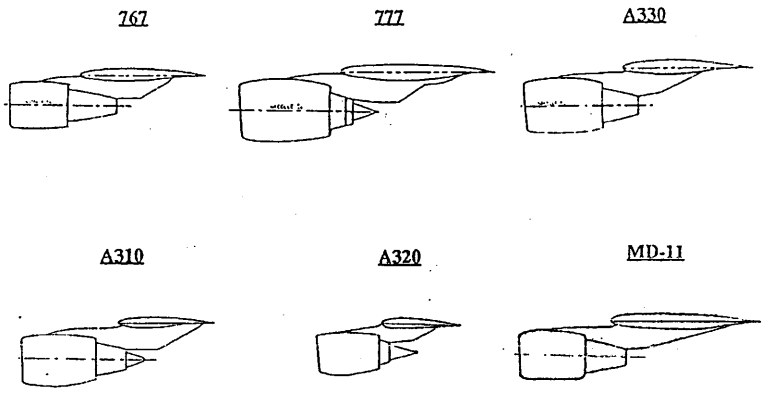

Figure 7.30 Typical engine installation of existing aircraft (Reference 7.56)

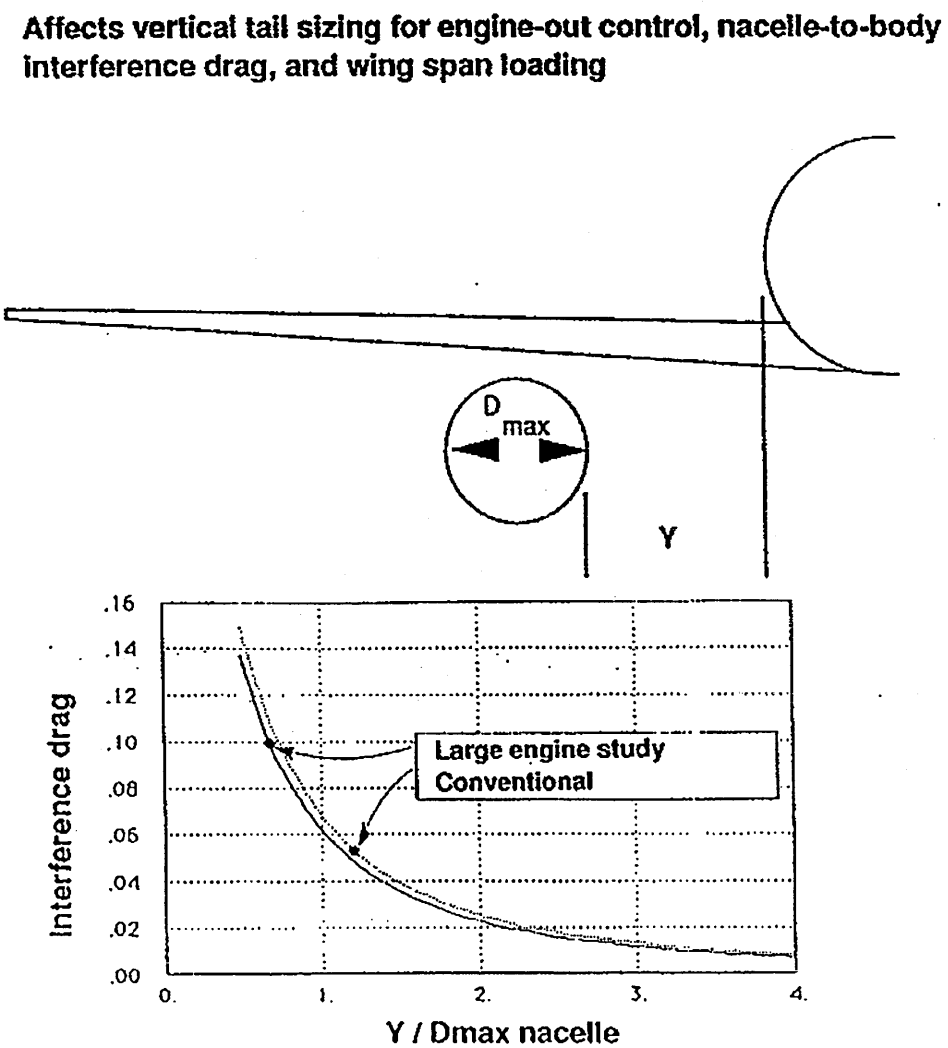

Figure 7.31 Effect of nacelle spanwise positioning (Reference 7.56)

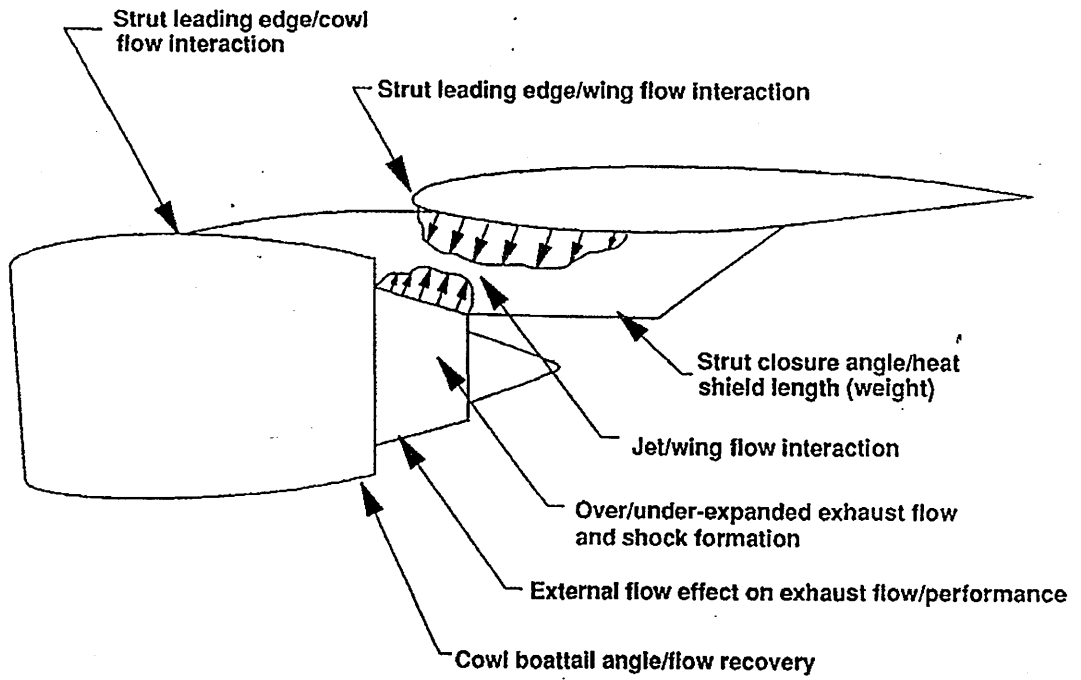

Figure 7.32 Exhaust system/strut aerodynamic design considerations (Reference 7.56)

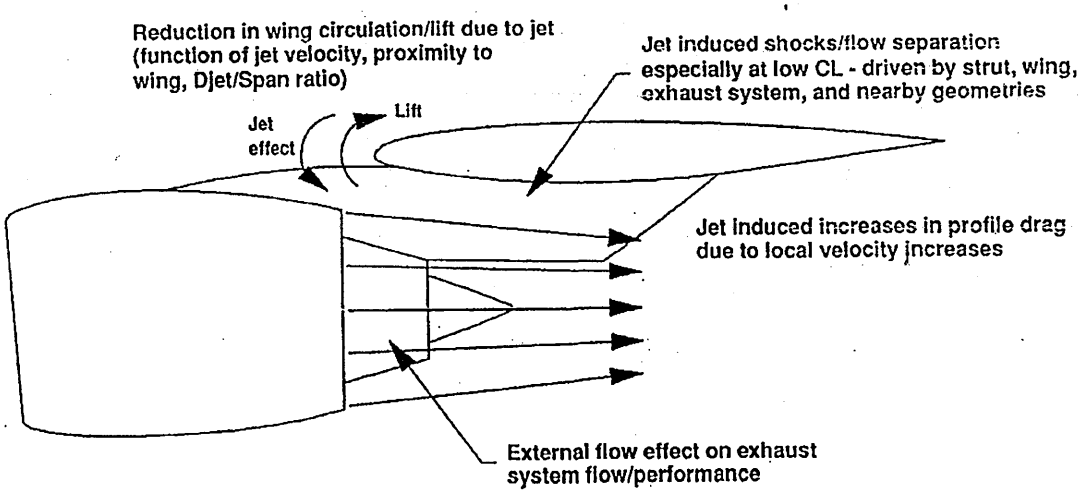

Figure 7.33 Blowing drag sources (Reference 7.56)

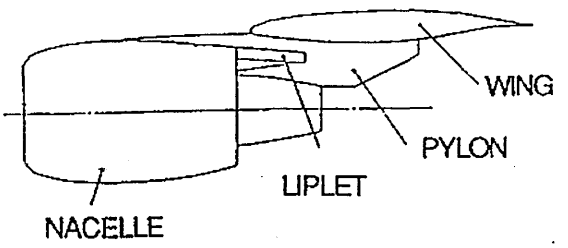

Figure 7.34 Schematic sketch of the liplet (Reference 7.61)

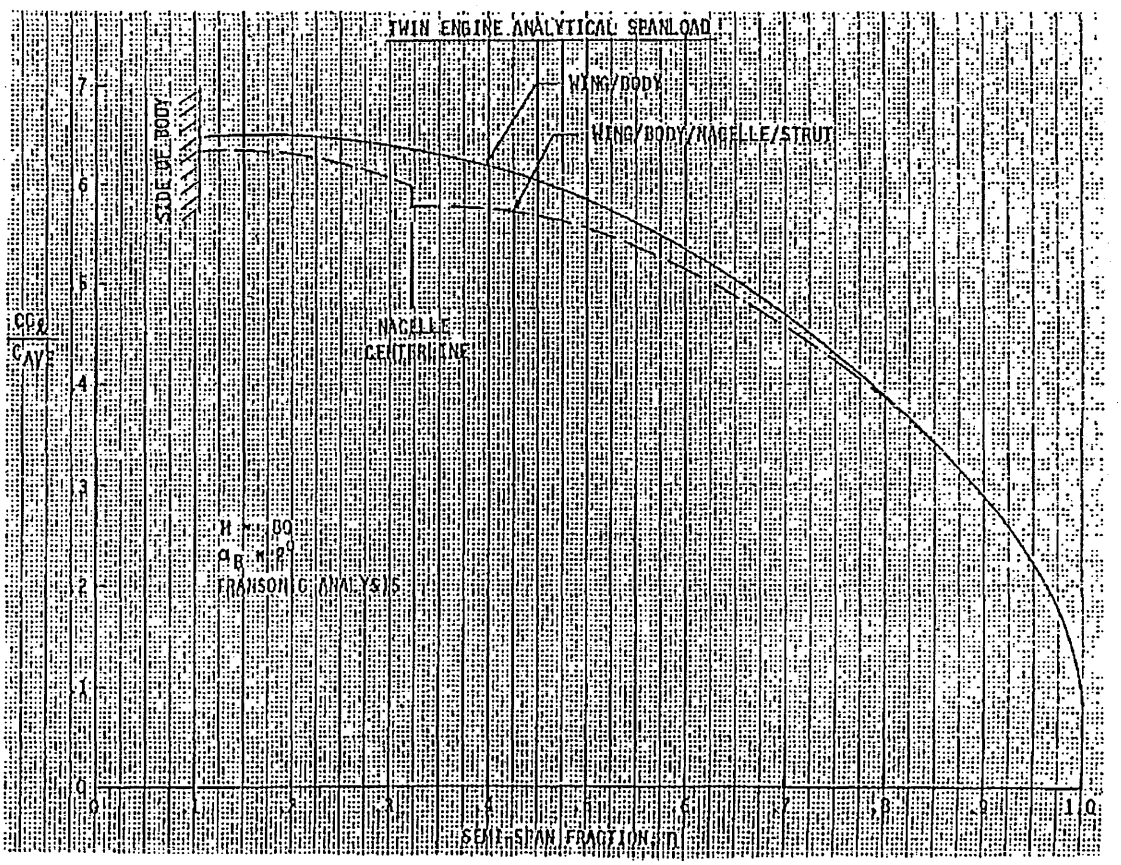

Figure 7.35 Nacelle effect on spanload (Reference 7.1)

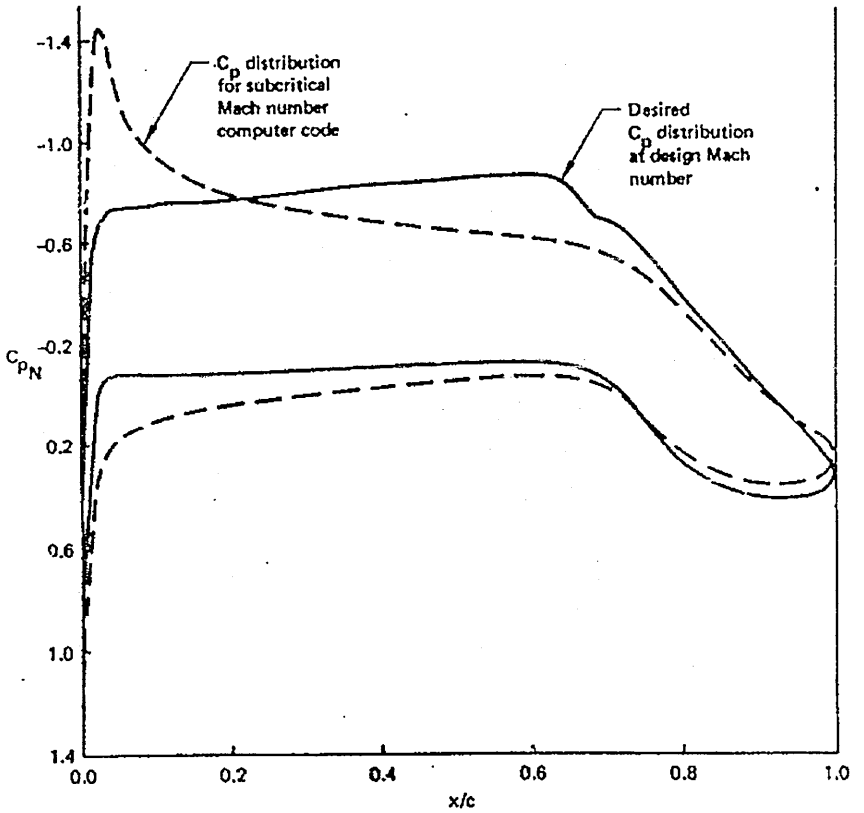

Figure 7.36 Modifications to target pressure distribution for subcritical three-dimensional computer code (Reference 7.28)

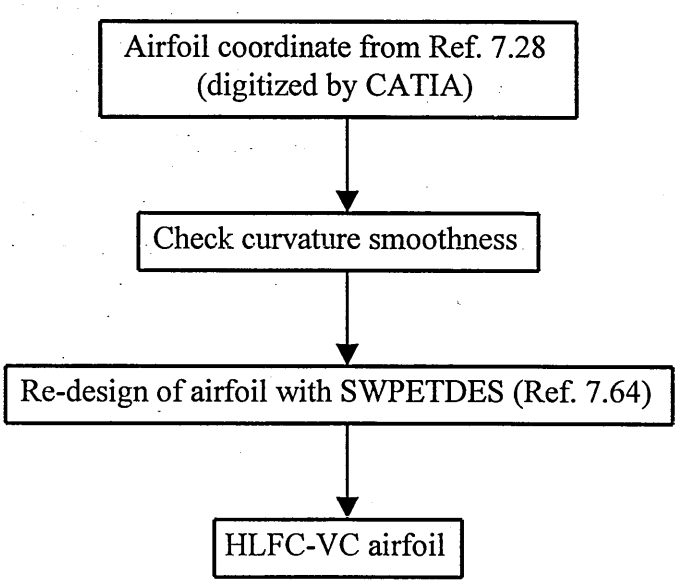

Figure 7.37 A simplified combine HLFC-VC wing design process

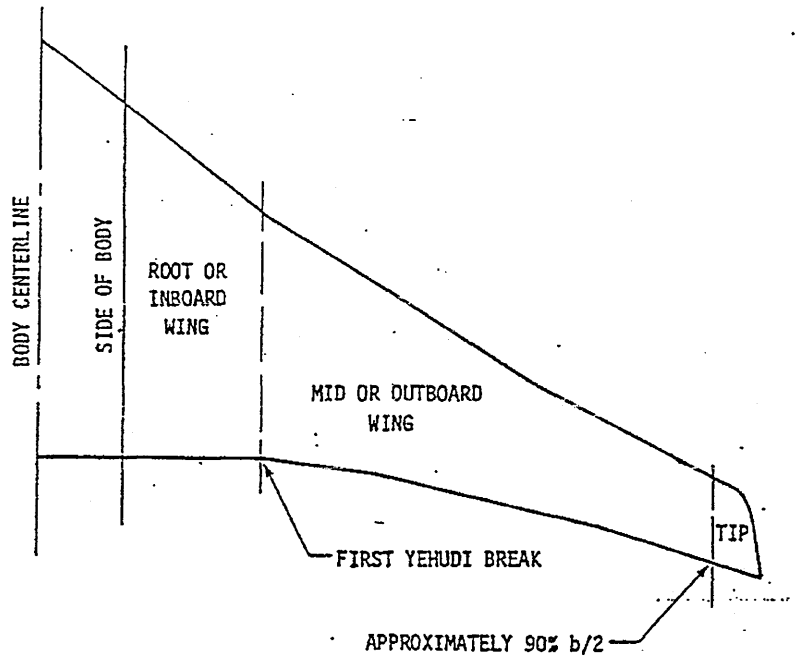

Figure 7.38 Wing geometry definitions (Reference 7.1)

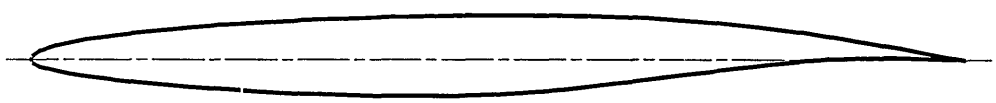

a. Constant upper surface :

$(Z_U/C)_{NEW} = (Z_U/C)_{OLD}$

Modify lower surface to achieve $t/c_{max,NEW}$

b. Chordline (transonic similarity) : RECOMMENDED

$(Z_U/C)_{NEW} = (Z_U/C)_{OLD}(t/c_{max,NEW})/(t/c_{max,OLD})$

$(Z_L/C)_{NEW} = (Z_L/C)_{OLD}(t/c_{max,NEW})/(t/c_{max,OLD})$

c. Camberline :

$(Z_U/C) = (Z_t/C) + (Z_c/C)$

$(Z_L/C) = (Z_c/C) - (Z_t/C)$

$(Z_U/C)_{NEW} = ((Z_t/C) + (Z_c/C))(t/c_{max,NEW})/(t/c_{max,OLD})$

$(Z_L/C)_{NEW} = ((Z_c/C) - (Z_t/C))(t/c_{max,NEW})/(t/c_{max,OLD})$

Figure 7.39 2D thickness scaling methods (Reference 7.1)

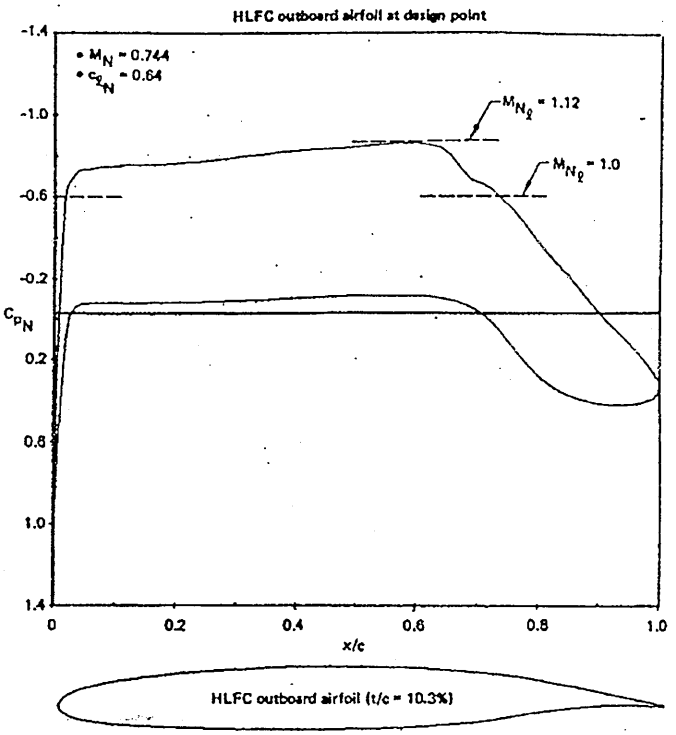

Figure 7.40 Pressure distribution and contour of outboard airfoil (Reference 7.28)

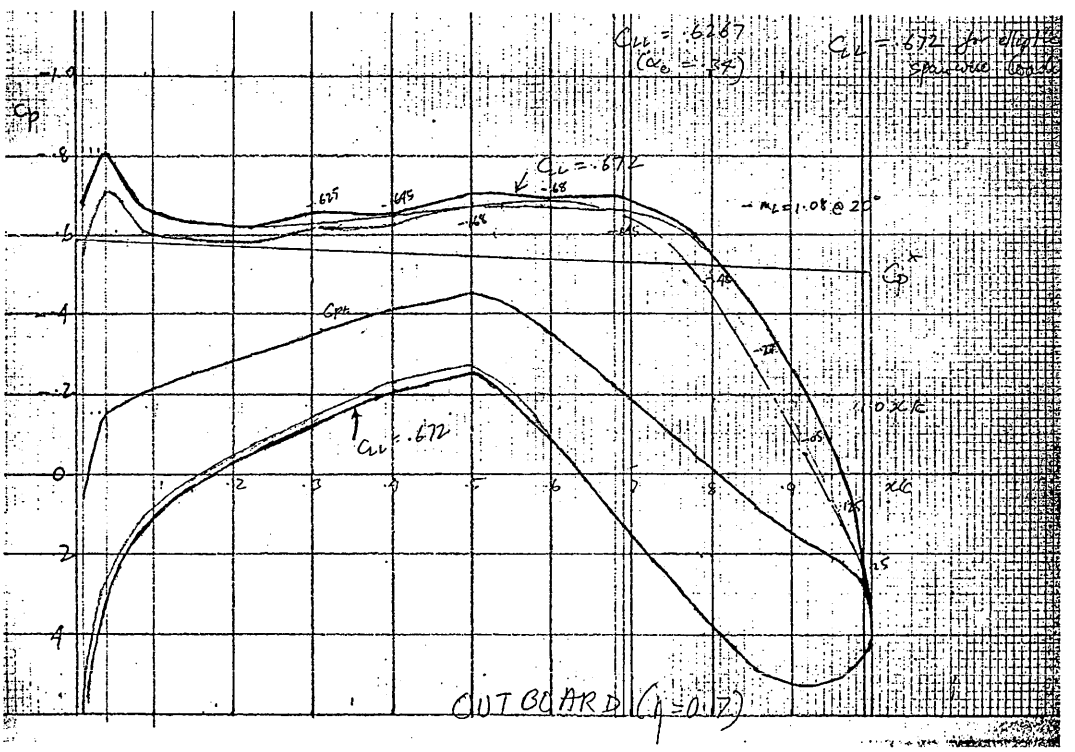

Figure 7.41 Subcritical pressure distribution of the ATRA-100's outboard wing airfoil section

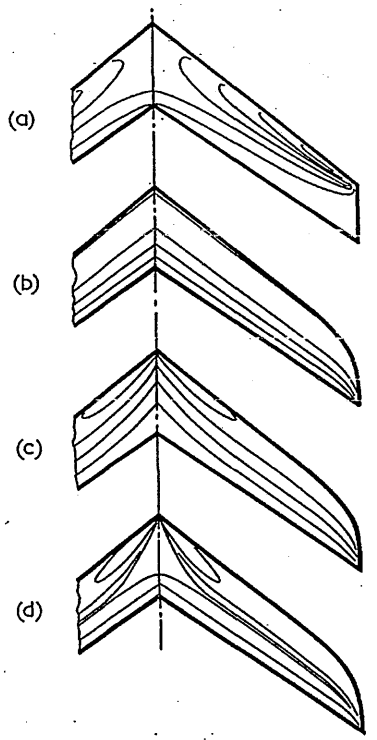

Figure 7.42 Isobar patterns on sweptback wings (schematic), from (Reference 7.27)

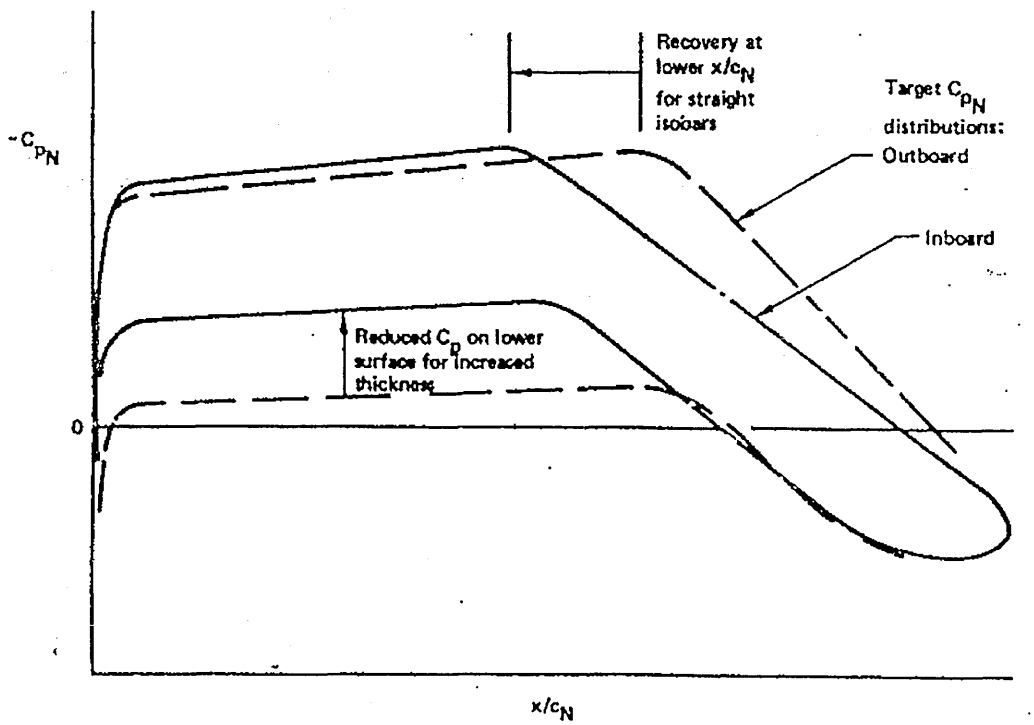

Figure 7.43 Root section pressure distribution considerations (Reference 7.28)

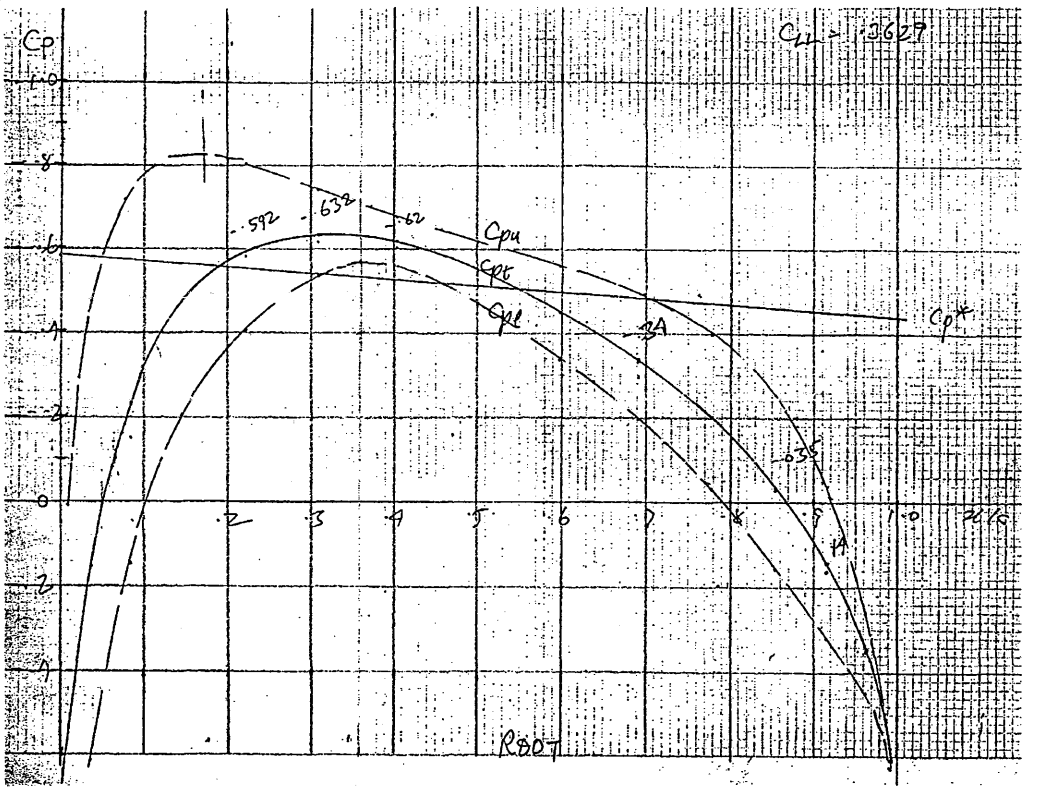

Figure 7.44 Subcritical pressure distribution of the ATRA-100's root wing airfoil section

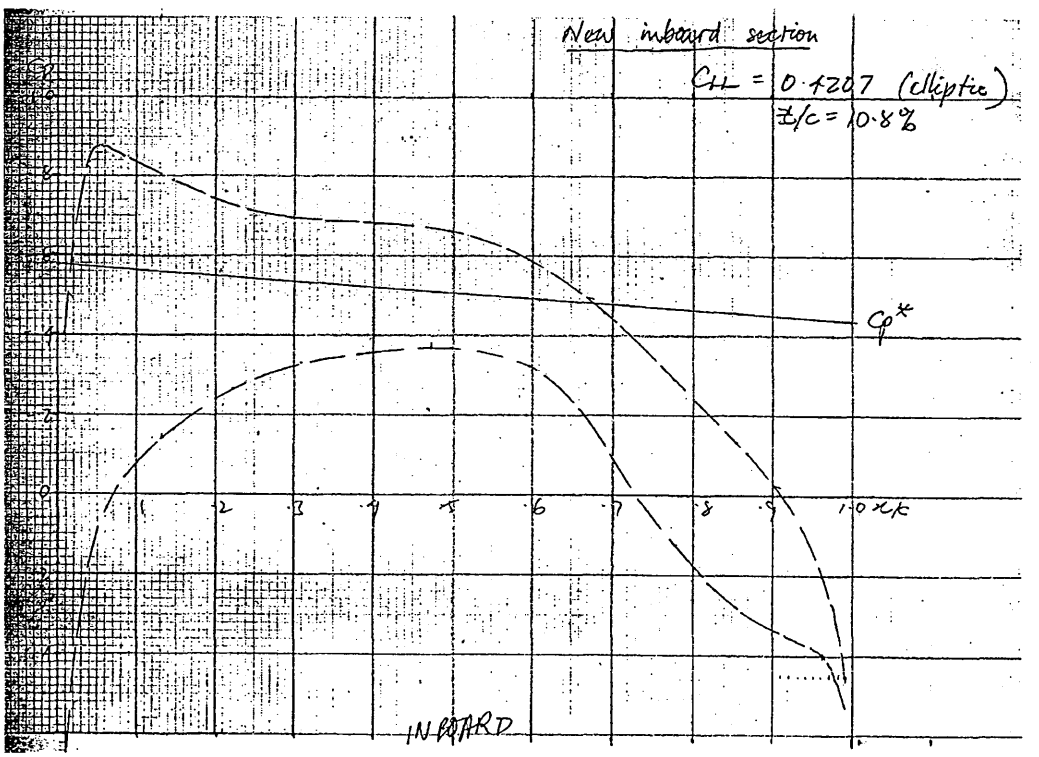

Figure 7.45 Subcritical pressure distribution of the ATRA-100's inboard wing airfoil section

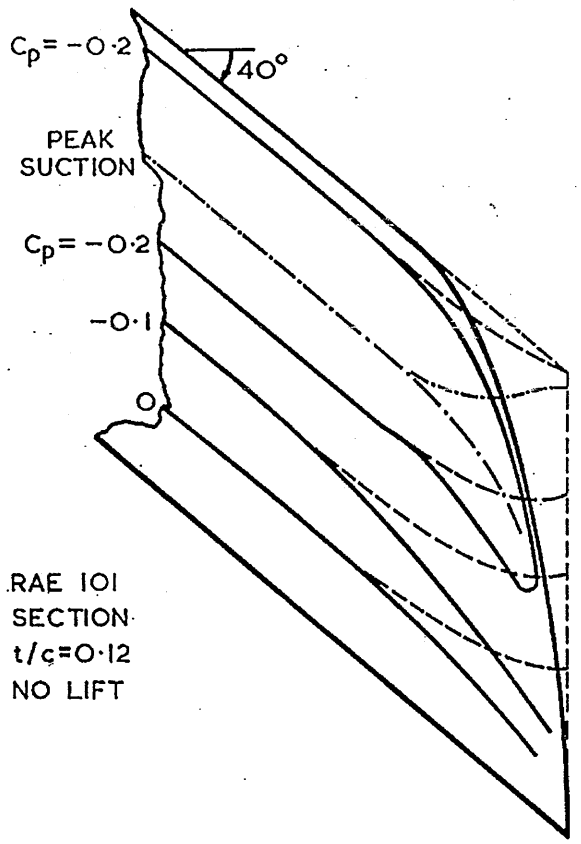

Figure 7.46 The Kuchemann tip (Reference 7.27)

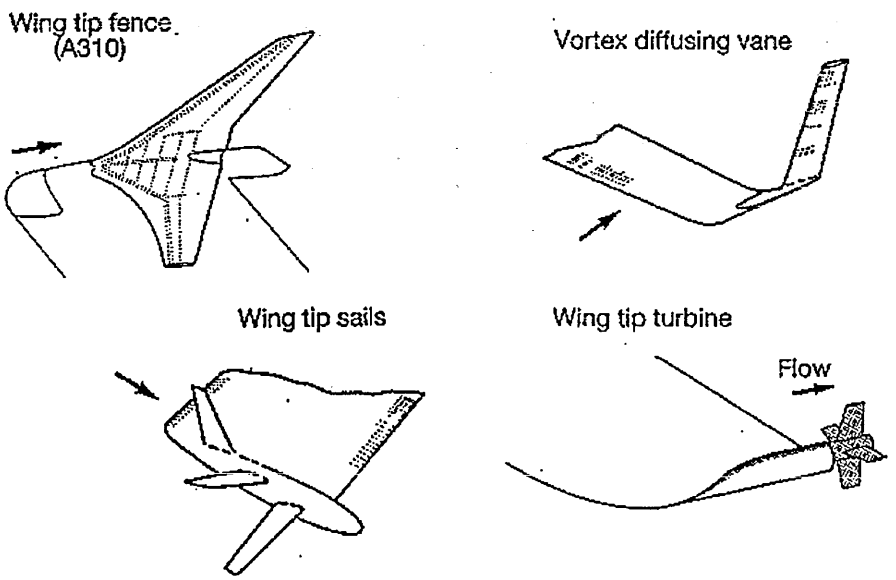

Figure 7.47 Wing tip devices (Reference 7.69)

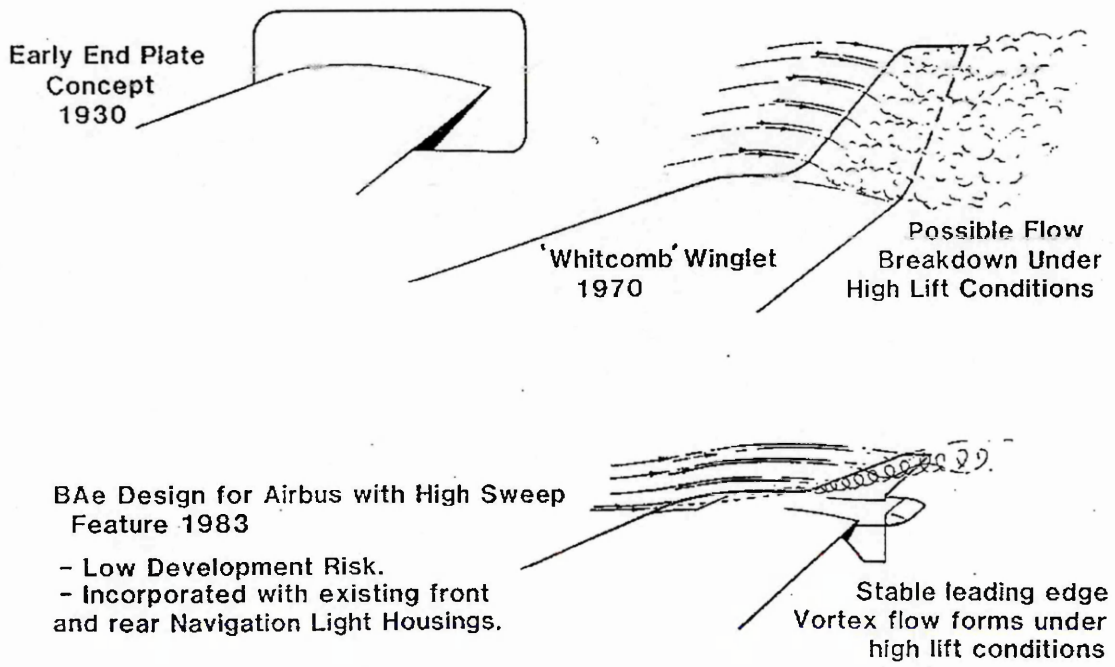

a. Winglets for the Airbus A300-600 and A310-300

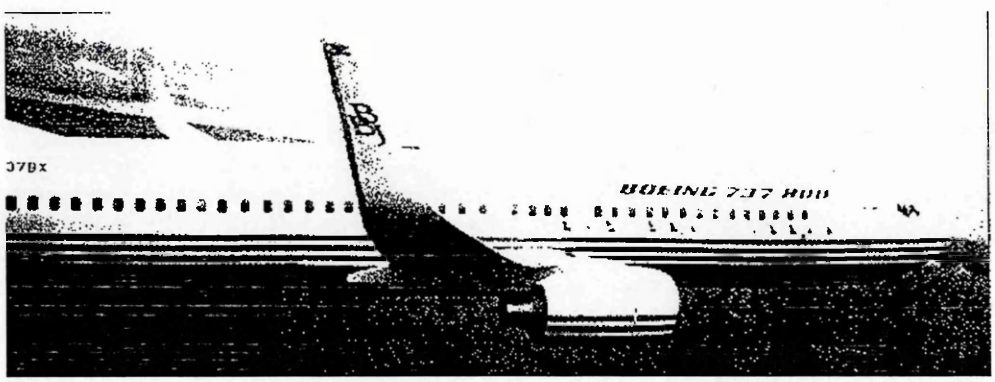

b. Winglets for the Boeing B737-800

Figure 7.48 Winglets for the Airbus A300-600, A310-300 and Boeing B737-800 (Reference 7.70 and 7.71)

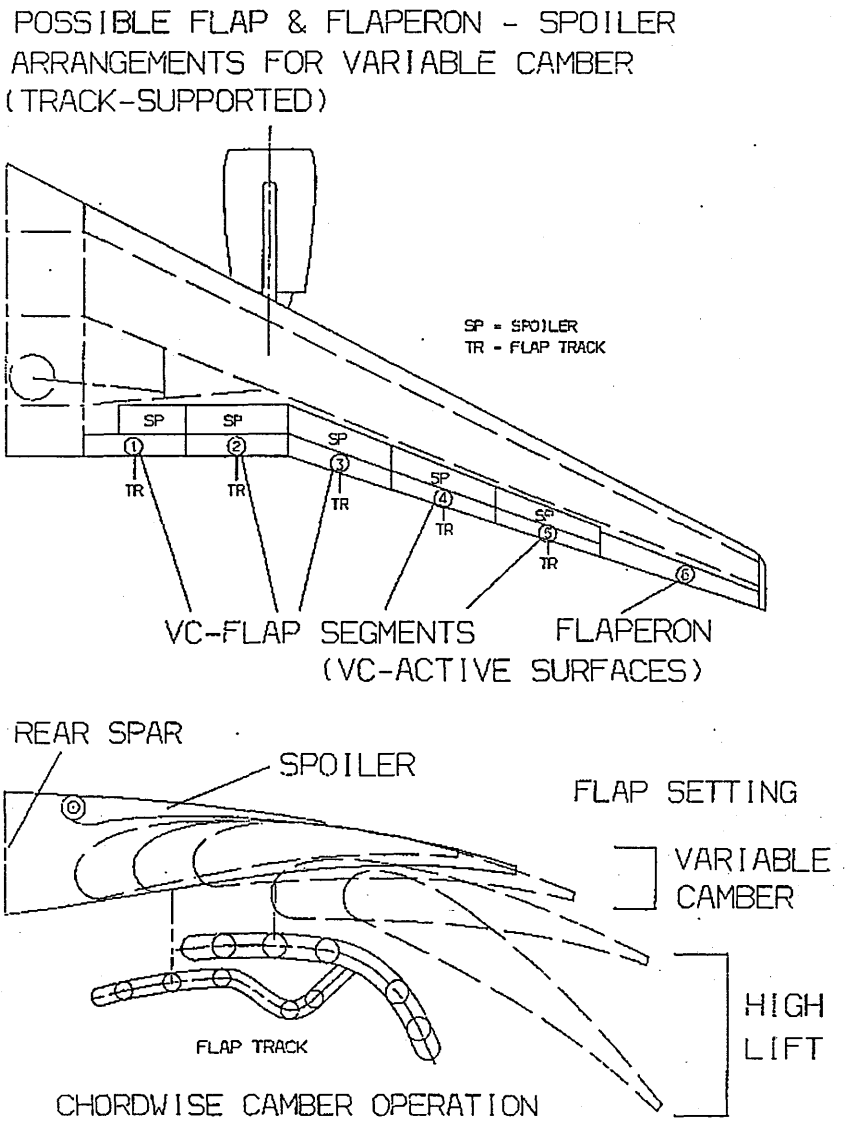

Figure 7.49 Principle of variable camber operation

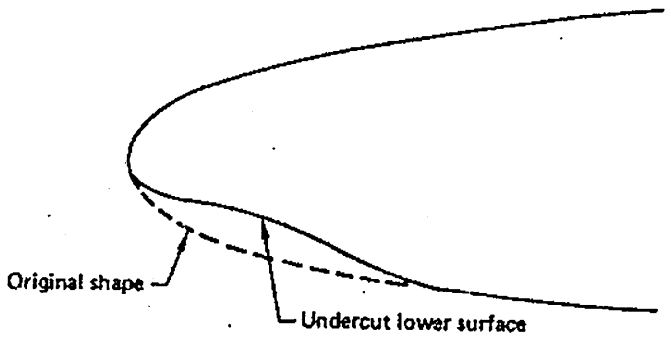

Figure 7.50 Geometric tailoring of leading-edge to prevent attachment line transition (Reference 7.28)

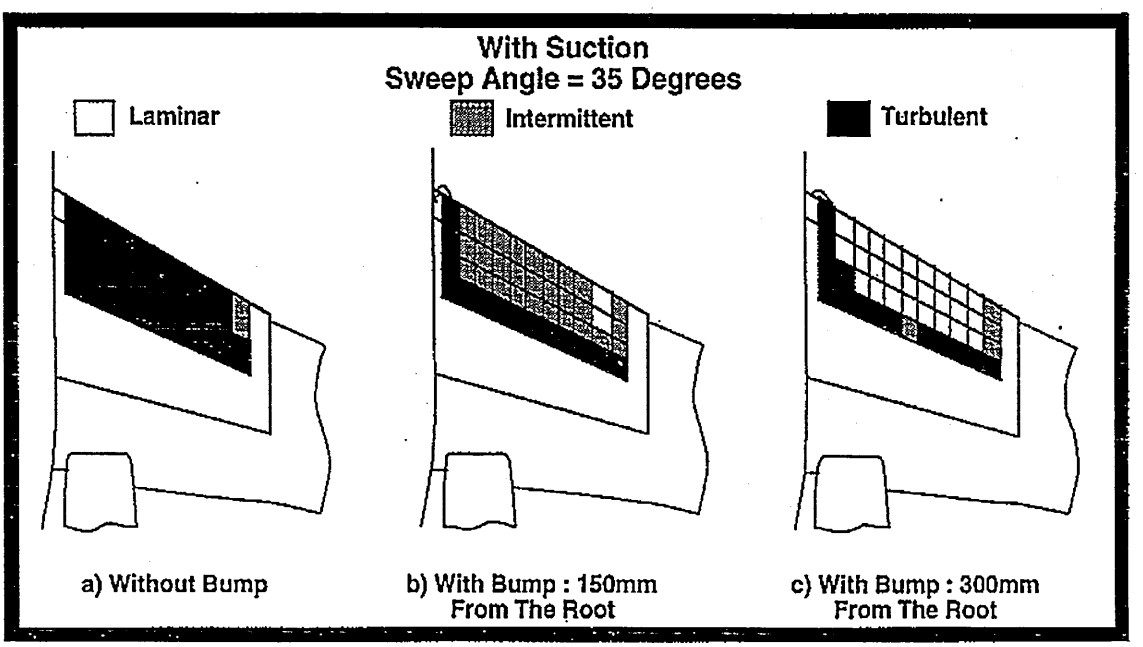

Figure 7.51 The effectiveness of the Gaster bump for turbulence contamination avoidance along the attachment line (Reference 7.77)

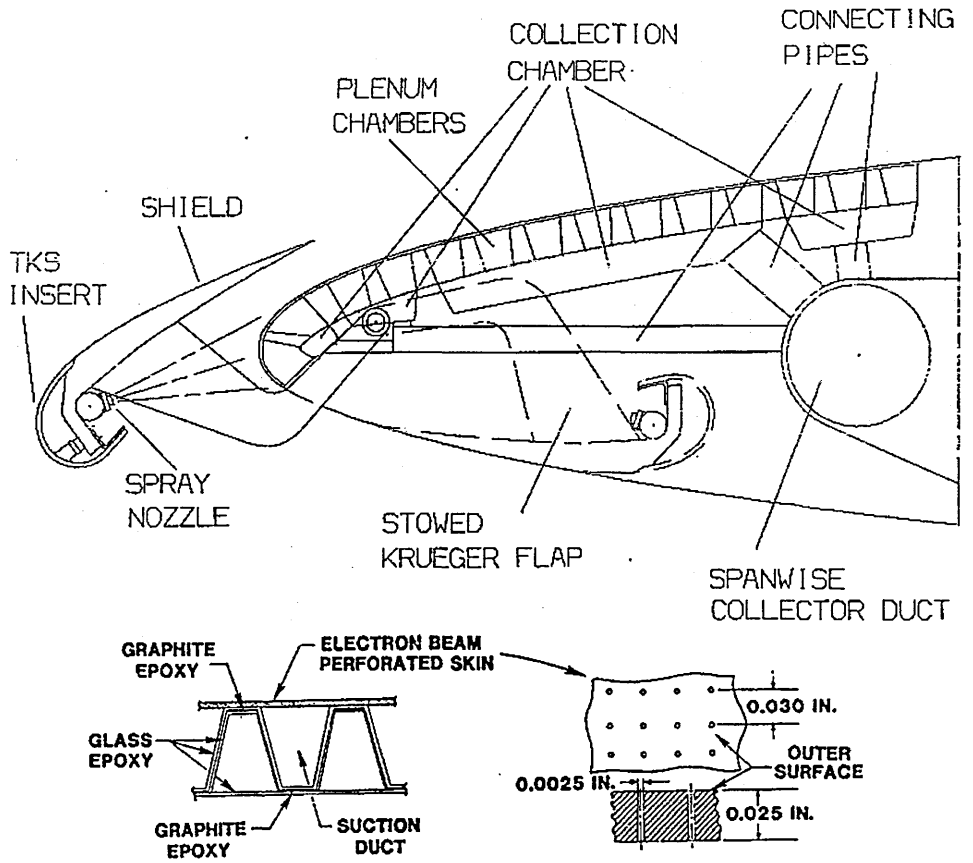

Figure 7.52 Leading edge systems design

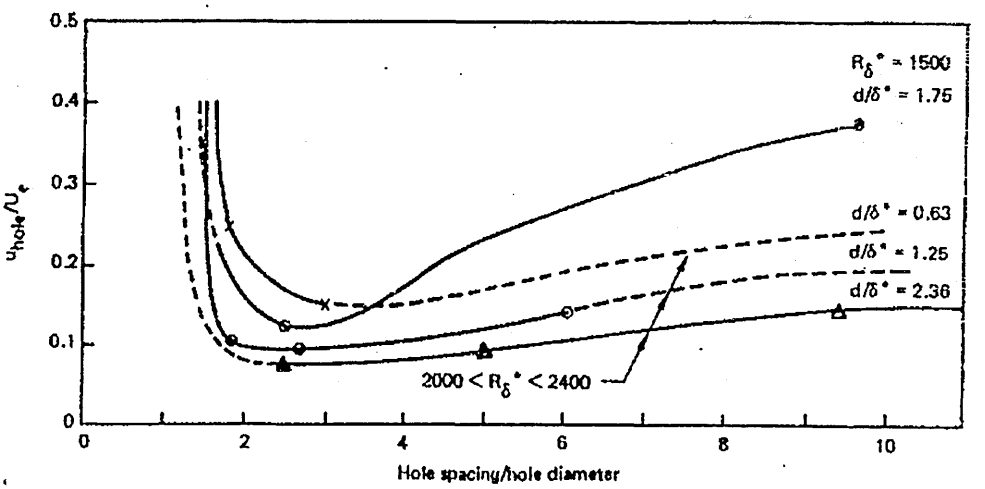

Figure 7.53 Hole spacing criterion (Reference 7.28)

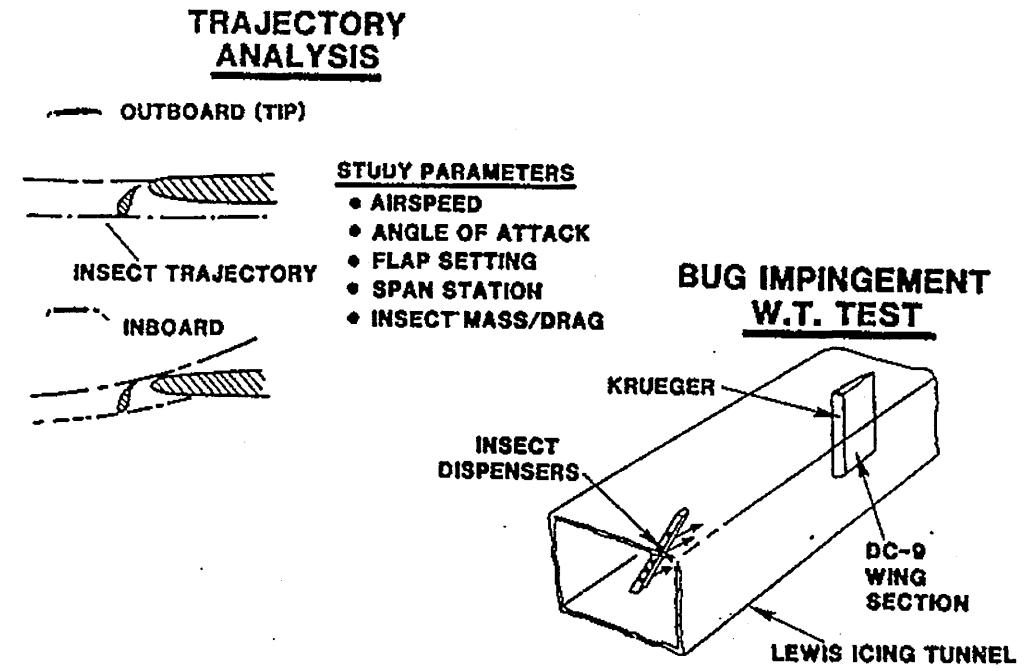

Figure 7.54 Krueger insect shield trajectory analysis and wind tunnel test (Ref. 7.81)

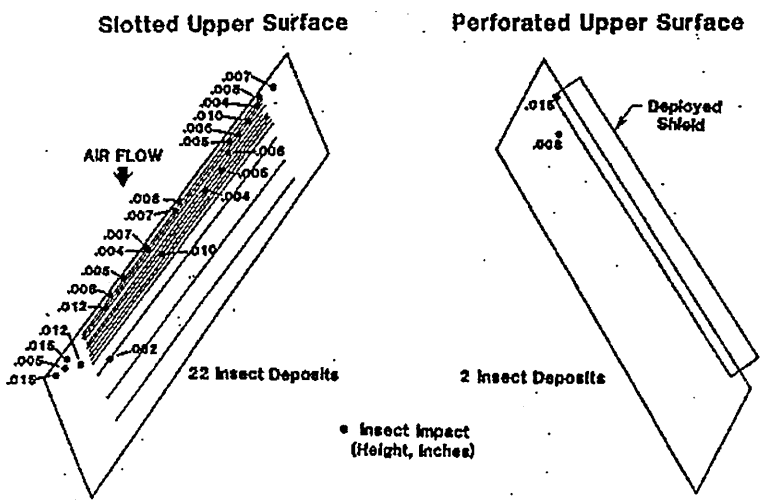

Figure 7.55 Typical insect contamination (Reference 7.81)

CHAPTER EIGHT

COMPUTATIONAL DESIGN ANALYSIS FOR ATRA WING WITH HLFC AND WITH AND WITHOUT VC DEVICES

8.1 INTRODUCTION

Many aircraft operate at transonic speed, where part of the flowfield is subsonic and part is supersonic. At these speeds shock waves form on the wings, which cause an increase in drag and variable changes in the lift. Multiple shock waves can develop and interact in ways that are difficult to predict, but that have a large influence on lift and drag.

With detailed knowledge of the flowfield and shock wave locations designers can shape the wing to delay the transonic drag rise and increase the lift to drag ratio. The results are higher transonic cruising speeds and reduced fuel consumption.

The main objective of this section is to analyse whether the ATRA-100's wing (which is designed in section 7.7) fulfils the design objectives (which are described in section 3.2 and 7.7.1) or not.

8.2 AERODYNAMIC PERFORMANCE PREDICTIONS

In this section, the transonic flow over the ATRA-100's wing-fuselage configuration is calculated. The computation was performed using RAMPANT (References 8.1 and 8.2), an unstructured, multigrid flow solver. A 3-D model of the ATRA-100's wing-fuselage configuration was created using CATIA (References 8.3 and 8.4). A corresponding grid was created using preBFC (Reference 8.5) and TGrid (Reference 8.6). The aerodynamic calculation procedures and their verification using the above codes are described in Appendix C.

8.2.1 Configuration Description

To simplify the problem and also to keep the grid size low as possible, the analysis was performed for a half wing-fuselage configuration only. Two configurations were used in this analysis, i.e. :

a. Configuration I : VC-flap undeployed
b. Configuration II : VC-flap deployed

The wing and fuselage geometry are described in Appendix B of this thesis. VC-flap deflection for Configuration II is shown in Table 8.1. For simplicity of modelling of the grid in preBFC and TGrid, rake tip was added to the ATRA-100's wing, so the wing span (b) became 16.972 m, instead of 16.179 m.

The wing-fuselage surface grid of the configuration I and II used for this

analysis are shown in Figure 8.1 and 8.2 respectively. The results shown here are for M_∞ = 0.8, angle of attack = 0 degree, and Reynolds number of 21.6×10^6. The computational domain is rectangular box that extends 5 fuselage length in front, behind, above, and below the wing, and 3 fuselage length (6.8 wing semispan) to the side of the wing. The size of the mesh of the above two configurations are as follow :

Configuration I =	35,019 Nodes	344,787 Faces	165,256 Cells
Configuration II =	36,215 Nodes	355,903 Faces	170,522 Cells

Both of the above configurations were run as an inviscid, fully laminar (RAMPANT cannot simulate the transition from laminar to turbulent boundary layer in a three-dimensional case) and fully turbulent flow (loss of laminar flow on the entire wing surface). The entire flowfield was initialized with freestream values, then run until the residual of the mass, momentum, and energy equations had all converged to 3 orders of magnitude.

8.2.2 Results

The wing surface pressure and Mach number distributions were measured at 6 different spanwise stations : 2y/b = 0.106, 0.191, 0.37, 0.578, 0.786 and 1.00. Figures 8.3 - 8.8 show pressure and Mach number contours on the surface of configuration I for the inviscid, fully laminar and fully turbulent flow assumption respectively. Figures 8.9 - 8.14 show pressure and Mach number contours on the surface of configuration II for the inviscid, fully laminar and fully turbulent flow assumption respectively.

The pressure and Mach number distribution at spanwise stations : 2y/b = 0.106, 0.191, 0.37, 0.578, 0.786 and 1.00 of configuration I for the inviscid, fully laminar and fully turbulent flow assumptions are shown in Figures 8.15 - 8.20 respectively. The pressure and Mach number distribution at spanwise stations : 2y/b = 0.106, 0.191, 0.37, 0.578, 0.786 and 1.00 of configuration II for the inviscid, fully laminar and fully turbulent flow assumptions are shown in Figures 8.21 - 8.26 respectively.

From the above Figures, for configuration I, it can be seen that all of the pressure distributions (especially on the outboard wing, i.e. : from the kink to the tip) is characterized by a steep initial gradient (rapidly falling pressure), followed by a negative pressure gradient (falling/favourable pressure) and a single weak shock wave and finally a recovery region with a soft aft pressure gradient. Based on section 7.3.2.1, with the above pressure distribution characteristics, it is possible to apply the HLFC concepts on the wing of configuration I. The same pressure distribution characteristic are seen on the wing of configuration II (VC-flap deployed). For a more detailed laminar flow analysis, see section 8.3 of this thesis.

From the above Figures, for both configurations, the average wing upper surface isobar sweep angle (taken at 50% chord) is approximately 21.8 degrees, instead of 25 degrees (wing quarter chord sweep angle). Thus, the isobar sweep efficiency is = 21.8/25 = 0.872. The inboard wing upper surface isobars are characterized by a more sweep forward at the front and less sweptback at the rear, and the shock strength is quite

weak.

With the deflection of VC-flap, the pressure distribution shape at the front of shock does not change too much; this is good for HLFC application. The VC-flap deflection makes the shock is stronger and increase aft loading (producing greater pitching moment and hence more trim drag).

The effects of angle of attack on pressure and Mach number distribution is quite strong, especially in the region near the leading edge, as shown in Figures 8.27 and 8.28. In real flight, the above phenomenon could have implications for a gust effects on aircraft performance. This phenomenon should be considered when designing HLFC wing.

Wing-fuselage lift coefficient ($C_{L_{WF}}$) versus angle of attack (α) for configuration I is shown in Figure 8.29. Lift curve slopes ($C_{L_{\alpha.WF}}$) for full-laminar and full-turbulent flow assumption are 0.1403/degree and 0.1337/degree respectively. Lift coefficient at zero angle of attack ($C_{L_{0.WF}}$) for the full-laminar and full-turbulent flow assumptions are 0.342 and 0.303 respectively. From the above figure, the aircraft design lift coefficient ($C_L = 0.5$) is attained at $\alpha = +1$ degrees.

At the aircraft design lift coefficient ($C_L = 0.5$), the comparisons between pressure distribution at subcritical Mach number and design Mach number for root, inboard and outboard wing sections are shown in Figures 8.30, 8.31 and 8.32 respectively (see also Figures 7.36, 7.41, 7.44 and 7.45).

The comparison of pressure distributions between inviscid, full-laminar and full-turbulent flow assumptions are shown in Figures 8.33. Based on this figure, pressure distributions between inviscid and full-laminar flow assumption is quite close, this is because boundary layer thickness on full-laminar flow assumption is quite thin. So to save an iteration time, especially during an initial design (where the iteration time is crucial), the inviscid flow assumption is quite reasonable. As shown in the above figure, the effect of turbulent is not so great.

As shown in Table 8.1, VC-flap deflection has a powerful effect (decrease/increase) on wing section lift. Careful VC-flap design (includes VC-flap shape, VC-flap chord ratio to the main wing, radius of rotation/ VC-flap deflection path, etc.) should be considered, if the maximum VC-flap effectiveness $(c_{l\,II}-c_{l.I})/\delta$, is the objective. As shown in Table 8.1, for positive VC-flap deflections, the VC-flap effectiveness is quite good; but for negative deflection, the VC-flap effectiveness is less satisfactory, as shown for the wing section SAOT, where VC-flap effectiveness is negative.

Figure 8.34 - 8.35 show spanload distribution for fully laminar flow of the configuration I and the configuration II respectively. It can be seen that both of the spanloads depart significantly from an elliptical distribution. The wing-fuselage lift coefficient for configuration I is about 0.342, which is less than the design requirement ($C_{L.design} = 0.5$), although the flow was assumed to be a fully laminar on the entire wing. The wing-fuselage lift coefficients for configuration II is 0.419 (see Figure 8.35).

The above wing configuration results from just the first iteration of a very

complex wing design. Regardless of its weakness, its performance appears quite reasonable. To improve the wing performance, it is recommended to optimized the airfoil sections, twist and VC-flap deflection distributions along the wing span.

8.3 LAMINAR FLOW ANALYSIS

It is beyond the scope of this work to undertake a complete laminar flow analysis on the ATRA-100's wing (i.e. : boundary layer stability analysis, transition prediction, suction requirements,...etc.). The codes necessary for such a design task were not available at Cranfield University.

The laminar analysis is performed only on the outboard wing (from the kink to the tip), as this region offers higher potential for HLFC application. Reference 8.7 states that on the mid to outer wing of subsonic transport aircraft the flow (normal to the 0.5 chord isobar) is two-dimensional in character (see also section 7.7.2.1). So, for purposes of this work, the laminar analysis is done by comparison of characteristics of the outboard wing sections (normal to the isobar) to the HLFC airfoil.

Taking into account the considerations described above, for purposes of this work, a simplified laminar flow analysis procedure was used, as follows :

a. Analyse the suitability of the ATRA-100's wing for HLFC application, by comparison of its pressure distribution characteristics described in section 8.2.2 with HLFC design requirements described in section 7.3.2. The results are shown in Table 8.1 and 8.2. Note for Table 8.1 and 8.2 : Kink (x = 17.0, y = 5.99), its means plane Kink is through point with co-ordinate x = 17.0 and y = 5.99 and normal to the wing upper surface 0.5 chord isobar; same definitions also for Saok, Saot and Stip.
b. It is assumed that the possibility of leading-edge attachment line contamination is eliminated by having $(dc_p/ds)_{le}$ between 40 – 100 and suction, cross-flow in the leading-edge region is suppressed by suction and instability due to cross-flow and Tollmien-Schlichting in the mid-chord is suppressed by the favourable pressure gradient.
c. Transition predictions. By assumptions that extended regions of favourable pressure gradient would correspond to extended regions of laminar flow, therefore the boundary layer transition is expected to be just in the front of the recovery point (see section C.5.2.2 for correction of shock position predicted by RAMPANT), see also section 7.3.2. The results are shown in Figure 8.34.
d. Suction requirements are predicted by using an empirical data as shown in Figure 6.5.

As shown in Tables 8.2 and 8.3, the leading-edge/initial pressure gradient ($(dc_p/ds)_{le}$) along the wing span from the KINK to near the wing tip (STIP) is about 42. For the ATRA-100 which has a wing leading-edge sweep angle of 27.3 degrees and cruise at Mach 0.8 (237 m/s) and Reynolds number of 21.6×10^6, based on Figure 6.5, the minimum suction quantity (V_s) is about - 0.00015 (or V_s = - 0.00015 x 237 m/s = - 0.03555 m/s).

The flow behind the shock can be expected to remain attached, as shown in Table 8.1 and 8.2, the maximum local Mach number (M_l) is less than Mach 1.2 and the aft pressure gradient both upper ($dc_p/d(x/c)_{aft.upper}$) and lower ($dc_p/d(x/c)_{aft.lower}$) are less than 3.

The following are transition locations both of configuration I and II, some occur beyond 65 % chord (the location of leading-edge of spoiler), see also Figure 8.36. It is impossible to have laminar flow behind the leading-edge of a spoiler, unless tight manufacturing tolerances and surface quality are attained (see section 7.4.6 of this thesis).

Wing section	Transition location, % local wing chord	
	Configuration I	Configuration II
Kink (x = 17.0, y = 5.99)	67	74
Saok (x = 18.5, y = 9.35)	65	69
Saot (x = 19.7, y = 12.71)	66	66
Stip (x = 21.0, y = 15.7)	57	62

8.4 AERODYNAMIC EFFECT OF GAP BETWEEN FLAP SEGMENT

In this section, the transonic flow over the gap between the VC-flap segments of a constant section wing is calculated. The computation was performed with same methods described in section 8.2.

8.4.1 Configuration Description

The basic properties of the wing and the gap geometries are given in table 8.4. The airfoil used in this wing is NLAM78, and its was taken from Reference 8.8. The wing and gap geometries and surface grid used for this analysis are shown in Figure 8.37. The results shown here are for $M_\infty = 0.8$, angle of attack = 0 degree, and Reynolds number of 21.6×10^6. The computational domain is rectangular box that extends 5 root chord in front, behind, above, and below the wing, and 3 wingspans to the side of the wing. The wing and gap surface mesh contains 291,809 faces. The resulting volume mesh contains 138,642 cells. Inviscid flow was assumed for the computations. The entire flowfield was initialized with freestream values, then run until the residual of the mass, momentum, and energy equations had all converged 3 orders of magnitude.

8.4.2 Results

Figure 8.38 shows pressure contours on the surface of the wing-gap configuration. Pressure and Mach number distribution of the wing-gap configuration across the center of the gap are shown in Figure 8.39 and 8.40 respectively.

From Figures 8.39 and 8.40, it can be seen that on the upper surface as a

flow reaches the gap, there is a steep positive pressure gradient and as a result a strong shock was formed. This phenomenon occurs because, after the flow on the upper surface reached the peak of its expansion, suddenly it is forced to reach the freestream value. The same phenomenon is seen in Figure 8.38.

Wing section, x and y in m	SOB	INB	KINK	SAOK	SAOT	STIP
Spanwise station, m	1.714	3.236	5.986	9.350	12.713	16.719
2y/b (b/2 = 16.179 m)	0.106	0.191	0.37	0.578	0.786	1
Configuration I :						
Chord (C.I), m	5.79	5.005	3.588	2.926	2.266	1.586
Lift coefficient ($c_{l.I}$)	0.258	0.298	0.38	0.439	0.343	0.24
Configuration II :						
Chord (C.II), m	5.873	5.082	3.649	2.96	2.239	1.558
VC-flap deflection (δ), deg.	2	1.822	1.5	1	-1	-1.5
Lift coefficient ($c_{l.II}$)	0.387	0.395	0.4534	0.4935	0.3463	0.1889
C.II/C.I	1.0143	1.0153	1.017	1.0115	0.9882	0.9822
$(c_{l.II}-c_{l.I})/\delta$, /deg.	0.0645	0.084	0.0489	0.0545	-0.003	0.0341

Table 8.1 Section lift coefficients for Configuration I and II

			$dc_p/d(x/c)$		
Wing section, x and y in m	$(dc_p/ds)_{le}$	M_l	middle-up.	aft-upper	aft-lower
Kink (x = 17.0, y = 5.99)	42	1.08	0.23	2.5	1.3
Saok (x = 18.5, y = 9.35)	42	1.1	0.293	2.83	1.5
Saot (x = 19.7, y = 12.71)	42	1.08	0.297	2.86	1.47
Stip (x = 21.0, y = 15.7)	42	1.025	0.477	2.44	1.36

Table 8.2 Pressure distribution characteristics for Configuration I

			$dc_p/d(x/c)$		
Wing section, x and y in m	$(dc_p/ds)_{le}$	M_l	middle-up.	aft-upper	aft-lower
Kink (x = 17.0, y = 5.99)	42	1.15	0.127	2.96	1.04
Saok (x = 18.5, y = 9.35)	42	1.19	0.396	2.98	1.04
Saot (x = 19.7, y = 12.71)	42	1.1	0.32	2.55	1.68
Stip (x = 21.0, y = 15.7)	42	0.99	0.44	1.92	1.54

Table 8.3 Pressure distribution characteristics for Configuration II

aspect ratio	9.5
span (b), M	16.2
tip Chord, M	1.586
root chord, M	4.763
taper ratio	0.333
quarter chord sweep, deg.	25
twist	none
airfoil section	NLAM78
gap wide, M	0.010
gap spanwise position, y/b	0.5

Table 8.4 Wing and gap geometries

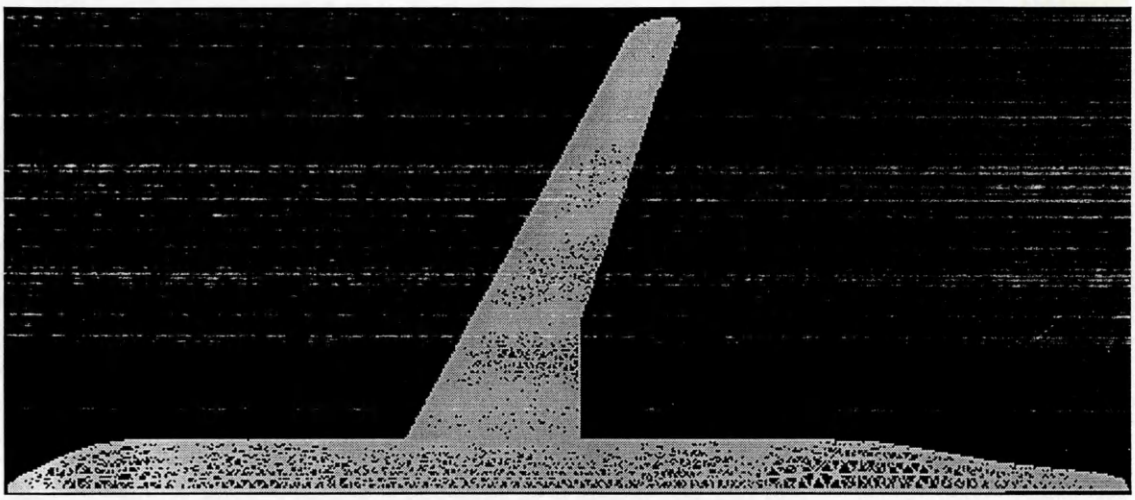

Figure 8.1 Configuration I surface mesh

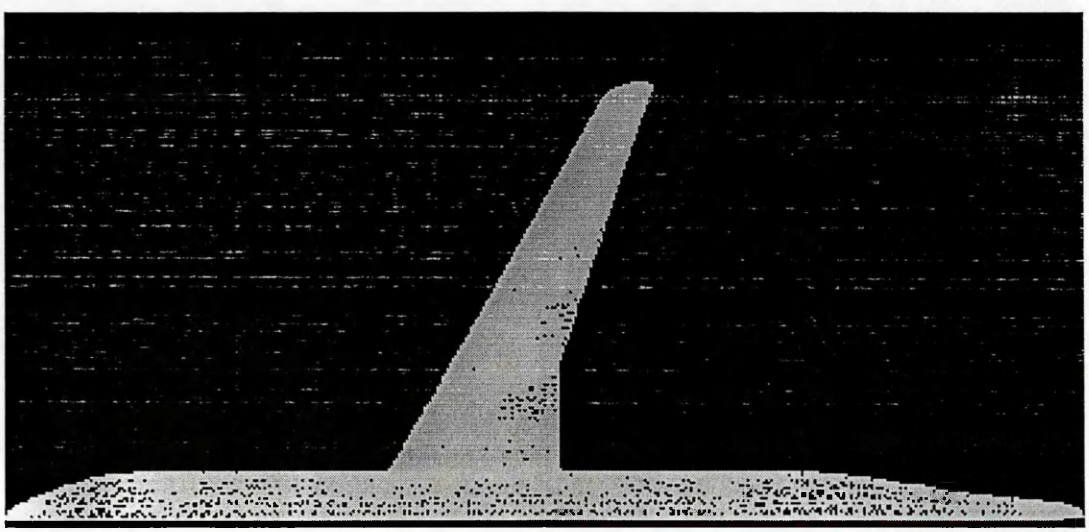

Figure 8.2 Configuration II surface mesh

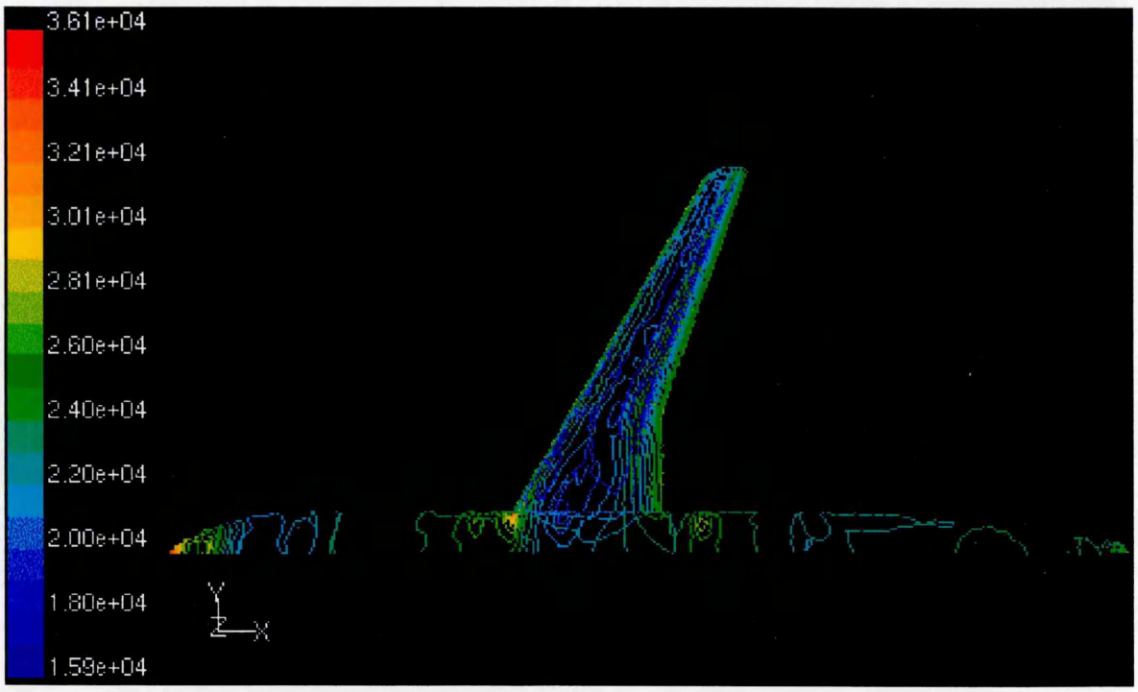

Figure 8.3 Configuration I : contours of static pressure, pascal (inviscid flow)

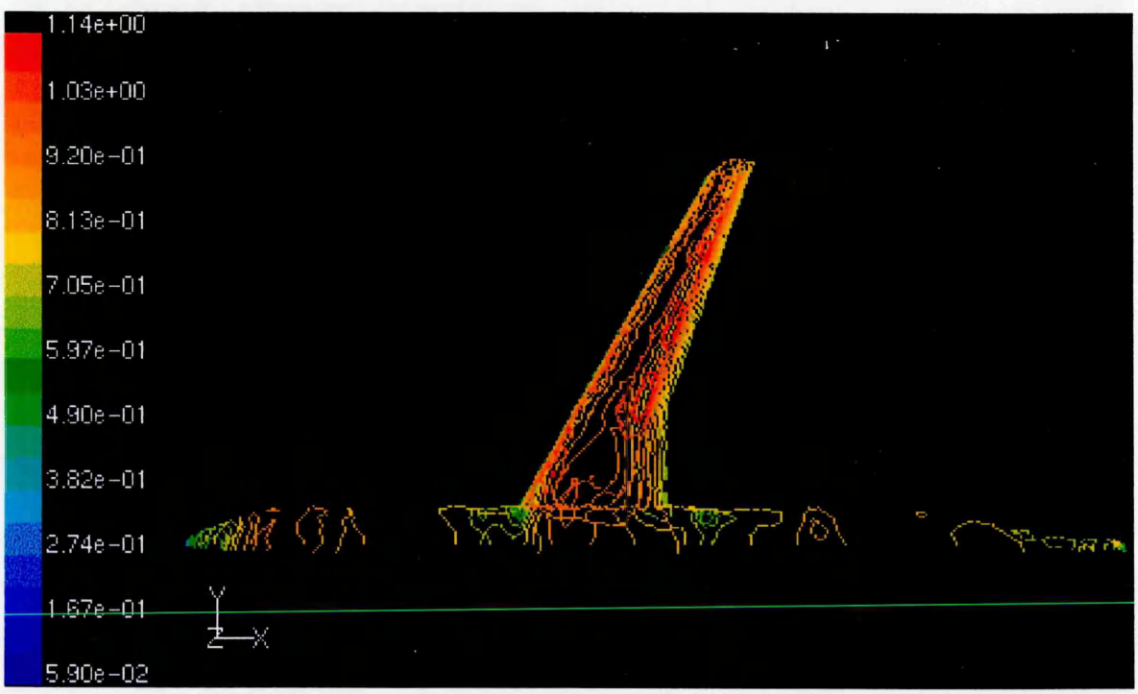

Figure 8.4 Configuration I : contours of Mach number (inviscid flow)

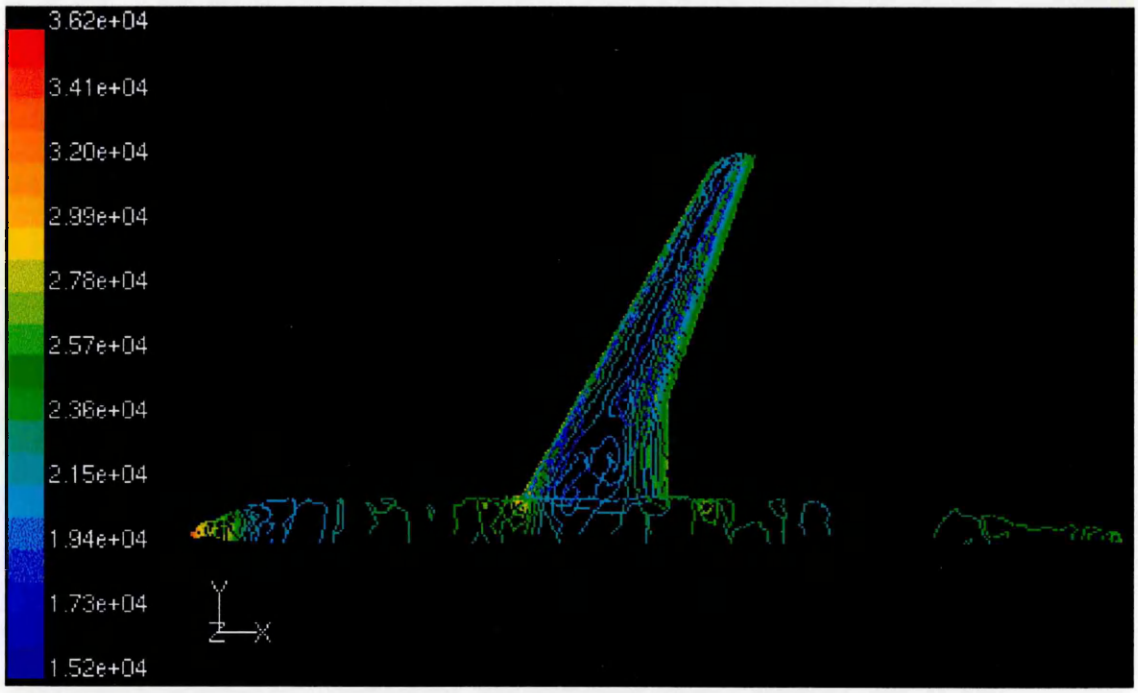

Figure 8.5 Configuration I : contours of static pressure, pascal (fully laminar flow)

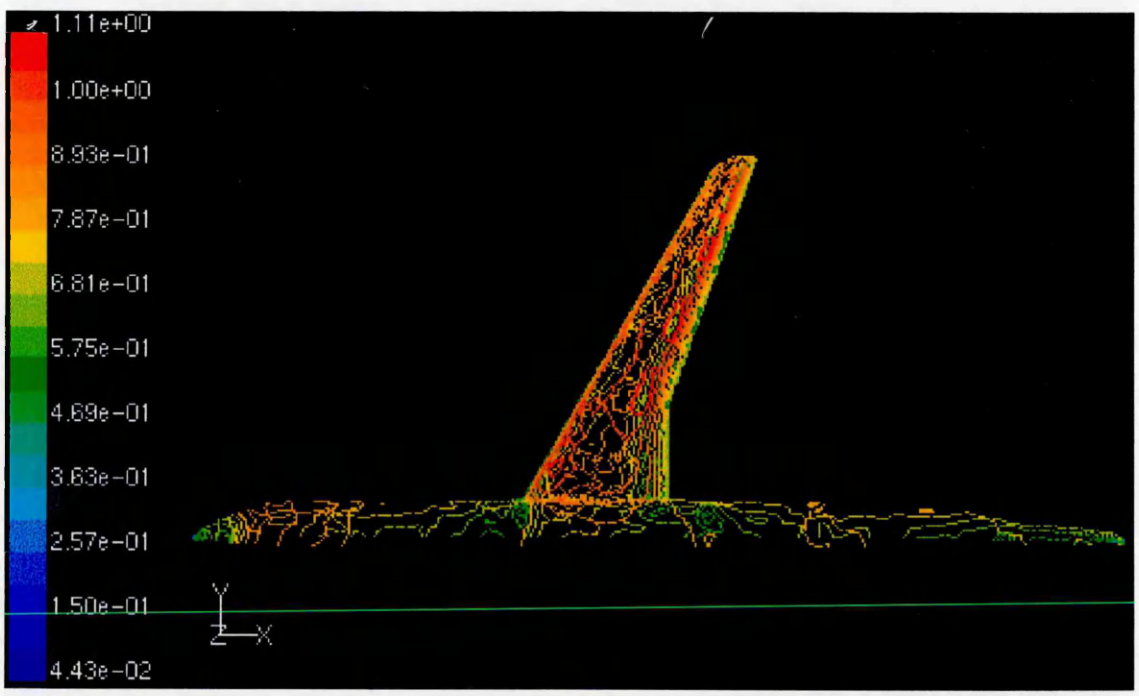

Figure 8.6 Configuration I : contours of Mach number (fully laminar flow)

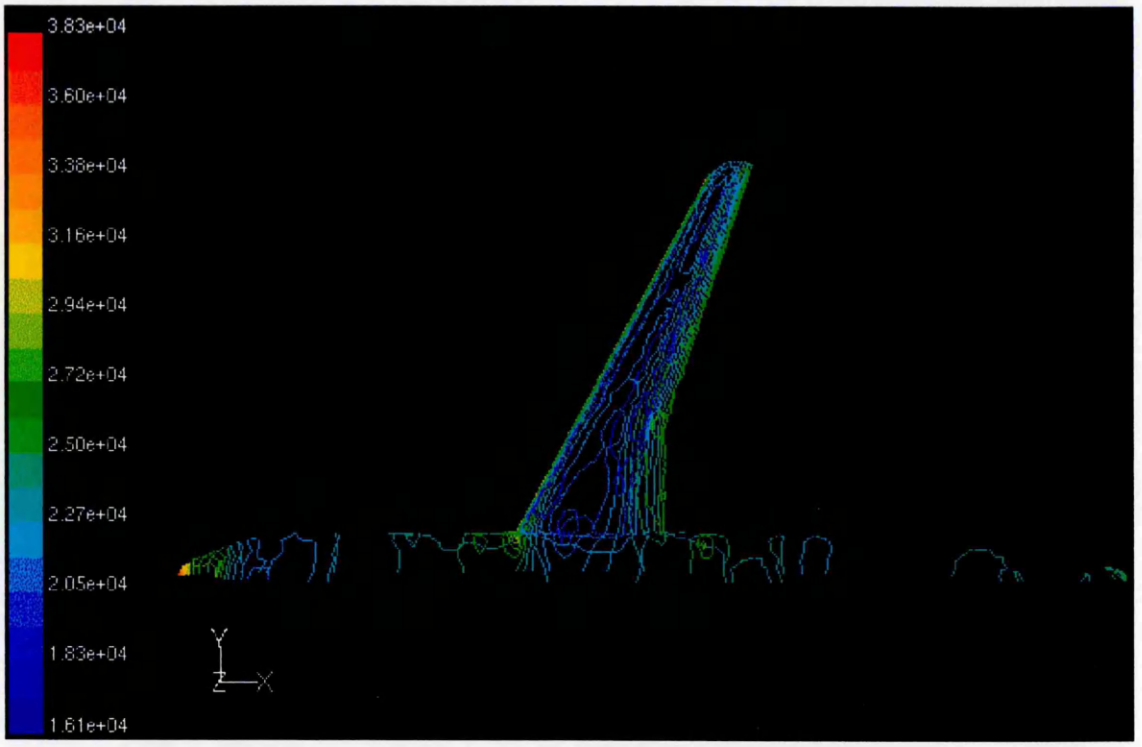

Figure 8.7 Configuration I : contours of static pressure, pascal (fully turbulent flow)

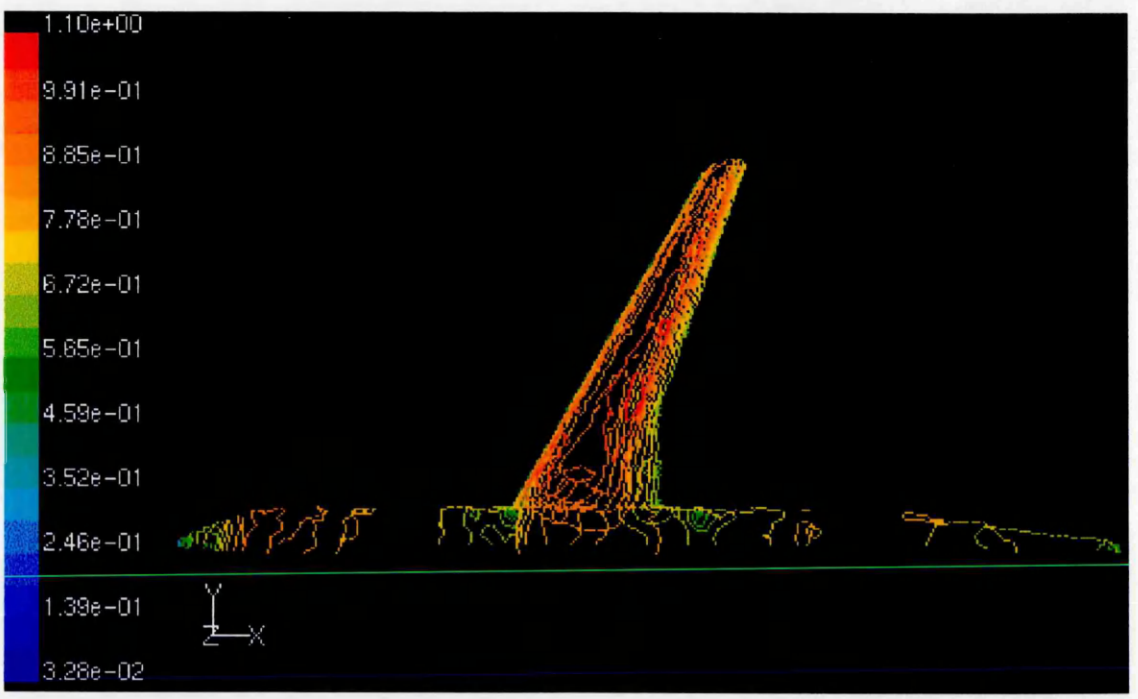

Figure 8.8 Configuration I : contours of Mach number (fully turbulent flow)

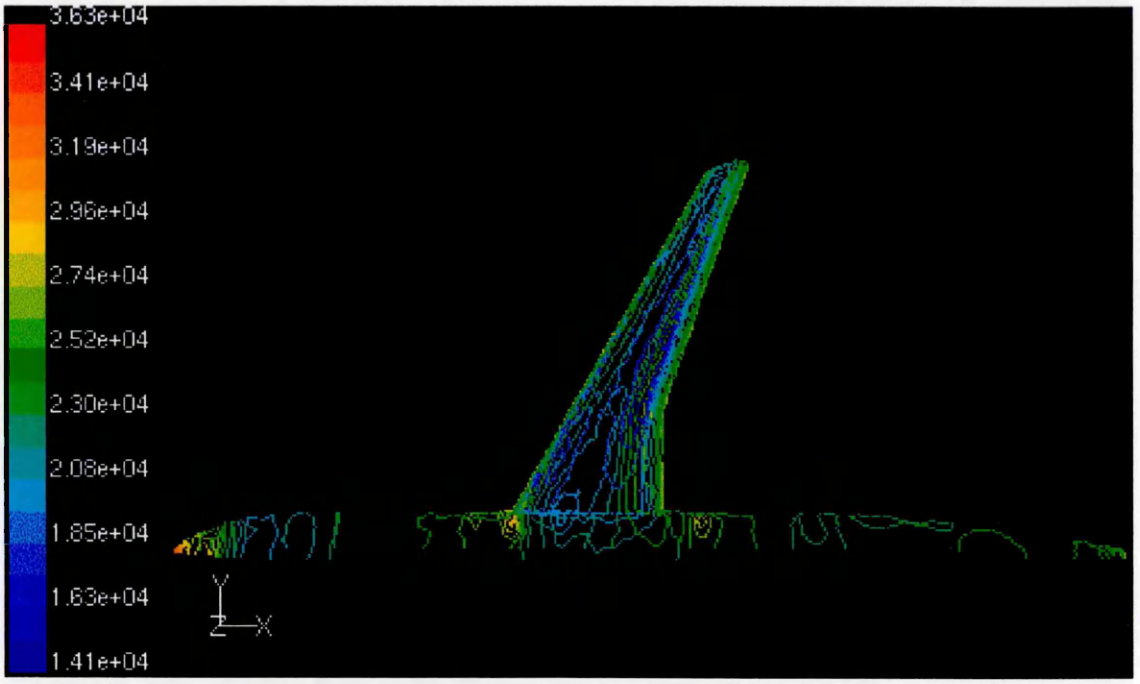

Figure 8.9 Configuration II : contours of static pressure, pascal (inviscid flow)

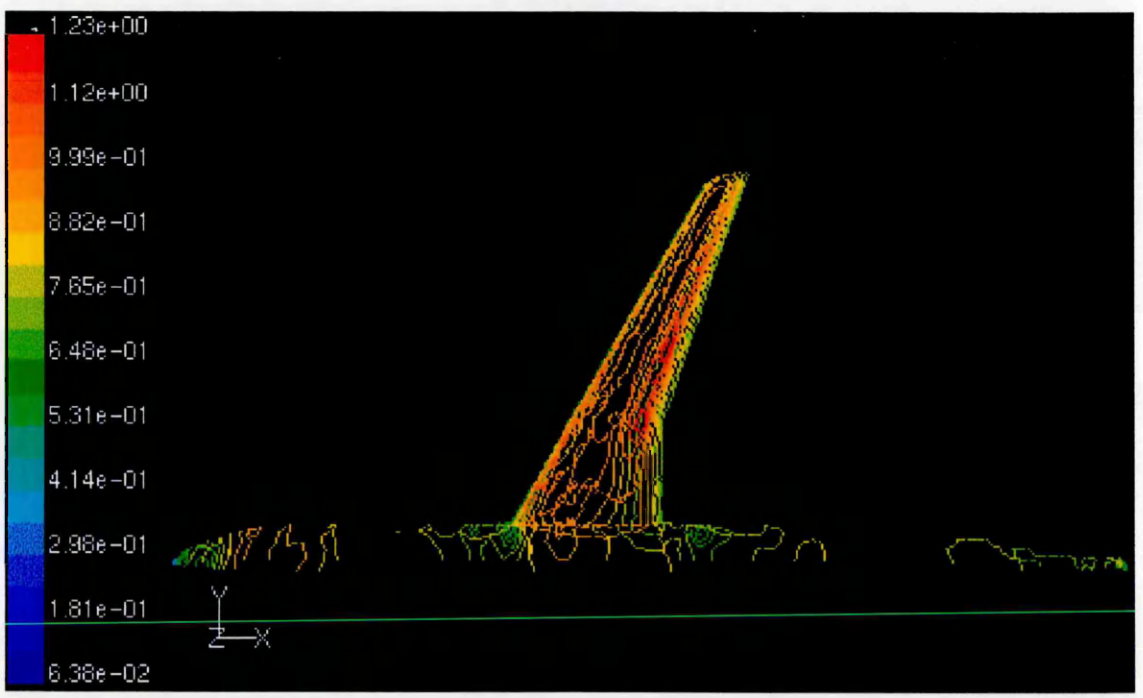

Figure 8.10 Configuration II : contours of Mach number (inviscid flow)

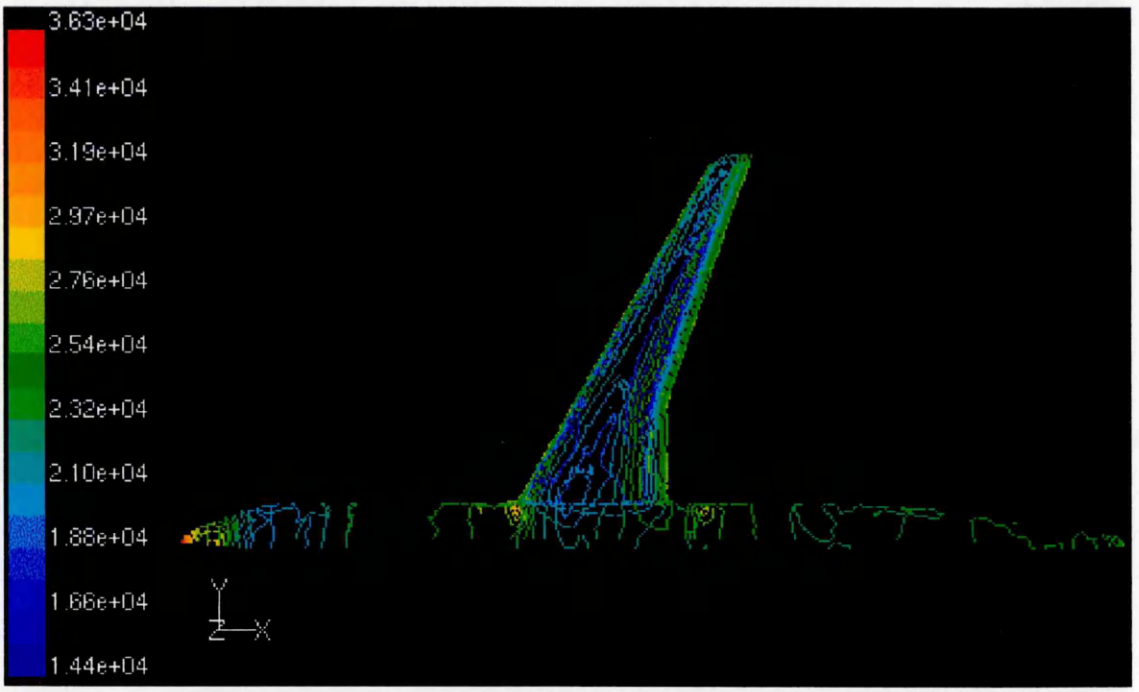

Figure 8.11 Configuration II : contours of static pressure, pascal (fully laminar flow)

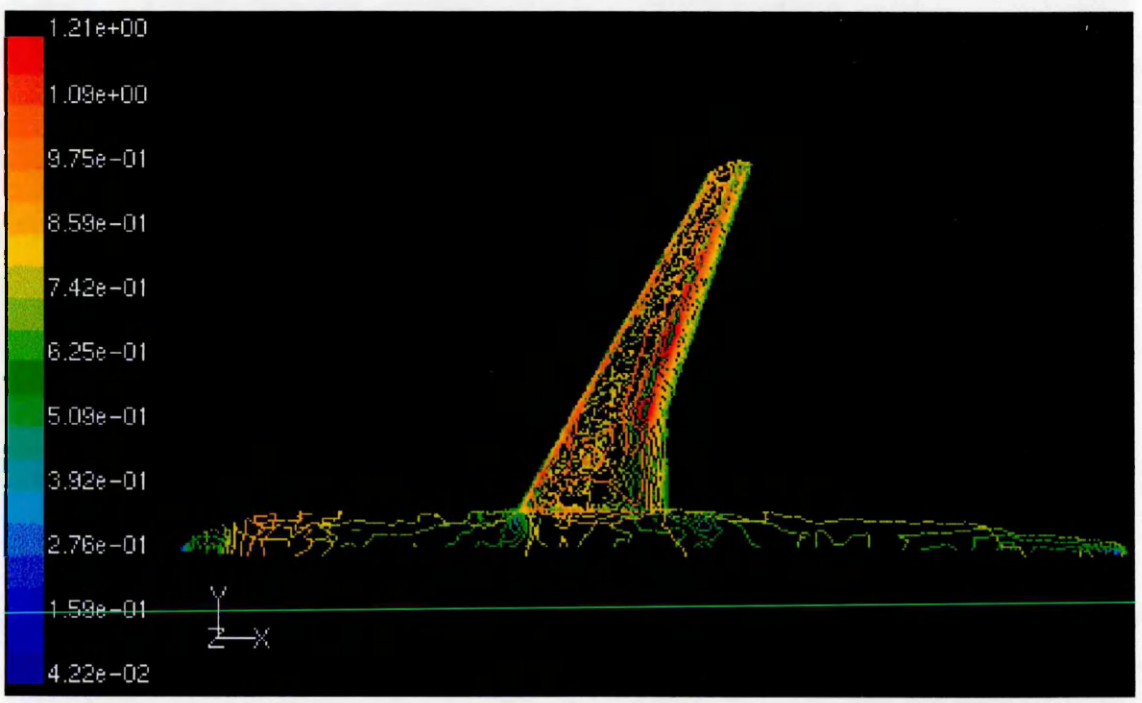

Figure 8.12 Configuration II : contours of Mach number (fully laminar flow)

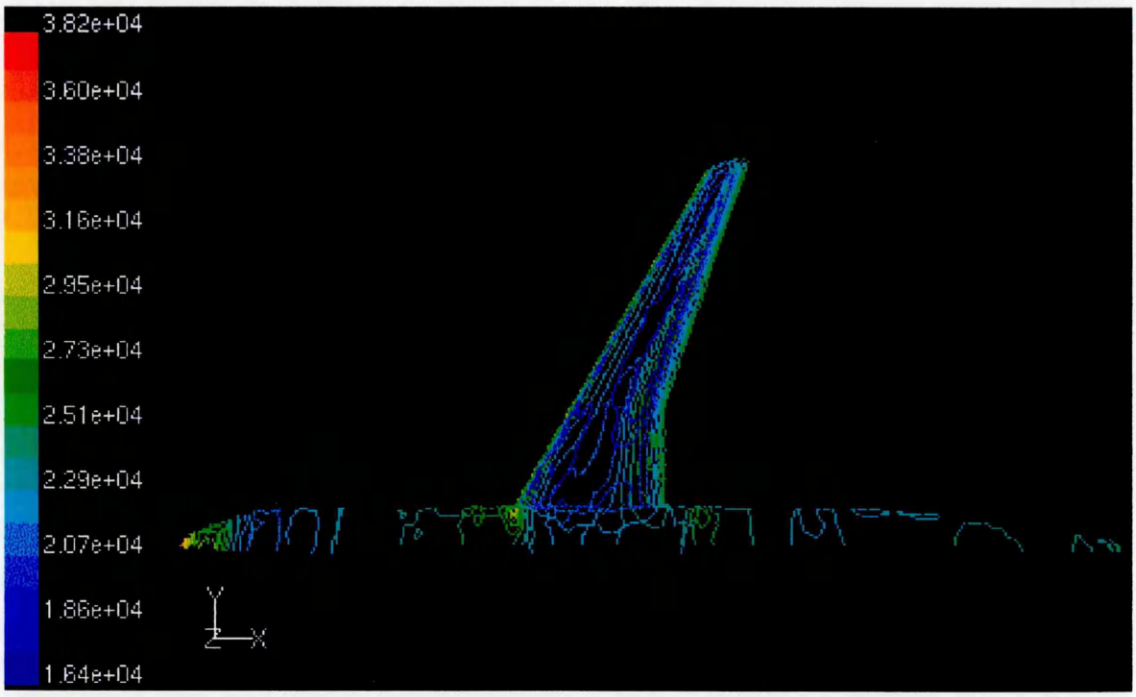

Figure 8.13 Configuration II : contours of static pressure, pascal (fully turbulent flow)

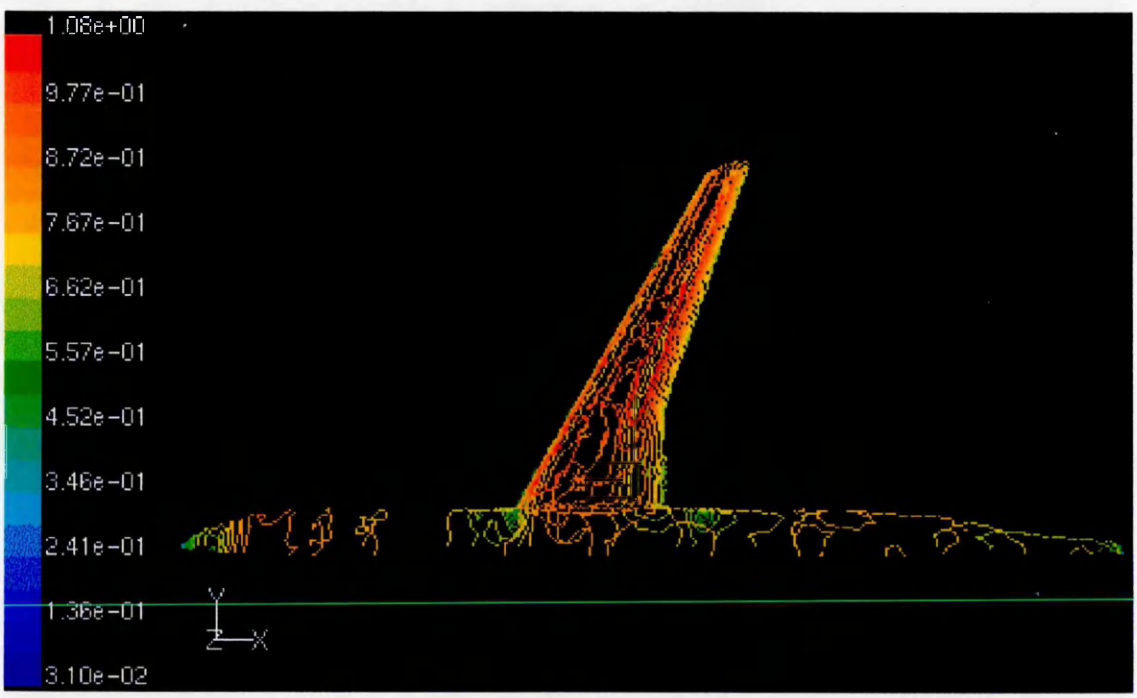

Figure 8.14 Configuration II : contours of Mach number (fully turbulent flow)

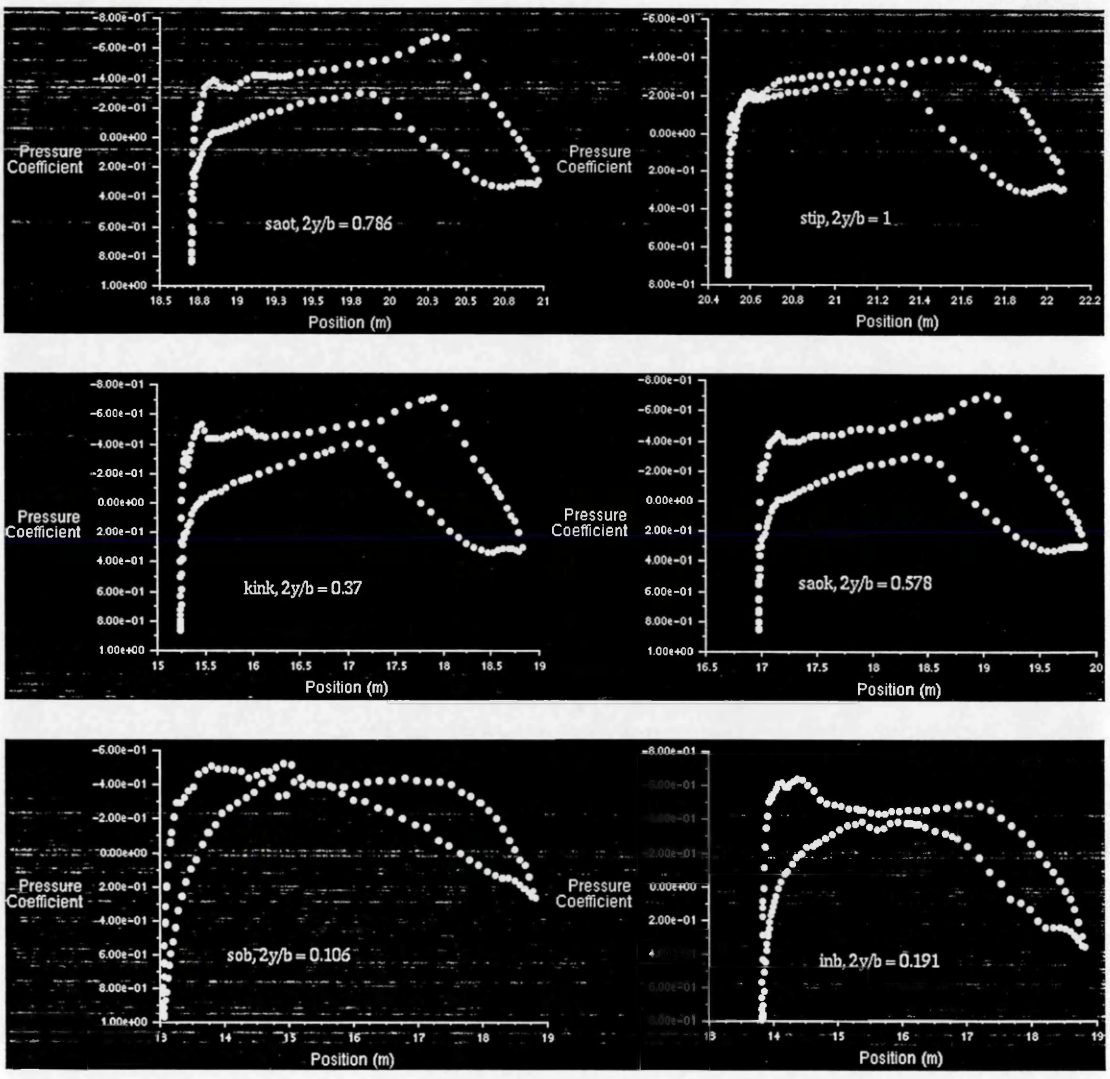

Figure 8.15 Configuration I : pressure distribution (inviscid flow)

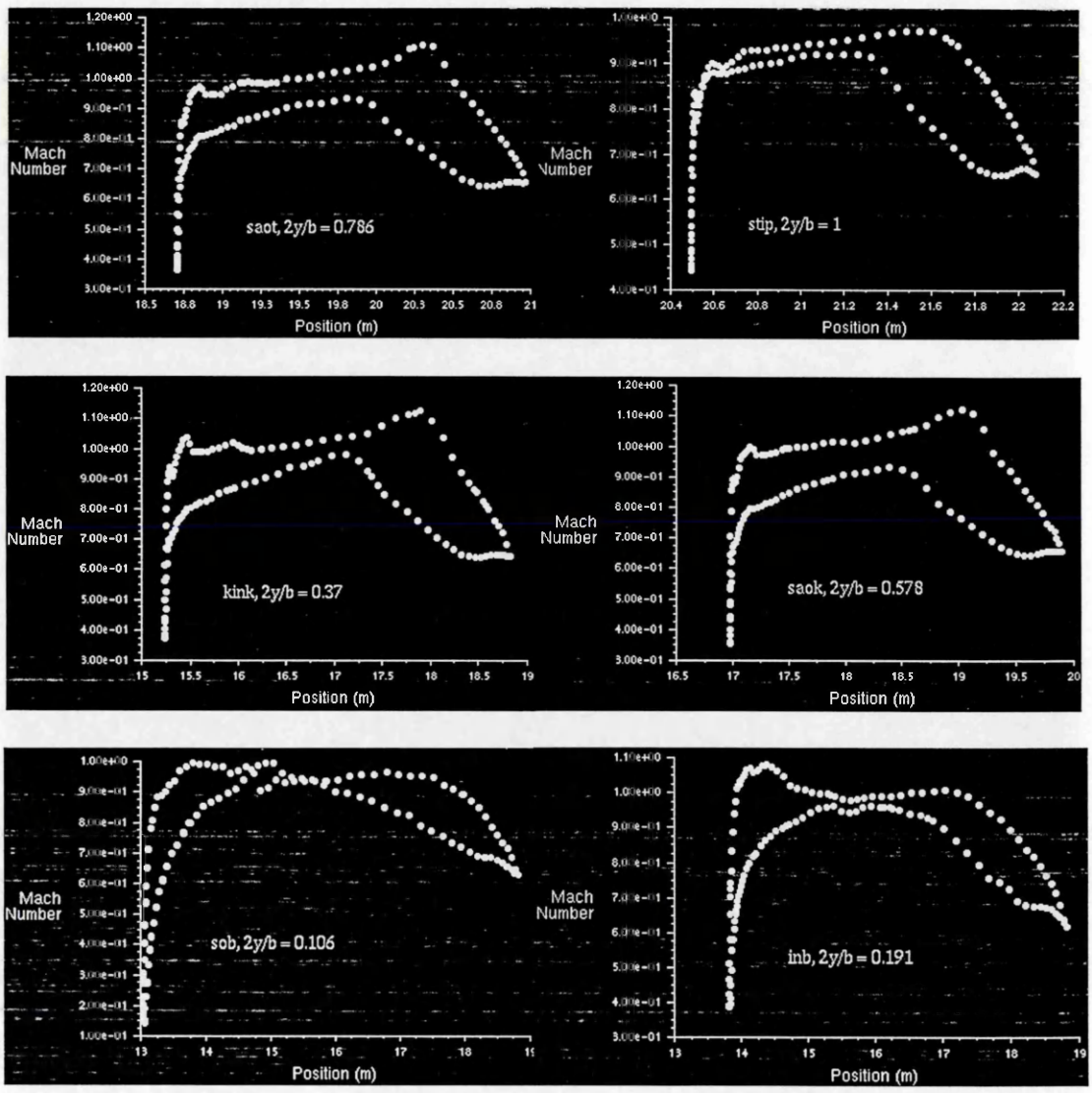

Figure 8.16 Configuration I : Mach number distribution (inviscid flow)

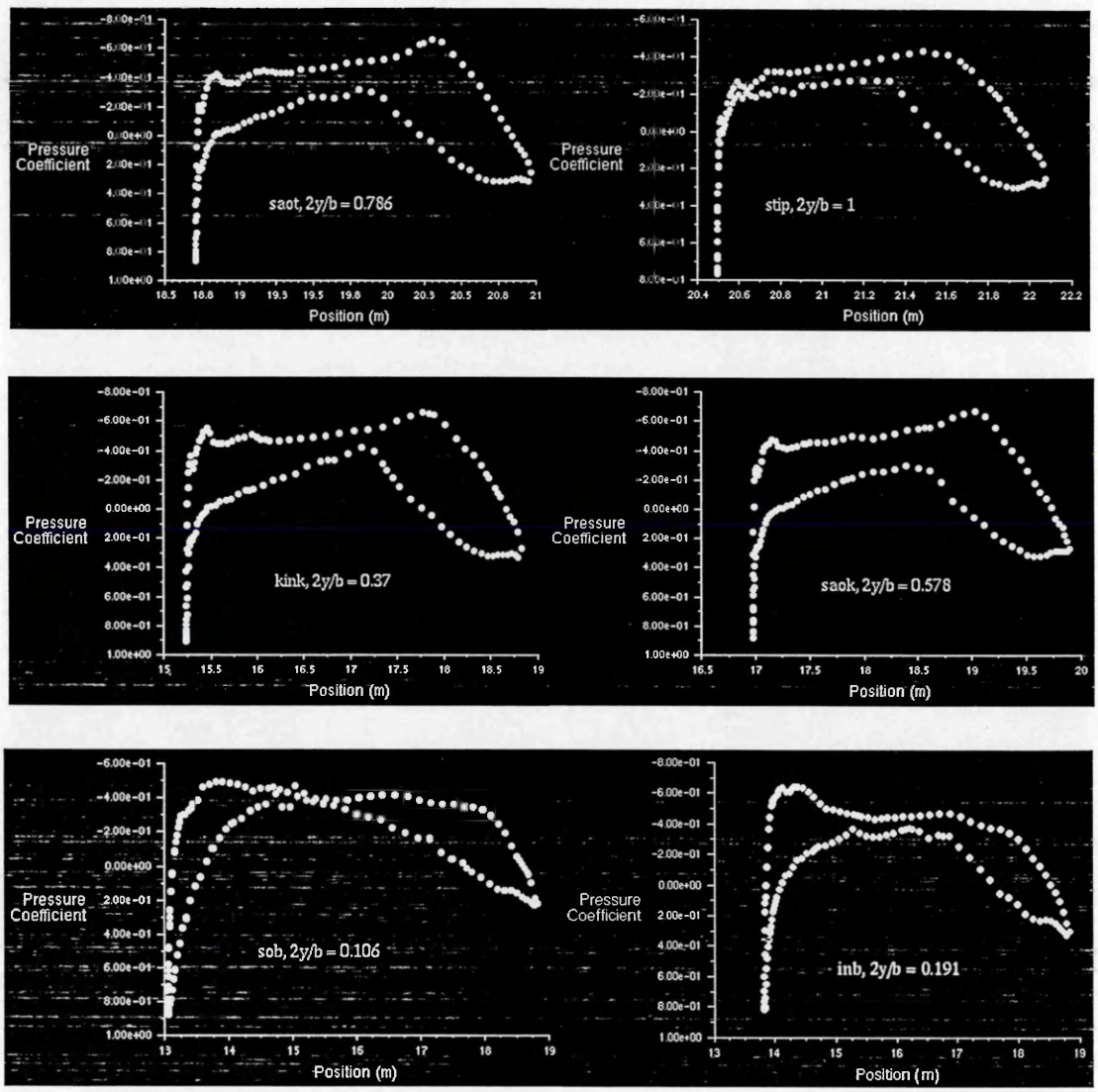

Figure 8.17 Configuration I : pressure distribution (fully laminar flow)

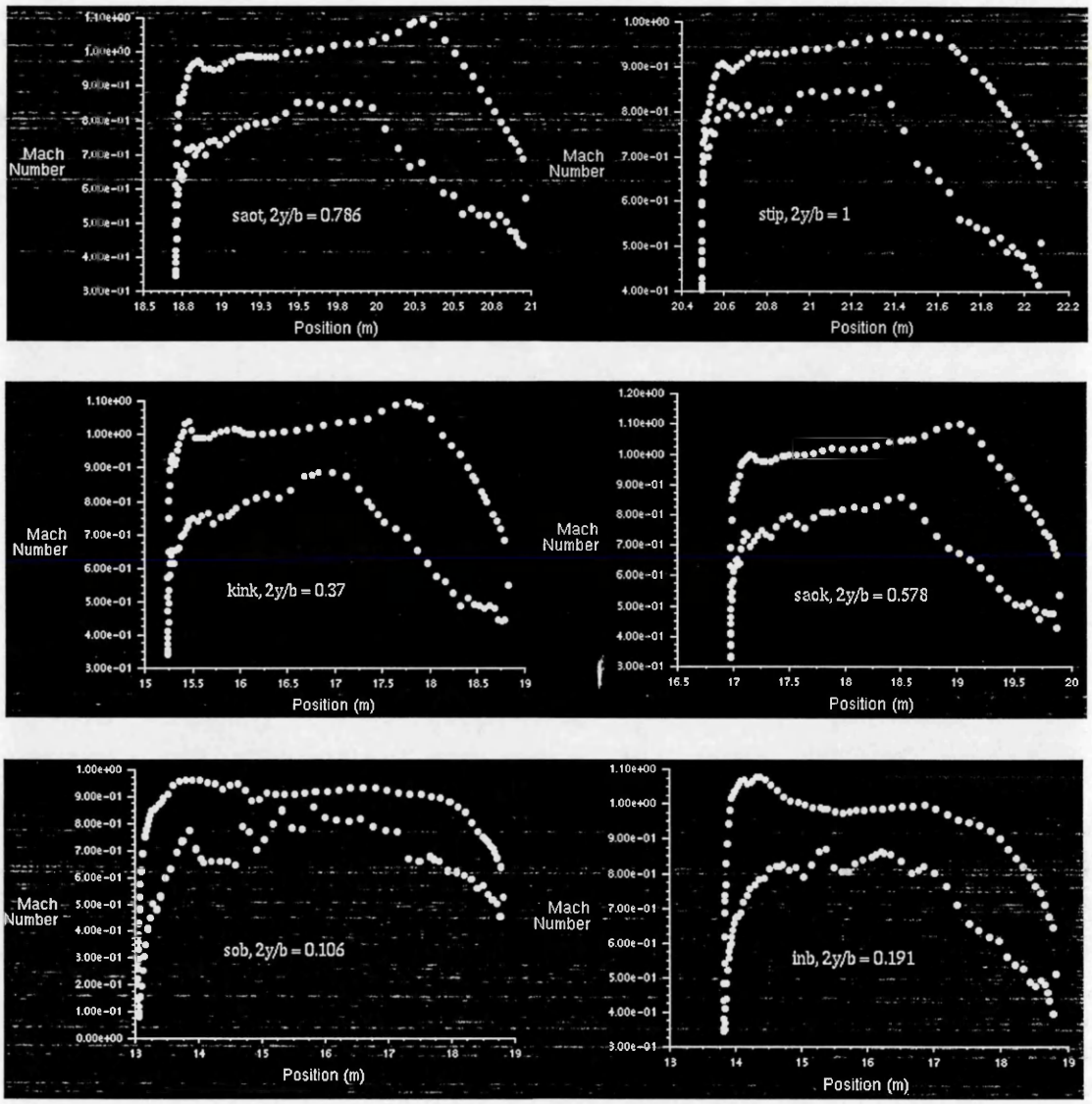

Figure 8.18 Configuration I : Mach number distribution (fully laminar flow)

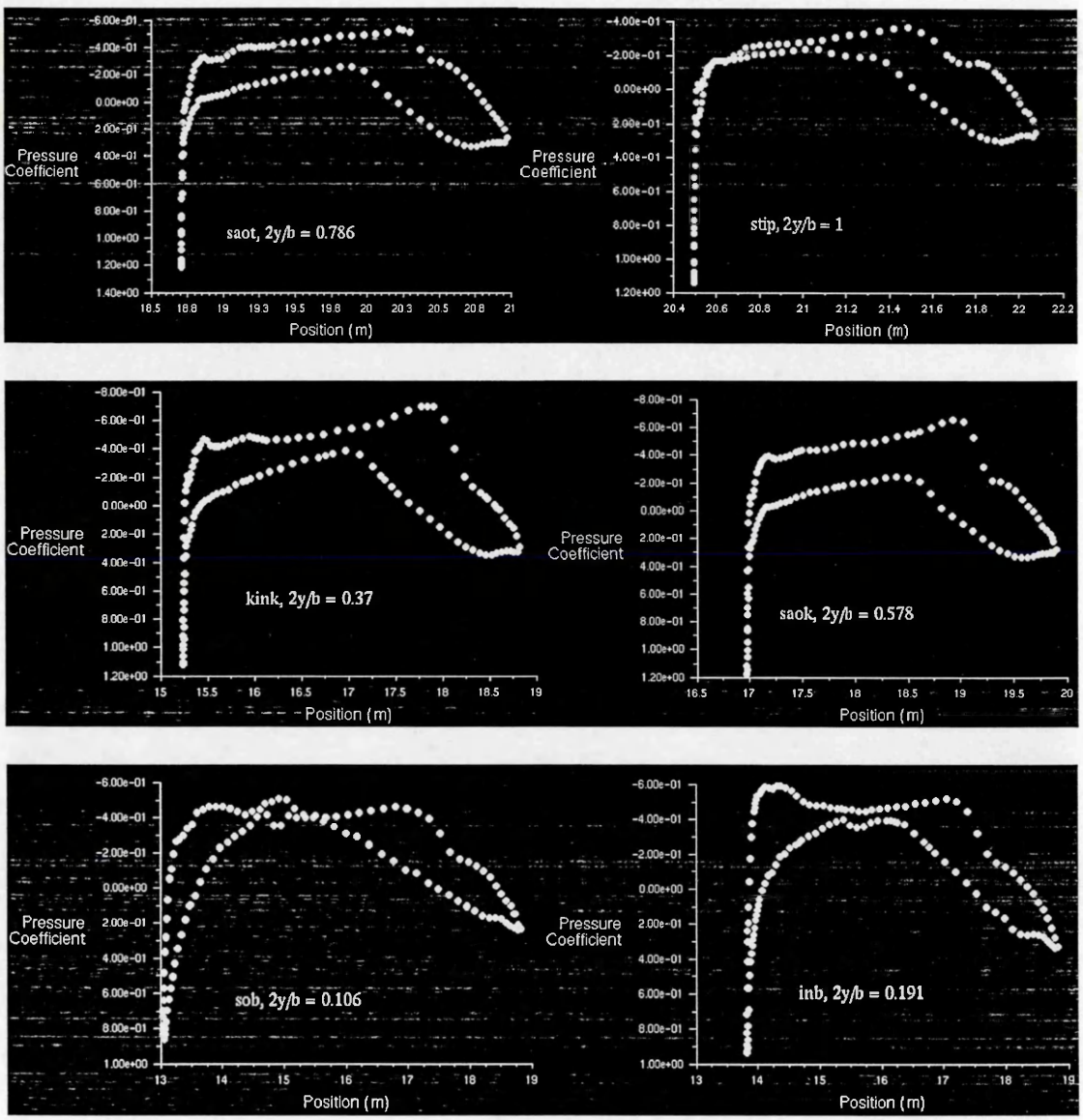

Figure 8.19 Configuration I : pressure distribution (fully turbulent flow)

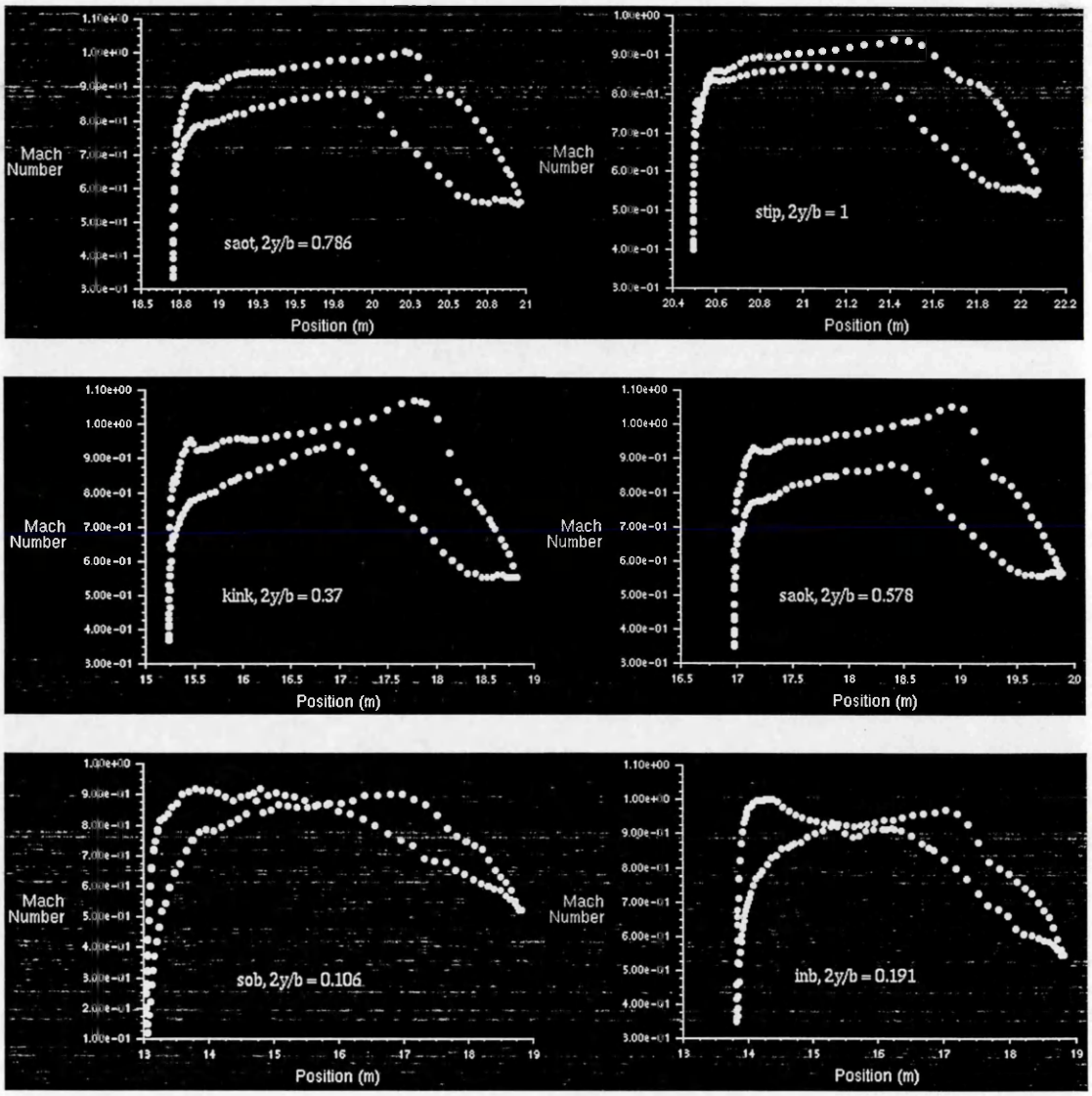

Figure 8.20 Configuration I : Mach number distribution (fully turbulent flow)

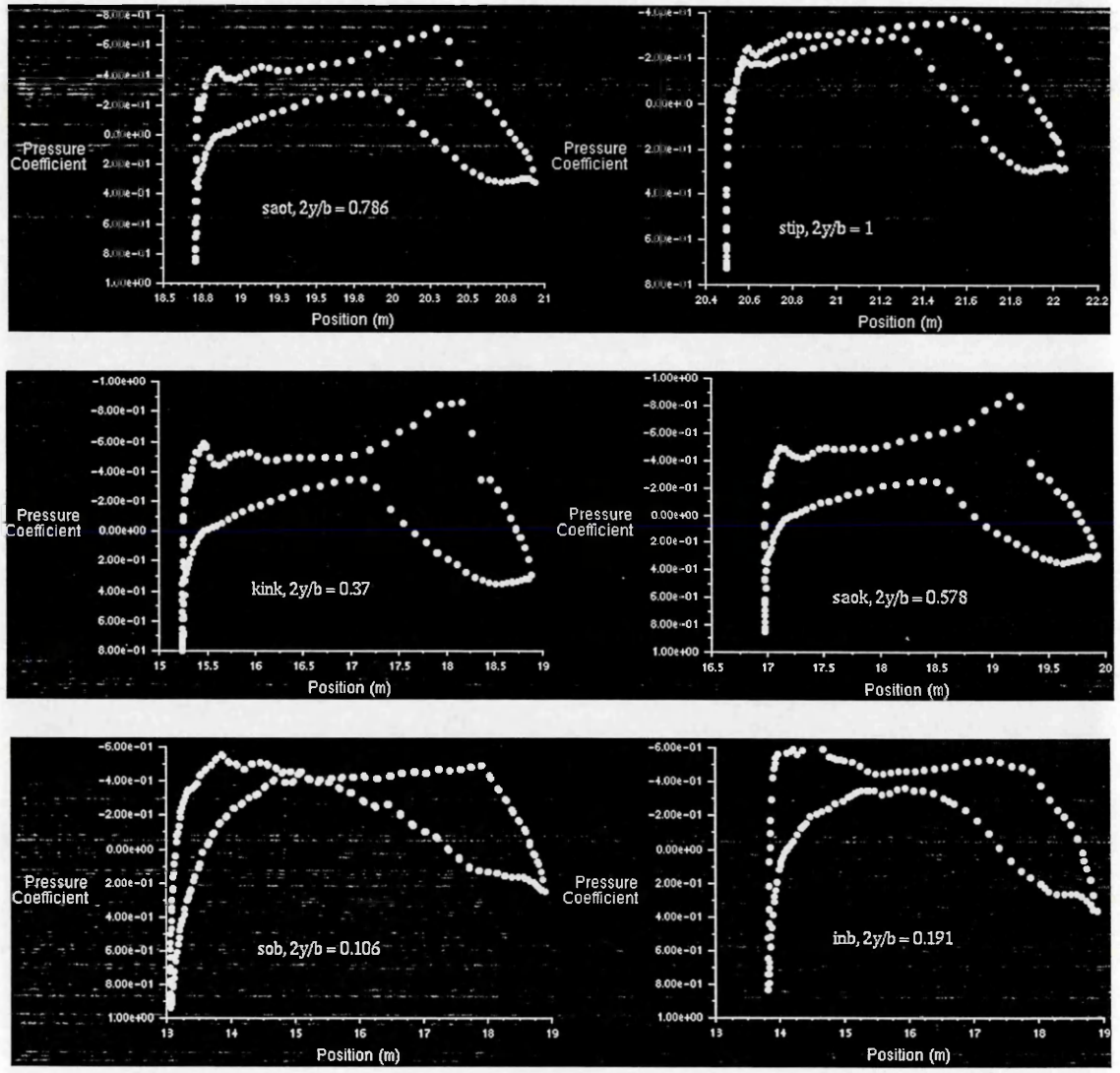

Figure 8.21 Configuration II : pressure distribution (inviscid flow)

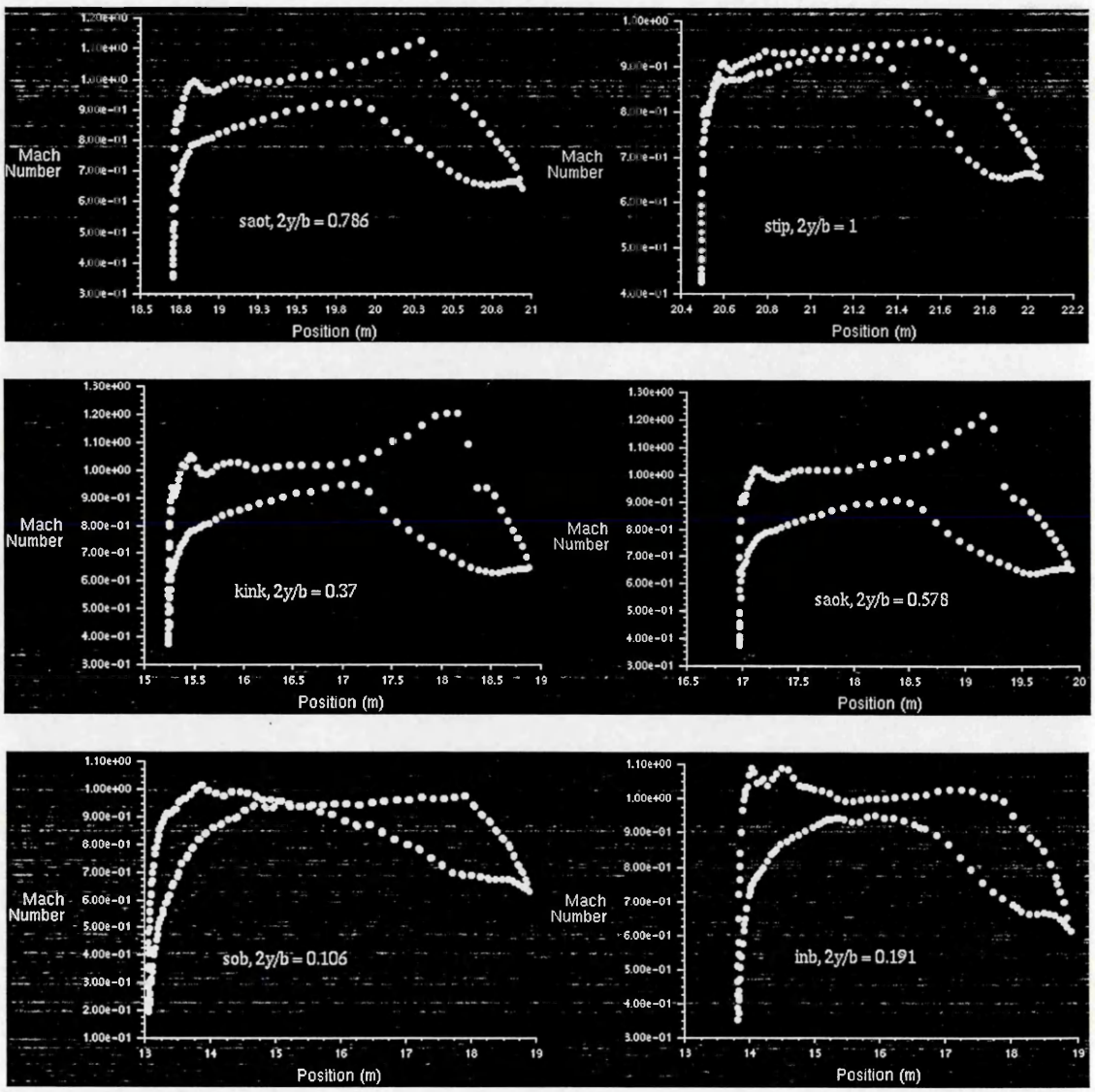

Figure 8.22 Configuration II : Mach number distribution (inviscid flow)

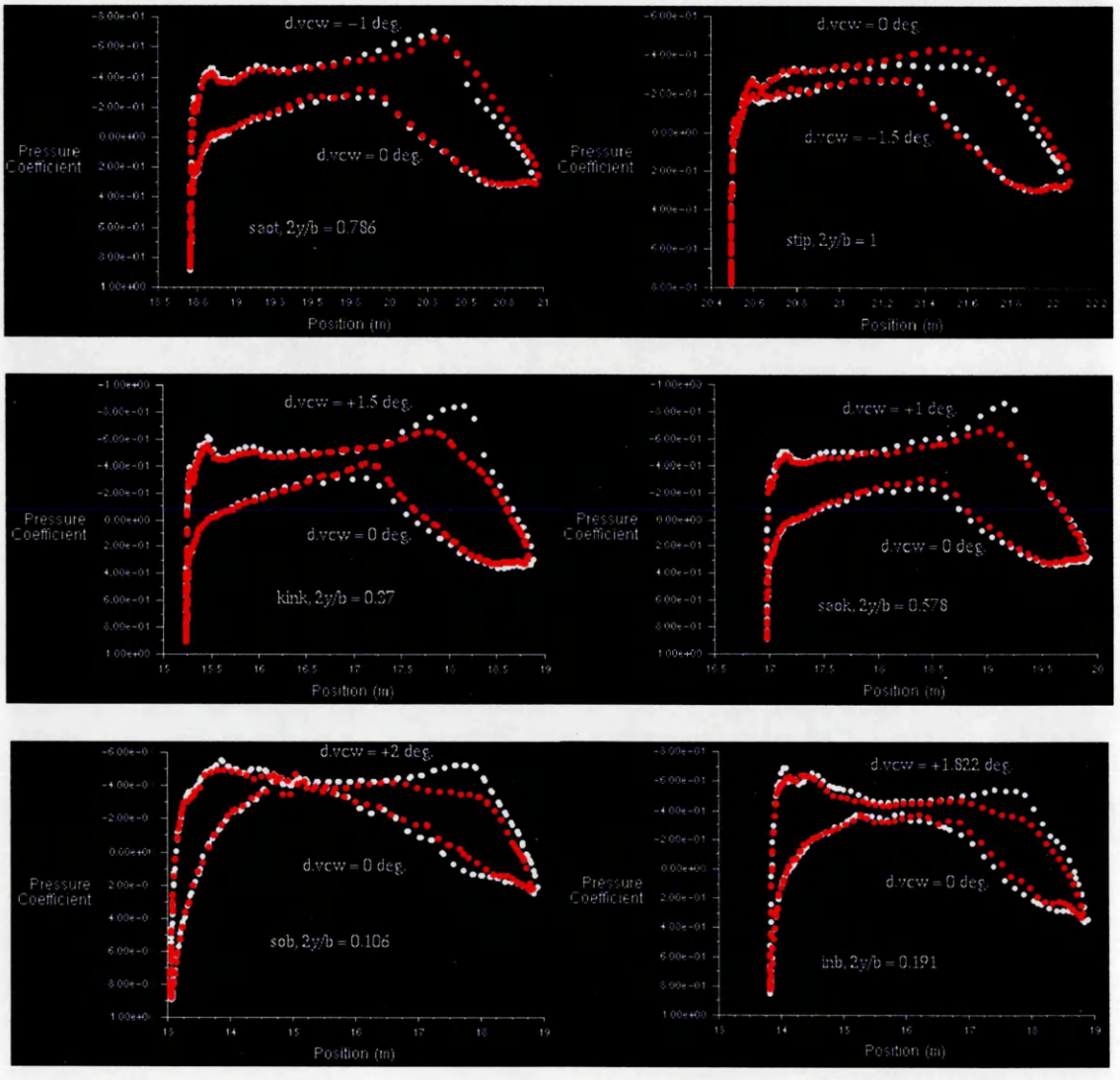

Figure 8.23 Configuration II : pressure distribution (fully laminar flow)
(red : VCW deflection = 0 deg.)

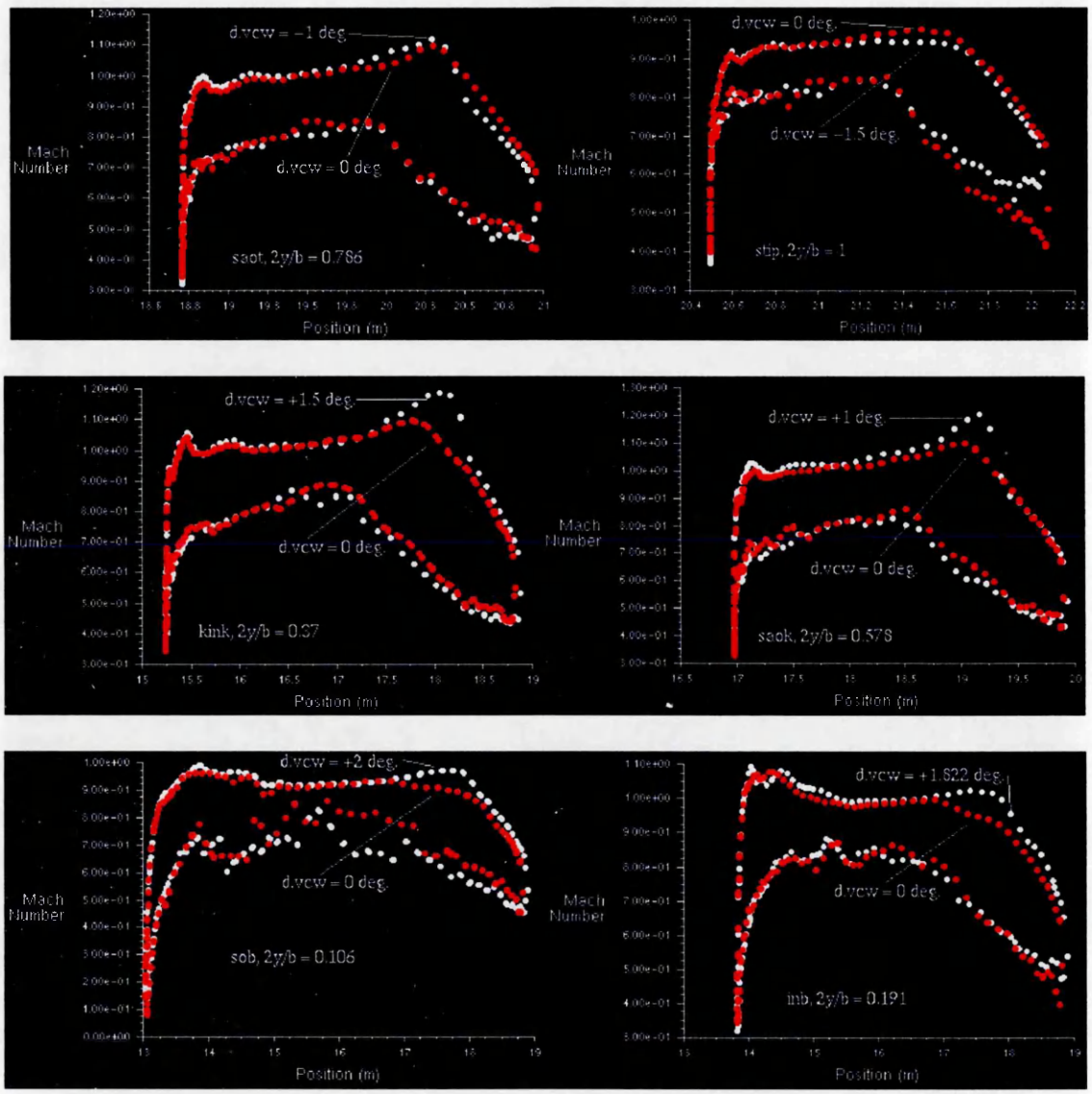

Figure 8.24 Configuration II : Mach number distribution (fully laminar flow)
(red : VCW deflection = 0 deg.)

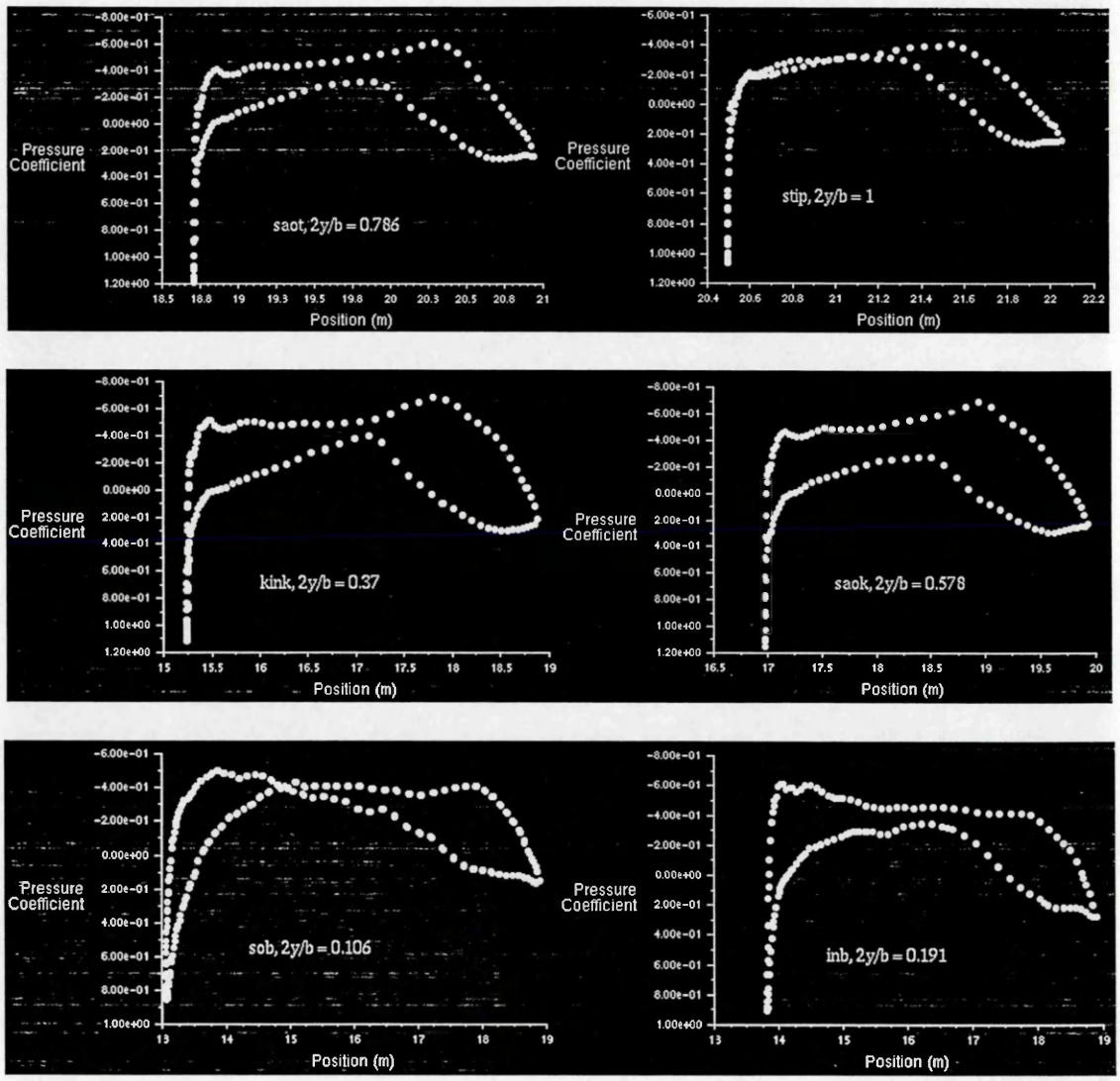

Figure 8.25 Configuration II : pressure distribution (fully turbulent flow)

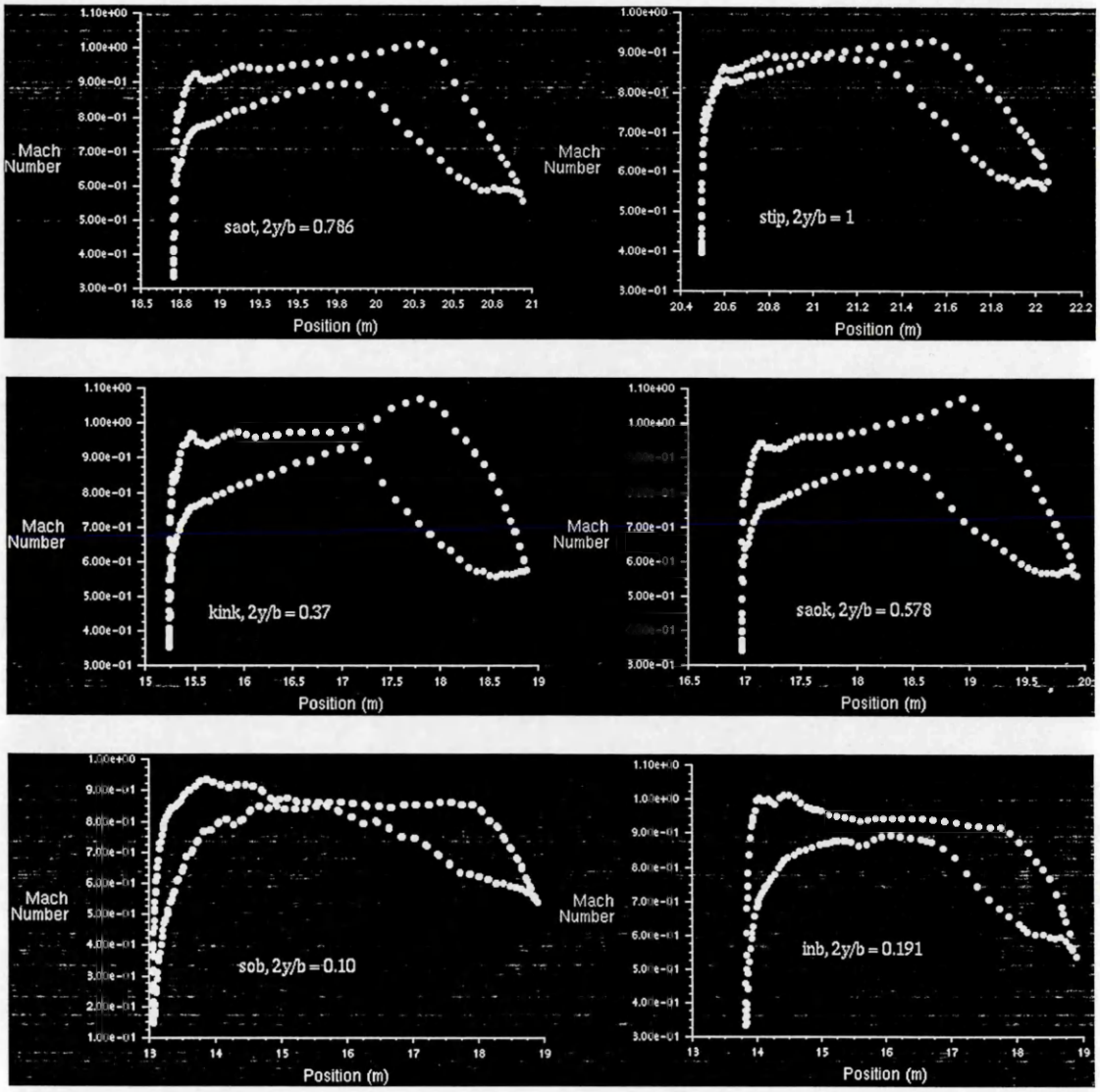

Figure 8.26 Configuration II : Mach number distribution (fully turbulent flow)

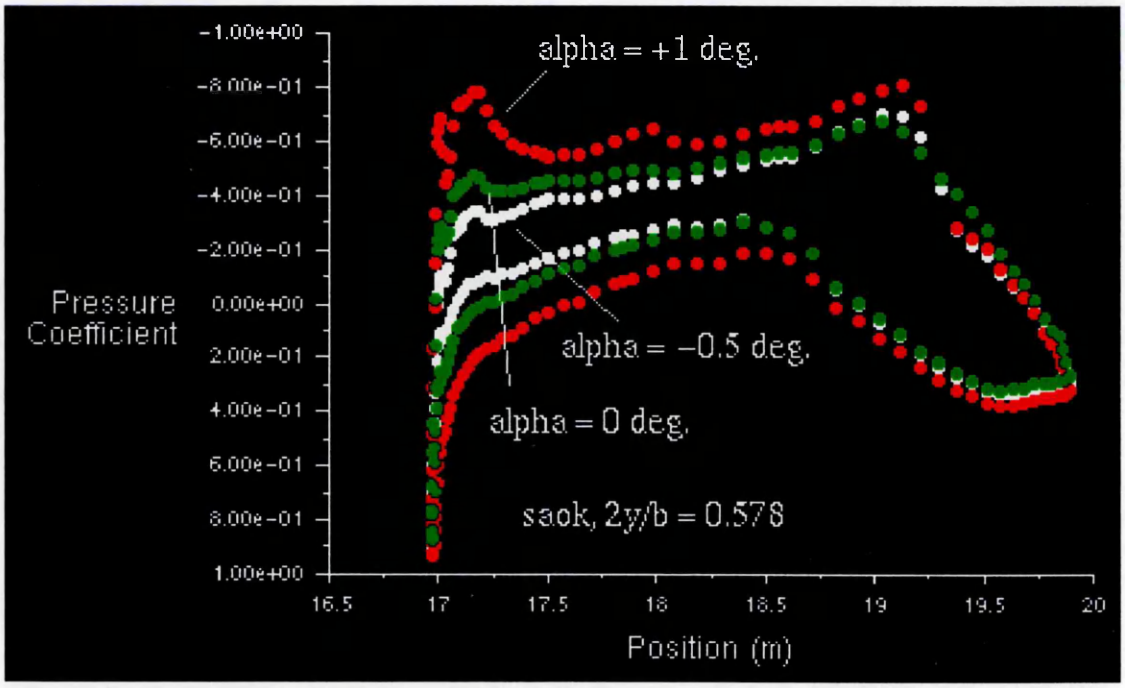

Figure 8.27 Configuration I : effect of angle of attack on pressure distribution (fully laminar flow)

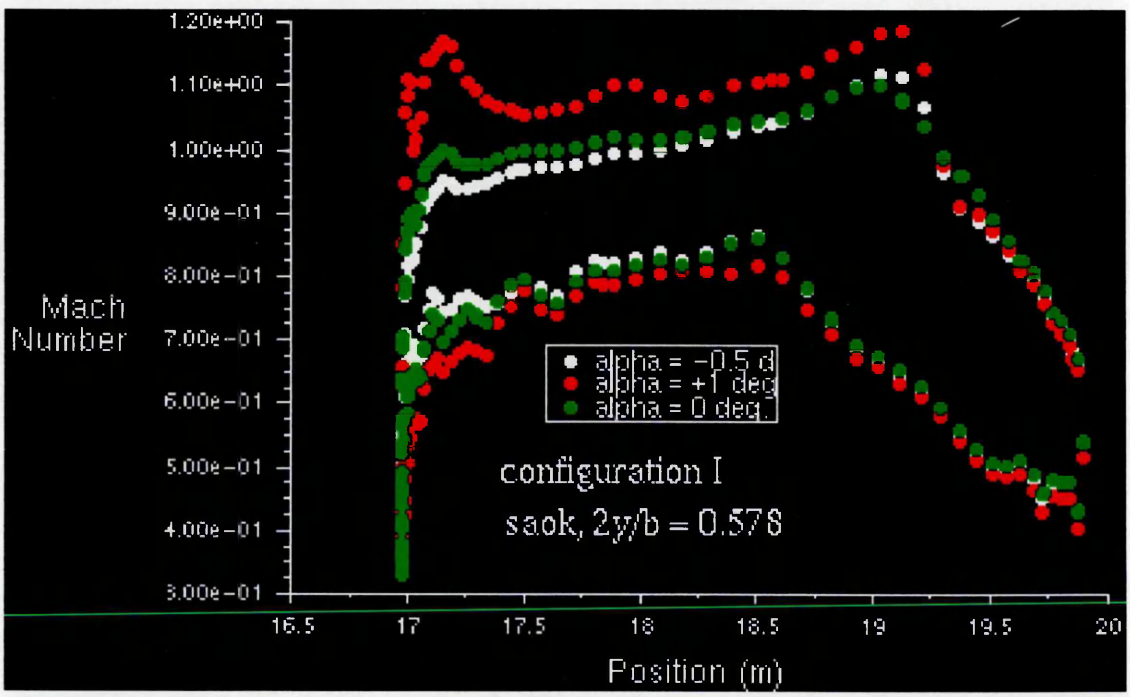

Figure 8.28 Configuration I : effect of angle of attack on Mach number distribution (fully laminar flow)

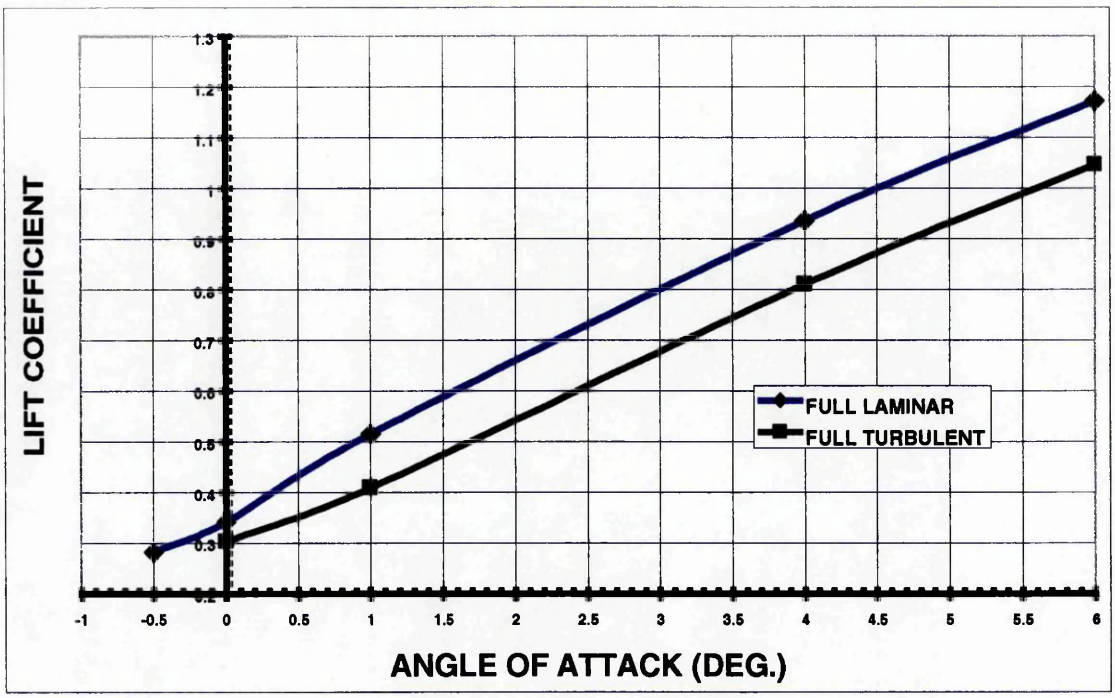

Figure 8.29 Configuration I : lift coefficient versus angle of attack (alpha)

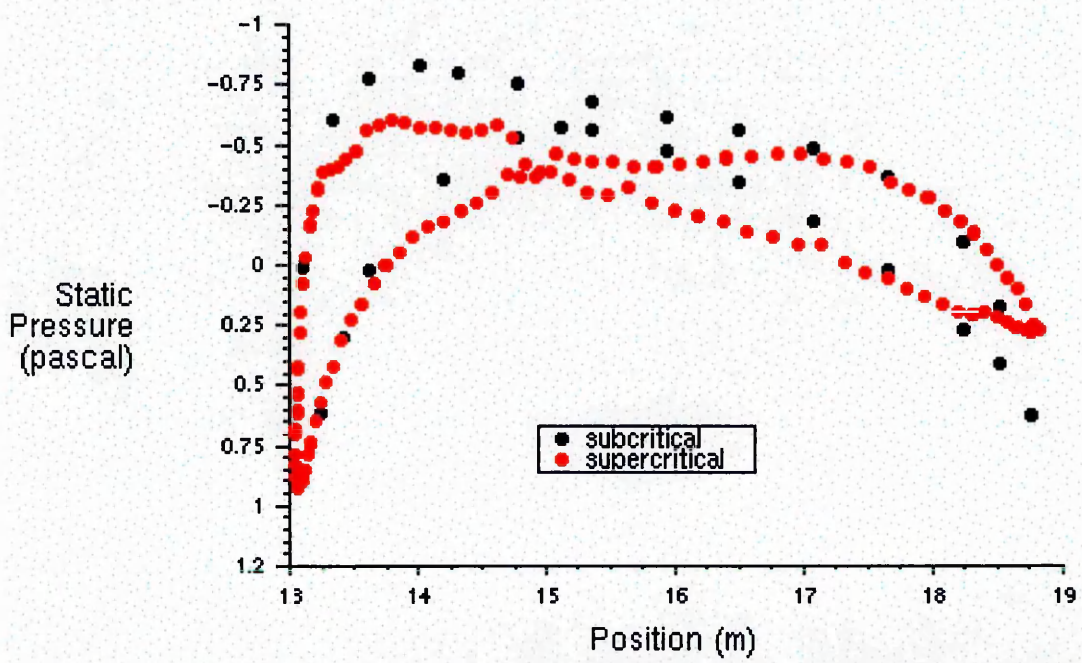

Figure 8.30 The comparisons between pressure distribution at subcritical Mach number and design Mach number for root wing section (at $C_L = 0.5$)

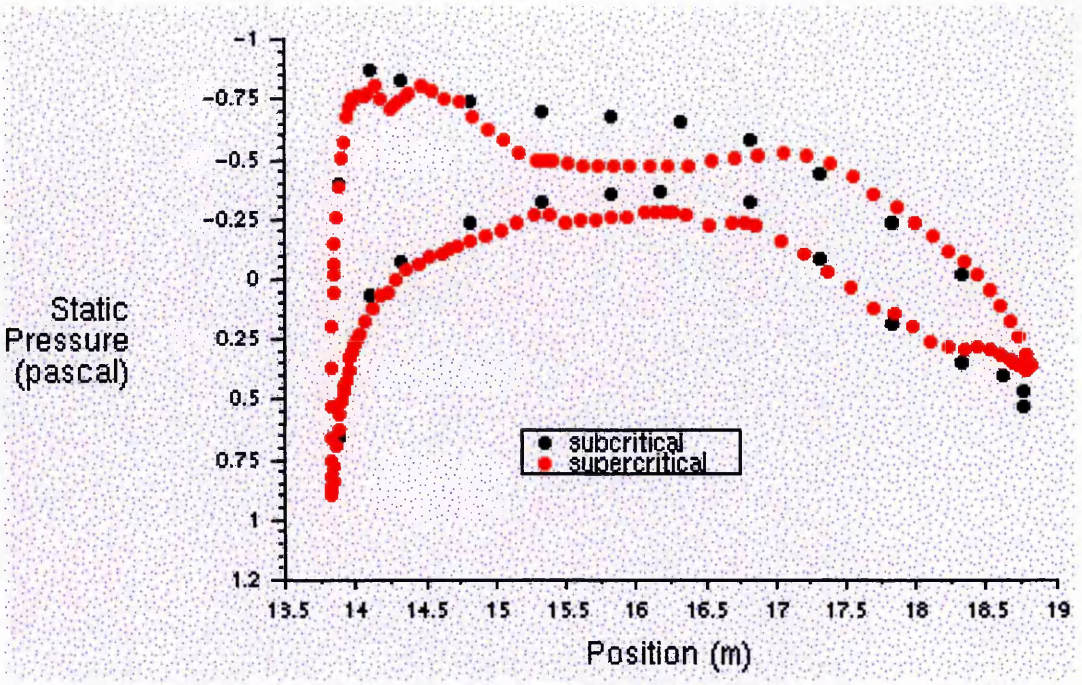

Figure 8.31 The comparisons between pressure distribution at subcritical Mach number and design Mach number for inboard wing section (at $C_L = 0.5$)

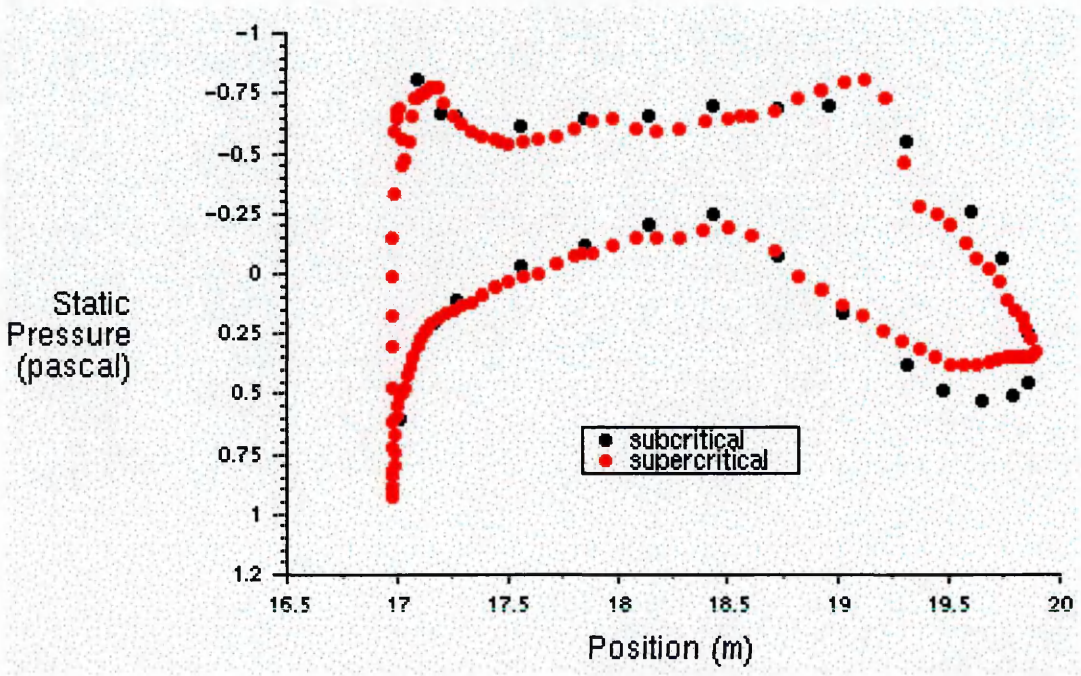

Figure 8.32 The comparisons between pressure distribution at subcritical Mach number and design Mach number for outboard wing section (at $C_L = 0.5$)

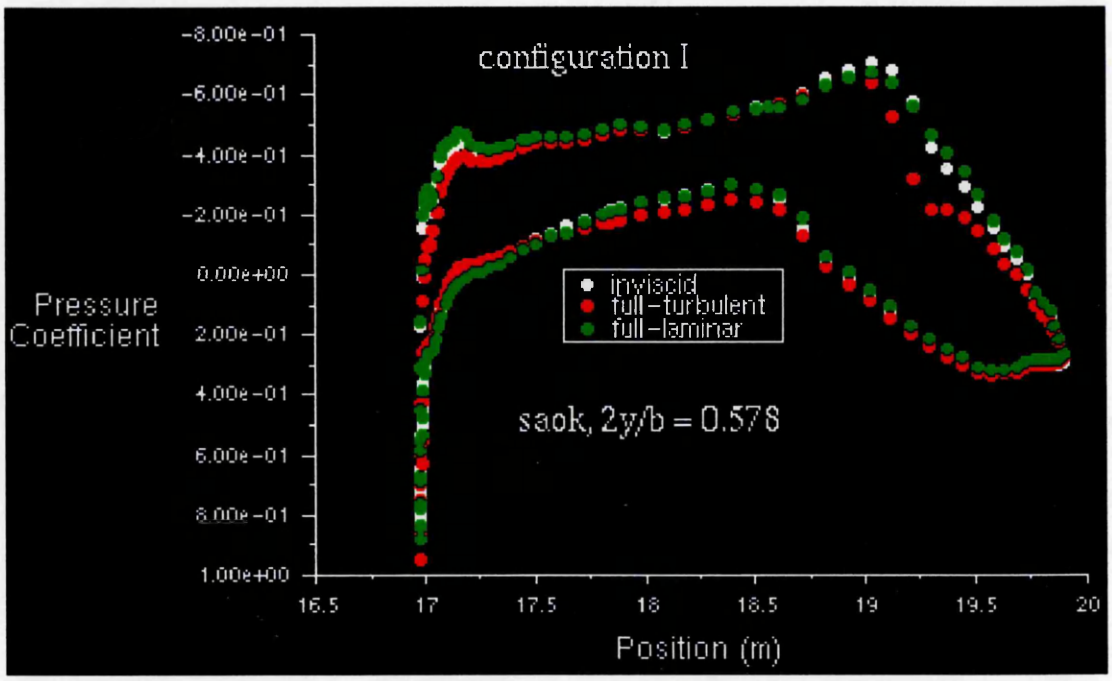

Figure 8.33 Configuration I : effect of flow model assumption on pressure distribution

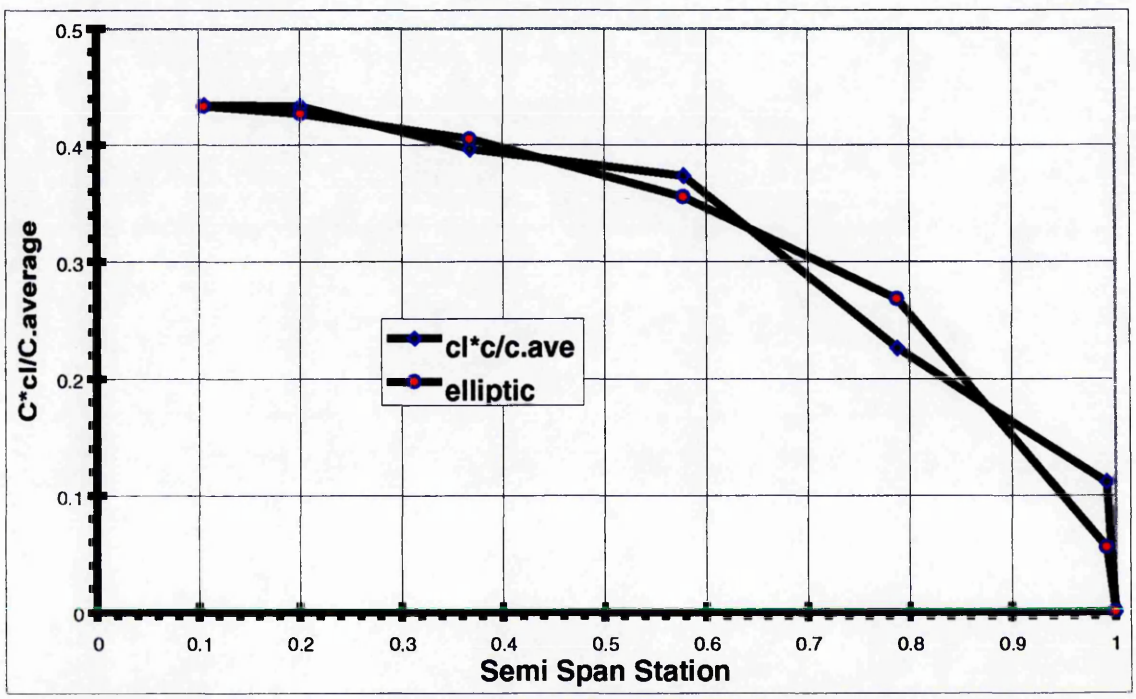

Figure 8.34 Configuration I : spanload distribution, C_L = 0.342 (fully laminar flow)

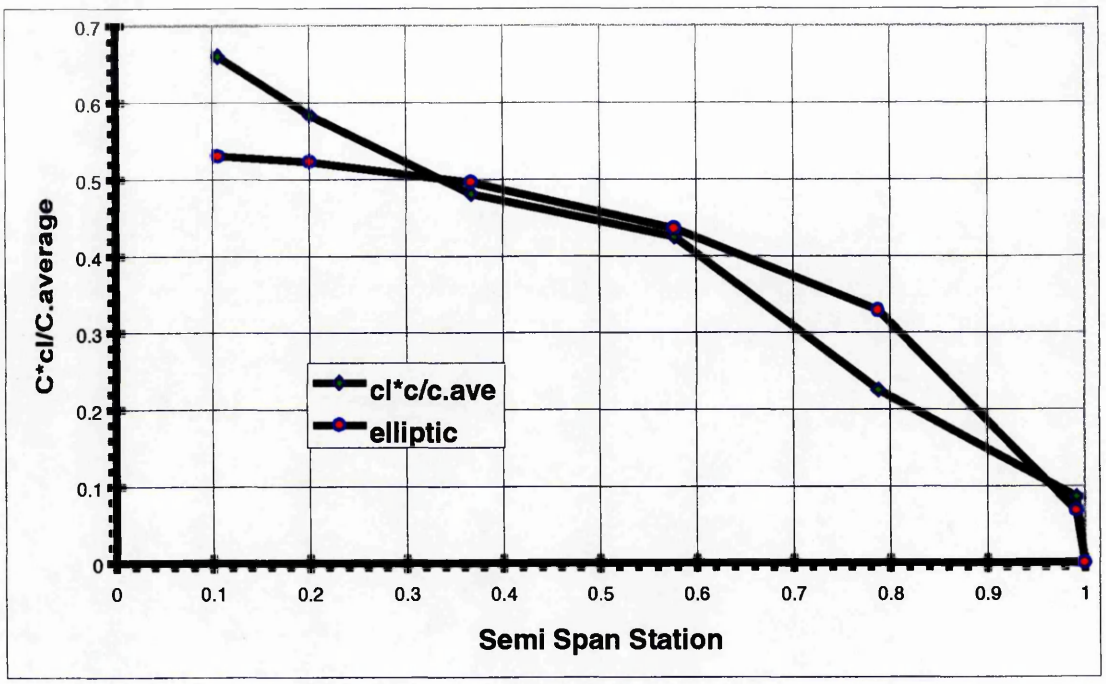

Figure 8.35 Configuration II : spanload distribution, C_L = 0.419 (fully laminar flow)

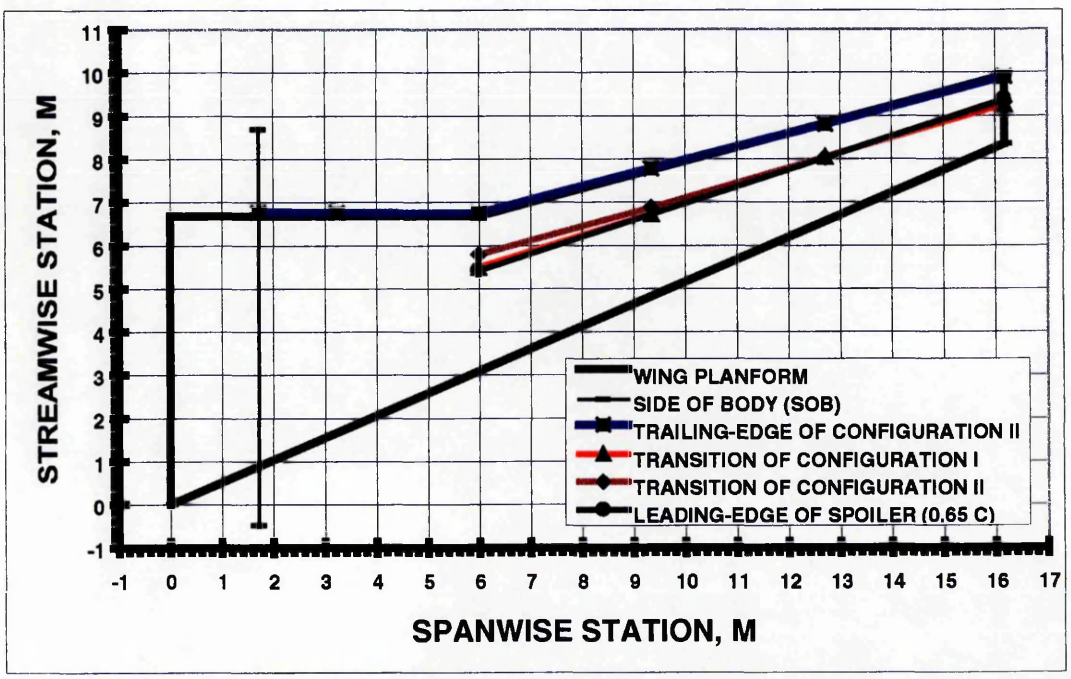

Figure 8.36 Transition predictions for ATRA-100's wing

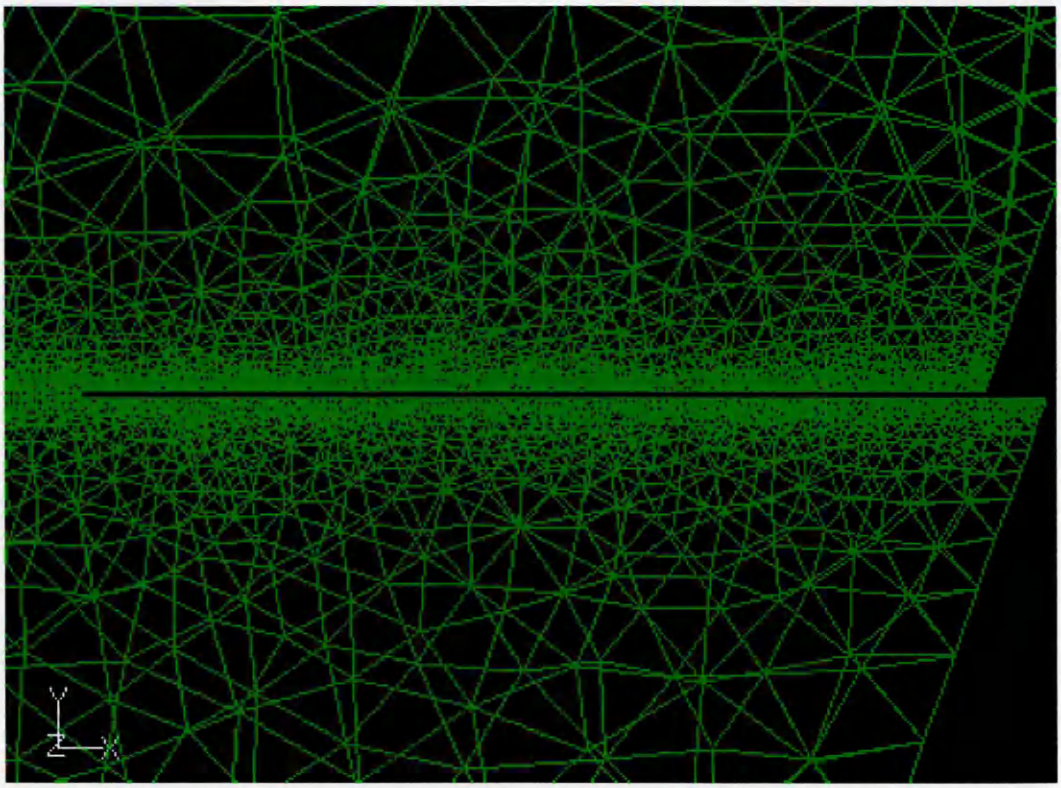

Figure 8.37 Wing and gap surface mesh

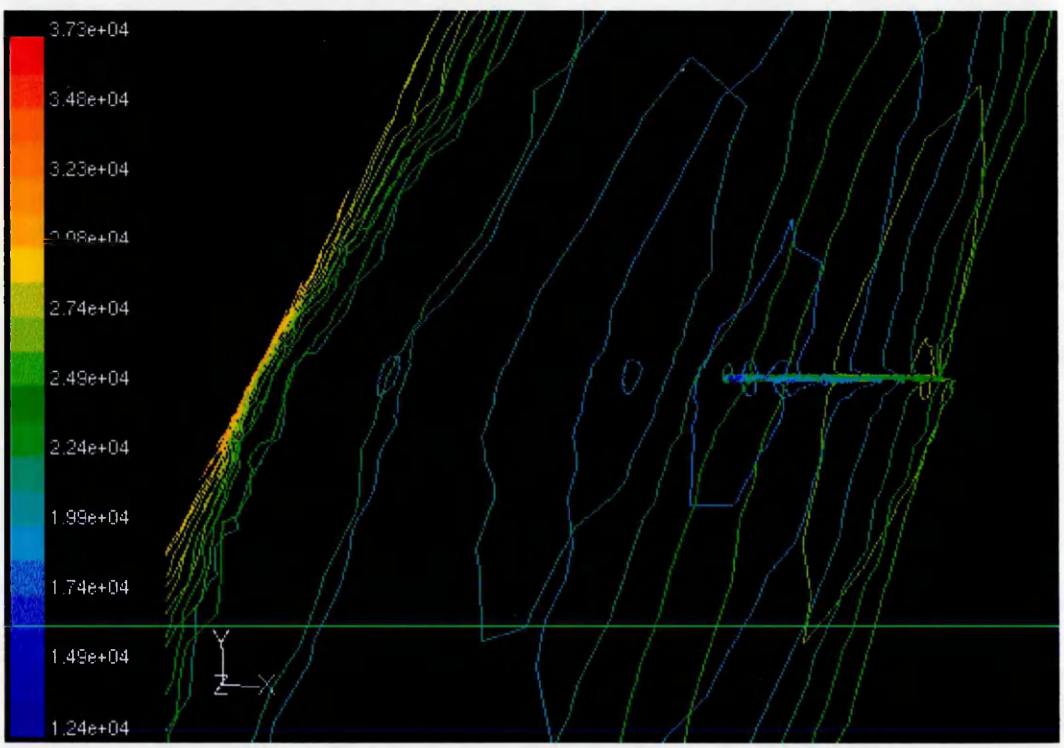

Figure 8.38 Wing and gap : contours of static pressure, pascal

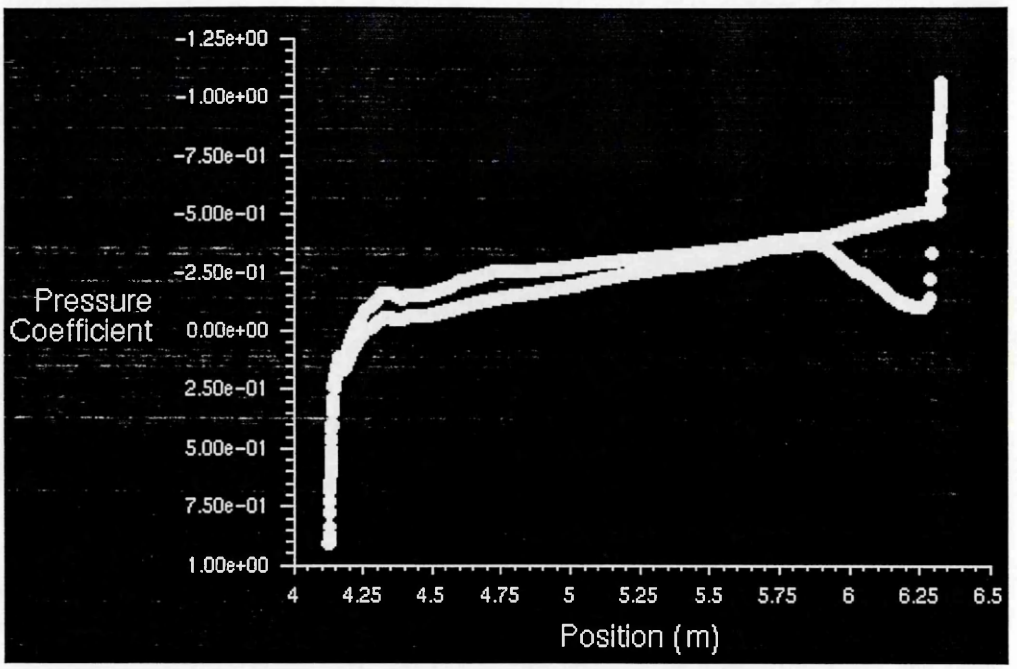

Figure 8.39 Wing and gap pressure distribution

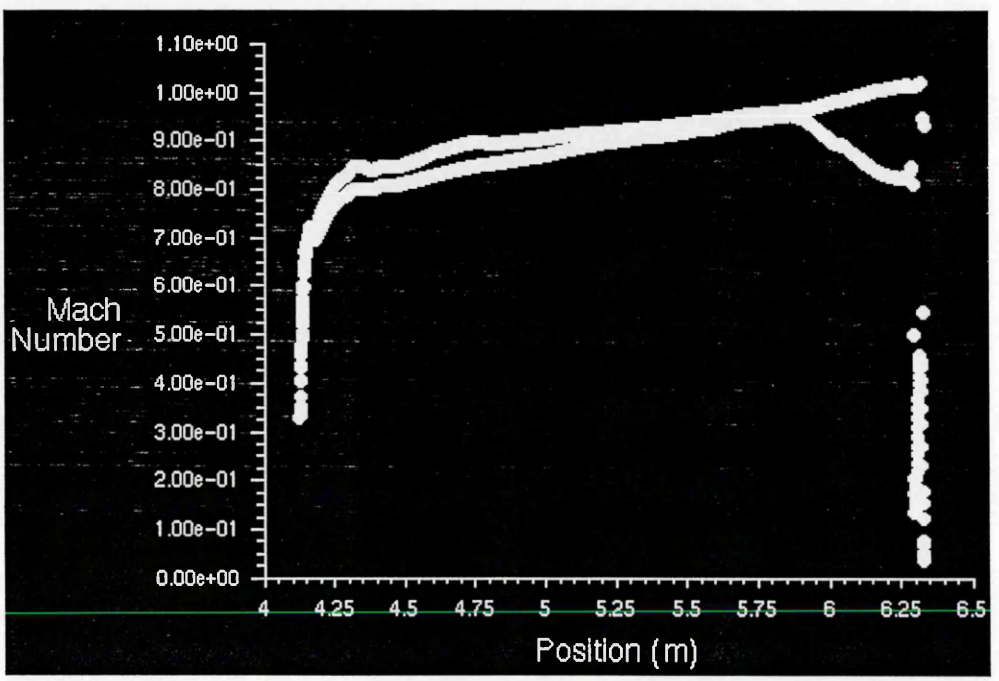

Figure 8.40 Wing and gap Mach number distribution

CHAPTER NINE

REVISION OF THE BASELINE AIRCRAFT CONFIGURATION

9.1 INTRODUCTION

Technically, the application of the combine HLFC-VCW to the civil transport aircraft appears to provide significant performance gains in terms of fuel consumption and payload range performance. However, in order to justify the implementation of the technology economically, it is necessary to consider the associated costs throughout the entire program.

It was judged that the most appropriate method of examining the cost implications of the combine HLFC-VCW would be to examine it's effects on the direct operating costs (DOC) of the aircraft. Due to lack of time, for the purposes of this research, aircraft weight reductions and increased range performance due to the application of the combine HLFC-VCW would be examine rather than DOC, with the assumption if the aircraft weight is reduced DOC would also reduce..

9.2. REVISION OF THE ATRA-100 AIRCRAFT

The lift/drag improvement due to the application of HLFC on the ATRA-100 aircraft compared to the turbulent version is predicted in Appendix D of this thesis. The aircraft lift/drag improvement at cruise (Mach 0.8, 35,000 ft and $R_N = 6.28e^6/m$) was 7.675 %.

The advantages and disadvantages of the application of the combined HLFC-VCW to civil transport aircraft compared to the turbulent version are described in Chapter 3 and 4 and section 7.2.3. Some of them are :

- HLFC systems weight = 0.373 % MTOW (Reference 9.1),
- VCW systems weight = 0.5 % wing weight (Reference 9.2),
- Lift/drag increment due to VCW application = 2.5 % (Reference 9.2),
- The increment in fuel flow to maintain the specified net thrust due to power offtake of HLFC suction systems = 0.2 % (Reference 9.3),
- Assumption : the reduction of wing sections t/c due to the application of the HLFC is eliminated by the application of VCW (see section 7.3.3 of this thesis) and wing sweep is unchanged.

The above values are from aircraft which does not closely match of the ATRA aircraft types included in this study, preventing any direct comparisons. However, the benefits and/or drawbacks associated with the various HLFC and/or VCW applications are provided. In the absence of a detailed investigation, it was decided to use the above values.

With the above predictions and assumptions and sizing method described in Chapter 2, the benefits of the combine HLFC-VCW to the ATRA-100 aircraft

compared to the turbulent version (see Table B.4) are :

1. Constant DR&O : MTOW reduction = 4.25 % (see Table 9.1).
2. Constant MTOW : range performance increased by 7.63 % (see Table 9.2).

A/C COMPONENT			WEIGHT KG	WEIGHT LB	% MTOW
WING (INC. AUXILLIARY SURFACES STRUCT.)			4284.12	9444.77	10.6036
HORIZONTAL TAIL (INC. ELEVATOR)			480.774	1059.91	0.89247
VERTICAL TAIL (INC. RUDDER)			406.809	896.85	0.75516
BODY			5285.12	11651.6	10.9009
MAIN LANDING GEAR			1791.18	3948.84	3.325
NOSE LANDING GEAR			255.883	564.121	0.475
NACELLE AND STRUT			1466.14	3232.25	2.72161
TOTAL STRUCTURE			13970	30798.3	25.9328
ENGINES (DRESSED)			3159.78	6966.05	5.86555
FUEL SYSTEM			487.718	1075.22	0.90536
FLYING CONTROLS SYSTEM			707.199	1559.09	1.31278
HYDRAULICS			1114.08	2456.1	2.06808
ELECTRICAL SYSTEM			776.413	1711.68	1.44127
A. P. U.			328.608	724.45	0.61
INSTRUMENTS AND NAVIGATIONS			980.438	2161.47	1.82
DE-ICE			410.18	904.282	0.76142
FIRE PROTECTION			161.611	356.287	0.3
FURNISHINGS (INC. SEAT, GALLEYS ETC.)			5193.09	11448.7	9.64
AIR CONDITIONING			699.565	1542.26	1.29861
TOTAL FIXED EQUIPMENT			10858.9	23939.5	20.1575
EXTERIOR PAINT			48.4832	106.886	0.09
OPTIONS			958.759	2113.68	1.77976
MANUFACTURER'S EMPTY WEIGHT			28995.9	63924.5	53.8256
STANDARD AND OPERATIONAL ITEMS			573	1263.24	1.06367
OPERATIONAL EMPTY WEIGHT			29568.9	65187.7	54.8893
PASSENGER AND BAGGAGE	108 PAX		10314	22738.2	19.146
MISSION FUEL (PAX, NM)	108	2250	13987.2	30836.2	25.9647
MAXIMUM ZERO FUEL WEIGHT			39882.9	87925.9	74.0353
MAXIMUM LANDING WEIGHT			48483.2	106886	90
MAXIMUM TAKE-OFF WEIGHT			53870.2	118762	100

Table 9.1 Weight breakdown for ATRA-100 (Revision : constant DR&O)

A/C COMPONENT			WEIGHT KG	WEIGHT LB	% MTOW
WING (INC. AUXILLIARY SURFACES STRUCT.)			4542.71	10014.9	10.7659
HORIZONTAL TAIL (INC. ELEVATOR)			498.413	1098.8	0.8859
VERTICAL TAIL (INC. RUDDER)			421.734	929.756	0.74961
BODY			5285.12	11651.6	10.4378
MAIN LANDING GEAR			1870.66	4124.05	3.325
NOSE LANDING GEAR			267.237	589.15	0.475
NACELLE AND STRUT			1531.19	3375.66	2.72161
TOTAL STRUCTURE			14417.1	31783.8	25.6256
ENGINES (DRESSED)			3299.98	7275.13	5.86554
FUEL SYSTEM			504.954	1113.22	0.89753
FLYING CONTROLS SYSTEM			730.604	1610.69	1.29861
HYDRAULICS			1138.53	2509.99	2.02367
ELECTRICAL SYSTEM			799.329	1762.2	1.42077
A. P. U.			343.188	756.593	0.61
INSTRUMENTS AND NAVIGATIONS			1023.94	2257.38	1.82
DE-ICE			422.836	932.184	0.75157
FIRE PROTECTION			168.781	372.095	0.3
FURNISHINGS (INC. SEAT, GALLEYS ETC.)			5423.5	11956.7	9.64
AIR CONDITIONING			726.808	1602.32	1.29186
TOTAL FIXED EQUIPMENT			11282.5	24873.3	20.054
EXTERIOR PAINT			50.6344	111.629	0.09
OPTIONS			993.197	2189.6	1.76536
MANUFACTURER'S EMPTY WEIGHT			30043.3	66233.5	53.4005
STANDARD AND OPERATIONAL ITEMS			573	1263.24	1.01848
OPERATIONAL EMPTY WEIGHT			30616.3	67496.8	54.419
PASSENGER AND BAGGAGE	108 PAX		10314	22738.2	18.3326
MISSION FUEL (PAX, NM)	108	2421.64	15330.1	33796.7	27.2484
MAXIMUM ZERO FUEL WEIGHT			40930.3	90235	72.7516
MAXIMUM LANDING WEIGHT			50634.4	111629	90
MAXIMUM TAKE-OFF WEIGHT			56260.4	124032	100

Table 9.2 Weight breakdown for ATRA-100 (Revision : constant MTOW)

CHAPTER TEN

DISCUSSION

10.1 INITIAL SIZING

Approximately 65% of the world's commercial jet fleet consists of narrow-body, single-aisle aircraft with a capacity of 70 to 170 seats. These are deployed on routes of 1,300 nautical miles or less. This sector also dominates the current order-book. More than 60% of aircraft on order are in the short-haul narrowbody category. The trend since deregulation in the US has been towards hub-and-spoke networks and a reduction in average aircraft size. The liberalization of the European market could exacerbate this trend (Reference 2.1). Because of congestion and the competitive environment the airlines are forced to buy technology and competitive aircraft at low cost and to ask to the manufacturers to provide more operational flexibility without drastic performance losses.

To correctly answer the market demands, both Aircraft Operational & Economic Analysis and Aircraft Configuration Design have to take active roles to ensure that requirements are correctly specified, complete, potentially realisable and economically rational.

To become a competitive product, the aircraft manufacturer should always actively study the introduction of advanced technology items. But technology for its own shake is of no great commercial value. We can learn from the Comet (the first jet transport aircraft) and Concorde (the first civil supersonic transport aircraft), where the talent to transfer the technical and technological advances into a commercial success was missing.

It is beyond this work to make a complete DR&O, as described secetion 2.3. The values of the DR&O for the ATRA family are taken as an average or an improvement of the data relative to the competitors. The design payload-range for the ATRA family and it's competitors are shown in Figure 2.3. This shows that the ATRA family may be seen as a complementary family rather than a competitor to the other narrowbodies. It fills a niche between small and big narrowbodies jets. The question is still, is there any market demand in those sector?

The empty weight versus maximum take-off weight for ATRA family and it's competitors is shown in Figure 2.4. As shown in this figure, the ATRA weight prediction, described in Chapter 2, is in the trend of existing aircraft.

Usually trade studies between several possible configurations will be required before the choice of the best configuration is made. The engine mounted on the wing configuration is typical transport aircraft and the most common for most airliners. It is beyond this work to make a trade study, as described above. For this study, engine mounted on the wing configuration was selected for the ATRA family (see Appendix B).

10.2 COMBINED HLFC-VCW SCHEME

The combined HLFC-VCW scheme used for the ATRA family is shown in Figure 5.8. The advantages of this scheme relative to upper and lower HLFC are (1) less potential insect contamination on the suction device (see Figure 7.55), hence laminar boundary layer will be more stable, (2) simpler trailing-edge high lift devices, (3) lower approach speeds and shorter take-off and landing field lengths, and (4) a smaller trim penalty (when the flaps are deployed). It's disadvantages and risks relative to upper and lower HLFC are (1) less drag reduction due to laminar flow only on the upper surface and (2) a more complex leading-edge system.

The main part of the HLFC application is the suction system. Clearly this must be capable of suppressing any boundary layer disturbances over the forward part of the surface, such that the flow remains laminar for some distance downstream of the suction surface. Air is drawn through the surface into the suction plenum chambers, where in this case it is gathered into a smaller number of collection chambers via metering holes. These chambers are connected by pipes to a main spanwise collector duct which transports the air to the suction unit (compressor). Downstream of the suction unit the air is exhausted to the atmosphere. This suction system is proposed in Reference 7.87 and is adopted to the ATRA-100's laminar wing.

In the present study, panels with holes are often considered for use as the suction surface because the structural design is more straightforward and because modern electron beam and laser drilling techniques permit economical fabrication of sheet metal with large numbers of small, uniform, evenly spaced holes (offering structural advantages). The problem is to establish criteria for suction system design and more specifically for the following parameters : Hole diamater, Hole spacing, Hole pattern and thickness of the sheet. The velocity in the holes must be small enough to prevent a premature transition due to horseshoe vortices. However, the chosen pattern must create pressure drops across the panel which are sufficiently high to avoid outflow in the compartments due to the external pressure gradients. The optimization of the design parameters is a compromise between these constraints (References 7.28 and 7.8).

The best configuration for an HLFC aircraft depends significantly on the degree of leading-edge high-lift protection that will be required. Until now, the severity of the insect contamination problem is not yet well defined.

This VC concept used in this research is engineerable and uses traditional high-lift devices without major mechanical additions in order to ease development and certification with low development costs.

Ideally the change in section profile aft of the rear spar should not cause separation of airflow, which would otherwise give rise to higher profile drag (Reference 5.7; see also section 7.3.2). To overcome the problem of separation, the radii of local curvature must be greater than half the chord (Reference 5.8), but not too high, as the section will have a higher pitching moment, and hence higher trim drag, which then will

reduce the benefit of variable camber itself. The radii should be optimized between these two constraints. The radius is inherent to the trailing-edge upper surface of the aerofoil, so when the aerofoil is used for a VC concept, the aerofoil should be designed taking into account the above considerations from the beginning (see also Figure 7.10 of this thesis).

The camber variation is achieved by small rotation motions (in two directions for positive and negative deflections). In VC-operation the flap body slides between the spoiler trailing edge and the deflector door. The radius of flap rotation is picked-up from the radius of curvature of the aerofoil trailing edge upper surface at about 90% chord. Camber variation is therefore performed with continuity in surface curvature at all camber settings. During this process the spoiler position is unchanged.

In low-speed conditions the flap exposes a slot between it and the spoiler in a similar manner to single-slotted flap.

10.3 INITIAL WING DESIGN

Designing the wing is one of the most complicated aspects of aicraft design. The wing must satisfy infrastructure requirements, mission/performance requirements, and design requirements. Wing design is a highly integrated process involving not only aerodynamicists but other disciplines such as marketing, sales, manufacturing, and design groups. Some of the wing design parameters are highlighted in the following sections.

Historically, wing aerodynamicists often ignored the engine installation during the wing design process. It was up to the Propulsion Integrator to do the best they could with the wing as provided. Today, it is recognized that the engine influence must be accounted for during the design process.

Planform is directly related to aspect ratio and taper. The main aerodynamic characteristics influenced by planform are the induced drag coefficient and the stalling characteristics (Reference 7.15).

Wing planform selection is based on a combination of criteria that require constant review during the design phase. Planform span, aspect ratio, sweep, and taper will be revised, based on the trade studies taking place during the design. As sweep increases, the MTOW, operating empty weight (OEW), mission fuel and engine size increase for a constant aspect ratio and wing loading. As aspect ratio increases, OEW and MTOW increase while engine size and fuel burn decrease (Reference 7.1 and 7.6).

Reference 7.7 suggests a new regional aircraft could have an aspect ratio as high as 11. Studies supported by wind tunnel results showed the feasibility of a lower sweep/high aspect ratio wing with similar aeroelastic distortion, but better cruise and field performance than the higher sweep/low aspect ratio (Reference 7.89).

For aeroelastic considerations, Figure 2.6 gives $(t/c)_{SOB}$ requirement for a given aspect ratio. Any combinations of wing aspect ratio and $(t/c)_{SOB}$ which lay under the boundary curve are safe from the structural point of view.

By the application of VCW, C_L buffet onset is enhanced (Reference 7.42), producing higher Mach-critical lift , hence allowing the aircraft to fly to a higher Mach number, and/or can have lower sweep, or higher thickness to chord ratio for the same flight Mach number. Both phenomena i.e. higher Mach critical drag, and Mach critical lift help VCW aircraft to be designed and optimised for higher thickness to chord ratio and/or alternatively lower sweep angles. Wings with lower sweep angle is preferred for HLFC application to reduce the possibility of attachment line contamination and cross flow instability. Wing with HLFC tend to have lower thickness to chord ratio for the same flight Mach number compared to the turbulent wing, but this phenomenon may be reduced or eliminated by the application of VCW concept (see also section 7.3.2.1).

The application of laminar flow on swept wings is effectively limited at high Reynolds numbers by a high sweep angle, as crossflow instability and attachment line transition lead to fully turbulent boundary layers on the wing. Theoretical and experimental investigations on finite swept wings show, because of three-dimensional displacement effects, an effective increase of wing sweep for backward swept wings and an effective decrease of wing sweep for forward swept wings compared to the geometrical sweep. For a laminar flow wing, the reduction in sweep in the case of a forward swept wing leads to a more stable laminar boundary layer concerning transition because of crossflow instability and attachment line transition. Thus, with this concept, a laminar forward swept wing can be realized more easily than a comparable swept back wing (Reference 7.9). An example of a forward swept laminar wing aircraft has been proposed by Airbus (Reference 7.10) as shown on Figure 7.2. The main problem for the forward swept wings is flutter (see also section 7.3.1).

ATRA-100's Outboard aerofoil section design goals were : (1) to sustain laminar flow to 55% chord (or more) on the upper surface with minimum suction requirements and (2) to suffer little or no flow separation or wave drag at Mach 0.8, a wing lift coefficient of 0.5, and 25 degrees quarter-chord sweepback.

It is beyond the scope of this work to design an airfoil. For purposes of this study, with help of Professor A. J. Bocci (Aerodynamics consultant, formerly based at ARA - Bedford), SWEPTDES was used to design the sections for ATRA-100 wing. Section data taken from Reference 7.28 were used as an initial input. The section co-ordinates were digitized by using CATIA (Reference 7.65), and then the sections curvature smoothness (d^2z_n/dx^2) were checked by the following equations (Reference 7.12) :

$$d^2z_n/dx^2 = ((z_{n+2} - z_{n+1}) - (z_{n+1} - z_n)) / dx^2 \qquad (7.8)$$

where : z_n = section ordinate
dx = absisca interval between z_{n+1} and z_n

Subcritical pressure distributions corresponding to this geometry were then computed by SWEPTDES. These pressure distributions were then adjusted to meet the previously-discussed requirements. The airfoil design process was necessarily iterative. A SWEPTDES airfoil design computer program was then used to design a set of wing sections, plus a twist distribution that gave the required spanwise lift variation. A preliminary transonic analysis was also undertaken using RAMPANT (Reference 7.66). Figures 7.41, 7.44 and 7.45 shows the subcritical pressure distribution of the ATRA-

100's outboard, side of body and inboard wing aerofoil section respectively obtained from SWEPTDES.

The thickness distribution requirements and the result from the initial study of ATRA's wing are shown in Figure B.10. As can be seen from this figure, t/c requirement was not achieved by this design because of insufficient sweep for Mach 0.8 and also because the VC had not yet been optimized. For comparison, a turbulent aircraft cruising at Mach 0.8, has a typical quarter chord sweep ($\wedge_{c/4}$) = 25 deg. and outboard section thickness chord ratio is about 11% (see Appendix A). As mention in section 7.3.2.1, laminar aerofoils are often prone to increased shock growth which result in earlier occurrence of drag rise conditions, relative to an aerofoil with an adverse 'roof-top' pressure gradient. In fundamental wing design terms this implies increased sweep, reduced thickness/chord ratio, and/or reduced wing loading, all of which reduce the aerodynamic and/or structural efficiency of the wing for a specified design condition. An alternate approach may be to use an aerofoil with a mildly adverse 'roof-top' pressure gradient to improve wave drag and lift capabilities, although with a reduced extent of laminar flow. Careful consideration would be required to select/design an aerofoil section to achieve maximum aircraft efficiency and minimum operating economics with laminar flow and a suitable off-design performance. In addition, it is necessary to ensure adequate efficiency and economics with turbulent boundary layers (References 7.28, 7.30 and 7.93). This would be a good subject for future work.

The influence of engine noise especially on the wing lower surface boundary layer is an area of concern. High-bypass-ratio fans typically radiate frequencies that coincide with the most critical T-S frequencies. These could excite rapidly amplified boundary layer oscillations and cause premature transition at high reynolds numbers. Acoustic treatment of the engines or increased suction in affected areas may therefore be required (Reference 7.). Detailed evaluation of the influence of noise on HLFC should be investigated.

The concept of varying the camber of an airfoil in the manner outlined in Chapter 5 appears relatively straightforward, if we restrict ourselves to two-dimensional considerations only. However, for the scheme to be adopted for the ATRA-100, it must be applied to a tapered wing with a kink (Yehudi) and 25 degree of a quarter-chord sweep (as shown in Figure B.8). For a workable scheme to result, it is necessary for the flap configuration to conform to a number of geometrical constraints, namely : flap segmentation, flap rotation,...etc.

The design objective of most variable camber wings has been the ability to vary the distribution of camber across the span of the wing. The provision of this capability inevitably adds to the complexity of a flap scheme, but it is necessary if the full performance benefits are to be obtained.

Ideally, from aerodynamic considerations, it is desirable to maintain a smooth and continuous wing surface across the whole of the span at all camber settings. However, this would necessitate the use of accurately supported wing skins that possess the ability to stretch, flex and warp. This was considered to be beyond current or immediately foreseeable engineering capabilities.

To control the load distribution across the span of the wing, it is necessary to resort to the application of spanwise variation in camber in a number of discrete spanwise steps or segments. This also prevents incompatibilities developing during wing flexure and enables the provision of roll control. The size of these segments depends on a number of criteria (Reference 7.72) which include :

1. Optimum load distribution characteristics with minimum structural and mechanical component weight.
2. Loss of lift and therefore increased rolling moment due to loss of a segment.
3. Flap flexure and bending moment and track positions (or hinge reaction points)
4. Practical restrictions, i.e. fuel space, engine positions, main wing pick up rib position.

Spillman (Reference 7.73) and Airbus (References 7.5 and 7.74) have proposed the use of about six spanwise segments in a typical subsonic wing. This figure represents a compromise between aerodynamic efficiency and mechanical complexity considerations. An additional factor is the ability to continue to fly safely with any one flap segment inoperative. In the absence of a detailed investigation, it was decided to use six flap segments per wing for the variable camber ATRA-100.

The objective of flap segmentation is to have spanloading as close as possible to the elliptic loading at any combination of camber settings at all flight regimes. The sizes of the individual flap segments were set to be : two inboard flap segments with same flap span, three outboard flap segments with same flap span, and one segment flaperon, as shown in Figure B.8.

Most swept, tapered-wing subsonic transport aircraft are forced to use flap movements that lie somewhere between a true conical (spanwise constant percentage of the chord) and streamwise motion for the outboard flap and a constant motion for the inboard flap. This is compromise results from the use of wing twist, spanwise variation of aerofoil section and a preference for constant chord inboard flaps in order to leave room for undercarriage stowage (Reference 7.52, 7.24 and 7.26).

The system concept of variable camber used in the ATRA-100's wing is very similar to traditional high lift devices; the flap motion used for the ATRA-100's variable camber wing is : natural conical motion (spanwise constant percentage of the chord) for the outboard flap and a constant motion for the inboard flap. The above concept has also been proposed by Airbus (Reference 7.5).

The spanwise split between the segments can cause excess drag due to induced vortices (Reference 7.75) and loss of lift. To reduce or prevent these vortices and lift loss, a plate may be introduced between each segment in order retain the airflow. These "splitter" plate are likely to be twice the depth of the airfoil in order to cover the full VC deflection range (Reference 7.72). The drag of splitter it's self must be considered.

An alternate approach to reduce or prevent these vortices and loss of lift involves closing the gap by connecting those adjacent flap segments with a flexible material (i.e. rubber).

10.4 AERODYNAMIC ANALYSIS

A study was made to verify the use of RAMPANT as a primary design tool in the design of combined VCW-HLFC. The verification was made both on two-dimensional and three-dimensional configurations.

The pressure distribution of the NLF-5 airfoil for the conditions described in section C.5.1.1 is shown in Figure C.6. The pressure distribution predicted by RAMPANT is in good agreement with the calculated data from Reference C.8. The shock position and strength are quite close. According to the RAMPANT predictions, the NLF-5 airfoil has more lift aft of the shock and less lift in the front of shock, hence more pitching moment.

The wing surface pressure distribution was measured at 3 different spanwise stations, $2y/b = 0.15$, 0.46, and 0.96. The pressure distributions for the three spanwise stations are shown in Figure C.8. The pressure distribution predicted by RAMPANT at spanwise station 0.46 is in good agreement with the calculated data by TIBLT (Transonic Interactive Boundary-Layer Theory, from Reference C.9) code. A shock is present on the upper surface of the wing. The shock position predicted by RAMPANT is about 5 % of the chord length aft of the TIBLT prediction. This may be because the grid is not fine enough (because the limitations of available computer memory) to capture the shock. The pressure distribution predicted by RAMPANT at spanwise stations 0.15 and 0.96 is not well matched with the data calculated by TIBLT code. This may be because the complex conditions at the wing root and the tip (3D effects more dominant) and the cylindrical fuselage geometry definition may be different.

Good agreement with experimental data also was achieved (Reference C.9), when TIBLT code is used to predict the pressure distributions for the M6 wing (Reference C.11). Reference C.12 reported that the pressure distributions of M6 wing predicted with RAMPANT (with the same procedure used by the author described above) are in good agreement with the experimental data.

For the purposes of this study, comparison to the NACA 0012 wing is used rather than the M6 wing, because the aspect ratio of the NACA 0012 wing is closer to the ATRA-100 wing (see section C.5.2).

10.5 AERODYNAMIC WING PERFORMANCE

From figures in Chapter 8, for configuration I, it can be seen that all of the pressure distributions (especially on the outboard wing, i.e. : from the kink to the tip) is characterized by a steep initial gradient (rapidly falling pressure), followed by a negative pressure gradient (falling/favourable pressure) and a single weak shock wave and finally a recovery region with a soft aft pressure gradient. Based on section 7.3.2.1, with the above pressure distribution characteristics, it is possible to apply the HLFC concepts on the wing of configuration I. The same pressure distribution characteristic

are seen on the wing of configuration II (VC-flap deployed). For a more detailed laminar flow analysis, see section 8.3 of this thesis.

From figures in Chapter 8, for both configurations, the average wing upper surface isobar sweep angle (taken at 50% chord) is approximately 21.8 degrees, instead of 25 degrees (wing quarter chord sweep angle). Thus, the isobar sweep efficiency is = 21.8/25 = 0.872. The inboard wing upper surface isobars are characterized by more sweep forward at the front and less sweptback at the rear, and the shock strength is quite weak.

With the deflection of VC-flap, the pressure distribution shape at the front of shock does not change too much; this is good for HLFC application. The VC-flap deflection makes the shock stronger and increases aft loading (producing greater pitching moment and hence more trim drag).

The effects of angle of attack on pressure and Mach number distribution is quite strong, especially in the region near the leading edge, as shown in Figures 8.27 and 8.28. In real flight, the above phenomenon could have implications for a gust effects on aircraft performance. This phenomenon should be considered when designing HLFC wings.

Wing-fuselage lift coefficient ($C_{L_{WF}}$) versus angle of attack (α) for configuration I is shown in Figure 8.29. Lift curve slopes ($C_{L_{\alpha.WF}}$) for full-laminar and full-turbulent flow assumption are 0.1403/degree and 0.1337/degree respectively. Lift coefficient at zero angle of attack ($C_{L_{0.WF}}$) for the full-laminar and full-turbulent flow assumptions are 0.342 and 0.303 respectively. From the above figure, the aircraft design lift coefficient ($C_L = 0.5$) is attained at $\alpha = +1$ degrees.

At the aircraft design lift coefficient ($C_L = 0.5$), the comparisons between pressure distribution at subcritical Mach number and design Mach number for root, inboard and outboard wing sections are shown in Figures 8.30, 8.31 and 8.32 respectively (see also Figures 7.36, 7.41, 7.44 and 7.45).

The comparison of pressure distributions between inviscid, full-laminar and full-turbulent flow assumptions are shown in Figures 8.33. Based on this figure, pressure distributions between inviscid and full-laminar flow assumption are quite similar. This is because the boundary layer thickness on the full-laminar flow assumption is quite thin. So to save iteration time, especially during an initial design (where the iteration time is crucial), the inviscid flow assumption is quite reasonable. As shown in the above figure, the effect of turbulencet is not so great.

As shown in Table 8.1, VC-flap deflection has a powerful effect (decrease/increase) on wing section lift. Careful VC-flap design (includes VC-flap shape, VC-flap chord ratio to the main wing, radius of rotation/ VC-flap deflection path, etc.) should be considered, if the maximum VC-flap effectiveness $(c_{l.II}-c_{l.I})/\delta$, is the objective. As shown in Table 8.1, for positive VC-flap deflections, the VC-flap effectiveness is quite good; but for negative deflection, the VC-flap effectiveness is less satisfactory, as shown for the wing section SAOT, where VC-flap effectiveness is negative.

Figure 8.34 - 8.35 show spanload distribution for fully laminar flow of the configuration I and the configuration II respectively. It can be seen that both of the spanloads depart significantly from an elliptical distribution. The wing-fuselage lift coefficient for configuration I is about 0.342, which is less than the design requirement ($C_{L.design}$ = 0.5), although the flow was assumed to be a fully laminar on the entire wing. The wing-fuselage lift coefficients for configuration II is 0.419 (see Figure 8.35).

The above wing configuration results from just the first iteration of a very complex wing design. Regardless of its weakness, its performance appears quite reasonable.

Figure 8.38 shows pressure contours on the surface of the wing-gap configuration. Pressure and Mach number distribution of the wing-gap configuration across the center of the gap are shown in Figure 8.39 and 8.40 respectively.

From Figures 8.39 and 8.40, it can be seen that on the upper surface as a flow reaches the gap, there is a steep positive pressure gradient and as a result a strong shock was formed. This phenomenon occurs because, after the flow on the upper surface reached the peak of its expansion, it was suddenly forced to reach the freestream value. The same phenomenon is seen in Figure 8.38.

10.6 TRANSITION PREDICTION

Comparing the various transition methods from different publications and experiments does not show a clear picture.

It is beyond the scope of this work to undertake a complete laminar flow analysis on the ATRA-100's wing (i.e. : boundary layer stability analysis, transition prediction, suction requirements,...etc.). The codes necessary for such a design task were not available at Cranfield University.

The laminar analysis was performed only on the outboard wing (from the kink to the tip), as this region offers higher potential for HLFC application. Reference 8.7 states that on the mid to outer wing of subsonic transport aircraft the flow (normal to the 0.5 chord isobar) is two-dimensional in character (see also section 7.7.2.1). So, for the purposes of this work, the laminar analysis was done by comparison of characteristics of the outboard wing sections (normal to the isobar) to the HLFC airfoil.

Taking into account the considerations described above, for purposes of this work, a simplified laminar flow analysis procedure was used (see section 8.3).

As shown in Tables 8.2 and 8.3, the leading-edge/initial pressure gradient ($(dc_p/ds)_{le}$) along the wing span from the KINK to near the wing tip (STIP) is about 42. For the ATRA-100 which has a wing leading-edge sweep angle of 27.3 degrees and cruise at Mach 0.8 (237 m/s) and Reynolds number of 21.6×10^6, based on Figure 6.5, the minimum suction quantity (V_s) is about - 0.00015 (or V_s = - 0.00015 x 237 m/s = - 0.03555 m/s).

The flow behind the shock can be expected to remain attached, as shown in Table 8.1 and 8.2, the maximum local Mach number (M_l) is less than Mach 1.2 and the

aft pressure gradient both upper ($dc_p/d(x/c)_{aft.upper}$) and lower ($dc_p/d(x/c)_{aft.lower}$) are less than 3.

Figure 8.36 shows the transition locations both of configuration I and II, some occur beyond 65 % chord (the location of leading-edge of spoiler). It is impossible to have laminar flow behind the leading-edge of a spoiler, unless tight manufacturing tolerances and surface quality are attained (see section 7.4.6 of this thesis).

10.7 DRAG PREDICTION

The drag breakdown described in Appendix D has the capability of drag prediction for the wing with some degree of laminar flow and was used in this research. The method is based on References D.1 and D.2

Where possible, it is important to compare the results from this study with those performed by other organisations, particularly as data from these has been extensively used within this study.

Boeing (Reference D.6).studied the implications of retro-fitting HLFC to the wing, fin and tailplane of a Boeing 757-200 aircraft. This does not closely match of the ATRA aircraft types included in this study, preventing any direct comparisons. However, the reduction in profile drag associated with the various HLFC applications are provided. These are compared with the corresponding drag reductions predicted by drag breakdown method described in Appendix D.

Cruise conditions : Mach 0.8, 37,000 ft and $R_N = 5.9e^6/m$

a. Laminar, basic trapezoidal wing spanwise from root to tip on both of upper surface (average : 0 - 0.5 chord) and lower surface (average : 0 - 0.38 chord) :
cruise drag reduction = 11.405 %, Reference D.6 quote 11 %.

b. Laminar, basic trapezoidal wing spanwise from root to tip on upper surface (average : 0 - 0.5 chord) only :
cruise drag reduction = 7.68 %, Reference D.6 quote 7 %.

10.8 REVISION OF THE ATRA-100 AIRCRAFT

The lift/drag improvement due to the application of HLFC on the ATRA-100 aircraft compared to the turbulent version is predicted in Appendix D of this thesis. The aircraft lift/drag improvement at cruise (Mach 0.8, 35,000 ft and $R_N = 6.28e^6/m$) was 7.675 %.

The advantages and disadvantages of the application of the combined HLFC-VCW to civil transport aircraft compared to the turbulent version are described in Chapter 3 and 4 and section 7.2.3. Some of them are :

- HLFC systems weight = 0.373 % MTOW (Reference 9.1),
- VCW systems weight = 0.5 % wing weight (Reference 9.2),

- Lift/drag increment due to VCW application = 2.5 % (Reference 9.2),
- The increment in fuel flow to maintain the specified net thrust due to power offtake of HLFC suction systems = 0.2 % (Reference 9.3),
- Assumption : the reduction of wing sections t/c due to the application of the HLFC is eliminated by the application of VCW (see section 7.3.3 of this thesis) and wing sweep is unchanged.

With the above prediction and assumptions and sizing method described in Chapter 2, the benefits of the combine HLFC-VCW to the ATRA-100 aircraft compared to the turbulent version are :

- Constant DR&O : MTOW reduction = 4.01 %
- Constant MTOW : range performance increased by 7.21 %

10.9 RESEARCH RESULT

The application of combined HLFC-VCW scheme to the ATRA family (see Figure 5.8) appears to provide the potential for significant performance improvements. This is in-spite of the difficulties associated with the installation of the such system on a moderately swept, tapered wing and have a kink..

Referred to a baseline aircraft with state-of-the-art technology, a cruise drag improvement potential of more than 10 % was identified. This drag reduction leads to MTOW reductions up to 4 % or increased range by more than 7 %.

Variable camber (VC) offers an opportunity to achieve considerable improvements in operational flexibility, buffet boundaries and performance and enable the use of one wing for a regional aircraft family. Although in this work the design lift requirement was not achieved, but the results showed that using VCW the lift could be increased and could be optimized to produce the desired lift range. The introduction of VC could set off a new generation of intelligent airliners which will optimize their camber schedule automatically throughout the entire mission. Variable Camber is a prerequisite for HLFC wing to control the pressure gradients and the off-design behaviour.

Before HLFC and VCW technology can be applied to the transport aircraft, a large multidisciplinary research effort is needed in order to master the technology and demonstrate it on flying test-beds and in-service operational tests.

CHAPTER ELEVEN

CONCLUSIONS AND RECOMMENDATIONS

11.1 CONCLUSIONS

The market are highly demands on a narrow-body, single-aisle aircraft with a capacity of 70 to 170 seats. Because of congestion and the competitive environment the airlines are forced to buy technology and competitive aircrafts at low cost and to ask to the manufacturers to provide more operational flexibility, without drastic performance losses.

In the feasibility phase of an Advanced Technology Regional Aircraft (ATRA) family, the combined HLFC-VCW concept was investigated to improve the overall efficiency and reduce weight as the weight-growth factor is a critical issue.

Referred to a baseline aircraft with current state-of-the-art technology, a cruise drag improvement potential of more than 10 % was identified. This drag reduction leads to MTOW reductions up to 4 % or increased range by more than 7 %.

The study showed that approximately 65 % of the wing upper surface from kink to tip can be laminarized in cruise by providing boundary layer suction only in the leading-edge region (see Figure 8.36). Hybrid laminar flow offers a high cruise drag reduction of more than 7.5 %. Although not studied in this research, there is further gain attainable with the application of HLFC to the empennage and engine nacelles. Variable Camber is a prerequisite for HLFC wing to control the pressure gradients and the off-design behaviour.

The variable camber (VC) system which is described in this thesis was designed for a typical new generation regional aircraft family the ATRA-80/-100/-130. This VC concept is engineerable and uses the traditional high lift devices without major mechanical additions in order to ease development and certification with low development costs; and is a powerful tool to enhance the operational flexibility and reduce weight through the reduction of limiting load cases. Moreover it can compensate for structural tolerances (e.g. twist). Variable camber will contribute an average reduction of 2.5 % (Reference 7.5) in cruise drag and enable the use of one wing for regional aircraft family. The introduction of VC can set off a new generation of intelligent airliners which will optimize their camber schedule automatically throughout the entire mission.

The ATRA's wing is not yet optimum. This can be seen from Figures 8.34 and 8.35, that C_L design (0.5) is not achieved and spanload distributions both for undeflected and deflected VC flap are not close to the elliptic distribution. Further revisions would be necessary to produce a more optimum design.

The conclusion can finally be drawn, that the combine HLFC - VCW concepts is feasible for an aircraft of the ATRA class and size, with the same reservations that apply to the feasibility of any laminar flow control (LFC) aircraft, i.e. the economic aspects depend on manufacturing and operational data.

11.2. RECOMMENDATIONS

As a result of the combined HLFC - VCW study, the following recommendations are made :

- The ATRA's wing needs to be optimized. The wing design parameters that need to be investigated include : aerofoil wing sections, t/c distribution, twist, aspect ratio, sweep, taper ratio, VC-flap shape, VC flap deflection, ...etc. This optimization, considering the combined HLFC-VCW design aspects from the beginning, should lead to significantly larger aircraft performance improvements.
- To improve the aerodynamic analysis with RAMPANT, a more fine grid or hybrid grid (structure grid near the wall and followed by unstructured grid) should be used.
- To improve drag prediction, more accurate methods should be used.
- Validation of the transition prediction methods in windtunnel and in flight.
- Research should be conducted to improve the definition of the transition criterion for mixed Tollmien-Schlichting (T-S) and crossflow (C-F) instabilities.
- Theoretical studies of the combined T-S and C-F instabilities would be valuable for interpretation of the experimental data and should be done.
- Study of techniques to delay attachment line transition.
- Study of roughness effects and wing surface smoothness requirements.
- Development of design criteria for perforated suction surface.
- Investigation of the possible leading-edge high lift devices to be used on a laminar wing.
- The best configuration for an HLFC aircraft depends significantly on the degree of leading-edge high-lift protection that will be required. Three studies should be made regarding this question : (1) to define the limits and trades for wings without leading-edge devices but considering the cruise requirements for HLFC, (2) to determine the acceptable size of surface discontinuities, considering application of locally increased suction, and (3) to determine the achievable smoothness of variable geometry leading-edges.
- The severity of the insect contamination problem should be better defined.
- The influence of engine noises especially on the wing lower surface boundary layer, is an area of concern. High-bypass-ratio fans typically radiate frequencies that coincide with the most critical T-S frequencies. These could excite rapidly amplified boundary layer oscillations and cause premature transition at high reynolds numbers. Acoustic treatment of the engines or increased suction in affected areas may therefore be required (Reference 7.). Detailed evaluation of the influence of noise on HLFC should be investigated.
- An alternate approach should be study to use an aerofoil with a mildly adverse 'roof-top' pressure gradient to improve wave drag and lift capabilities, although with a reduced extent of laminar flow.

- A further improvement potential of VC concept due to leading edge camber devices and spanwise differential camber is emphasized and should be investigated.
- The benefits of combined HLFC-VCW concept on a shorter flight segment should be studied.
- Before HLFC and VCW technology can be applied to the transport aircraft, a large multidisciplinary research effort is needed in order to master the technology and demonstrate it on flying test-beds and in-service operational tests.

REFERENCES

CHAPTER 2

2.1 **Aircraft Economics**. A Euromoney Publication, Number 20 July/August 1995.

2.2 **Flight International.** A Reed Business Publication, 12 - 18 November 1997.

2.3 **Aviation Week & Space Technology.** A Publication of the McGraw-Hill Companies, July 3, 1995.

2.4 **Flight International.** A Reed Business Publication, 16 - 22 August 1955.

2.5 **Jane's**. All The World's Aircraft 1996 - 1997. Jane's Information Group Ltd., Surrey - UK, 1996.

2.6 **E. Greff, K. Becker, M. Karwin, S. Rill**. Integration of High Bypass Ratio Engines on Modern Transonic Wings for Regional Aircraft. Aeronautical Journal Paper No. 1896. January, 1993.

2.7 **Mike Jenisco**, Boeing Technical Assistant. Preliminary Aircraft Design Course Note. IPTN-Bandung, Indonesia. 1989.

2.8 **Airbus Industrie**. A319 Briefing. AI/CM-T 316.0010 Issue 4. August 1994

2.9 **AVRO International Aerospace**. The RJ Avroliners. England. August 1994

2.10 **Alan Blythe, C.Eng. FRAeS**. Aircraft Design Course : 100 Seater Design Philosophy. CoA/Cranfield University. December, 1988.

2.11 **AVT-AVD 9665.** Derivation of Specifications for Civil Airliners. Lecture Note. AVT/CoA/Cranfield University.Cranfield. UK

2.12 **DAeT 9330.** Preliminary Design of Subsonic Civil Aircraft. Lecture Note. AVT/CoA/Cranfield University.Cranfield. UK

2.13 **DAeT 9439**. Aircraft Design Lecture Note. AVT/CoA/Cranfield University.Cranfield. UK

2.14 **DES 7413.** Lecture Note. AVT/CoA/Cranfield University.Cranfield. UK

2.15 **Egbert Torenbeek**. Synthesis of Subsonic Airplane Design. Delft University Press. 1982.

2.16 **Daniel P. Raymer**. Aircraft Design : A Conceptual Approach. AIAA Education Series. 1992.

2.17 **Dr. Jan Roskam**. Airplane Design Parts I-VIII. Roskam Aviation and Engineering Corporation. Ottawa, KS. 1989.

2.18 **L. M. Nicolai**. Fundamentals of Aircraft Design. METS Inc., 1975

2.19 **D. Stinton**. The Design of the Airplane. BSP Professional Books. 1983

2.20 **D. Stinton**. The Anatomy of the Airplane. BSP Professional Books. 1985

2.21 **D. Kuchemann**. The Aerodynamic Design of Aircraft. Pergamon Press Ltd. Oxford, England. 1978

2.22 **S. F. Hoerner**. Fluid Dynamic Drag. Hoerner Fluid Dynamics. P.O. Box 342, Brick Town, N. J., 08723. 1965

2.23 **R. W. Taylor**. Twin-Engine Transports a Look at the Future. Boeing Commercial Airplane Group. Seattle, Washington, USA. AIAA 90-3215. AIAA//AHS/ASEE Aircraft Design, Systems and Operations Meeting. September 17 - 19, 1990. Dayton, Ohio.

2.24 **Fred W. Tiegarden**. GE90 Integration with the B777 - a Success Story. Royal Aeronautical Society Paper, RAes Conference. October, 1992. Nottingham, England.
2.25 **D. L. Berry**. Civil Aircraft Propulsion Integration : Current & Future. SAE 932624, AeroTech 93 Conference. Anaheim, Ca. September, 1993.
2.26 **Dennis L. Berry**. The Boeing 777 Engine/Aircraft Integration Aerodynamic Design Process. Boeing Commercial Airplane Group. Seattle, Washington, USA. ICAS 94-6.4.4.
2.27 **A. W. Chen, M. M. Curtin, R. Carlson, E. N. Tinoco**. TRANAIR Applications to Engine/Airframe Integration. AIAA-89-2165CP. August, 1989.
2.28 **E. F. Kraus, P. Park, D. P. Raymer, J. H. McMasters**. AIAA Short Course. Prespectives in Aircraft System Design. February 20-21, 1993. Irvine, Ca.
2.29 **P. A. Henne.** MD-90 Transport Aircraft Design. AIAA-89-2023. Douglas Aircraft Company. McDonnell Douglas Corporation. Long Beach, CA. 1989.
2.30 **Aviation Week & Space Technology.** A Publication of the McGraw-Hill Companies, June 26, 1995
2.31 **S. Losch**. Influence of Flow Mixing on the Performance of a Turbofan Engine of High Bypass Ratio. Z. Flugwiss. 1990.
2.32 **Horst M. Homar** (Boeing Associated Technical Fellow). Trip Report to BMW/Rolls-Royce. IPTN. May, 1994.
2.33 **Prasetyo Edi.** F-93A Powerplant Installation. Project Thesis (M.Sc.) Supervisor: Dr. J. P. Fielding. AVT/CoA/Cranfield University, Cranfield - UK, 1994.
2.34 **DES 8308.** Lecture Note. AVT/CoA/Cranfield University.Cranfield. UK
2.35 **DES 8161.** Lecture Note. AVT/CoA/Cranfield University.Cranfield. UK
2.36 **J. C. Klein**, Boeing Technical Assistant. Stability and Control Course Note. IPTN-Bandung, Indonesia. 1989.
2.37 **D.E. Hoak**. "USAF Stability and Control Datcom". Flight Control Division, Air Force Flight Dynamics Lab, WPAFB. Ohio. 1978.
2.38 **Boeing Company**. http://www.boeing.com/commercial/737family/737.html
2.39 **P. J. Fennell and Prof. H. C. Muir**. The Influence of Hatch Weight and Seating Configuration on the Operation of a Type III Hatch. CAA Paper 93015. CAA London August 1993.
2.40 **Dr. E. Greff (Deutsche Airbus GmbH, Bremen, FRG).** Aerodynamic Design For A New Regional Aircraft. 17th ICAS Congress - Stockholm, 9th-14th September 1990; Paper No. 90-2.7.1.

CHAPTER 3

3.1. **F. S. Collier, Jr.**(NASA Langley Research Center, Hampton, VA 23681-0001). Recent Progress In The Development Of Laminar Flow Aircraft. ICAS Proceedings 1994; 19th Congress Of The International Council Of The Aeronautical Sciences; Anaheim, California, USA, 18-23 September, 1994. Volume III; Paper No. 94-4.7.1.
3.2. **Frank T. Lynch and Mark D. Klinge** (Douglas Aircraft Company). Some Practical Aspects of Viscous Drag Reduction Concepts. AIAA 91-2129.

3.3. **Boeing Commercial Airplane Company**. Hybrid Laminar Flow Control Study Final Technical Report. October 1982; NASA CR 165930.
3.4. **J. Reneaux and A. Blanchard**. The Design and Testing of an Airfoil with Hybrid Laminar Flow Control. First European Forum on Laminar Flow Technology. March 1992. Paper No. 92-01-021.
3.5. **R. D. Wagner, D. V. Maddalon and D. F. Fisher**. Laminar Flow Control Leading-Edge Systems in Simulated Airline Service. Journal of Aircraft, Vol. 27, No. 3, March 1990.
3.6. **Dr. E. Greff** (Deutsche Airbus GmbH, Bremen, FRG). Aerodynamic Design and Technology Concepts for A New Ultra-High Capacity Aircraft. ICAS Paper No. 96-4.6.3.
3.7. **J. J. Thibert (ONERA), A. Quast (DLR) and J. P. Robert (Airbus Industrie).** The A320 Laminar Fin Programme. ICAS-92-01-004.
3.8. **P. K. Bhutiani, D. F. Keck, D. J. Lahti, and M. J. Stringas**. Investigating the Merits of a Hybrid Laminar Flow Nacelle, in The Leading Edge, General Electric Company, Spring 1993, pp. 32-35.
3.9. **J. L. Lecordix (Snecma), A. Mullender (Rolls-Royce), E. Lecossais (Hispano-Suiza), J. L. Godard (ONERA) and M. Hepperle (DLR).** Hybrid Laminar Flow Nacelle Design. ICAS-96-2.3.4. 1996.

CHAPTER 4

4.1. **E. Greff**, "The Development and Design Integration of A Variable Camber Wing for Long/Medium Range Aircraft", Aeronautical Journal, November 1990.
4.2. "Assessement of Variable Camber for Application to Transport Aircraft", **Boeing Commercial Airplane Company**, NASA CR 158430, November 1980.
4.3. **William W. Gilbert**, "Mission Adaptive Wing System for Tactical Aircraft", General Dynamics/Fort Worth Division, Fort Worth, Texas, 1980.
4.4. **J.J. Spillman**, "The Use of Variable Camber to Reduce Drag, Weight and Cost of Transport Aircraft". Aeronautical Journal, January 1992, Royal Aeronautical Society, Paper No. 1844.
4.5. **J.P. Fielding, S.H.M. Macci, A.V. Mackinnon, J.L. Stollery**, "The Aerodynamic and Structural Design of A Variable Camber Wing (VCW)", ICAS-92-1.6.4, 1992.

CHAPTER 5

5.1. **Boeing Commercial Airplane Company**. Hybrid Laminar Flow Control Study Final Technical Report. October 1982; NASA CR 165930.

5.2. **Dr. E. Greff** (Deutsche Airbus GmbH, Bremen, FRG). Aerodynamic Design and Technology Concepts for A New Ultra-High Capacity Aircraft. ICAS Paper No. 96-4.6.3.

5.3. **J. Rao**. Variable Camber Wing for a Transport Aircraft. PhD Thesis Supervisor : Prof. J. J. Spillman. CoA/Cranfield University, Cranfield - UK, 1989.

5.4. **J. J. Spillman**. The Use of Variable Camber to Reduce Drag, Weight and Cost of Transport Aircraft. Aeronautical Journal, January 1992, Royal Aeronautical Society, Paper No. 1844.

CHAPTER 6

6.1. **G. Redeker, K. H. Horstmann, H. Koster and A. Quast** (German Aerospace Research Establishment (DFVLR), Braunschweig, FRG). Investigations On High Reynolds Number Laminar Flow Airfoils. Journal of Aircraft, Vol. 25, No. 7; July 1988.

6.2. **Boeing Commercial Airplane Company**. Hybrid Laminar Flow Control Study Final Technical Report. October 1982; NASA CR 165930.

6.3. **D. I. A. Poll**. Transition Description and Prediction in Three-Dimensional Flows. CoA/CIT/Cranfield University. CoA Report 8332. 1983.

6.4. **D. I. A. Poll**. Three Dimensional Boundary Layer Transition via the Mechanisms of Attachment Line Contamination and Cross Flow Instability. CoA/CIT/Cranfield University. CoA Report 7904. September 1979.

6.5. **Schlichting, H.**; "Boundary Layer Theory"; 7th ed. McGraw-Hill, New York; 1979.

6.6. **Gray, W. E.**; "The Effect of Wing Sweep on Laminar Flow"; RAE TM Aero. 255; 1952.

6.7. **Owen, P. R. and Randall, D. J.**; "Boundary Layer Transition on the Swept back Wing"; RAE TM Aero. 277; 1952.

6.8. **Boltz, F. W.; Kenyon, G. C. and Allen, C. Q.**; "Effects of Sweep Angle on the Boundary Layer Stability Characteristics of an Untapered Wing at Low Speeds"; NASA TN D-338; 1960.

6.9. **Skrokowski, A. J. and Orzaq, S. A.**; "Mass Flow Requirements for LFC Wing Design"; AIAA Aircraft Systems and Technology Meeting Paper 77-1222; 1977.

6.10. **Pfenninger, W.**; "Laminar Flow Control; Laminarization"; AGARD-R-654; 1977; pp. 3-1 to 3-75.

6.11. **Poll, D. I. A.**; "Transition in the Infinite Swept Attachment Line Boundary Layer"; The Aeronautical Quarterly; Vol. 30; 1979; pp. 607-629.

6.12. **J. Reneaux** (Office National d'Etudes et de Recherches Aerospatiales, Chatillon, France); A. Blanchard (ONERA/CERT, Toulouse, France); "The Design and Testing of an Airfoil with Hybrid Laminar Flow Control"; Paper 92-01-021.

6.13. **Mack, L. M.**; "On the Stability of the Boundary Layer on a Transonic Swept Wing"; AIAA 17th Aerospace Sciences Meeting Paper 79-0264; New Orleans, La.; January 15-17, 1979.

6.14. **Betchov, R. and Criminale, W. O.**; "Stability of Parallel Flows"; Academic Press; New York; 1967.

6.15. **Dagenhardt, J. R.**; "Amplified Crossflow Disturbances in the Laminar Boundary Layer on Swept Wings with Suction"; NASA TP 1902; 1981.

6.16. **Gregory, N.; Stuart, J. W. and Walker, W. S.**; "On the Stability of Three Dimensional Boundary Layer with Application to the Flow Due to a Rotating Disc"; Philosophical Transactions of the Royal Society of London; Series A; No. 943; Vol. 248; 1955; pp. 155 - 199.

6.17. **Runyan, J. and George Falvy, D.**; "Amplification Factors at Transition on an Unswept Wing in Free Flight and on Swept Wing in Wind Tunnel"; AIAA 17th Aerospace Sciences Meeting Paper 79-0267; New Orleans, La.; January 15-17, 1979.

6.18. **Jaffe, N. A.; Okamura, T. T. and Smith, A. M. O.**; "Determination of Spatial Amplification Factors and Their Application to Predicting Transition"; AIAA Journal Vol. 8; 1970; pp. 301 - 308.

6.19. **Obara, C. J. and Holmes, B. J.**; "Flight Measured Laminar Boundary Layer Transition Phenomena Including Stability Theory Analysis"; NASA TP 2417; 1985.

6.20. **Hefner, Jerry N. and Bushnell, Dennis N.**; "Status of Linear Boundary Layer Stability Theory and the e^n Method, with Emphasis on Swept Wing Applications"; NASA TP-1645; 1980.

6.21. **Bushnell, Dennis N. and Tuttle, Marie H.**; "Survey and Bibliography on Attainment of Laminar Flow Control in Air Using Pressure Gradient and Suction"; Vol. 1; NASA RP-1035; 1979.

6.22. **Arnal D.**; "Transition Prediction in Transonic Flow"; IUTAM Symposium Transsonicum III; Gottingen; 1988.

6.23. **D. Arnal, M. Habiballah and E. Coustols**. Laminar Instability Theory and Transition Criteria in Two and Three Dimensional Flow. La Recherche Aerospatiale, No. 1984-2, 1984.

6.24. **P. S. Granville**. The Calculation of the Viscous Drag of Bodies of Revolution. David Taylor Model Basin Report 849, 1953.

6.25. **R. Michel**. Critere de Transition et Amplification des Ondes d'Instabilite Laminaire. La Recherche Aerospatiale, No. 70, 1979.

6.26. **J. A. Beasley**. Calculation of the Laminar Boundary Layer and the Prediction of Transition on a Sheared Wing. ARC R&M 3787, 1973.

6.27. **D. I. A. Poll and D. J. Paisley**. On the Effect of Wing Taper and Sweep Direction on Leading Edge Transition. Aeronautical Journal, March 1985.

6.28. **P. W. C. Wong and M. Maina**. Study of Methods and Philosophies for Designing Laminar Flow Wings. ARA CR M275/1. August 1995.

6.29. **P. Hall, M. R. Malik and D. I. A. Poll**. On the Stability of an Infinite Swept Attachment Line Boundary Layer. Proc. R. Soc. A 395, pp 229-245, 1984.

6.30. **D. I. A. Poll**. Some Observations of the Transition Process on the Windward Face of a Long Yawed Cylinder. J. Fluid Mechanics, Vol. 150, pp 329-356, 1985.

6.31. **C. J. Atkin and D. I. A. Poll**. The Correlation Between Linear Stability Analysis and Crossflow Transition Near an Attachment Line. Presented at the Colloquium on Transitional Boundary Layers in Aeronautics, Amsterdam, December 1995.

6.32. **E. W. Warren and H. A. Hassan**. Alternate to the e^n Method for Determining Onset of Transition. AIAA Journal, Vol. 36, No. 1, page 111-113.

6.33. **W. S. Saric**. Physical Description of Boundary Layer Transition : Experimental Evidence. AGARD Rept. 793, March 1993.
6.34. **T. Herbert**. Parabolized Stability Equations. AGARD Rept. 794, March 1993.

CHAPTER 7

7.1 **Conceptual Design Staff**. ATRA-100 Multi National Project Aircraft (Boeing, MBB, Fokker, IPTN). Wing Design Document. 1987.
7.2 **DAeT 9573.** Wing Design Requirements and Construction Methods. Lecture Note. AVD/CoA/Cranfield University.Cranfield. UK
7.3 **D. Stinton**. The Anatomy of the Airplane. BSP Professional Books. 1989
7.4 **R. A. L. Wilson and R. I. Jones**. Project Design Studies on Aircraft Employing Natural and Assisted Laminar Flow Technologies. PhD Thesis. AVT-CoA-Cranfield University. 1996. SAE 952038.
7.5 **Dr. E. Greff (Deutsche Airbus GmbH, Bremen, FRG).** Aerodynamic Design And Integration Of A Variable Camber Wing For A New Generation Long/Medium Range Aircraft. ICAS-88-2.2.3.
7.6 **DAeT 9439**. Aircraft Design Lecture Note. AVT-CoA-Cranfield University. Cranfield. UK
7.7 **Dr. E. Greff (Deutsche Airbus GmbH, Bremen, FRG).** Aerodynamic Design For A New Regional Aircraft. 17th ICAS Congress - Stockholm, 9th-14th September 1990; Paper No. 90-2.7.1.
7.8 **J. Reneaux and A. Blanchard.** The Design and Testing of an Airfoil with Hybrid Laminar Flow Control. First European Forum on Laminar Flow Technology. March 1992. Paper No. 92-01-021.
7.9 **G. Redeker and G. Wichmann**. Forward Sweep-a Favorable Concept for a Laminar Flow Wing. J. Aircraft Vol. 28, No. 2, page 97 - 102. February 1991.
7.10 **Aviation Week & Space Technology**. Airbus Transport Concept Relies on Radical Design. A Publication of the McGraw-Hill Companies. Oct 27, 1986, p 26.
7.11 **L. M. Nicolai**. Fundamentals of Aircraft Design. METS Inc., 1975
7.12 **A. J. Bocci**. Modern Wing Aerodynamic Design. A course of lectures. Originally prepared by **P.R. Ashill.** High Speed and Weapon Aerodynamics Department. DRA Bedford. 1997
7.13 **D. Schmitt and K. H. Vahle**. The Impact of Hybrid Laminar Flow Control on the Performance of a Commercial Transport Aircrfat. First European Forum on Laminar Flow Technology. March 1992.
7.14 **R. W. Barnwell and M. Y. Hussaini (Editors).** Natural Laminar Flow And Laminar Flow Control. ICASE/NASA LaRC Series; 1992. Hampton, VA 23665, USA.
7.15 **Julian Moxon**. Drag Down 15% with Laminar Flow Wing. Fokker 100 with Laminar Flow Wing-Glove (ELFIN). Flight International 25 Dec., 1991 - 7 Jan., 1992.
7.16 **F. S. Collier, Jr.(NASA Langley Research Center, Hampton, VA 23681-0001).** Recent Progress In The Development Of Laminar Flow Aircraft. ICAS

Proceedings 1994; 19th Congress Of The International Council Of The Aeronautical Sciences; Anaheim, California, USA, 18-23 September, 1994. Volume III; Paper No. 94-4.7.1.

7.17 **Frank T. Lynch and Mark D. Klinge (Douglas Aircraft Company).** Some Practical Aspects of Viscous Drag Reduction Concepts. AIAA 91-2129.

7.18 **J. Szodruch.** Viscous Drag Reduction on Transport Aircraft. AIAA 91-0685.

7.19 **H. Bieler and J. Preist.** HLFC for Commercial Aircraft. First ELFIN Test Results. First European Forum on Laminar Flow Technology. Paper No. 92-01-031. March 1992.

7.20 **D. Schmitt, J. Reneaux, and J. J. Thibert.** Design and Experimental Investigation of a Laminar Horizontal Tail. AIAA-90-3042.

7.21 **J. J. Thibert, A. Quast and J. P. Robert.** The A320 Laminar Fin Progamme. First European Forum on Laminar Flow Technology. Paper No. 92-01-004. March 1992

7.22 **F. S. Collier, Jr and P. C. Arcara Jr.** Hybrid Laminar Flow Control Applied to Advanced Turbofan Engine Nacelles. SAE Technical Paper No. 920962.

7.23 **D. P. Coiro and F. Nicolosi.** Design of Natural Laminar Flow Fuselages. ICAS Paper No. 94-4.7.4. Anaheim, California, USA. 18-23 September, 1994.

7.24 **P. Macey.** A Feasibility Study on the Application of Variable Camber Flaps on a Military Tactical Transport Aircraft. Research Thesis (MSc) Supervisor : Dr. J. P. Fielding. AVT/CoA/Cranfield University, Cranfield - UK, 1993.

7.25 **Mohammad Ali (F) Vaziry-Zanjany.** Aircraft Conceptual Design Modelling Incorporating Reliability and Maintainability Predictions. PhD Thesis Supervisor : Dr. J. P. Fielding. AVT/CoA/Cranfield University, Cranfield - UK, 1996.

7.26 **Prasetyo Edi.** A Feasibility Study on the Application of Variable Camber Wings on a Military Tactical Transport Aircraft. Research Thesis (MSc) Supervisor : Dr. J. P. Fielding. AVT/CoA/Cranfield University, Cranfield - UK, 1994.

7.27 **D. Stinton.** The Design of the Aeroplane. BSP Professional Books. 1989

7.28 **Boeing Commercial Airplane Company.** Hybrid Laminar Flow Control Study Final Technical Report. October 1982; NASA CR 165930

7.29 **Boeing Commercial Airplane Company.** Natural Laminar Flow Airfoil Analysis and Trade Studies Final Report. August 1977 - June 1979; NASA CR 159029.

7.30 **P. W. C. Wong and M. Maina.** Study of methods and Philosophies for Designing Laminar Flow Wings. ARA - Bedford - UK. Contractor Report M275/1. August 1995.

7.31 **Egbert Torenbeek.** Synthesis of Subsonic Airplane Design. Delft University Press. 1982.

7.32 **Bertil Dillner, Fred W. May and John H. McMasters.** Aerodynamic Issues in the Design of High-Lift Systems for Transport Aircraft. Boeing Aircraft Company. AGARD-CP-365.

7.33 **D. S. Woodward and D. E. Lean.** Where is High-Lift Today? - A Review of Past UK Research Programmes. DRA Farnborough - UK. AGARD-CP-515. Sept. 1993.

7.34 **A. Flaig and R. Hilbig**. High-Lift Design for Large Civil Aircraft. Deutsche Airbus Gmbh. AGARD-CP-515. Sept. 1993.

7.35 **D. J. Butter**. Recent Progress on Development and Understanding of High-Lift Systems. AGARD-CP-365

7.36 **J. R. Wedderspoon**. The High Lift Development of the A320 Aircraft. BAe - UK. ICAS-86-2.3.2.

7.37 **Walter O. Valarezo, Chet J. Dominik, Robert J. McGhee and Wesley L. Goodman**. High Reynolds Number Configuration Development of a High-Lift Airfoil. AGARD-CP-515. Sept. 1993

7.38 **Walter O. Valarezo, Chet J. Dominik, Robert J. McGhee, Wesley L. Goodman and Keith B. Paschal.** Multi Element Airfoil Optimization for Maximum Lift at High Reynolds Numbers. AIAA-91-3332-CP.

7.39 **P. Capbern.** Theoretical and Experimental Study of High-Lift Device for a Natural Laminar Flow Airfoil. ICAS 92-01-032.

7.40 **H. L. Morgan**. High-Lift Flaps for Natural Laminar Flow Airfoils. NASA CP-2413, 1985.

7.41 **Dr. E. Greff** (Deutsche Airbus GmbH, Bremen, FRG); "Aerodynamic Design For A New Regional Aircraft"; 17th ICAS Congress - Stockholm, 9th-14th September 1990; Paper No. 90-2.7.1.

7.42 **Dr. E. Greff** (Deutsche Airbus GmbH, Bremen, FRG); "Aerodynamic Design And Integration Of A Variable Camber Wing For A New Generation Long/Medium Range Aircraft; ICAS-88-2.2.3.

7.43 **J. Reneaux** (Office National d'Etudes et de Recherches Aerospatiales, Chatillon, France); **A. Blanchard** (ONERA/CERT, Toulouse, France); "The Design and Testing of an Airfoil with Hybrid Laminar Flow Control"; Paper 92-01-021.

7.44 **G. Redeker, K. H. Horstmann, H. Koster and A. Quast** (German Aerospace Research Establishment (DFVLR), Braunschweig, FRG); "Investigations On High Reynolds Number Laminar Flow Airfoils"; Journal of Aircraft, Vol. 25, No. 7; July 1988.

7.45 **M. Khalid and D. J. Jones**. A Summary of Transonic Natural Laminar Flow Airfoil Development at NAE. Aeronautical Note, NAE-AN-65, NRC No. 31608. Ottawa May 1990

7.46 **Dr. Jan Roskam**. Airplane Design Parts I-VIII. Roskam Aviation and Engineering Corporation. Ottawa, KS. 1989.

7.47 **D. E. Hoak and D. E. Ellison**. USAF Stability and Control DATCOM. Flight Control Division, Air Force Flight Dynamics Laboratory, WPAFB, Ohio, 45433-0000, 1978, revised.

7.48 **Hermann Schlichting and Erich Truckenbrodt**. Aerodynamics of the Airplane. McGraw-Hill International Book Company. 1979.

7.49 **D. Kuchemann**. The Aerodynamic Design of Aircraft. Pergamon Press Ltd. Oxford, England. 1978

7.50 **David Nixon** (Ed.). Transonic Aerodynamics. Progress in Astronautics and Aeronautics Vol. 81. February 18-20, 1981.

7.51 **Daniel P. Raymer**. Aircraft Design : A Conceptual Approach. AIAA Education Series. 1992.

7.52 **Michael C. Y. Niu**. Airframe Structural Design. Pracrtical Design Information and Data on Aircraft Structures. Conmilit Press Ltd. 1988.

7.53 **Bernard Etkin and Lloyd Duff Reid**. Dynamics of Flight. Stability and Control. Third edition. 1996. John Wiley &Sons, Inc.

7.54 **McRuer, Ashkenas, and Graham**. Aircraft Dynamics and Automatic Control. Princeton University Press. 1990.

7.55 **M. V. Cook**. Flight Dynamics Principles. College of Aeronautics, Cranfield University. Arnold. 1997.

7.56 **D. L. Berry**. Civil Aircraft Propulsion Integration : Current & Future. SAE 932624, AeroTech 93 Conference. Anaheim, Ca. September, 1993.

7.57 **B. C. Clem, J. K. Elliott, T. L. B. Tamigniaux, and E. N. Tinoco**. Recent CFD Applications on Jet Transport Configurations. Boeing Commercial Airplane Group. AIAA-92-2658-CP.

7.58 **W. H. Jou, W. P. Huffman, D. P. Young, R. G. Melvin, M. B. Bieterman, C. L. Hilmes, and F. T. Johnson**. Practical Considerations in Aerodynamic Design Optimization. The Boeing Company. AIAA-95-1730.

7.59 **T. J. Kao, T. Y. Su, and N. J. Yu**. Navier-Stokes Calculations for Transport Wing-Body Configurations with Nacelles and Struts. Boeing Commercial Airplane Group. AIAA-93-2945.

7.60 **Leigh Ann Smith and Richard L. Campbell**. Applications of a Direct/Iterative Design Method to Complex Transonic Configurations. NASA TP 3234. 1992.

7.61 **Yasuhiro Tani and Kanichi Amano**. Experimental and Numerical Investigation on Liplets for Wing/Nacelle Interference Drag Reduction. ICAS-94-6.4.5. 1994.

7.62 **J. A. Jupp and T. Markham**. The Prediction and Reduction of Interference and Parasite Drag of Transport Aircraft with Reference to the A310 Wing Development. Royal Aeronautical Society Symposium on "The Prediction and Reduction of Aircraft Drag", 2nd March 1983.

7.63 **J. P. Robert.** Hybrid Laminar Flow Control. A Challange for a Manufacturer. First European Forum on Laminar Flow Technology. March 1992. Paper No. 92-01-031.

7.64 **SWEPTDES**. A Computer program of RAeS TDM 6312 for calculating the subcritical inviscid flow over a finite wing, with compressibility effects updated to the standard of ESDU TDM 7312.

7.65 **CATIA** Base Geometry Interface Reference Manual"; 2nd Edition, IBM Publication No. SH50-0091-01; 1988.

7.66 **RAMPANT** User's Guide; Fluent Incorporated; January 1995.

7.67 **H. Zimmer**. The Aerodynamic Optimization of Wings at Subsonic Speeds and the Influence of Wingtip Design. NASA TM-88534. May 1987.

7.68 **J. J. Spillman**. Wing Tip Sails

7.69 **Dieter Schmitt**. Advanced Technology Constant Challenge and Evolutionary Process. L'Aeronautique et l'Astronautique. No. 145-1990-6-17.

7.70 **J. A. Jupp**. Winglets for the Airbus.

7.71 **Flight International**. Number 4629 Volume 153. June 10 - 16 1998.

7.72 **S. H. M. Macci**. Structural and Mechanical Feasibility Study of a Variable Camber Wing (VCW) for a transport Aircraft. PhD Thesis Supervisor : Dr. J. P. Fielding. AVT/CoA/Cranfield University, Cranfield - UK, August 1992.

7.73 **J. J. Spillman**. The Use of Variable Camber to Reduce Drag, Weight and Cost of Transport Aircraft. Aeronautical Journal, January 1992, Royal Aeronautical Society, Paper No. 1844.

7.74 **Josef Mertens**. German National Technology Programme on Cruise Drag Reduction (RaWid). Daimler-Benz Aerospace Airbus GmbH. 28-5-1996.

7.75 **A. J. Rao**. Variable Camber Wing for a Transport Aircraft. PhD Thesis Supervisor : Prof. J. J. Spillman. CoA/Cranfield University, Cranfield - UK, 1989.

7.76 **W. Pfenninger.** Flow Problems of Swept Low-Drag Suction Wings of Practical Constraction at High Reynolds Numbers. Annals of the N.Y. Academy of Sciences, Vol. 154, Art. 2, page 672-703, November 1968.

7.77 **C. Bulgubure and D. Arnal.** DASSAULT FALCON 50 Laminar Flow Flight Demonstrator. First European Forum on Laminar Flow Technology. March 16-18, 1992, page 11-18.

7.78 **Douglas Aircraft Company Staff.** Laminar Flow Control Leading Edge Flight Test Article Development. NASA CR-172137, 1984.

7.79 **Douglas Aircraft Company Staff.** Evaluation of Laminar Flow Control System Concepts for Subsonic Commercial Transport Aircraft. NASA CR-159251, 1983.

7.80 **N. Gregory.** Research on Suction Surfaces of Laminar Flow, Boundary Layer and Flow Control, edited by G. V. Lachman. Pergamon Press, page 924-960. 1961.

7.81 **R. D. Wagner, D. V. Maddalon and D. F. Fisher**. Laminar Flow Control Leading-Edge Systems in Simulated Airline Service. Journal of Aircraft, Vol. 27, No. 3, March 1990.

7.82 **Anon**. Evaluation of Laminar Flow Control System Concepts for Subsonic Commercial Transport Aircraft. NASA CR-159253, September 1983.

7.83 **Kohlman, D. L. et al**. Icing Tunnel Tests of a Glycol-Exuding Porous Leading Edge Ice Protection System on a General aviation Airfoil. AIAA Paper 81-0405, January 1981.

7.84 **Northrop Report NOR 67-136**. Final Report on LFC Aircraft Design Data, Laminar Flow Control Demonstration Program. X-21A Engineering Section, June 1967.

7.85 **I. Tani**. Effect of Two-Dimensional and Isolated Roughness on Laminar Flow. Edited by G. V. Lachman, Bondary Layer Control, Vol 2, Pergamon Press, 1961.

7.86 **A. E. Von Doenhoff and A. L. Braslow**. The Effect of Distributed Surface Roughness on Laminar Flow. Edited by G. V. Lachman, Bondary Layer Control, Vol 2, Pergamon Press, 1961.

7.87 **D. H. Jagger and A. J. Davies**. Design and Engineering Issues of a Hybrid laminar Flow Wing. Paper 12.3, 2nd European Forum for Laminar Flow Technology, Bordeaux, June 1996.

7.88 **Boeing Commercial Airplane Company**. F-111 Natural Laminar Flow Glove Flight Test Data and Boundary Layer Stability Analysis. January 1984. NASA CR 166051.

7.89 **Dr. E. Greff** (Deutsche Airbus GmbH, Bremen, FRG); "Aerodynamic Design And Technology Concepts For A New Ultra-High Capacity Aircraft. ICAS-96-4.6.3.

7.90 **P. R. Ashill, J. L. Fulker and A. Shires (DRA, Bedford, UK).** A Novel Technique for Controlling Shock Strength of Laminar-Flow Aerofoil Sections. ICAS 92-01-022.

7.91 **Claus Bauer, Willi Martin, Hans-Friedrich Siegling and Helmut Schurmann.** A New Structural Approach to Variable Camber Wing Technology of Transport Aircraft. AIAA-98-1756.

7.92 **A. V. Mackinnon.** An Experimental Study of a Variable Camber Wing. PhD Thesis, Cranfield University, 1992.

7.93 **R. A. L. Wilson**. The Introduction of Laminar Flow to the Design and Optimisation of Transport Aircraft. PhD Thesis, Supervisor : DR. R. I. Jones, Cranfield University March 1997.

CHAPTER 8

8.1 **Rampant** User's Guide; Fluent Incorporated; January 1995.

8.2 **Fluent** User's Guide; Fluent Incorporated; January 1995.

8.3 **CATIA** 3D Design, Interactive Functions Reference Manual. 1st Edition, IBM Publication No. SH50-0091-01; 1988.

8.4 **CATIA** Base Geometry Interface Reference Manual"; 2nd Edition, IBM Publication No. SH50-0091-01; 1988.

8.5 **PreBFC** User's Guide; Fluent Incorporated; January 1993.

8.6 **TGrid** User's Guide; Fluent Incorporated; January 1993.

8.7 **A. J. Bocci**. Modern Wing Aerodynamic Design. A course of lectures. Originally prepared by **P.R. Ashill.** High Speed and Weapon Aerodynamics Department. DRA Bedford. 1997

8.8 **Preliminary Design Department** (Boeing Commercial Aircraft Company). F-111 Natural Laminar Flow Glove Flight Test Data Analysis and Boundary Layer Stability Analysis. NASA CR 166051. August 1981 - July 1983.

CHAPTER 9

9.1 **Boeing Commercial Airplane Company**. Hybrid Laminar Flow Control Study Final Technical Report. October 1982; NASA CR 165930

9.2 **Dr. E. Greff (Deutsche Airbus GmbH, Bremen, FRG).** Aerodynamic Design And Integration Of A Variable Camber Wing For A New Generation Long/Medium Range Aircraft. ICAS-88-2.2.3.

9.3 **R. A. L. Wilson and R. I. Jones**. Project Design Studies on Aircraft Employing Natural and Assisted Laminar Flow Technologies. PhD Thesis. AVT-CoA-Cranfield University. 1996. SAE 952038.

APPENDIX A

COMPETITOR AIRCRAFT DATA

A.1 WING PARAMETER, WEIGHT AND PERFORMANCE

AIRCRAFT	S M^2	b M	AR	C_R M	C_T M	λ	$\Lambda_{C/4}$ DEG	i_{root} DEG	i_{tip} DEG	t/c_{root}	t/c_{tip}
AVRO RJ-70/-85/-100/-115	77.29	26.21	9	2.75	0.91	0.331	15	3.1	0	15.3	12.2
FOKKER F-70/-100	93.5	28.08	8.4	5.28	1.26	0.239	17.45			12.3	9.6
FOKKER F-130		31.09			1.26		17.45				
BOEING 737-500/-300/-400	105.4	28.88	7.9	4.71							
BOEING 737-600/-700/-800	125	34.31	9.4								
BOEING MD-95-30/-90-50	112.3	32.87	9.6								
BOEING MD-87	115.11	32.87	9.6	7.05	1.1	0.156	24.5	1.25		11 (mean)	
AIRBUS A319/A320	122.4	33.91	9.4				25			10.8 (out board)	
AIRBUS A321	122.4	34.09	9.49								
IPTN N-2130-IO3/AO3/GO3	102.8	28.95	8.2								
CRJ-X	68.56	23.01	7.7								

Table A.1.a Competitor aircraft wing parameter

AIRCRAFT	Passenger	Range NM	OEW KG	MTOW KG	T KG	W/S KG/M^2	T/W	$S_{T.O.}$ M	S_{LAND} M	M_{CRUISE} Mach
AVRO RJ-70	70	1,660	23,587	43,091	12,701	558	0.295	1,192	1,173	0.73 (M_{MO})
AVRO RJ-85	85	1,600	24,267	43,998	12,701	569	0.289	1,385	1,189	0.73 (M_{MO})
AVRO RJ-100	100	1,490	25,174	46,039	12,701	596	0.276	1,655	1,268	0.73 (M_{MO})
AVRO RJ-115	116	1,490	25,310	46,039	12,701	596	0.276	1,811	1,268	0.73 (M_{MO})
FOKKER F-70-D	79	2,015	22,784	41,730	12,565	446	0.301	1,665	1,274	0.77 (M_{MO})
FOKKER F-100-C	107	1,680	24,747	45,810	12,565	490	0.274	1,825	1,350	0.77 (M_{MO})
FOKKER F-130-Optional	137	2,365	31,555	58,965				1,825	1,430	0.77 (M_{MO})
BOEING 737-500-B	108	2,420	32,223	60,555	18,144	575	0.3	2,633	1,356	0.745
BOEING 737-300-B	128	2,600	33,266	62,820	19,958	596	0.318	2,286	1,433	0.745
BOEING 737-400-B	146	2,090	35,162	68,040	19,958	646	0.293	2,664	1,539	0.745
BOEING 737-600	108	3,230	36,441	65,090	19,958	521	0.307	1,877	1,268	0.782
BOEING 737-700	128	3,245	37,584	69,399	21,773	555	0.314	2,042	1,356	0.781
BOEING 737-800	162	2,930	41,463	78,244	23,769	626	0.304	2,316	1,600	0.785

Table A.1.b Competitor aircraft weight and performance

AIRCRAFT	Passenger	Range NM	OEW KG	MTOW KG	T KG	W/S	T/W	$S_{T.O.}$ M	S_{LAND} M	M_{CRUISE} Mach
BOEING MD-95-30-ER	106	2,001	31,480	54,885	16,783	590	0.306	2,012	1,469	0.76 (max level)
BOEING MD-87-Optional	130	2,833	33,965	67,810	18,144	589	0.268	1,859	1,429	0.76. 0.8 (max)
BOEING MD-90-50	153	3,022	41,685	78,245	25,402	697	0.325	2,435	1,670	0.76
AIRBUS A319-B	124	2,650	40,149	70,000	21,319	572	0.305	1,970	1,356	
AIRBUS A320-2nd Option-B	150	2,950	42,069	77,000	22,680	629	0.295	2,294	1,442	
AIRBUS A321-C3-one ACT	185	2,650	47980	89,000	29,030	727	0.326	2,345	1,587	
IPTN N-2130-IO3	80	1,550		43,500	16.795	423	0.386	1,800		0.8
IPTN N-2130-AO3	100	1,850		49,500	16,779	482	0.339	1,850		0.8
IPTN N-2130-GO3	130	1,850		55,800	16,807	543	0.301	1,850		0.8
CRJ-X -Optional	70	2,040	19,641	34,019	11,857	496	0.349	1,762	1,413	0.77

Table A.1.b Competitor aircraft weight and performance (continue)

A.2 GENERAL ARRANGEMENT

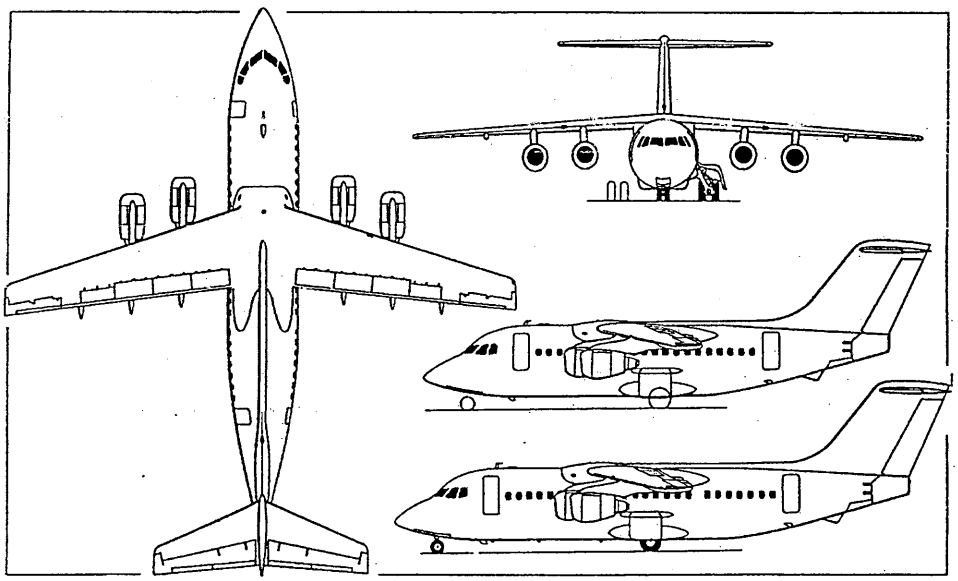

Figure A.1 Avro RJ85 with additional side view (upper) of RJ70 (Ref. 2.9)

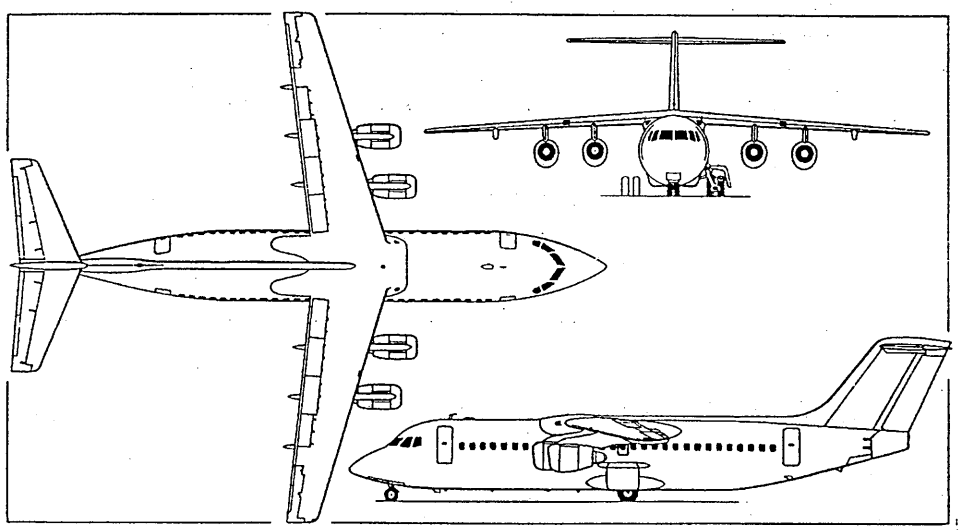

Figure A.2 Avro RJ115 with up to 128 seats (Ref. 2.9)

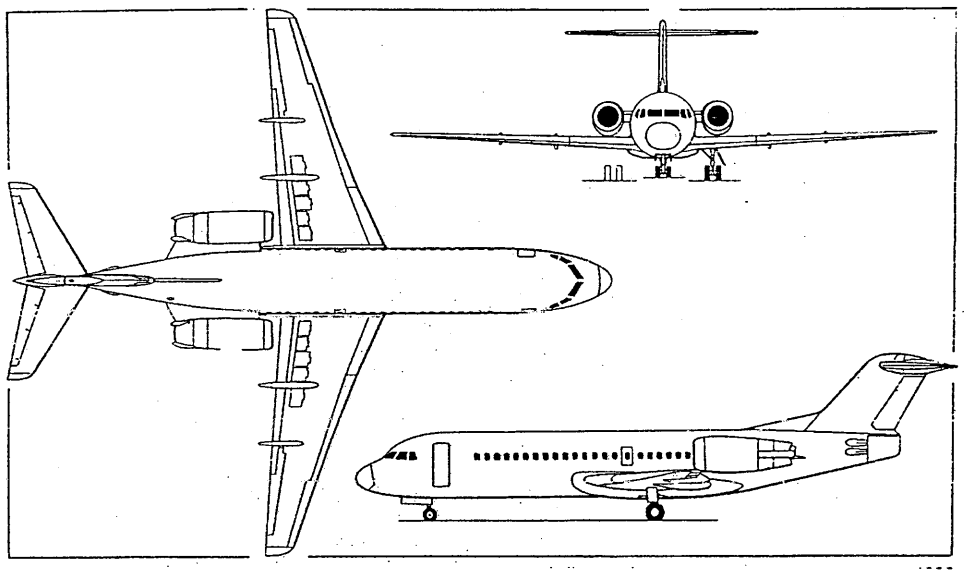

Figure A.3 Fokker 70, shortened version of the Fokker 100 (Ref. 2.5)

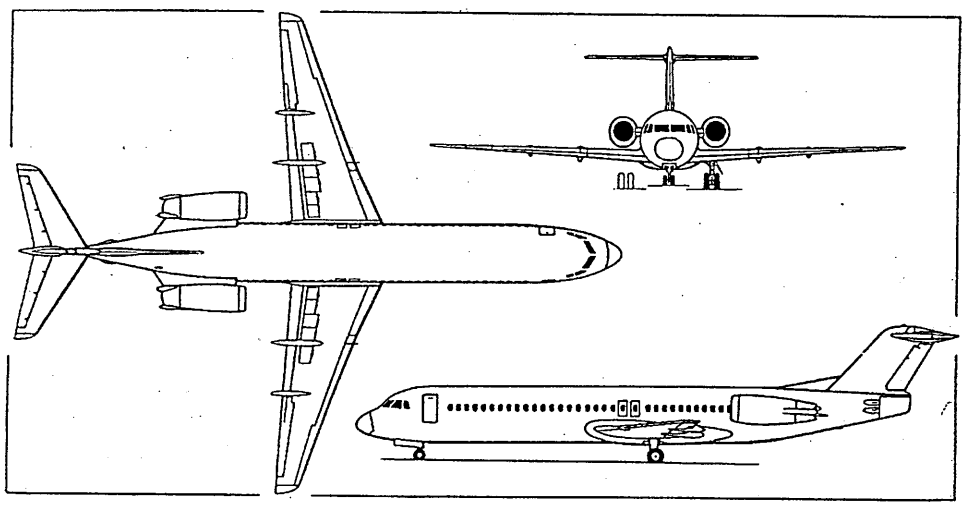

Figure A.4 Fokker 100 short/medium-haul transport (Ref. 2.5)

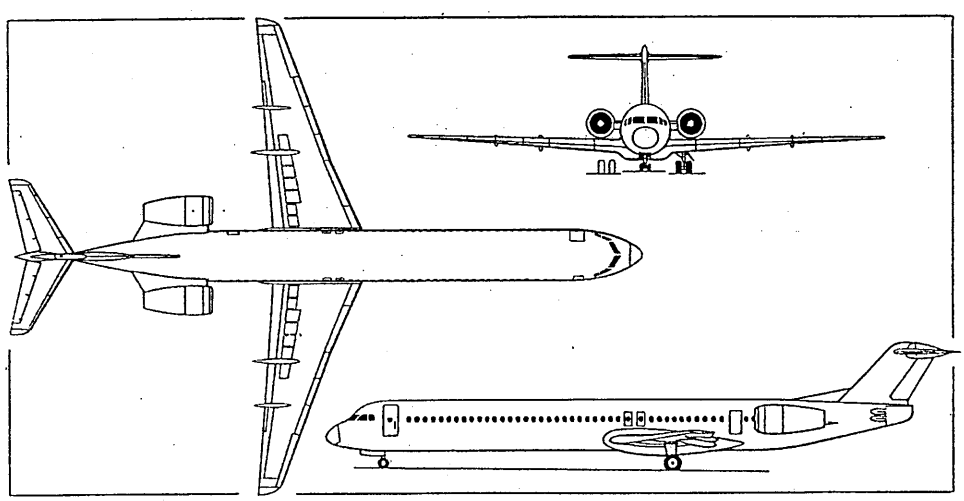

Figure A.5 Fokker 130 proposed stretched derivative of the Fokker 100 (Ref. 2.5)

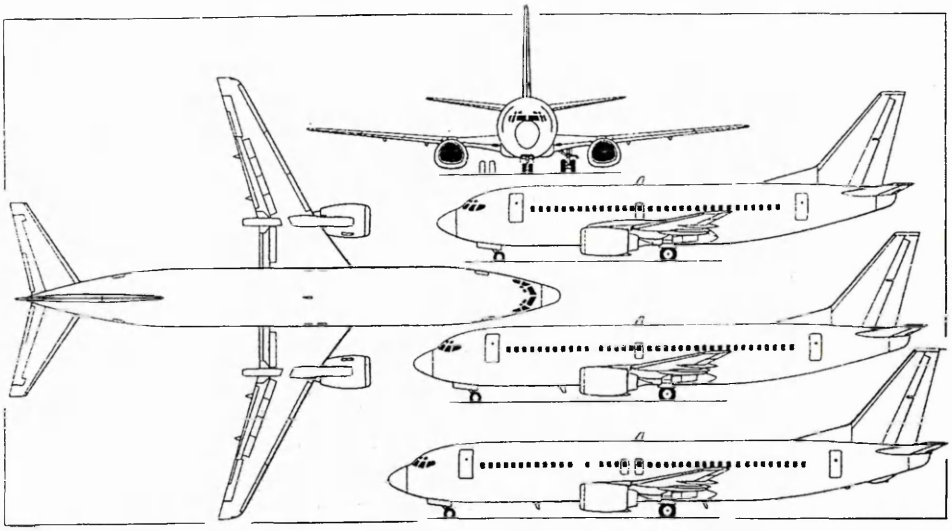

Figure A.6 Boeing 737-400, with additional side views of 737-500 (top) and 737-300 (centre), Ref. 2.5

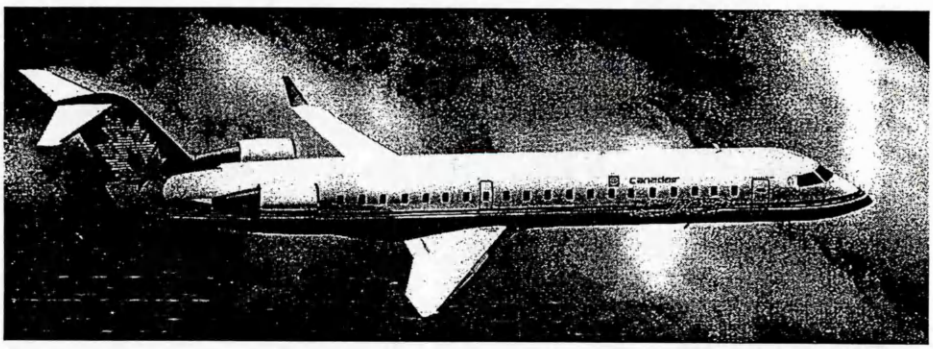

Figure A.7 Computer-generated impression of Canadair CRJ-X (Ref. 2.5)

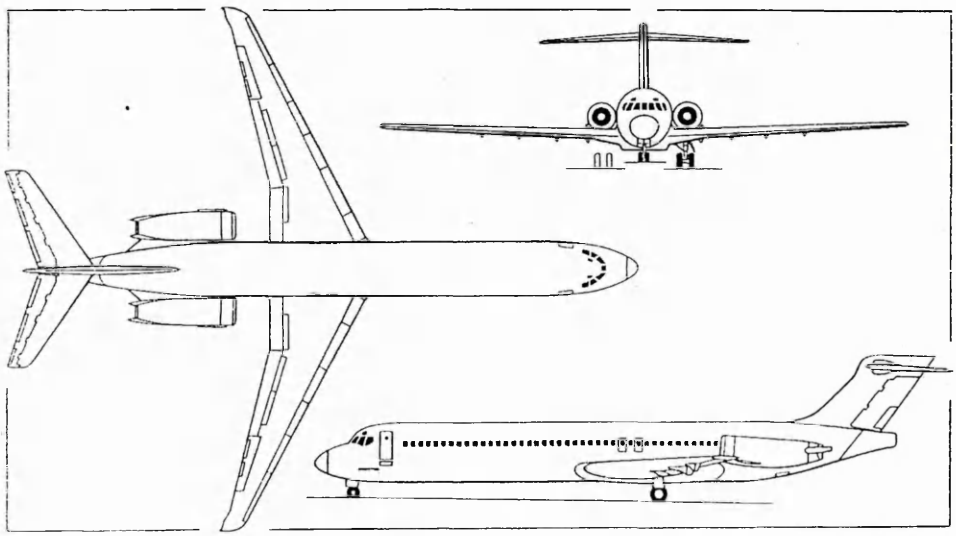

Figure A.8 MD-87, a short-fuselage variant of the MD-80 (Ref. 2.5)

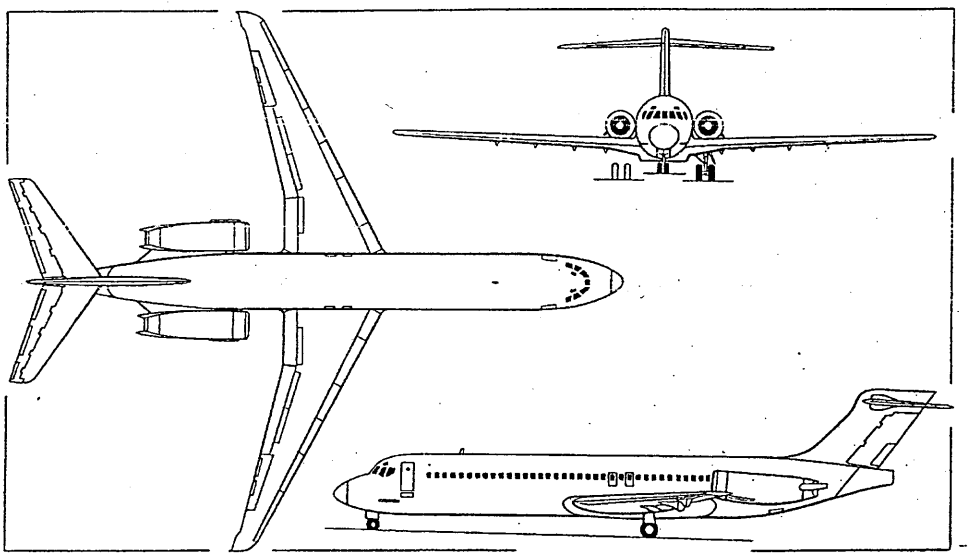

Figure A.9 McDonnell Douglas MD-95 airliner (two BR715 turbofans), Ref. 2.5

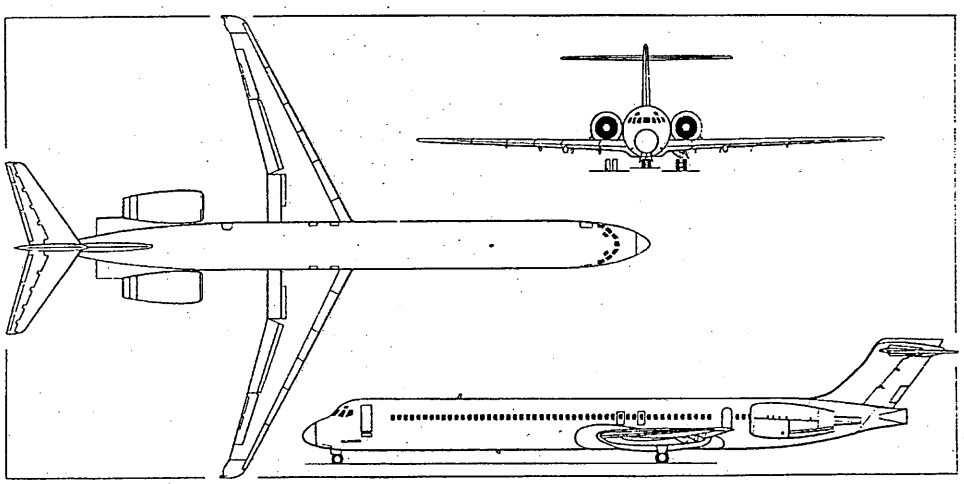

Figure A.10 McDonnell Douglas MD-90-30 airliner (two IAE V2525-D5 turbofans), Ref. 2.5

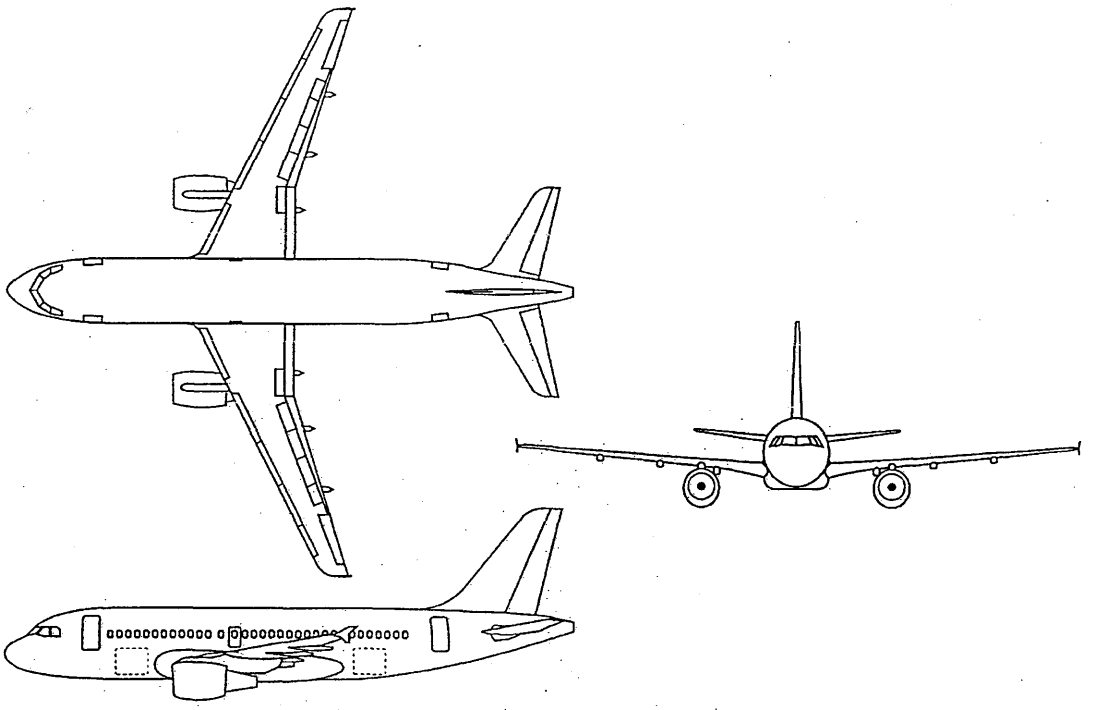

Figure A.11 Airbus A319, a short-fuselage variant of the A320 (Ref. 2.8)

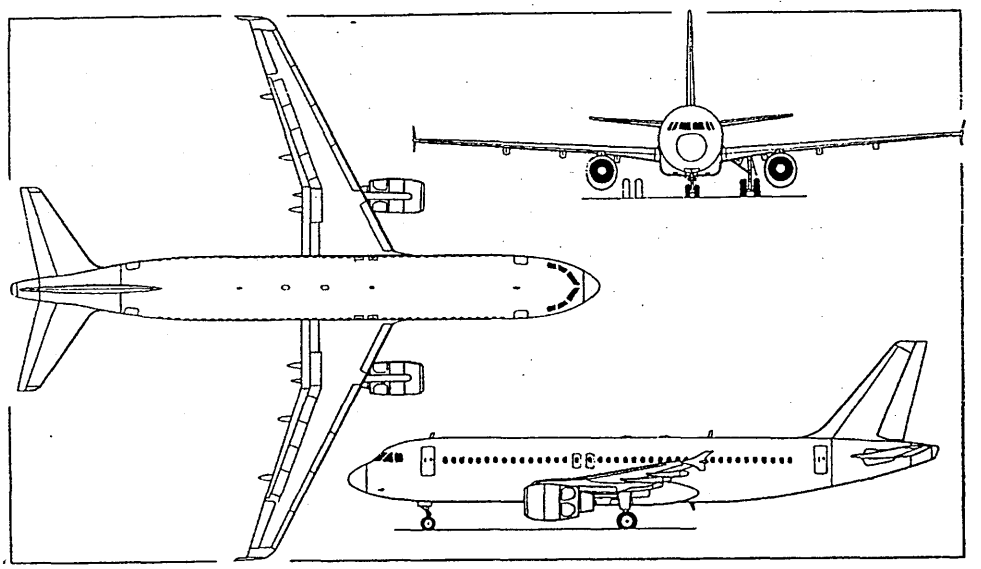

Figure A.12 Airbus A320 twin-turbofan single-aisle 150/179-seat airliner (Ref. 2.5)

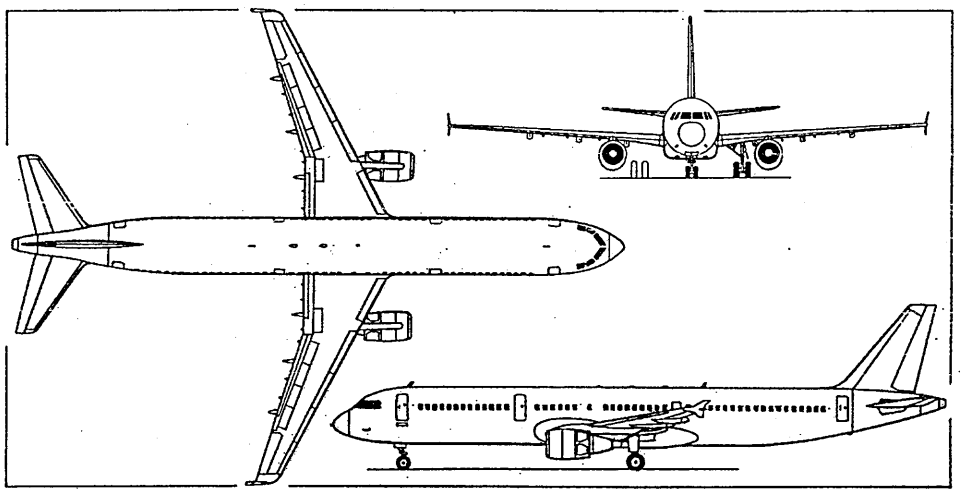

Figure A.13 Airbus A321 stretched development of the Airbus A320 (Ref. 2.5)

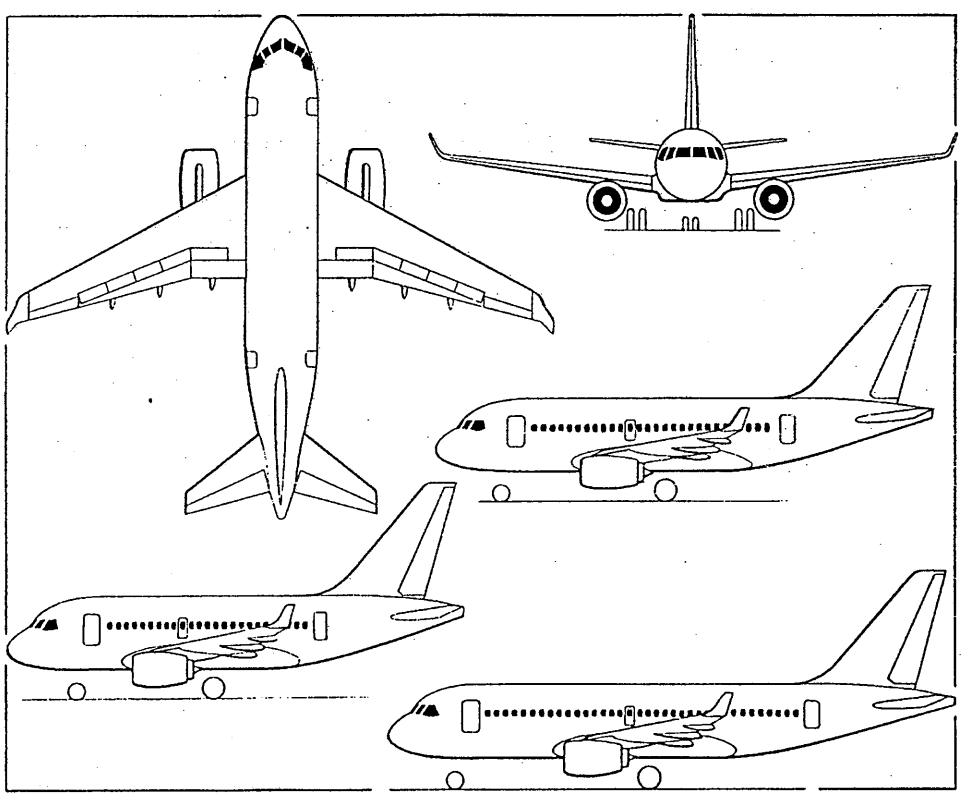

Figure A.14 IPTN N-2130 in basic 100-seat (A03) configuration (main drawing), with additional side views of the 80- and 130-seat (I03 and G03) model (Ref. 2.5)

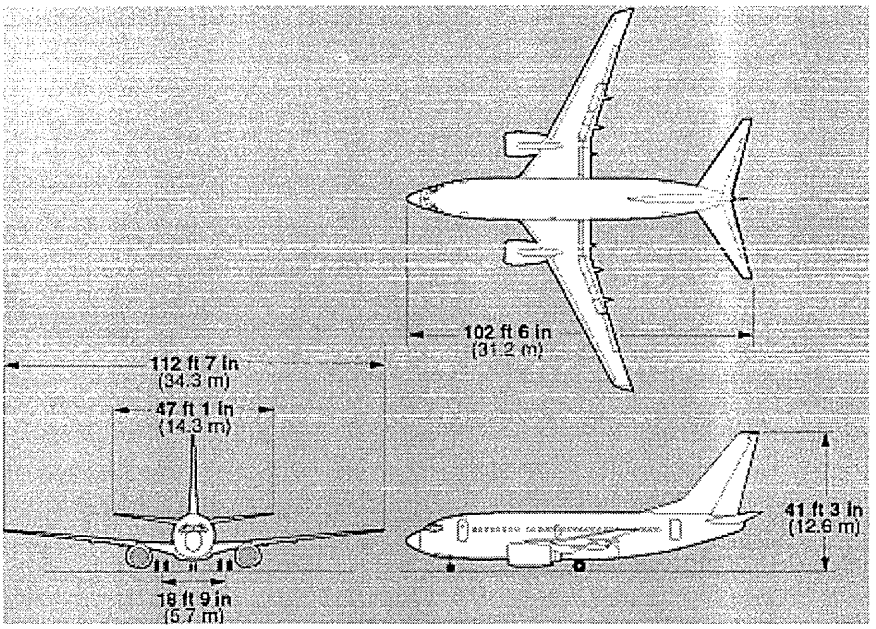

Figure A.15 Boeing 737-600 twin-turbofan single-aisle 108-seat airliner (Ref.2.38)

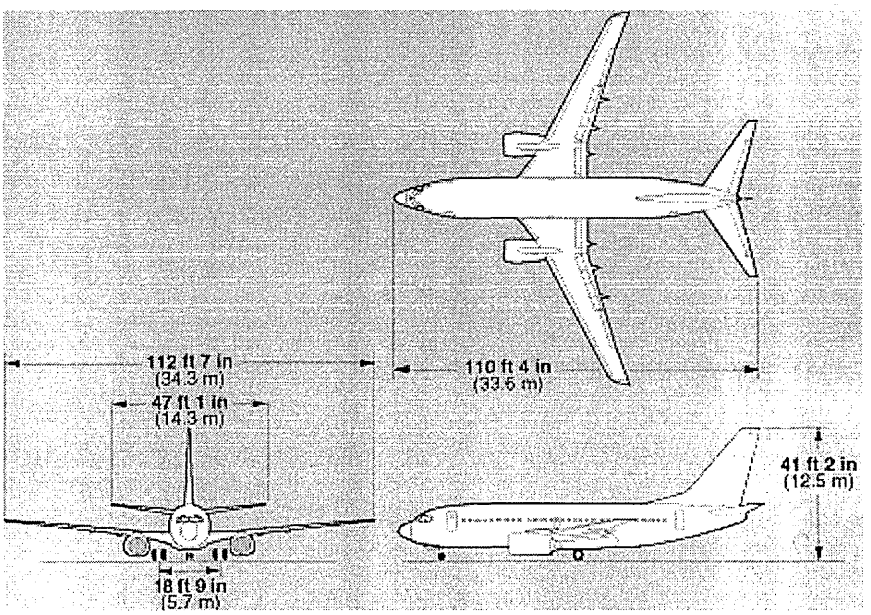

Figure A.16 Boeing 737-700 twin-turbofan single-aisle 128-seat airliner (Ref.2.38)

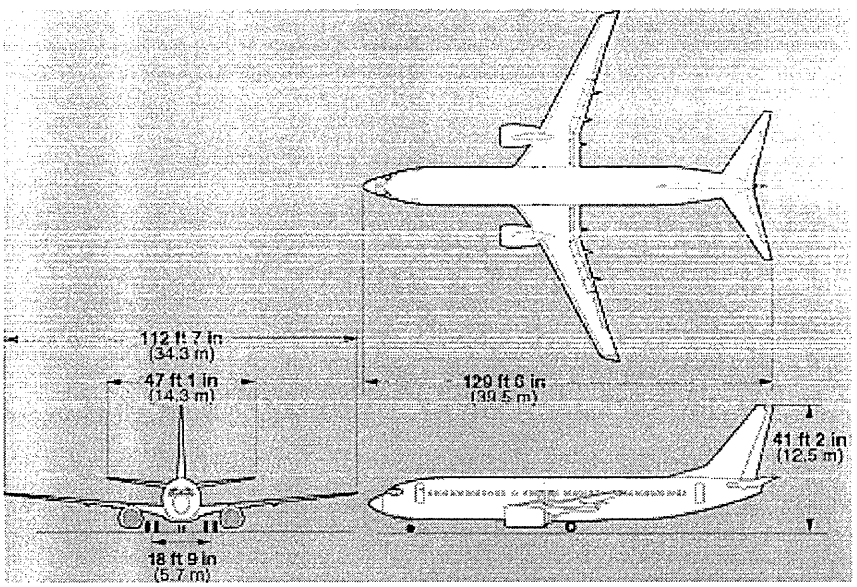

Figure A.17 Boeing 737-800 twin-turbofan single-aisle 162-seat airliner (Ref.2.38)

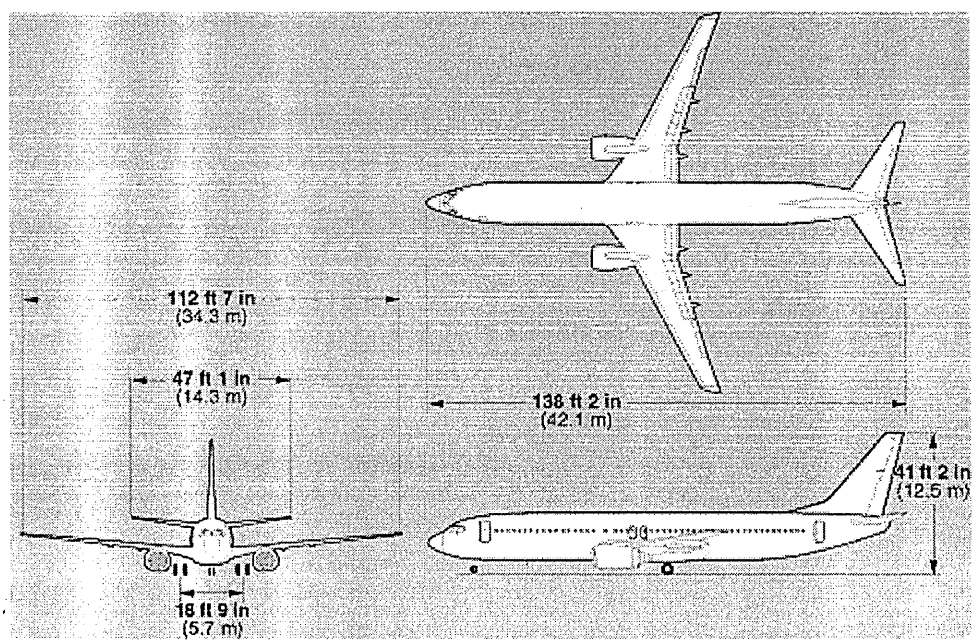

Figure A.18 Boeing 737-900 twin-turbofan single-aisle 177-seat airliner (Ref.2.38)

A.3 CABIN CROSS SECTION

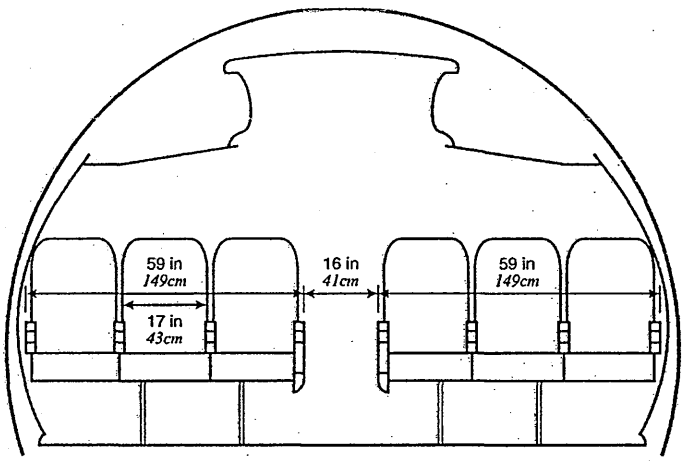

Figure A.19a Cabin cross section for AVRO RJ family (economy class), Ref. 2.9

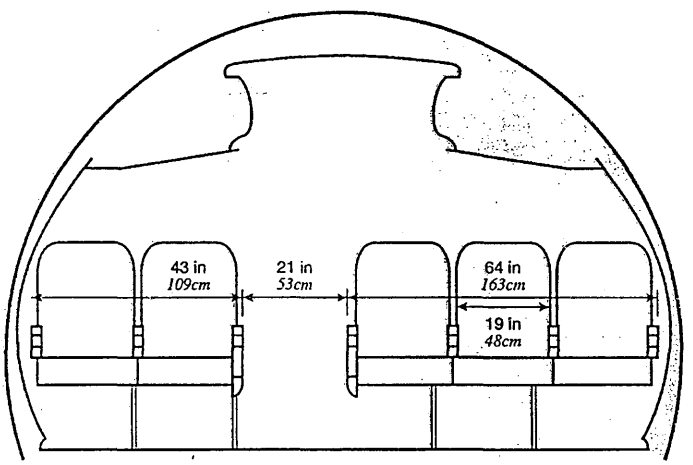

Figure A.19b Cabin cross section for AVRO RJ family (bisnis class), Ref. 2.9

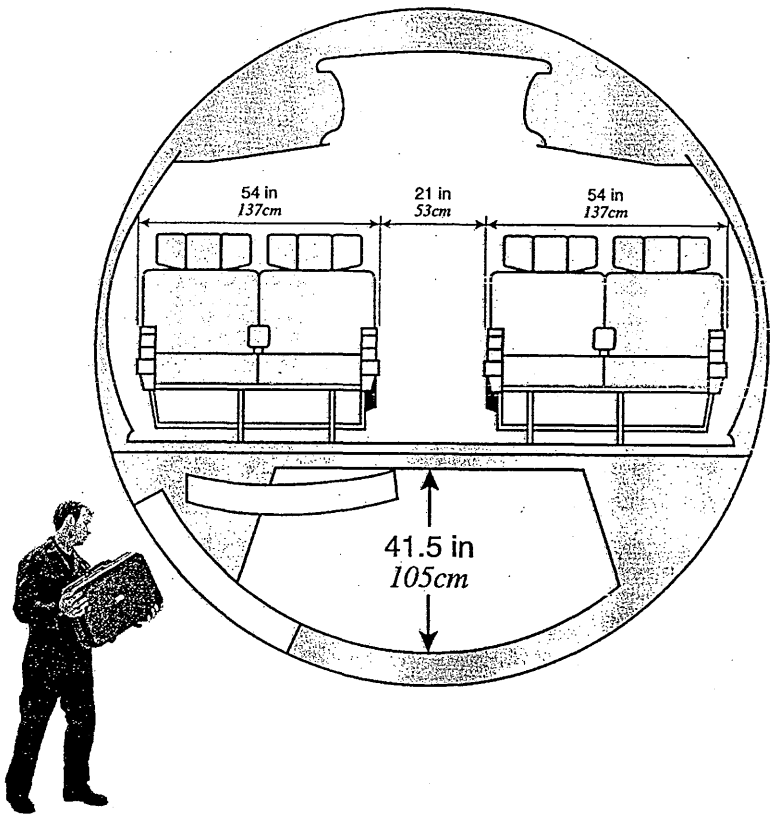

Figure A.19c Cabin cross section for AVRO RJ family (first class), Ref. 2.9

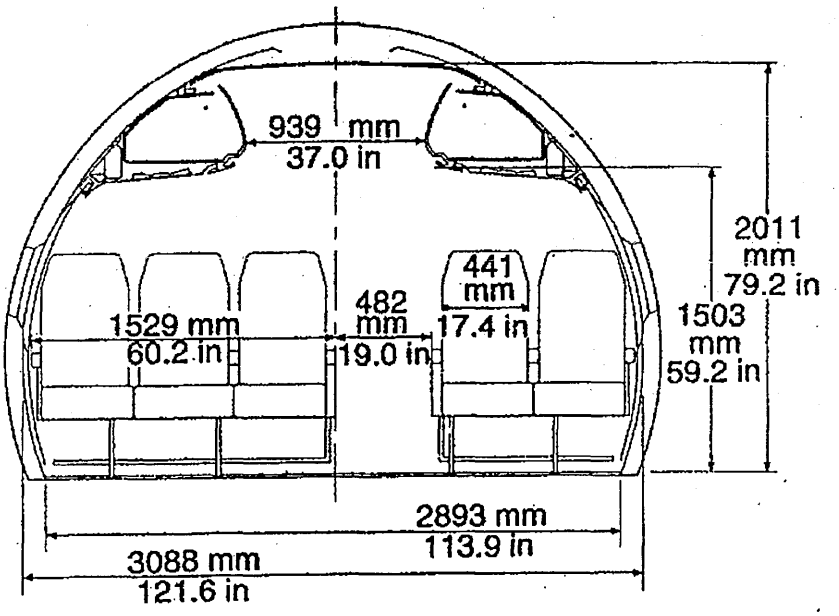

Figure A.20 Cabin cross section for Fokker F-70/-100/-130, (Ref. 2.5)

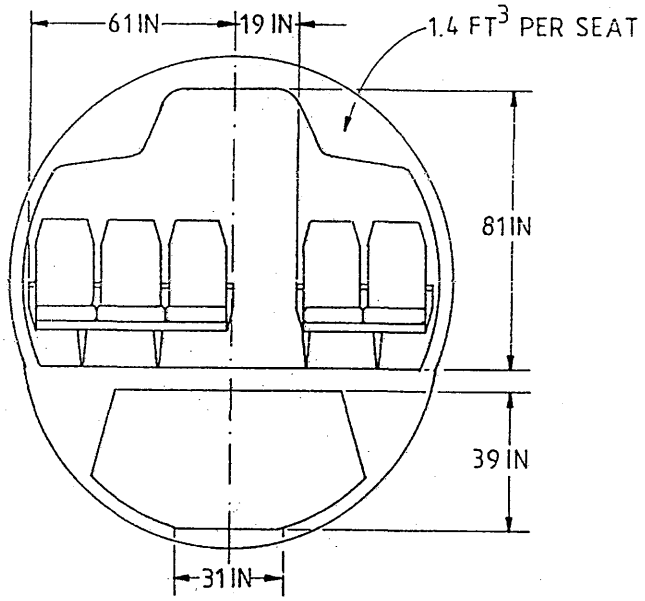

Figure A.21 Cabin cross section for DC-9 (Ref. 2.17)

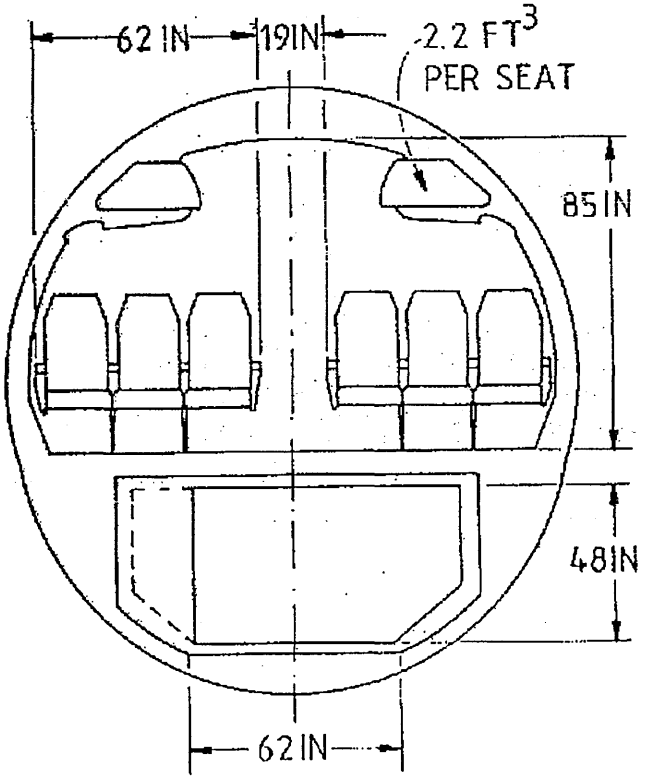

Figure A.22 Cabin cross section for Airbus A320/A319/A321 (Ref. 2.17)

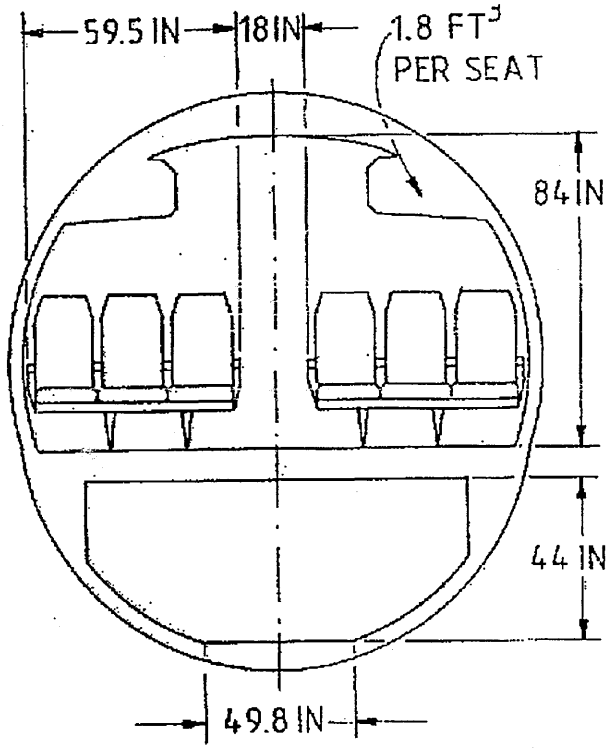

Figure A.23 Cabin cross section for Boeing B-737 family (Ref. 2.17)

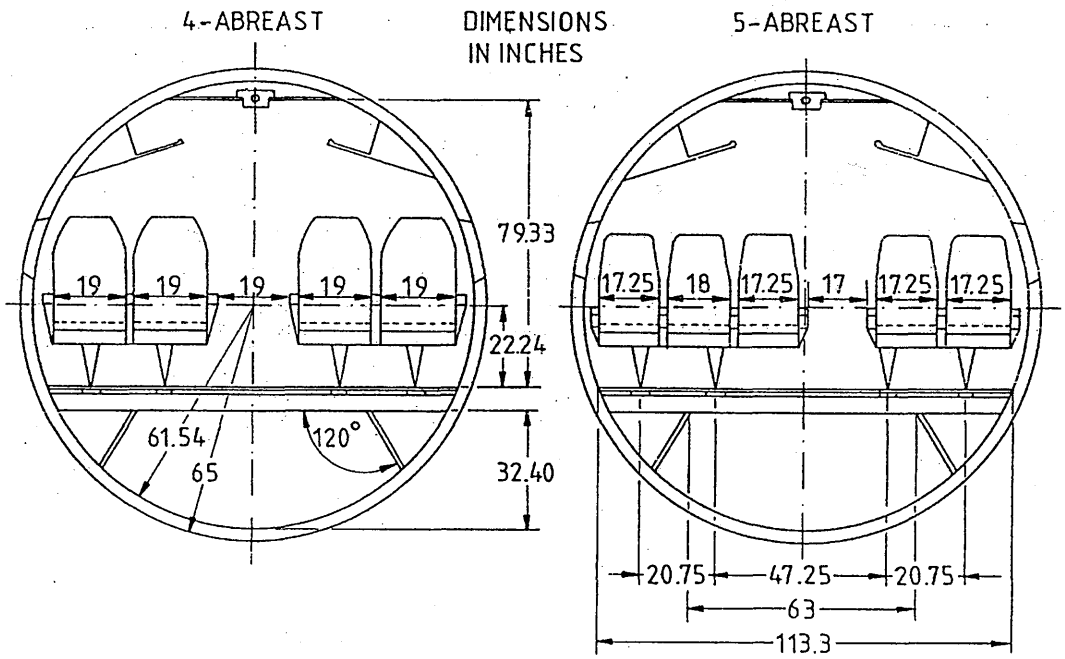

Figure A.24 Cabin cross section for Fokker F-28 (Ref. 2.17)

A.4 INTERIOR ARRANGEMENT

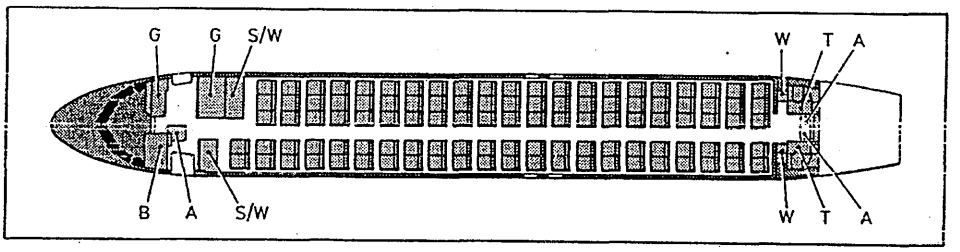

Figure A.25 Fokker 100 standard configuration (107 seats at 81 cm; 32 in pitch) Ref. 2.5

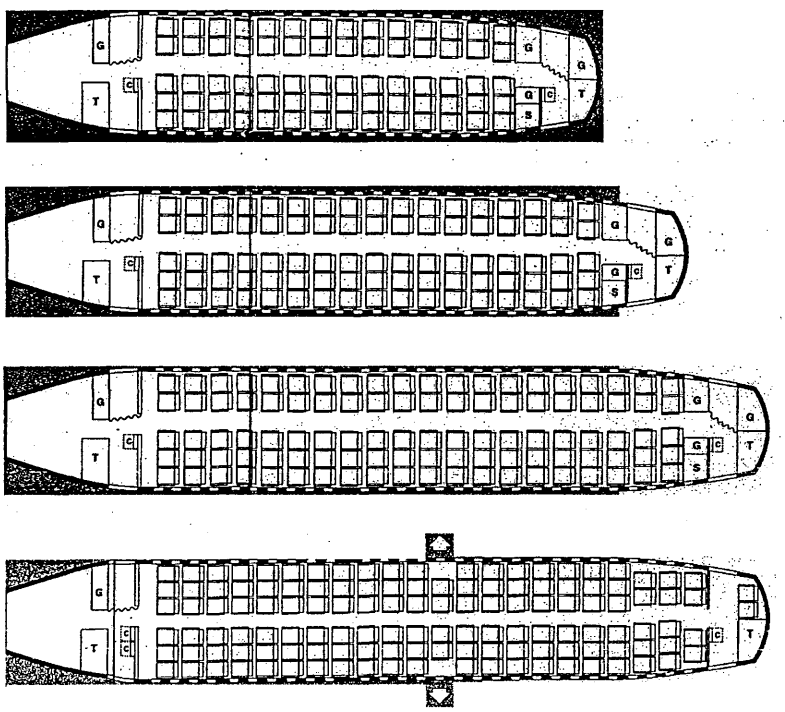

Figure A.26a AVRO RJ family typical business 5-abreast with 31 inch seat pitch. From the top : AVRO RJ70 with 70 passengers; AVRO RJ85 with 85 passengers, AVRO RJ100 with 100 passengers and AVRO RJ115 with 128 passengers (high capacity 6-abreast with 29 inch seat pitch), Ref.2.9

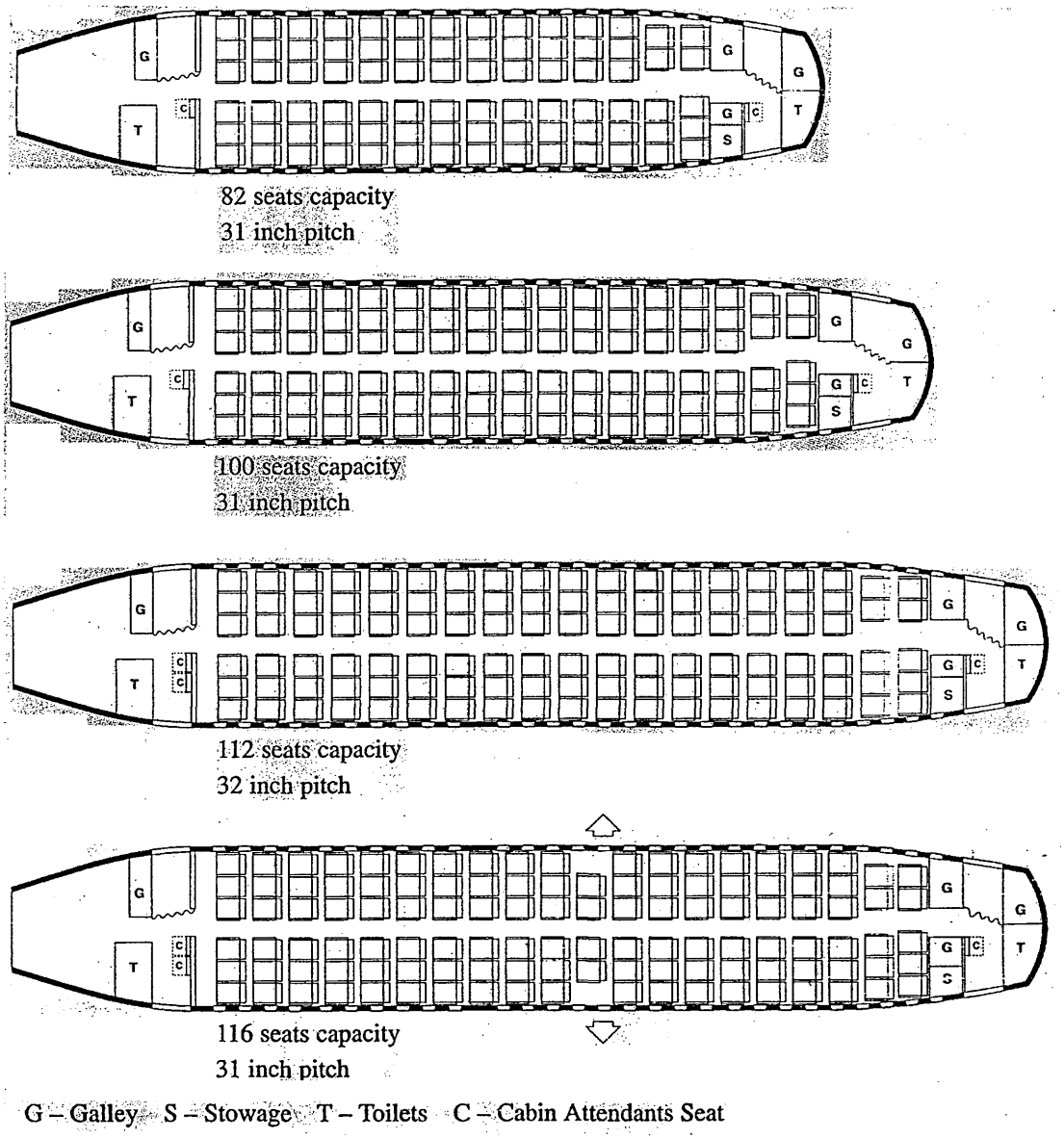

Figure A.26b AVRO RJ family typical economy 6-abreast with 31 inch seat pitch. From the top : AVRO RJ70 with 82 passengers; AVRO RJ85 with 100 passengers, AVRO RJ100 with 112 passengers and AVRO RJ115 with 116 passengers, Ref.2.9.

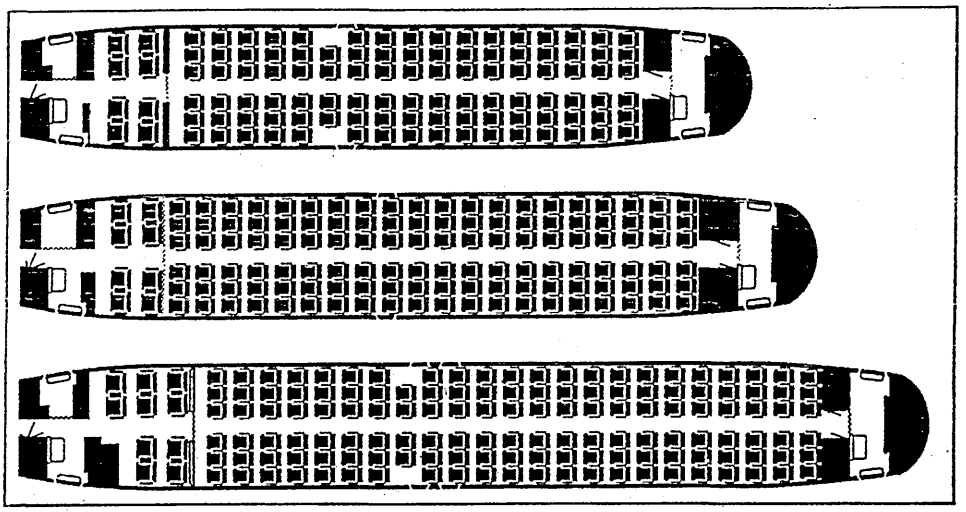

Figure A.27 Boeing 737 typical interior arrangements. Top : 737-500 with 108 passengers; centre : 737-300 with 128; bottom : 737-400 with 146. Seat pitches are 91 cm (36 in) for first class, 81 cm (32 in) for economy class, Ref. 2.5

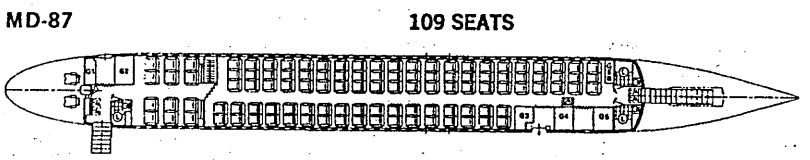

Figure A.28 MD-87 typical cabin layout with 109 seats in two classes, Ref. 2.5

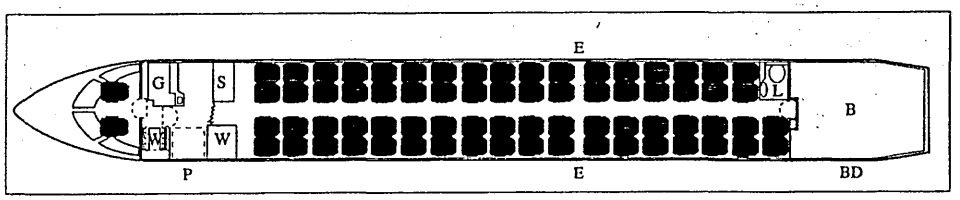

Figure A.29 Typical CRJ-X seating plan for 70 passengers at 79 cm (31 in) pitch, with 15.7 m^3 (555 cu ft) of baggage, Ref. 2.5.

Single-class

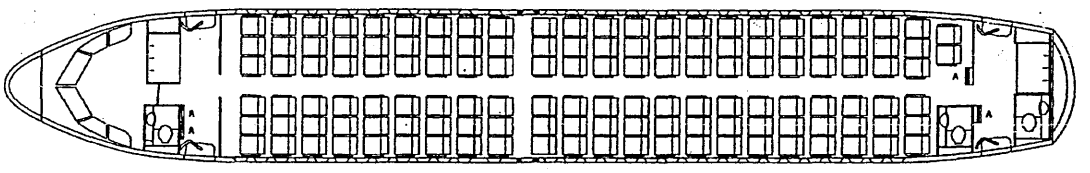

134 seats

Seat pitch : 32in

Two-class

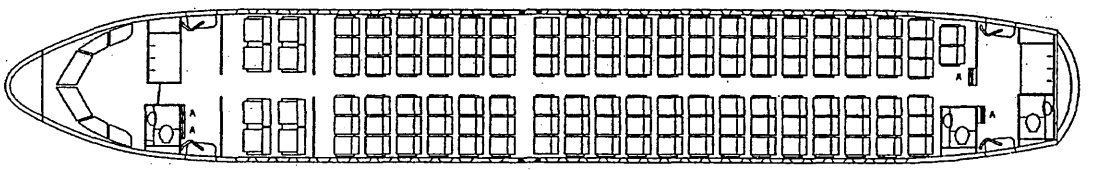

8 Super First + 116 Economy = **124 seats**

Seat pitches : First 36in, Economy 32in

Alternative two-class

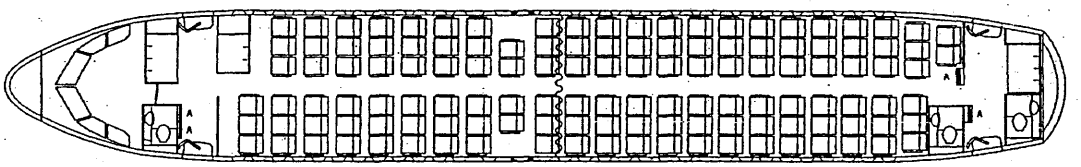

55 Business + 74 Economy =**129 seats**

Seat pitches : Business 34in, Economy 31/32in

High-density

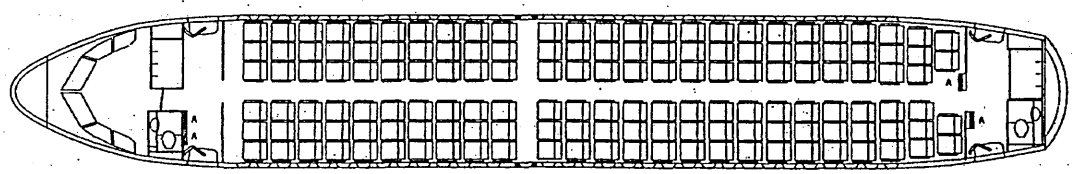

148 seats

Seat pitch : 29/30in

Figure A.30 Airbus A319 typical cabin layouts (Ref. 2.8)

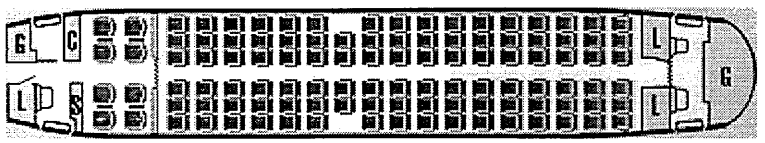

Figure A.31 Boeing 737-600 interior arrangement, 108 passengers (two class), first class at 36-in pitch, economy class at 31-/32-in pitch (Ref. 2.38)

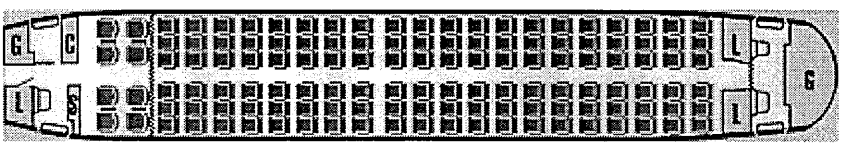

Figure A.32 Boeing 737-700 interior arrangement, 128 passengers (two class), first class at 36-in pitch, economy class at 31-/32-in pitch (Ref. 2.38)

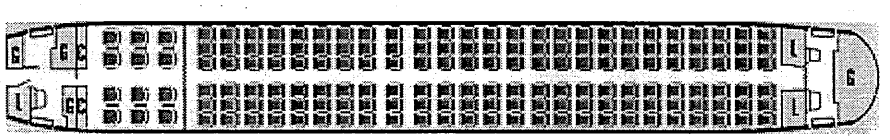

Figure A.33 Boeing 737-800 interior arrangement, 162 passengers (mixed class), first class at 36-in pitch, economy class at 32-in pitch (Ref. 2.38)

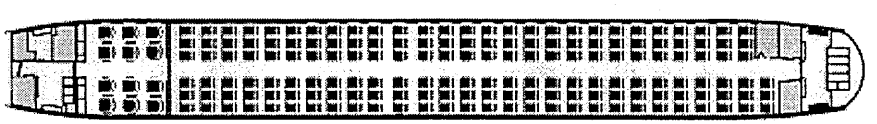

Figure A.34 Boeing 737-900 interior arrangement, 177 passengers (mixed class), first class at 36-in pitch, economy class at 32-/31-in pitch (Ref. 2.38)

APPENDIX B

BASELINE AIRCRAFT DESCRIPTION

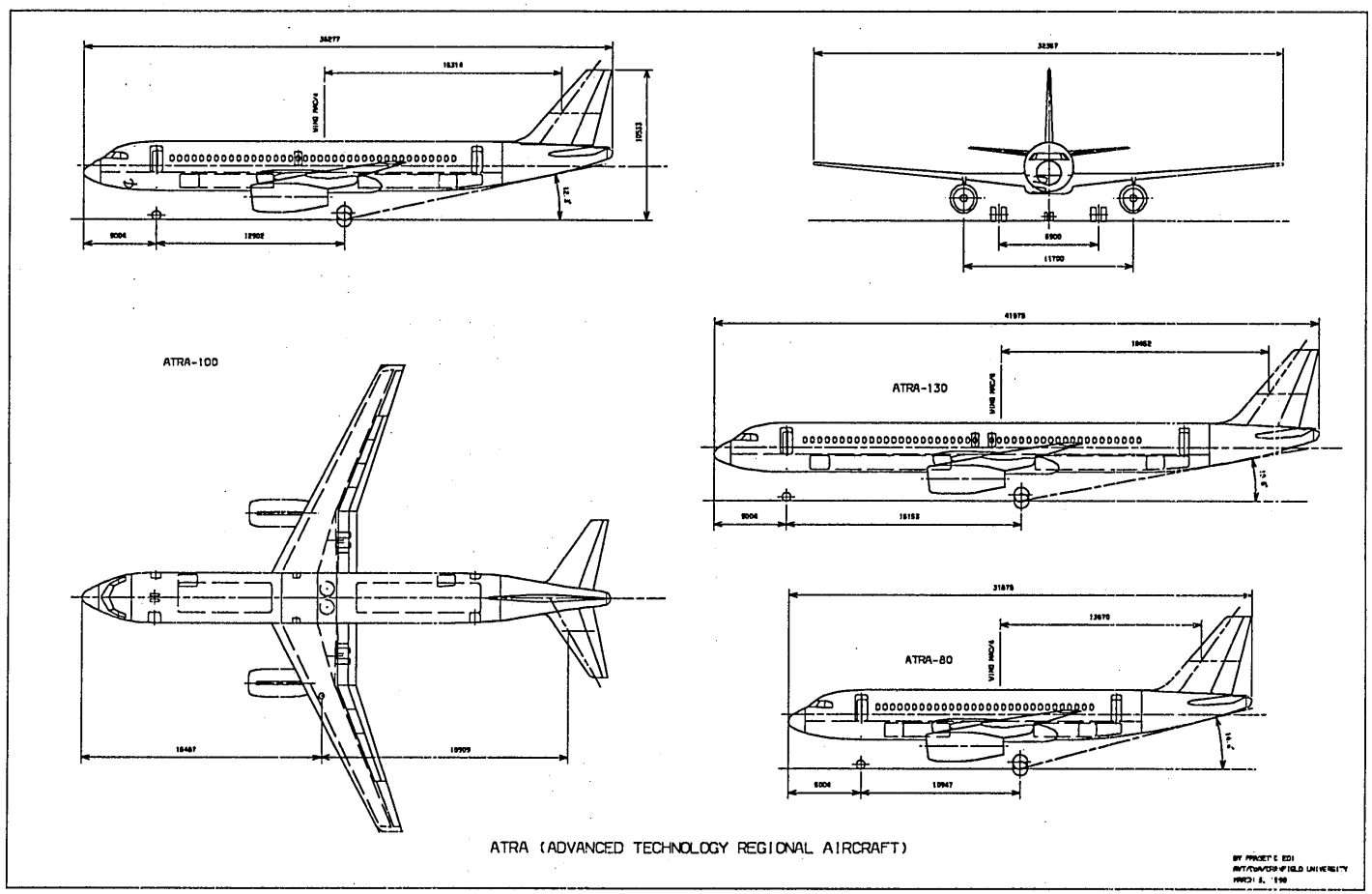

Figure B.1 ATRA-100, with additional side views of ATRA-130 (centre) and ATRA-80 (below)

B.2 FUSELAGE

B.2.1 Fuselage Cross-Section

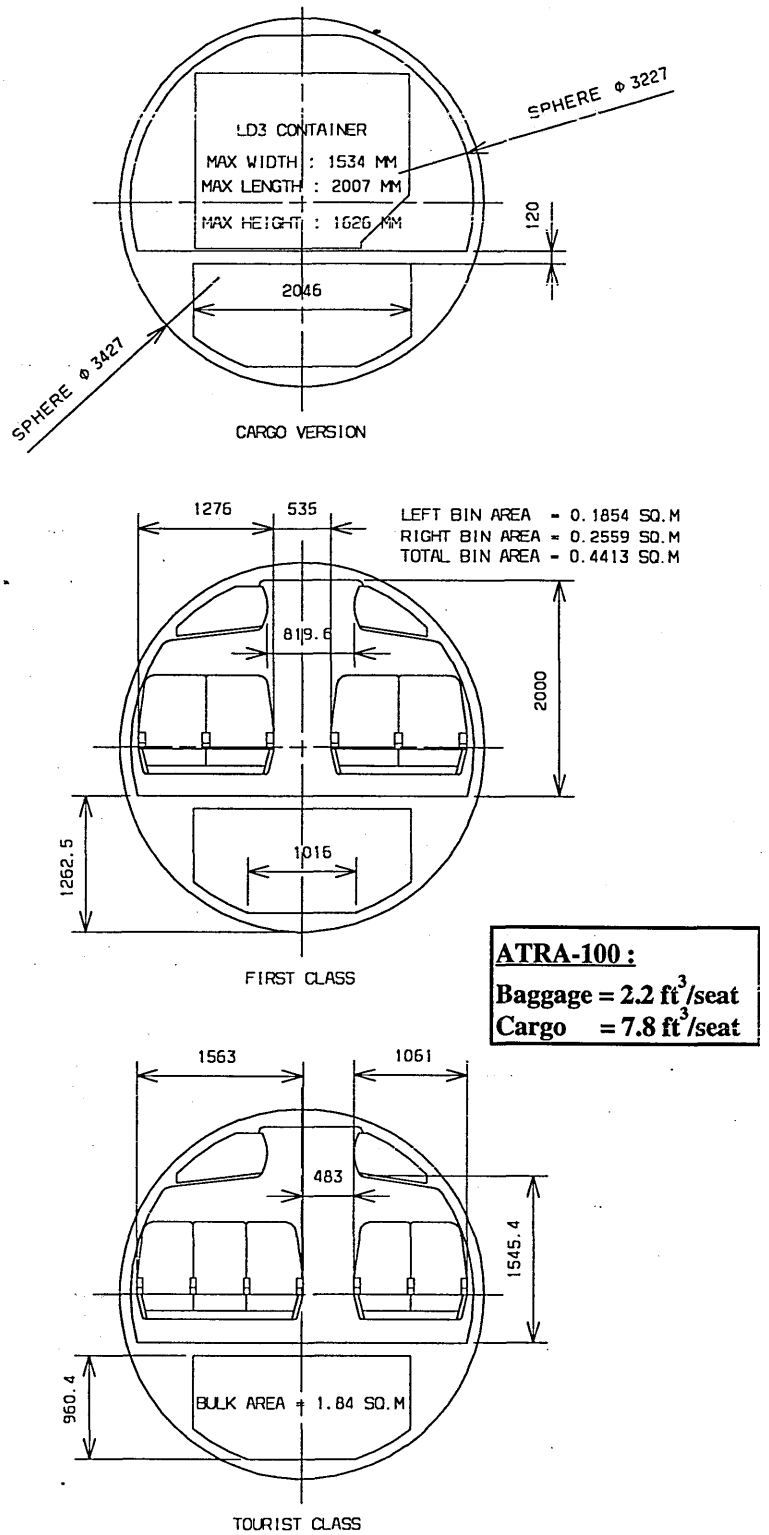

Figure B.2 ATRA-100 cross section

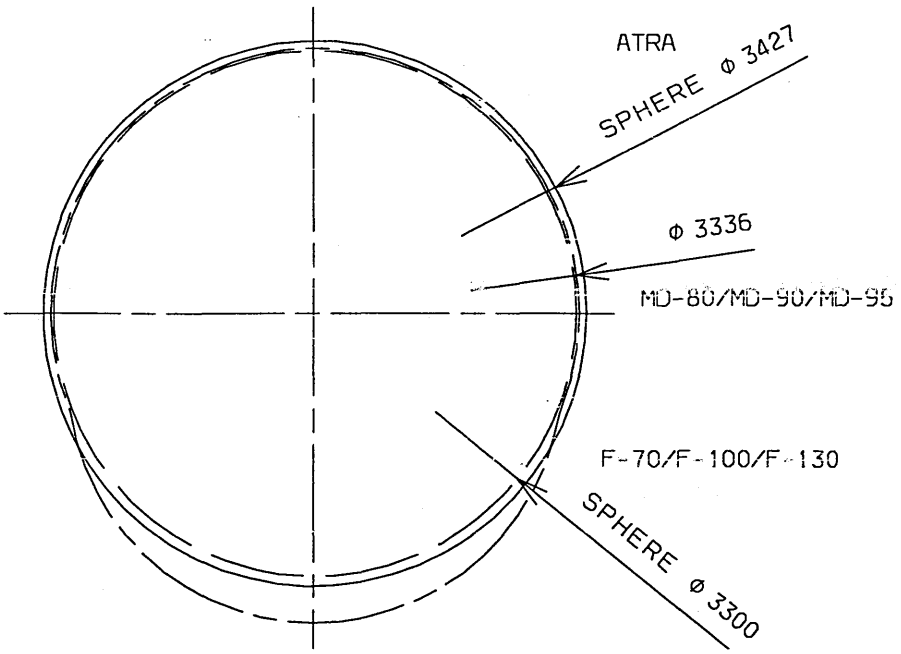

Figure B.3 Comparison of ATRA-100 cross section with competitors

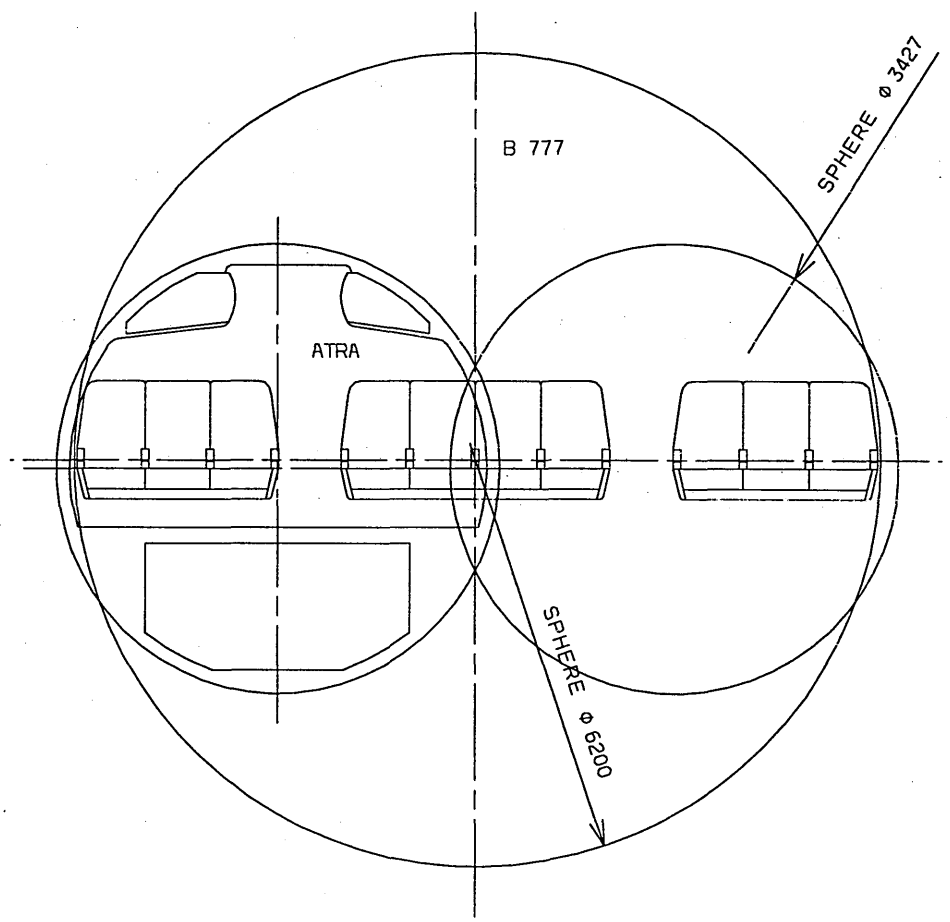

Figure B.4 Comparison of ATRA-100 cross section with Boeing 777

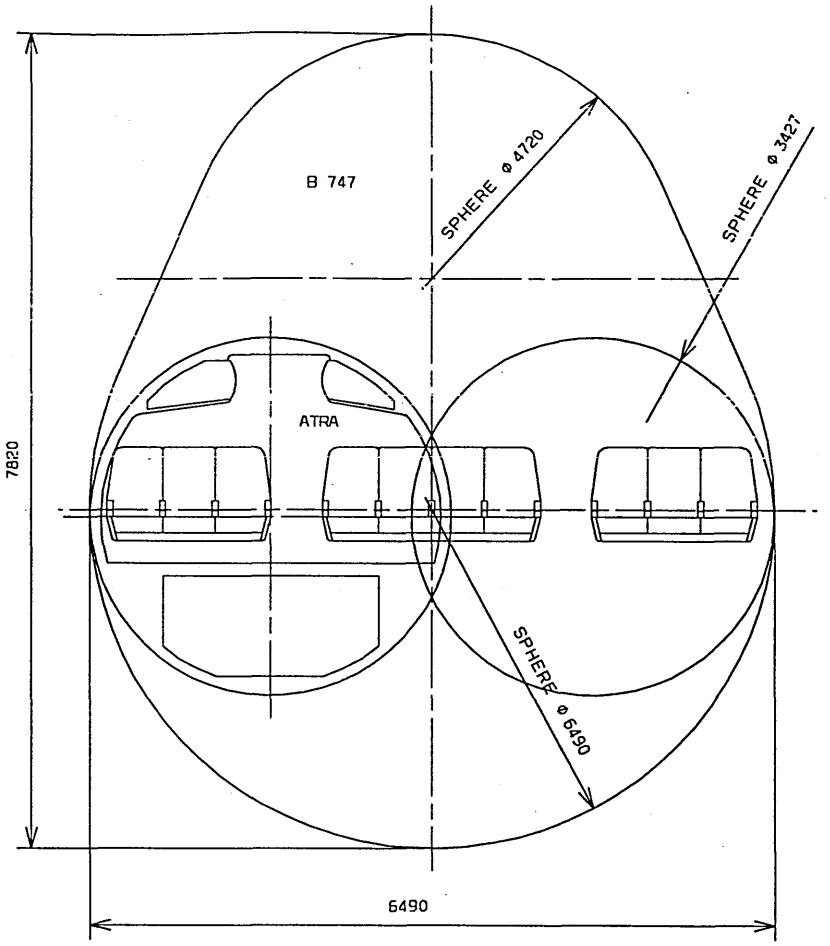

Figure B.5 Comparison of ATRA-100 cross section with Boeing 747

B.2.2 Seat Abreast Trade-Off Study

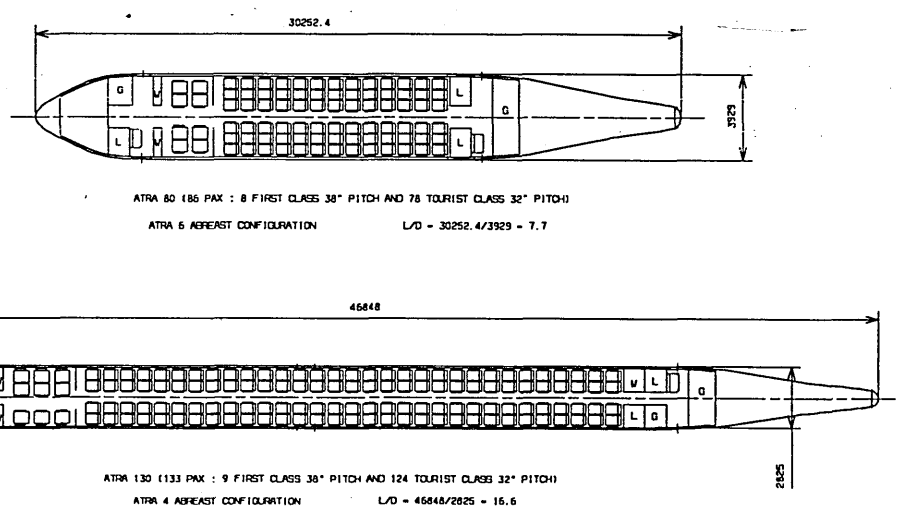

Figure B.6 ATRA-100 : seat abreast trade-off study

B.2.3 Interior Arrangement

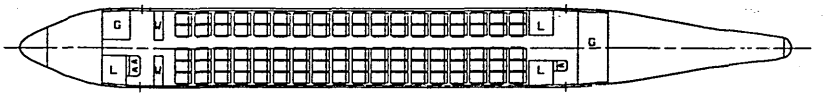

ATRA 80 (90 PAX ALL TOURIST CLASS 32" PITCH)

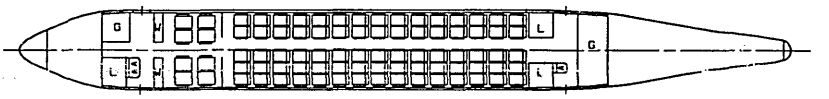

ATRA 80 (83 PAX : 8 FIRST CLASS 38" PITCH AND 75 TOURIST CLASS 32" PITCH)

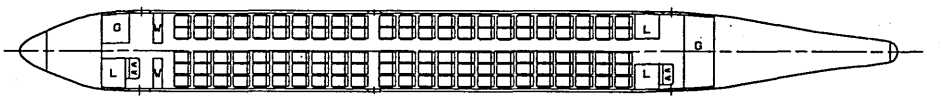

ATRA 100 (115 PAX ALL TOURIST CLASS 32" PITCH)

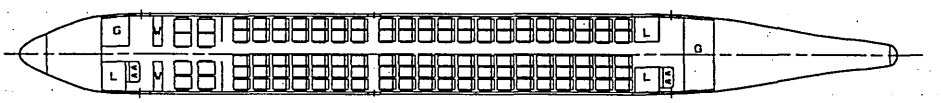

ATRA 100 (108 PAX : 8 FIRST CLASS 38" PITCH AND 100 TOURIST CLASS 32" PITCH)

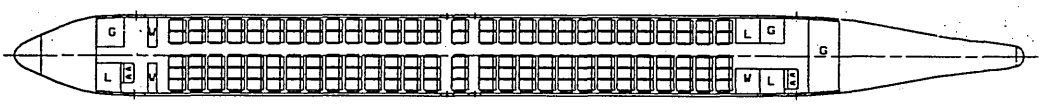

ATRA 130 (140 PAX ALL TOURIST CLASS 32" PITCH)

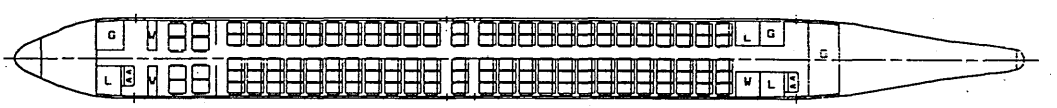

ATRA 130 (133 PAX : 8 FIRST CLASS 38" PITCH AND 125 TOURIST CLASS 32" PITCH)

Figure B.7 Typical interior arrangement for ATRA family

B.3 WING

B.3.1 Planform

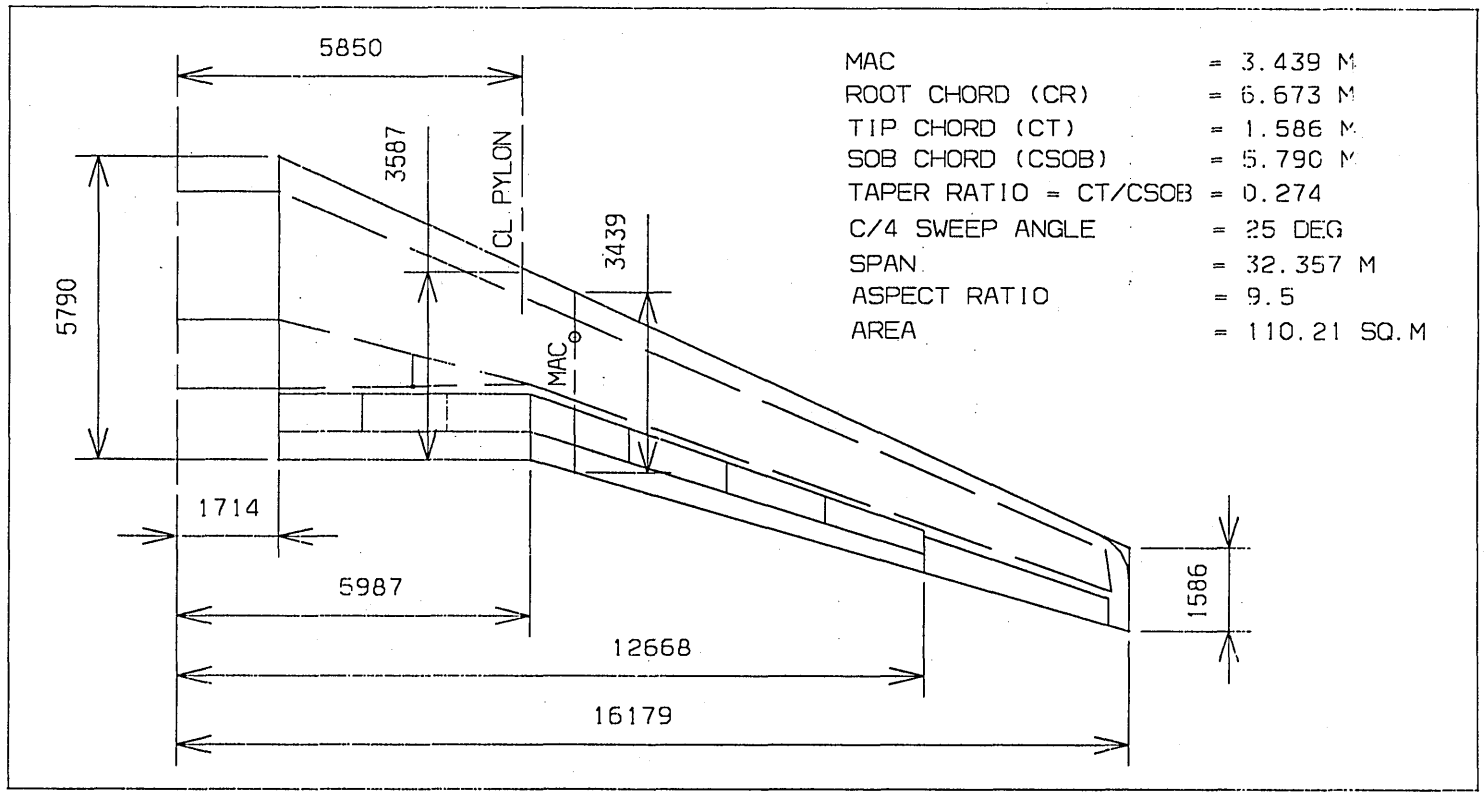

Figure B.8 ATRA wing concept

B.3.2 Twist

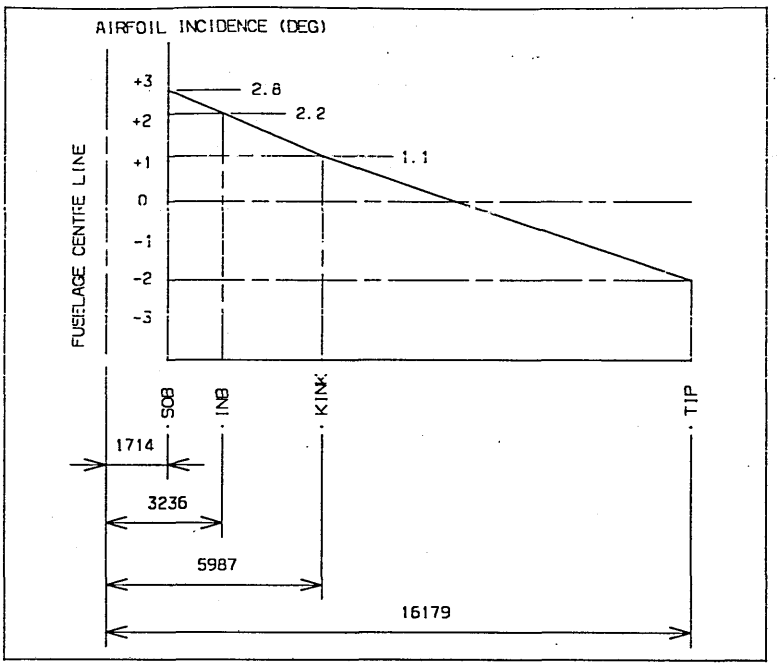

Figure B.9 ATRA wing twist

B.3.3 Thickness Distribution

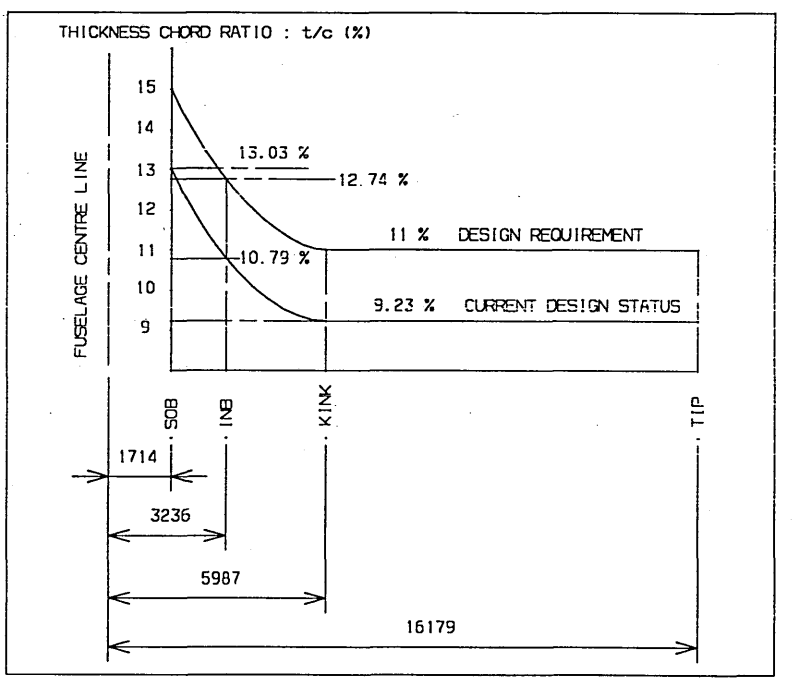

Figure B.10 ATRA wing thickness distribution

B.3.4 Airfoil Section

B.3.4.1 Side of Body (SOB) Section, y = 0.106

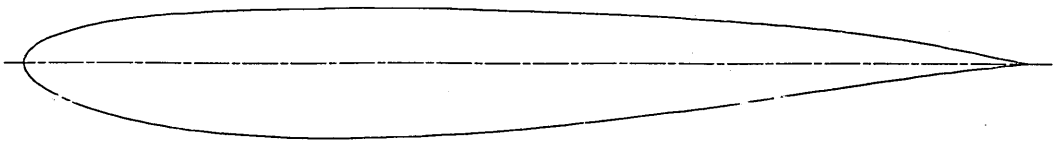

X	Y
1.000000E+01	0.000000E+00
9.903930E+00	1.650000E-02
9.619400E+00	7.560000E-02
9.157350E+00	1.697500E-01
8.535530E+00	2.717400E-01
7.777850E+00	3.621000E-01
6.913420E+00	4.352400E-01
5.975450E+00	4.903300E-01
5.000000E+00	5.282400E-01
4.024550E+00	5.497200E-01
3.086580E+00	5.533800E-01
2.222150E+00	5.359400E-01
1.464470E+00	4.901000E-01
8.426500E-01	4.108300E-01
3.806000E-01	2.980600E-01
9.607000E-02	1.596100E-01
0.000000E+00	0.000000E+00
9.607000E-02	-1.711500E-01
3.806000E-01	-3.443500E-01
8.426500E-01	-5.104900E-01
1.464470E+00	-6.405100E-01
2.222150E+00	-7.204200E-01
3.086580E+00	-7.498200E-01
4.024550E+00	-7.268200E-0
5.000000E+00	-6.555600E-01
5.975450E+00	-5.511300E-01
6.913420E+00	-4.300000E-01
7.777850E+00	-3.026600E-01
8.535530E+00	-1.849400E-01
9.157350E+00	-9.633000E-02
9.619400E+00	-3.980000E-02
9.903930E+00	-8.170001E-03

Figure B.11 Side of Body (SOB) section, y = 0.106

B.3.4.2 Inboard Section, y = 0.2

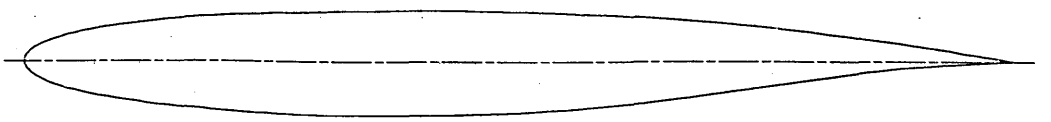

X	Y
1.000000E+01	0.000000E+00
9.903930E+00	1.384000E-02
9.619400E+00	6.190000E-02
9.157350E+00	1.362200E-01
8.535530E+00	2.248800E-01
7.777850E+00	3.184500E-01
6.913420E+00	4.044500E-01
5.975450E+00	4.713700E-01
5.000000E+00	5.121900E-01
4.024550E+00	5.252600E-01
3.086580E+00	5.130700E-01
2.222150E+00	4.794700E-01
1.464470E+00	4.258500E-01
8.426500E-01	3.504900E-01
3.806000E-01	2.537600E-01
9.607000E-02	1.358000E-01
0.000000E+00	0.000000E+00
9.607000E-02	-1.373700E-01
3.806000E-01	-2.601200E-01
8.426500E-01	-3.648400E-01
1.464470E+00	-4.510600E-01
2.222150E+00	-5.159800E-01
3.086580E+00	-5.517400E-01
4.024550E+00	-5.541900E-01
5.000000E+00	-5.240000E-01
5.975450E+00	-4.565700E-01
6.913420E+00	-3.456100E-01
7.777850E+00	-2.149700E-01
8.535530E+00	-1.121700E-01
9.157350E+00	-5.035000E-02
9.619400E+00	-1.764000E-02
9.903930E+00	-2.100000E-03

Figure B.12 Inboard section, y = 0.2

B.3.4.3 Outboard Section, y = 0.37 - 1

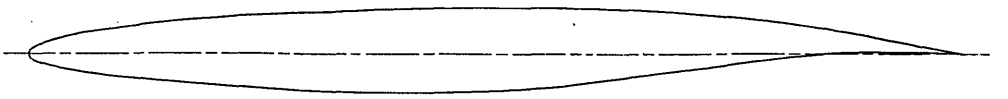

X	Y
1.000000E+01	0.000000E+00
9.903930E+00	1.825000E-02
9.619400E+00	7.069000E-02
9.157350E+00	1.595000E-01
8.535530E+00	2.688200E-01
7.777850E+00	3.736100E-01
6.913420E+00	4.533200E-01
5.975450E+00	4.950300E-01
5.000000E+00	5.044000E-01
4.024550E+00	4.889000E-01
3.086580E+00	4.551000E-01
2.222150E+00	4.047300E-01
1.464470E+00	3.405200E-01
8.426500E-01	2.647200E-01
3.806000E-01	1.839700E-01
9.607000E-02	9.437000E-02
0.000000E+00	0.000000E+00
9.607000E-02	-8.583000E-02
3.806000E-01	-1.582300E-01
8.426500E-01	-2.278800E-01
1.464470E+00	-2.935800E-01
2.222150E+00	-3.536700E-01
3.086580E+00	-3.998000E-01
4.024550E+00	-4.184000E-01
5.000000E+00	-4.001000E-01
5.975450E+00	-3.145700E-01
6.913420E+00	-1.923800E-01
7.777850E+00	-7.779000E-02
8.535530E+00	1.200000E-04
9.157350E+00	2.350000E-02
9.619400E+00	1.539000E-02
9.903930E+00	5.250000E-03

Figure B.13 Outboard section, y = 0.37 - 1

B.4 PROPULSION

B.4.1 BR 700 Engine

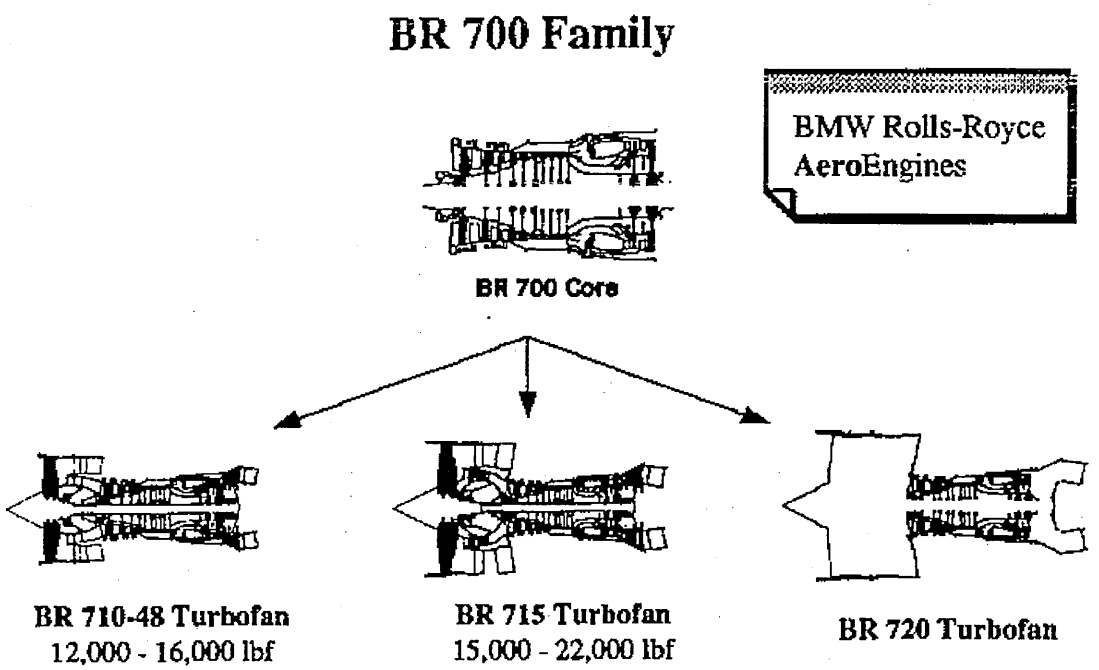

Figure B.14 BR 700 family

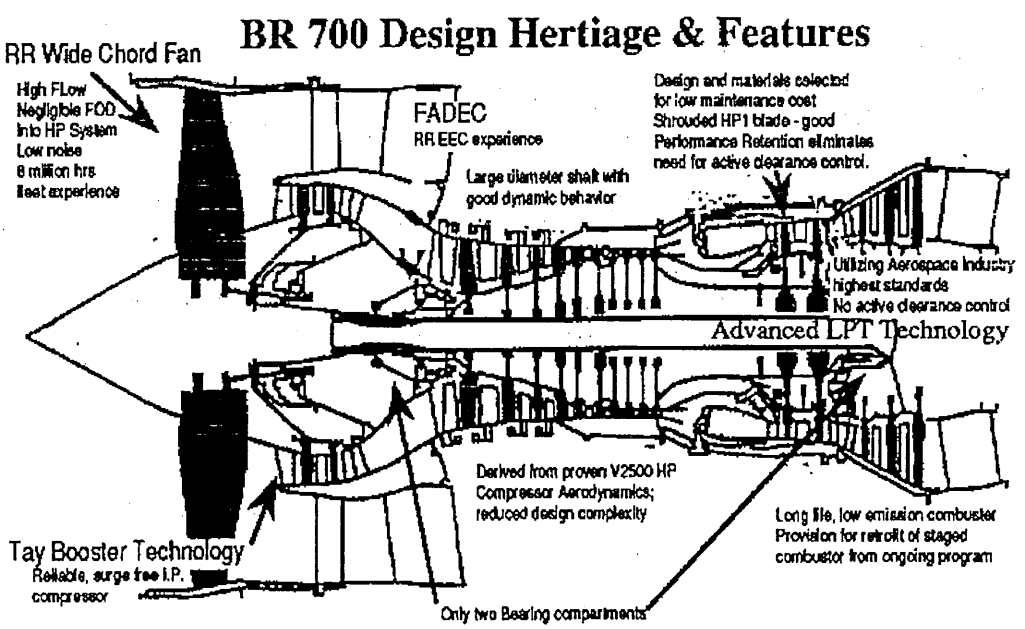

Figure B.15 BR 700 design heritage & features

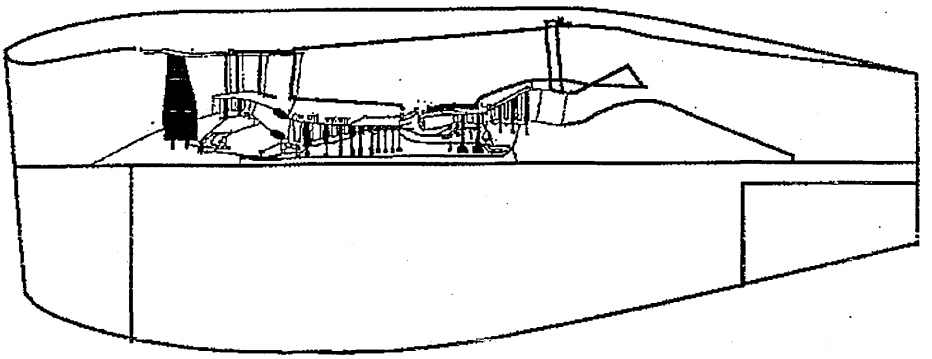

Figure B.16 BR 715 turbofan typical mixed flow long duct engine/nacelle

B.4.2 Engine Performance

	Take-off	Cruise at 35,000 ft and Mach 0.8
Thrust, LB	20,005	4,159
SFC, LB/LB.H	0.36	0.644

Table B.1 BR715-58 performance data

B.4.3 Fuel Tank Capacity

Capacity (L)	Wing with $(t/c)_{\text{design status}}$	Wing with $(t/c)_{\text{design requirement}}$
Outboard tank	5,430	6,282
Inboard tank	7,305	8,452
Total	12,735	14,734
Central tank	4,927	5,700
Total	17,662	20,434
Net capacity	16,955	19,616

Note :
Fuel density (JP-4) = 0.80892 KG/L = 6.75 LB/US.Gallons
Mission fuel at design payload and design range for ATRA-100 = 19,189 L
= 15,522 KG
= 34,220 LB

Table B.2 Fuel tank capacity

B.5 WEIGHT DATA

B.5. 1 ATRA-80 (Shortened Version)

A/C COMPONENT		WEIGHT KG	WEIGHT LB	MTOW %
WING (INC. AUXILLIARY SURFACES STRUCT.)		4116.31	9074.82	12.0525
HORIZONTAL TAIL (INC. ELEVATOR)		418.186	921.933	0.91833
VERTICAL TAIL (INC. RUDDER)		353.85	780.097	0.77705
BODY		4353.56	9597.85	10.6226
MAIN LANDING GEAR		1514.13	3338.05	3.325
NOSE LANDING GEAR		216.304	476.864	0.475
NACELLE AND STRUT		1398.52	3083.18	3.07113
TOTAL STRUCTURE		12370.9	27272.8	27.1662
ENGINES (DRESSED)		3014.06	6644.79	6.61882
FUEL SYSTEM		426.37	939.976	0.9363
FLYING CONTROLS SYSTEM		623.46	1374.48	1.36911
HYDRAULICS		1024.3	2258.17	2.24934
ELECTRICAL SYSTEM		752.237	1658.38	1.6519
A. P. U.		277.78	612.394	0.61
INSTRUMENTS AND NAVIGATIONS		828.787	1827.14	1.82
DE-ICE		364.661	803.933	0.80079
FIRE PROTECTION		136.613	301.177	0.3
FURNISHINGS (INC. SEAT, GALLEYS ETC.)		4389.84	9677.83	9.64
AIR CONDITIONING		603.404	1330.26	1.32506
TOTAL FIXED EQUIPMENT		9427.45	20783.8	20.7025
EXTERIOR PAINT		40.9839	90.3532	0.09
OPTIONS		851.102	1876.34	1.869
MANUFACTURER'S EMPTY WEIGHT		25704.4	56668	56.4465
STANDARD AND OPERATIONAL ITEMS		477.5	1052.7	1.04858
OPERATIONAL EMPTY WEIGHT		26181.9	57720.7	57.4951
PASSENGER AND BAGGAGE	83 PAX	7926.5	17474.8	17.4064
MISSION FUEL (PAX, NM)	83 2000	11429.3	25197	25.0985
MAXIMUM ZERO FUEL WEIGHT		34108.4	75195.5	74.9015
MAXIMUM LANDING WEIGHT		40983.9	90353.2	90
MAXIMUM TAKE-OFF WEIGHT		45537.7	100392	100

Table B.3 Weight breakdown for ATRA-80

B.5.2 ATRA-100 (Baseline)

A/C COMPONENT			WEIGHT KG	WEIGHT LB	MTOW %
WING (INC. AUXILLIARY SURFACES STRUCT.)			4358.35	9608.42	10.329
HORIZONTAL TAIL (INC. ELEVATOR)			498.414	1098.8	0.8859
VERTICAL TAIL (INC. RUDDER)			421.735	929.756	0.74961
BODY			5285.12	11651.6	10.4378
MAIN LANDING GEAR			1870.66	4124.05	3.325
NOSE LANDING GEAR			267.237	589.151	0.475
NACELLE AND STRUT			1531.19	3375.66	2.72161
TOTAL STRUCTURE			14232.7	31377.4	25.2979
ENGINES (DRESSED)			3299.98	7275.14	5.86555
FUEL SYSTEM			504.955	1113.22	0.89753
FLYING CONTROLS SYSTEM			730.604	1610.69	1.29861
HYDRAULICS			1138.53	2509.99	2.02367
ELECTRICAL SYSTEM			799.329	1762.2	1.42077
A. P. U.			343.189	756.593	0.61
INSTRUMENTS AND NAVIGATIONS			1023.94	2257.38	1.82
DE-ICE			422.836	932.184	0.75157
FIRE PROTECTION			168.781	372.095	0.3
FURNISHINGS (INC. SEAT, GALLEYS ETC.)			5423.5	11956.7	9.64
AIR CONDITIONING			726.808	1602.32	1.29186
TOTAL FIXED EQUIPMENT			11282.5	24873.3	20.054
EXTERIOR PAINT			50.6344	111.629	0.09
OPTIONS			985.595	2172.84	1.75184
MANUFACTURER'S EMPTY WEIGHT			29851.4	65810.4	53.0593
STANDARD AND OPERATIONAL ITEMS			573	1263.24	1.01848
OPERATIONAL EMPTY WEIGHT			30424.4	67073.6	54.0778
PASSENGER AND BAGGAGE	108 PAX		10314	22738.2	18.3326
MISSION FUEL (PAX, NM)	108	2250	15522	34219.9	27.5896
MAXIMUM ZERO FUEL WEIGHT			40738.4	89811.8	72.4104
MAXIMUM LANDING WEIGHT			50634.4	111629	90
MAXIMUM TAKE-OFF WEIGHT			56260.4	124032	100

Note :

Centre of gravity (c.g.) range for ATRA-100 (Baseline) are 15 - 35 % MAC for take-off/landing and flight.

Table B.4 Weight breakdown for ATRA-100 (Baseline)

B.5.3 ATRA-130 (Stretched Version)

A/C COMPONENT			WEIGHT KG	WEIGHT LB	MTOW %
WING (INC. AUXILLIARY SURFACES STRUCT.)			4578.99	10094.8	8.80999
HORIZONTAL TAIL (INC. ELEVATOR)			592.557	1306.35	0.85167
VERTICAL TAIL (INC. RUDDER)			501.394	1105.37	0.72065
BODY			6507.84	14347.2	10.4342
MAIN LANDING GEAR			2304.23	5079.89	3.31182
NOSE LANDING GEAR			329.175	725.699	0.47312
NACELLE AND STRUT			1860.44	4101.52	2.67397
TOTAL STRUCTURE			16674.6	36760.9	23.9661
ENGINES (DRESSED)			4009.56	8839.48	5.76288
FUEL SYSTEM			596.591	1315.24	0.86088
FLYING CONTROLS SYSTEM			854.24	1883.26	1.23267
HYDRAULICS			1263.59	2785.72	1.82337
ELECTRICAL SYSTEM			910.747	2007.83	1.31421
A. P. U.			422.73	931.951	0.61
INSTRUMENTS AND NAVIGATIONS			1261.26	2780.57	1.82
DE-ICE			489.264	1078.63	0.70601
FIRE PROTECTION			207.9	458.336	0.3
FURNISHINGS (INC. SEAT, GALLEYS ETC.)			6680.52	14727.9	9.64
AIR CONDITIONING			873.145	1924.94	1.25995
TOTAL FIXED EQUIPMENT			13560	29894.4	19.4895
EXTERIOR PAINT			62.37	137.501	0.09
OPTIONS			1162.68	2563.24	1.67775
MANUFACTURER'S EMPTY WEIGHT			35469.2	78195.4	50.9793
STANDARD AND OPERATIONAL ITEMS			573	1263.24	0.82684
OPERATIONAL EMPTY WEIGHT			36042.2	79458.7	51.8029
PASSENGER AND BAGGAGE	133 PAX		12701.5	28001.7	18.3283
MISSION FUEL (PAX, NM)	133	2500	20832	45926.2	30.0606
MAXIMUM ZERO FUEL WEIGHT			48743.7	107460	70.0585
MAXIMUM LANDING WEIGHT			62618.2	138048	90
MAXIMUM TAKE-OFF WEIGHT			69575.7	153387	100

Table B.5 Weight breakdown for ATRA-130 (Stretched Version)

B.6 ACCESSIBILITY/SERVICEABILITY OF ATRA-100

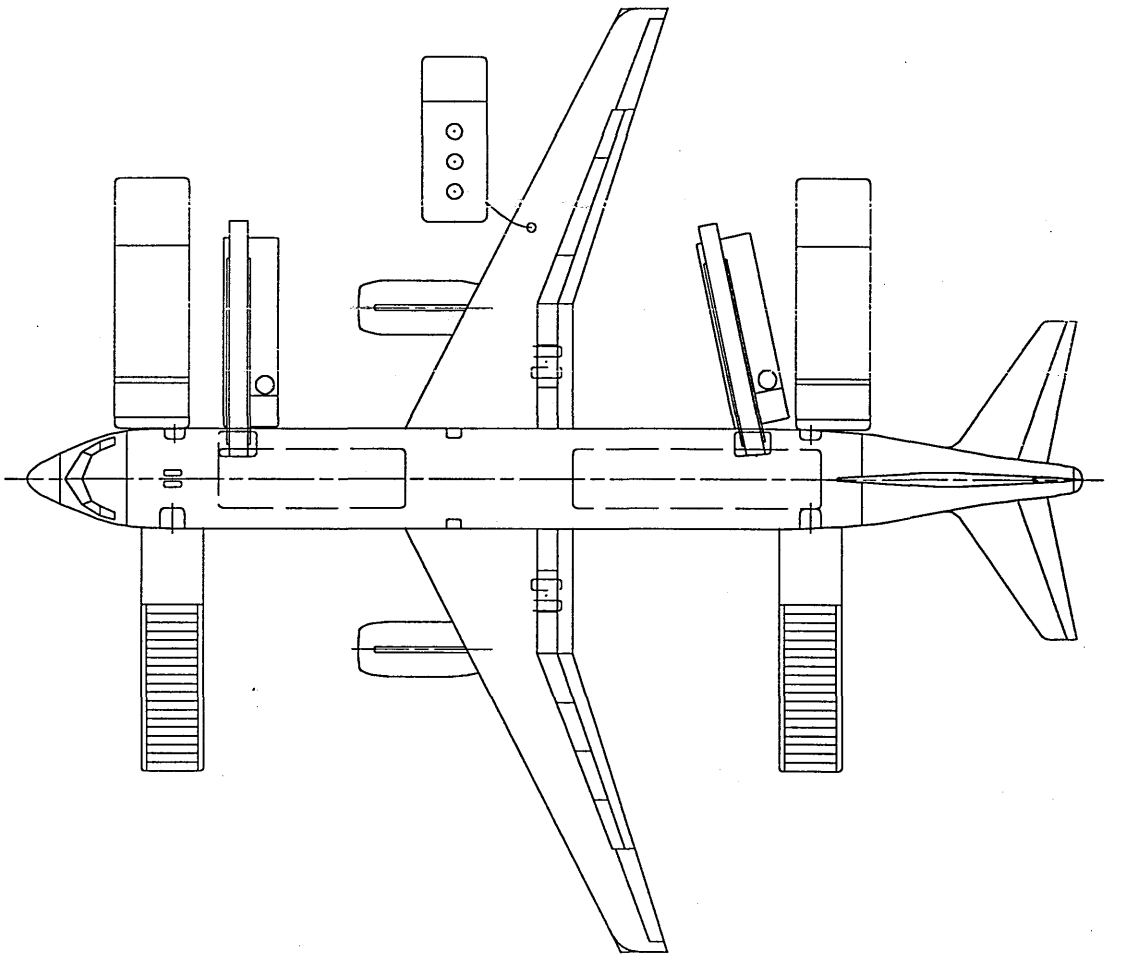

- Passenger and service doors at front and rear end
- Separation of servicing activities from passenger embarkation/disembarkation
- Ease of galley servicing and cabin reconfiguration
- Good accessibility for servicing activities
- Ease of on-line maintenance

Figure B.17 ATRA-100 : accessibility/serviceability

APPENDIX C

AERODYNAMIC CALCULATIONS

C.1 INTRODUCTION

Computational Fluid Dynamics or CFD is the analysis of systems involving fluid flow, heat transfer and associated phenomena such as chemical reactions by means of computer-based simulation. The technique is very powerful and spans a wide range of industrial and non-industrial application areas (Reference C.1). Some examples are : aerodynamics of aircraft, hydrodynamics of ships, power plant, chemical process engineering, marine engineering, meteorology, etc.

The use of computational fluid dynamics (CFD) to predict internal and external flows has risen dramatically in the past decade. In the 1980s the solution of fluid flow problem by means of CFD was the domain of the academic, postdoctoral or postgraduate researcher or the similarity trained specialist with many years of grounding in the area. The widespread availability of engineering workstations together with efficient solution algorithms and sophisticated pre- and post-processing facilities enable the use of commercial CFD codes by graduate engineers for research, development and design tasks in industry. The codes that are now on the market may be extremely powerful, but their operation still requires a high level of skill and understanding from the operator to obtain meaningful results in complex situations.

Commercial CFD codes based on the finite element method have more recently entered the fray. The market is currently dominated by four codes, PHOENICS, FLUENT, FLOW3D and STAR-CD, that are all based on the finite volume method (Reference C.1).

There are several unique advantages of CFD over experiment-based approaches to fluid systems design :

- substantial reduction of lead times and cost of new designs
- ability to study systems where controlled experiments are difficult or impossible to perform (e.g. very large systems)
- ability to study systems under hazardous conditions at and beyond their normal performance limits (e.g. safety studies and accident scenarios)
- practically unlimited level of detail of results

For disadvantages of CFD, see Section 7.7 of this thesis.

The variable cost of an experiment, in terms of facility hire and/or man-hour costs, is proportional to the number of data points and the number of configurations tested. In contrast CFD codes can produce extremely large volumes of results at virtually no added expense and it is very cheap to perform parametric studies, for instance to optimise equipment performance.

CFD codes are structured around the numerical algorithms that can tackle fluid flow problems. In order to provide easy access to their solving power all commercial CFD packages include sophisticated user interfaces to input problem parameters and to examine the results. Hence all codes contain three main elements : (i) a pre-processor, (ii) a solver and (iii) a post-processor.

The aerodynamic computation uses in this research consists of four components :

- **CATIA**, pre-processor for 2D and 3D geometry modeling. For 3D complex geometry modeling, CATIA has better capability than preBFC.
- **preBFC**, pre-processor for 2D and 3D simple geometry modeling, unstructured 2D-mesh generator, and unstructured surface mesh generator.
- **TGrid**, a 2D (triangular) and 3D (tetrahedral) mesh generator.
- **RAMPANT**, the solver.

Figure C.1 shows the organizational structure of these components.

CATIA (Computer Aided Three-Dimensional Interactive Application) from IBM and Dassault Systems is widely uses in aircraft companies. Surface geometry created by CATIA can be imported to mesh generators by an IGES (Initial Graphics Exchange Specification) file; for more information of CATIA, see References C.2, C.3 and C.10.

PreBFC (Reference C.4) is a CAD-style program for geometry set-up and grid generation in 2D or 3D for the computational fluid dynamics (CFD) software packages, FLUENT, NEKTON, and RAMPANT.

The unstructured grid generation capability in preBFC provides a way to make grids for RAMPANT or FLUENT/UNS from any preBFC geometry. Currently only 2D grids and surface grids for 3D grids can be made with preBFC. To generate a 3D-volume mesh, firstly a surface grid must be generated with preBFC and then a volume mesh is created with TGrid.

TGrid (Reference C.5) is a highly efficient, easy to use, unstructured triangular/tetrahedral grid generation program that can handle grids of virtually unlimited size and complexity. For input TGrid requires a discretized boundary mesh consisting of either nodes and edges in 2D, or nodes and triangular faces in 3D. TGrid contains a number of tools for checking and repairing the boundary mesh to ensure a good starting point for the mesh. A complete mesh can be generated from the boundary mesh automatically or by exercising control of the process.

RAMPANT (Reference C.6) is a state-of-the-art computer program for modeling fluid flow and heat transfer in complex geometries. RAMPANT uses unstructured meshes (triangular in 2D and tetrahedral in 3D) that can be generated around complex geometries with relative ease. RAMPANT also allows a triangular or tetrahedral grid to be refined or coarsened, based on the flow solution. For added flexibility, Rampant can also use grids composed of quadrilateral and hexahedral elements, such as those generated by single or multiple block, structured grid laws.

This solution-adaptive grid capability is particularly useful for accurately predicting flow fields in regions with large gradients, such as shock waves, free shear layers, and boundary layers. In comparison to solutions on structured or block-structured grids, these features significantly reduce the time required to generate a "good" grid. They also reduce the computational effort required to achieve a desired

level of accuracy by limiting mesh refinement to those regions where greater mesh resolution is needed.

C.2 PROBLEM SOLVING WITH CFD

When solving fluid flow problems it is necessary to be aware that the underlying physics is complex and the results generated by a CFD code are at best as good as the physics (and chemistry) embedded in it and at worst as good as its operator.

C.2.1 Planning the CFD Analysis

Careful consideration of the following issues before begining the CFD analysis will contribute significantly to the success of the modeling effort (Reference C.6).

- **Definition of the Modeling Goals** : What specific results are required from the CFD model and how will they be used ? What degree of accuracy is required from the model ?
- **Choice of the Computational Model** : How will the complete physical system to be modelled ?. Where will the computational domain begin and end ? What boundary conditions will be used at the boundaries of the model ? Can the problem be modelled in two dimensions or is a three-dimensional model required ? What type of grid topology is best suited for this problem ?
- **Choice of Physical Models** : Is the flow laminar or turbulent ?. Is the flow unsteady or steady ? Is heat transfer important ? Will the fluid to be treated as incompressible or compressible ? Are there other physical models that should be applied ?
- **Determination of the Solution Procedure** : Can the problem be solved simply, using the default solution parameters in the CFD code ? Can convergence be accelerated with a more judicious solution procedure ? Will the problem fit within the memory constraints of the computer, including the use of multigrid ?. How long will the problem take to converge on the computer ?

C.2.2 Problem Solving Steps

Once the important features of the problem being solved are determined, usually the basic procedural steps shown below are followed.

1. Create the model geometry and grid.
2. Choose the basic equations to be solved : 2D or 3D, non-turbulent or turbulent.
3. Import the grid.
4. Check the grid.
5. Identify additional models needed : fans, heat exchangers, porous media, etc.
6. Specify material properties.
7. Specify the boundary conditions.

8. Adjust the solution control parameters.
9. Initialize the flow field.
10. Calculate a solution.
11. Examine the results.
12. Save the results.
13. If necessary, refine the grid or consider revisions to the numerical or physical model.

C.3 GEOMETRIC DEFINITION

The numerical simulation of fluid flows requires, as a starting point, description of the flow passage geometry and the creation of the discrete elements or volumes to be used in the calculation.

PreBFC is ideally suited for generating simple geometries (for example, an airfoil), while for complex geometries (for example, a wing-fuselage fairing) it is better to use CATIA instead of preBFC. To generate a complex geometry, firstly define the shape with CATIA, then import the complex geometry to the mesh generator through IGES.

C.4 GRID GENERATION

The mesh must be suitable for the discretization technique and also for the flow. The basic parts, or primitives, from which meshes are built are as follows :

- points, sometimes called nodes,
- volumes, also known as cells in some documentation,
- elements,

Moreover, which of these primitives are needed for a mesh depends on the discretization method being used. In all discussion that follows the terms 'volume', 'cell', 'element' are used to describe sub-domain without implying that a particular discretization technique is being used. Figure C.2 shows some of the commonly used sub-domains (Reference C.7).

The arrangement of the mesh is known as the **structure** of the mesh or the **topology** of the mesh. There are two ways in which the mesh structure can be arranged. These are as follows :

- **A regular structure or topology**, where the points of the mesh can be imagined as a grid of points placed in a regular way throughout a cuboid (also known as a 'shoebox'). These points can then be stretched to fit a given geometry and this is shown in Figure C.3. Sometimes these meshes are called **structured meshes** as they have a well-defined structure, or **mapped meshes** as they can be seen as a cuboid mesh that has been mapped onto some other geometry.

- **An irregular structure or topology**, where the points fill the space to be considered but are not connected with a regular topology. Figure C.4 shows a 2D example of this type of mesh formed with triangular elements. Note that the cell faces do not overlap. A mesh with an irregular structure is often referred to as an **unstructured mesh** or a **free mesh.**

C.4.1 Acceptable Grid Topologies

Since RAMPANT is an unstructured solver that can handle both quadrilateral/hexahedral and triangular/tetrahedral grid elements, it is able to solve problems on a wide variety of grids. O-type grids, grids with zero-thickness walls, C-type grids, conformal block-structured grids, multi-block structured grids, and unstructured triangular, tetrahedral, quadrilateral, and hexahedral grids are all accepted by RAMPANT. Note that while RAMPANT does not require a cyclic branch cut in an O-type grid, it will accept a grid that contains one (Reference C.6). Figures C.5 and C.7 show examples of valid grids for RAMPANT.

C.4.2 Grid Requirements and Considerations

This section contains information about special geometry/grid requirements, choosing the appropriate mesh type, and general comments on mesh quality.

C.4.2.1 Geometry/Grid Requirements.

For axisymmetric geometries and periodic boundaries, there are geometry set-up and grid construction requirements. For a more extensive discussion of these requirements, the reader is referred to Reference C.6.

C.4.2.2 Choice of Mesh Types

The choice of which mesh type to use will depend on the application. When choosing the mesh type, the following issues should be consider (Reference 5) :

- Set-up time
- Computational expense
- Ability to adapt
- Numerical diffusion effects

To clarify the trade-offs inherent in the choice of mesh type, these issues are discussed further.

Set-up time

Many flow problems solved in engineering practice are extremely complex. The creation of structured or block-structured grids consisting of quadrilateral or hexahedral elements for such problems can be extremely time-consuming, if not impossible. Set-up time for complex geometries is, therefore, the major motivation for using unstructured grids employing triangular or tetrahedral cells.

If the geometrical configuration is very simple, however, there may be no clear saving in set-up time with either approach.

Computational expense

When geometries are complex or the range of length scales of the flow are large, a triangular/tetrahedral mesh can often be created with far fewer cells than the equivalent mesh consisting of quadrilateral/hexahedral elements. This is because a triangular/tetrahedral mesh allows cell to be clustered in regions where there are large gradients in the flow, while fewer cells can be used where the gradients are small. A quadrilateral/hexahedral mesh generated using a structured approach will generally contain cells that are not needed.

One characteristic of quadrilateral/hexahedral elements that might make them more economical in some situations is that they permit a much larger aspect ratio than triangular/tetrahedral cells. (A large aspect ratio in a triangular/tetrahedral cell will invariably affect the skewness of the cell, which is undesirable as it may impede accuracy and convergence). So for a relatively simple geometry in which the flow conforms well to the shape of the geometry, such as a long thin duct, a mesh of high-aspect-ratio quadrilateral/hexahedral cells could be used. The mesh is likely to have far fewer cells than if triangular/tetrahedral cells are to be used.

Ability to Adapt

RAMPANT does not currently have the ability to adapt meshes that contain quadrilateral or hexahedral cells. So if the solution adaptation could be used, a triangular or tetrahedral cells should be used.

Numerical Diffusion

A dominant source of error in multidimensional situations is numerical diffusion, also termed false diffusion. (The term "false diffusion" is used because the diffusion is not a real physical phenomenon, yet its effect on a flow calculation is analogous to that of increasing the real diffusion coefficient). Numerical diffusion is minimised when the flow is aligned with the grid. It is clear that if a triangular or

tetrahedral mesh will be used the flow can *never* be aligned with the grid. See Reference 5 for more information of the numerical diffusion.

C.4.2.3 Mesh Quality

The quality of the mesh plays a significant role in the accuracy and stability of the numerical computation. The attributes that characterize a mesh are node point distribution, smoothness and skewness.

Node Density and Clustering

For discretely defining a continuous domain, resolution of the salient features of the flow field, such as shear layers, separated regions, shock waves, boundary layers, and mixing zones, depends on the density and distribution of nodes in the mesh. Poor resolution in critical regions can dramatically alter the flow characteristics.

Resolution of the boundary layer (i.e., mesh spacing near walls) also plays a significant role in the accuracy of the computed shear stress and heat transfer coefficient at the wall. This is particularly true in laminar flow where the grid adjacent to the wall should obey (Reference C.6) :

$$y_p \sqrt{\frac{u_\infty}{\nu x}} \leq 1 \qquad \text{(C.1)}$$

where y_p = distance to the wall from the adjacent cell centroid
u_∞ = free-stream velocity
ν = kinematic viscocity of the fluid
x = distance along the wall from the starting point of the boundary layer

Turbulent flow calculations in RAMPANT are especially sensitive to the near-wall mesh spacing. This is because wall functions are used to provide a boundary condition for the rate of dissipation of turbulent kinetic energy, ε, as well as to estimate the production of turbulent kinetic energy, (see Reference C.6 for a more complete explanation of wall functions). It is necessary to maintain as smooth a distribution of cell volume along a surface as possible. This is because the wall functions rely on the value of y^+ in the wall cells, which is a function of the distance of the cell centroid from the wall. Typical values of y^+ are 50 to 200. The y^+ is defined as follows :

$$y^+ = y_p \frac{\sqrt{\tau_w / \rho_w}}{\nu_w} \qquad \text{(C.2)}$$

where τ = shearing stress
ρ = density of the fluid
subscribe 'w' indicates y^+ is only defined in the cells adjacent to walls.

In general, no flow passage should be represented by fewer than 5 cells, and many more cells are normally required to adequately resolve the passage.

Smoothness

Lack of a smooth rate of change in cell volume between adjacent cells translates into larger truncation errors. Truncation error is the difference between the partial derivatives in the governing equations and their discrete approximations. RAMPANT provides the capability to improve the smoothness by refining the mesh based on the change in cell volume or the gradient of cell volume.

Cell Shape

The shape of the cell, including skewness and aspect ratio, also plays a role in the accuracy of the mesh. Skewness is basically a measure of the difference between the cell's shape and an equilateral cell of equivalent volume. Highly skewed cells can decrease accuracy and destabilize the solution. However, a general rule of thumb is to avoid aspect ratios in excess of 5:1.

Flow-Field Dependency

The effect of resolution, smoothness and cell shape on the accuracy and stability of the solution process is strongly dependent on the flow field being simulated. For example, very skewed cells can be tolerated in benign flow regions, but can be very damaging in regions with strong flow gradients.

C.4.2.4 Partitioning the Grid for Parallel Processing

Rampant has capability to partition the grid into separate clusters of cells for separate processors on a parallel computer. See Reference C.6 for more discussion on this procedure.

C.4.3 Creating the Grid

This section provides a quick overview of how to use preBFC and TGrid for generating grid. Should a more explanation of this subject be needed, the reader is referred to References C.4 and C.5.

C.4.3.1 Using preBFC

Starting from a given geometry (a geometry file can be obtained from a number of sources including preBFC itself or from CATIA). The major steps involved in generating an unstructured grid using preBFC are as follows :

1. Create/Read a geometry file using/into preBFC.
2. Specify the nodes along the bounding curves
3. Adjust the node distribution (if necessary)
4. In 2D , mesh the boundary nodes to generate the initial grid, or in 3D, generate surface grids
5. Refine the initial grid (2D only)
6. Display and verify the grid
7. Modify the grid (if necessary)
8. Save the geometry and grid

The steps that follow perform the actual grid generation in 2D. For 3D geometries, the surface grid created in step 3 must be transferred to TGrid where the interior mesh can be generated.

Swapping and Smoothing

Swapping and Smoothing in preBFC are performed as follows (Reference C.4). First, every pair of triangles with a common edge is examined. These two triangles form a quadrilateral with their common edge as one of the diagonals. If the triangles formed by dividing the quadrilateral with the other diagonal are better then the existing triangles, then the edge (diagonal) is swapped. Then, for each swapping pass, a number of smoothing iterations can be performed. Node smoothing moves each interior node to the average of the neighbouring node locations, and is also referred to as Laplace smoothing. The node is always constrained to lie on surface. Rather than fully moving the node, the smoothing can be relaxed. To have the nodes evenly distributed would take many iterations, but even distribution is not usually desired. Only a few iterations are required to minimize face skewness on the surface mesh.

Many surface meshes can be improved with one swapping iteration and a couple of smoothing iterations. It is a good to remember : any improvement to the surface mesh can make a substantial improvement in the 3D interior mesh.

Meshing Problems

To make the surface meshes conforming, the nodes are placed on the edge curves. If the curve parameterization does not match the surface's parameterization, however, the mesh will be distorted. This mismatch can occur when the curves used to create a surface patch have different numbers of points and different point distributions. The distortion is evident when the surface is displayed because of the uneven spacing of

the constant u-lines or v-lines used in drawing the surface. To make the surface parameterization match its curves, the curves must be modified.

C.4.3.2 Using TGrid

Starting from a given boundary mesh, TGrid generates a 2D triangular or 3D tetrahedral unstructured grid. In 2D the boundary mesh consists of nodes and straight edges, whereas in 3D it consists of nodes and triangular faces. A boundary mesh file can be obtained from a number of sources including preBFC. From the boundary mesh TGrid creates an interior mesh and writes it to a new file. This file can then be read into RAMPANT, where the solution process and postprocessor occur.
The basic steps for using TGrid are the following :

1. Read a boundary mesh file into TGrid.
2. Examine the boundary mesh for topological problems such as free edges and duplicate nodes. Once the boundary is topologically correct, a 3D surface mesh can be checked for poor face quality. Many quality-related problems can be solved easily with edge swapping, but more difficult problems may require direct manipulation of the faces and nodes
3. Generate the interior mesh. This can be done automatically or by proceeding through a series of steps. The basic steps are to generate an initial mesh, select the cell zones, refine the cell zones, and perform face swapping. At each step various parameters to control the process can be set.
4. Check the mesh for problems. Look carefully at the worst cells both their skewness and their location. The presence of degenerate cells will prevent RAMPANT from obtaining a solution, and very poor cells in critical areas will cause serious convergence problems. If the bad cells cannot be removed, a new mesh must be generate using different mesh parameters.
5. Write the mesh to a new file for input to RAMPANT.

Meshing Problems

Most problems with the mesh generation process can be traced back to problems with the boundary mesh. These will usually become manifest in the failure to generate an initial mesh. If the boundary mesh has problems, it is unlikely that TGrid will be able to create a mesh. The problems with boundary meshes can be loosely classified as either topological problems or problems related to poor boundary mesh quality and/or smoothness. Topological problems include such things as extraneous nodes or faces, intersecting boundaries, and connectivity problems. See Reference C.5 for a more discussion on the above issues.

C.5 VERIFICATION

A study was made to verify the use of RAMPANT as a primary design tool in the design of combined VCW-HLFC. The verification was made both on two-dimensional and three-dimensional configurations.

C.5.1 Two-Dimensional Problem

A laminar flow airfoil, developed by Boeing (Reference C.8), was selected for this study. The name of this airfoil is : NLF-5 airfoil. This airfoil has a thickness of 10.1 % chord, a design section lift coefficient of 0.5, and is intended to cruise at M = 0.78.

C.5.1.1 Problem Description

Geometric definition of the NLF-5 airfoil is contained in Table C.1. The airfoil geometry and surface grid used for this analysis are shown in Figure C.5. The results shown here are for $M_\infty = 0.78$, angle of attack = 0 degree, and Reynolds number of 20.6×10^6. The computational domain is rectangular box that extends 25 chord lengths in front, behind, above, and below the airfoil. The NLF-5 airfoil mesh contains 6,218 nodes, 17,627 faces and 11,409 cells. Inviscid flow was assumed for the computations. The entire flowfield was initialized with freestream values, then run until the residual of the mass, momentum, and energy equations had all converged 3 orders of magnitude.

C.5.1.2 Results

The pressure distribution of the NLF-5 airfoil for the conditions described in section C.5.1.1 is shown in Figure C.6. The pressure distribution predicted by RAMPANT is in fair agreement with the calculated data from Reference C.8. The shock position and strength are quite close. According to the RAMPANT predictions, the NLF-5 airfoil has more lift aft of the shock and less lift in the front of shock, hence more pitching moment.

C.5.2 Three-Dimensional Problem

The NACA 0012 wing, based on Reference C.9, was selected for this study. The wing has an aspect ratio of eight and a NACA 0012 cross-section, without twist. The planform has a taper ratio of 0.5 and a leading-edge sweep angle of 20 degrees. The wing is attached to a cylindrical fuselage (no fuselage geometry data's are given).

C.5.2.1 Problem Description

The NACA 0012 wing geometry and surface grid used for this analysis are shown in Figure C.7. The results shown here are for M_∞ = 0.85, angle of attack = 2 degrees, and Reynolds number based on the mean aerodynamic chord of $9x10^6$. The computational domain is rectangular box that extends 8.3 fuselage lengths in front, behind, above, and below the wing, and 8.3 fuselage lengths (78 wing semispans) to the side of the wing. The domain mesh contains 55,593 nodes, 556,852 faces, and 267,874 cells. Inviscid flow was assumed for the computations. The entire flowfield was initialized with freestream values, then run until the residuals of the mass, momentum, and energy equations had all converged 3 orders of magnitude.

C.5.2.2 Results

The wing surface pressure distribution was measured at 3 different spanwise stations, 2y/b = 0.15, 0.46, and 0.96. The pressure distributions for the three spanwise stations are shown in Figure C.8. The pressure distribution predicted by RAMPANT at spanwise station 0.46 is in fair agreement with the calculated data by TIBLT (Transonic Interactive Boundary-Layer Theory, from Reference C.9) code. A shock is present on the upper surface of the wing. The shock position predicted by RAMPANT is about 5 % of the chord length aft of the TIBLT prediction. This may be because the grid is not fine enough (because the limitations of available computer memory) to capture the shock. The pressure distribution predicted by RAMPANT at spanwise stations 0.15 and 0.96 is not well matched with the data calculated by TIBLT code. This may be because the complex conditions at the wing root and the tip (3D effects more dominant) and the cylindrical fuselage geometry definition may be different.

Good agreement with experimental data also was achieved (Reference C.9), when TIBLT code is used to predict the pressure distributions for the M6 wing (Reference C.11). Reference C.12 reported that the pressure distributions of M6 wing predicted with RAMPANT (with the same procedure used by the author described above) are in good agreement with the experimental data.

For the purposes of this study, comparison to the NACA 0012 wing is used rather than the M6 wing, because the aspect ratio of the NACA 0012 wing is closer to the ATRA-100 wing (see section C.5.2).

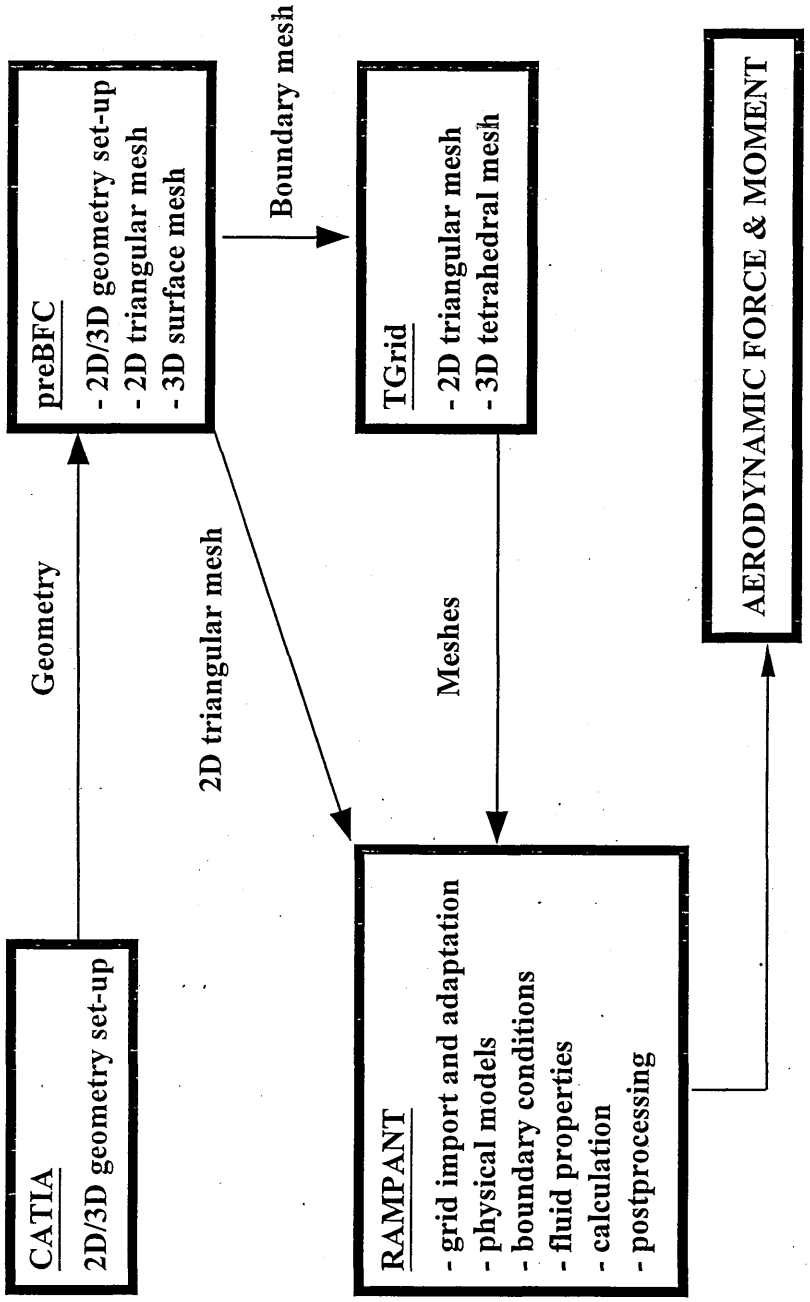

Figure C.1 Aerodynamic calculations program structure

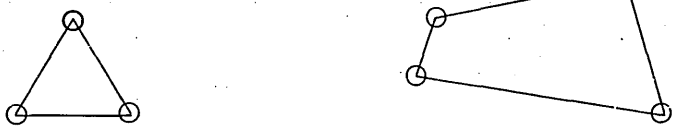

3-Noded triangle 4-noded quadrilateral

(a) Two dimensions

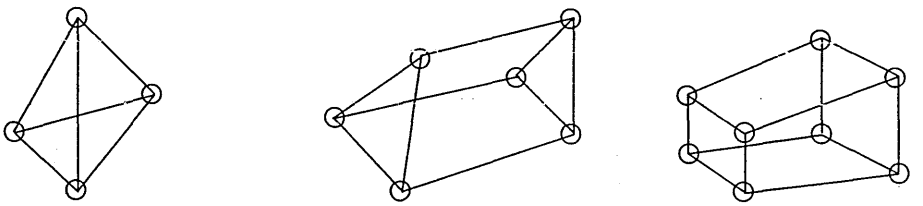

4-noded tetrahedron 6-noded prism (wedge) 8-noded hexahedron (brick)

(b) Three dimensions

Figure C.2 Some common sub-domains (Reference C.7)

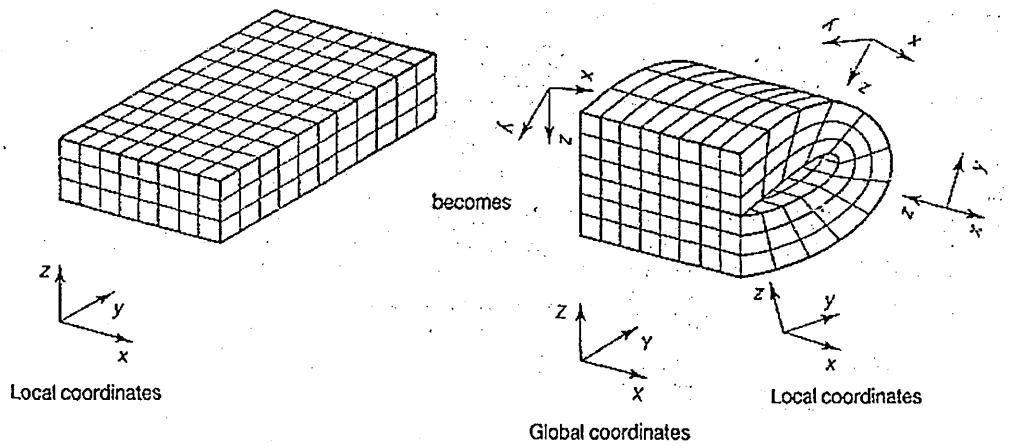

Figure C.3 Transformation of a mesh with a regular structure (Reference C.7)

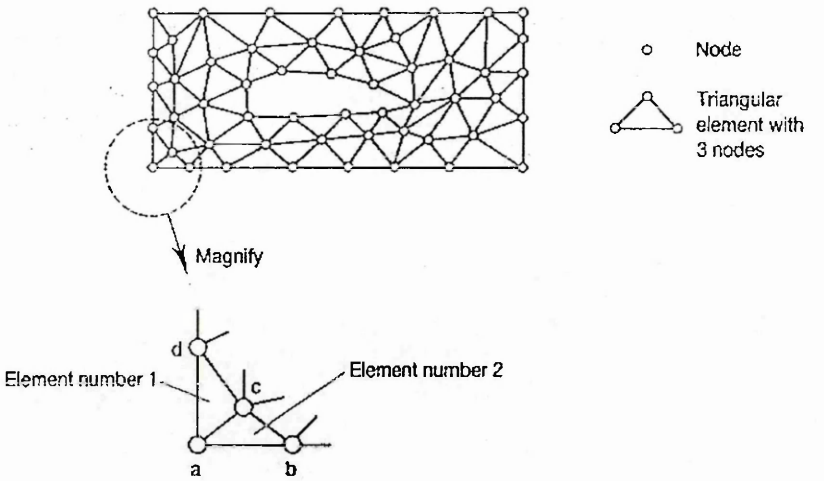

Figure C.4 A mesh with an irregular structure (Reference C.7)

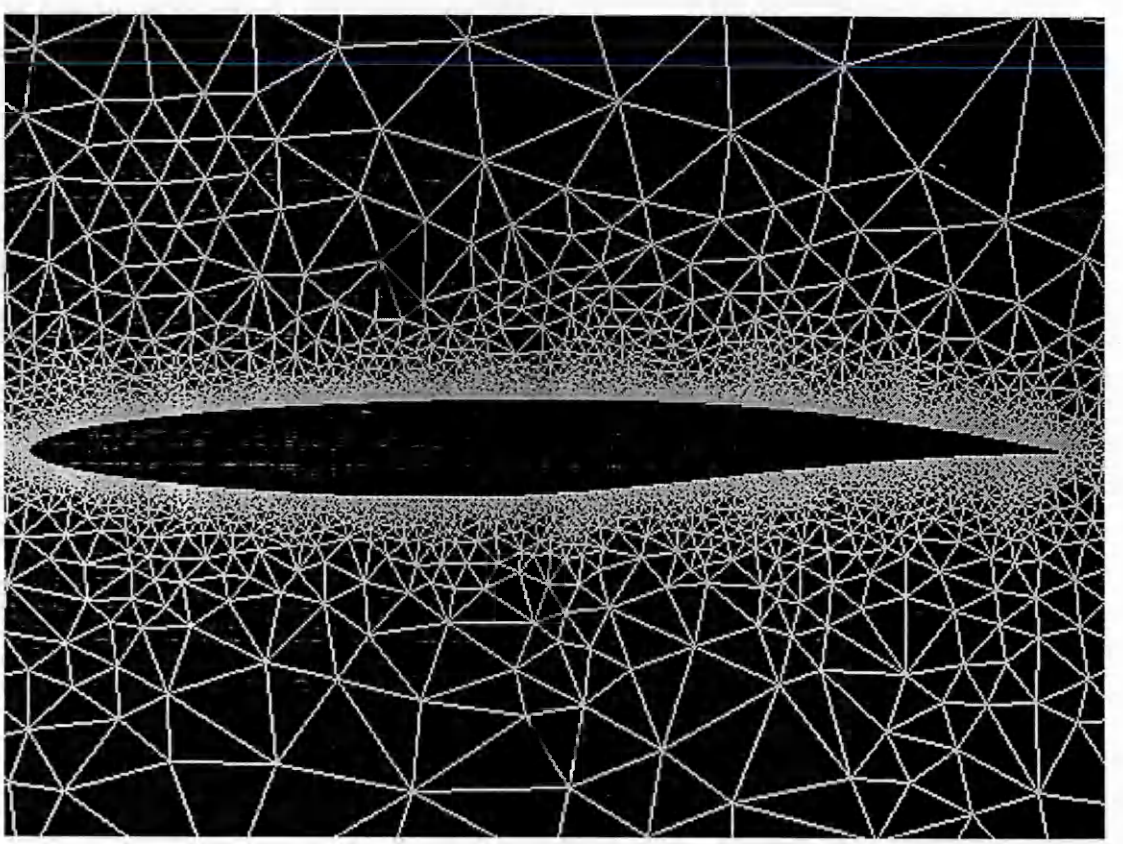

Figure C.5 NLF-5 airfoil mesh

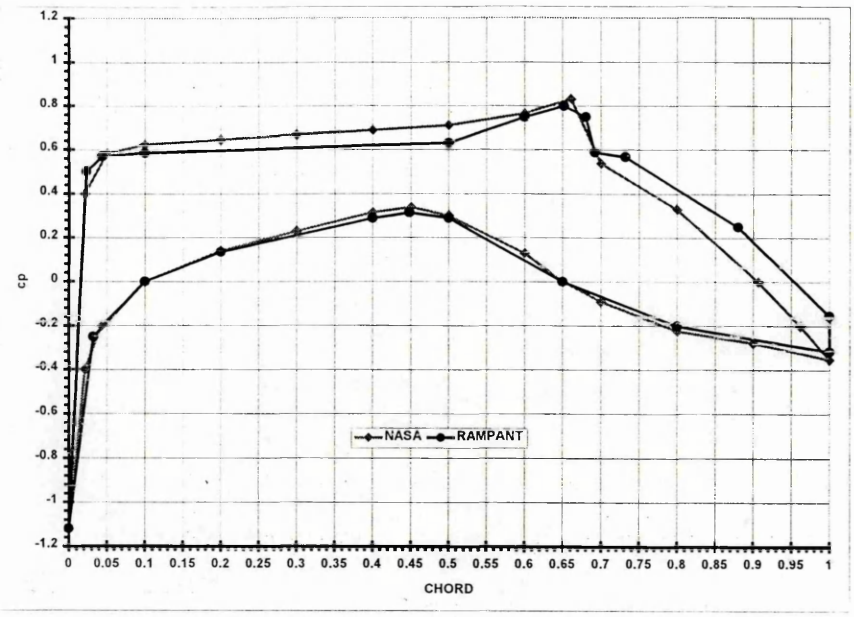

Figure C.6 Pressure distribution of NLF-5 Airfoil

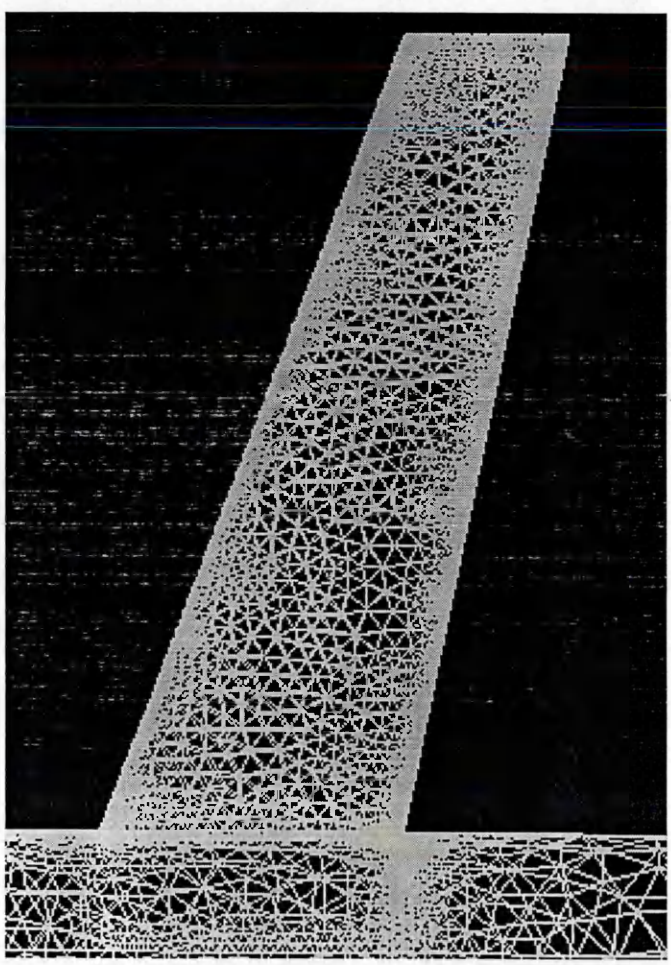

Figure C.7 NACA 0012 wing surface mesh

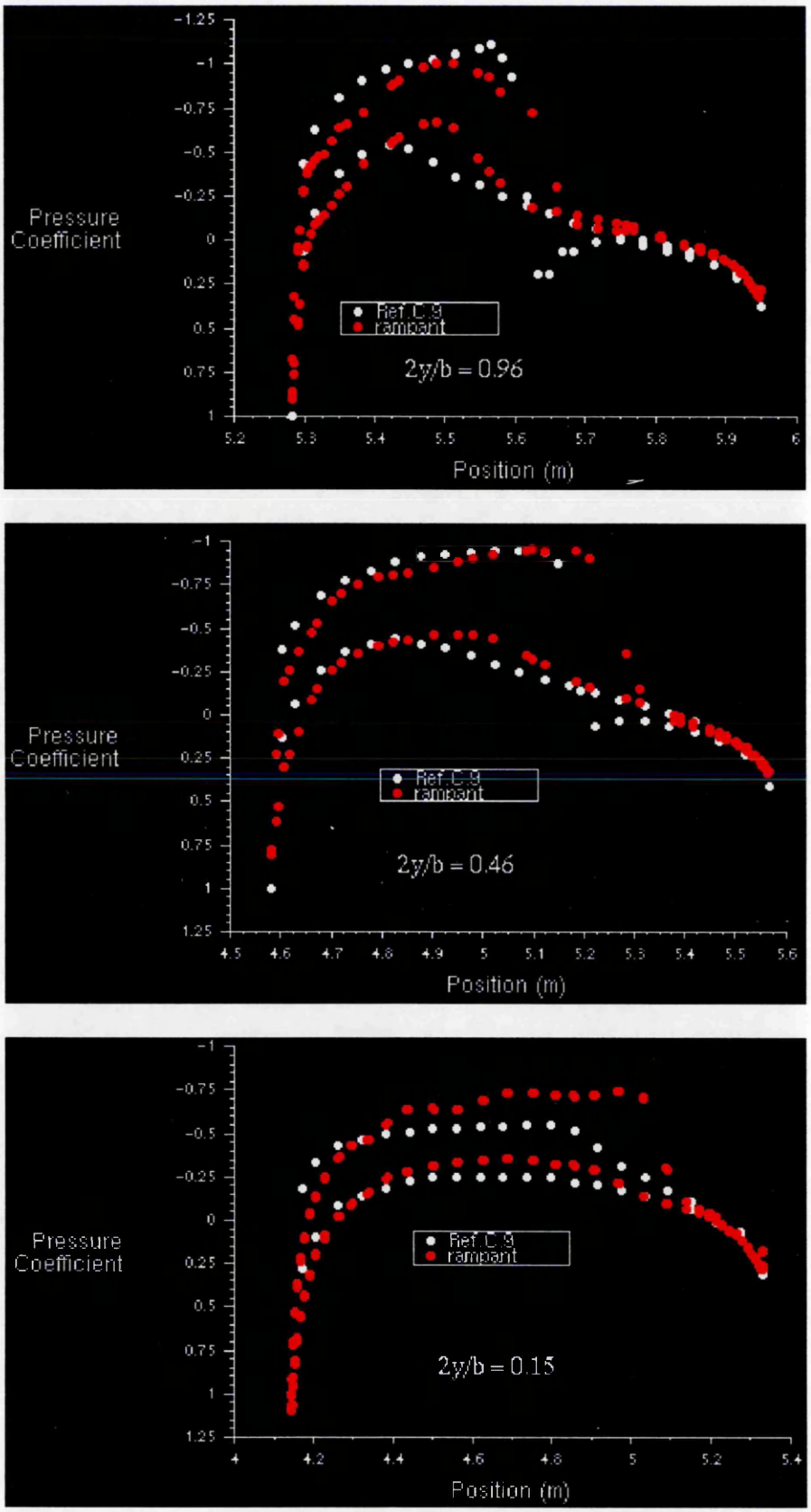

Figure C.8 NACA 0012 pressure distributions

Upper Surface

x/c	z/c	x/c	z/c	x/c	z/c
0.00010	0.002110	0.17121	0.041920	0.53886	0.056126
0.00080	0.004443	0.18584	0.043259	0.55738	0.055904
0.00231	0.006498	0.20091	0.044580	0.57576	0.055582
0.00441	0.008545	0.21642	0.045783	0.59393	0.056128
0.00719	0.010674	0.23232	0.046977	0.61202	0.054540
0.01067	0.012576	0.24861	0.048082	0.64761	0.052882
0.01485	0.014570	0.26524	0.049138	0.66516	0.052008
0.01973	0.016617	0.28221	0.050106	0.68256	0.050905
0.02531	0.018446	0.29948	0.051014	0.71681	0.048343
0.03159	0.020357	0.31703	0.051843	0.73351	0.046902
0.03855	0.022241	0.33483	0.052604	0.75006	0.045324
0.04619	0.024076	0.35286	0.053295	0.78208	0.041873
0.05450	0.025885	0.37109	0.053917	0.81261	0.038063
0.06347	0.027655	0.38948	0.054469	0.82725	0.036060
0.07309	0.029407	0.40801	0.054962	0.85522	0.031935
0.08334	0.031122	0.42664	0.055376	0.88141	0.027725
0.09419	0.032789	0.44533	0.055709	0.90556	0.023557
0.10565	0.034428	0.46406	0.055971	0.92746	0.019582
0.11767	0.036018	0.48280	0.056141	0.95562	0.014212
0.13027	0.037561	0.50153	0.056228	0.97094	0.011200
0.14340	0.039056	0.52023	0.056222	1.00000	0.005400
0.15706	0.040512				

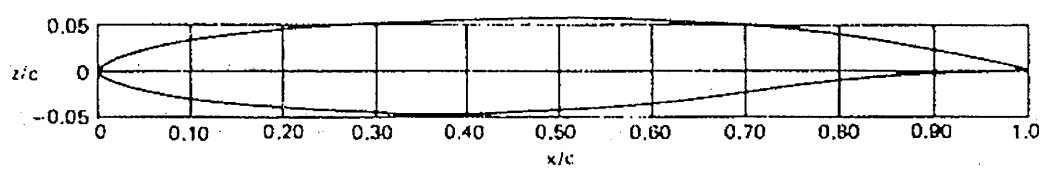

Lower Surface

x/c	z/c	x/c	z/c	x/c	z/c
0.00000	0.000000	0.10000	0.028781	0.70000	−0.022603
0.00120	0.003418	0.12000	0.031347	0.74000	−0.017930
0.00200	0.004381	0.14000	0.033615	0.77000	−0.014833
0.00300	0.005334	0.16000	0.035637	0.80000	0.011738
0.00500	0.006725	0.19000	0.038272	0.83000	0.009066
0.00800	0.008333	0.22000	0.040503	0.85000	0.007252
0.01200	0.010079	0.26000	0.042926	0.87000	0.005726
0.01800	0.012250	0.30000	0.044762	0.89000	0.004199
0.02400	0.014133	0.35000	0.046207	0.91000	0.003054
0.03200	0.016336	0.40000	0.046621	0.93000	0.002099
0.04000	0.018294	0.45000	0.045813	0.95000	−0.001241
0.05000	0.020467	0.50000	0.043518	0.97000	0.000668
0.06000	0.022422	0.55000	0.039757	0.98000	0.000477
0.07000	0.024208	0.60000	0.034778	0.99000	0.000387
0.08000	0.025846	0.65000	0.028855	1.00000	0.000382

Table C.1 NLF-5 airfoil geometric definition (Reference C.8)

APPENDIX D

DRAG PREDICTION

D.1 INTRODUCTION

Total drag may be broken down in different ways. To compound the confusion, drag component definitions are not consistent between different authors. The drag breakdown describes in the following sections is used in this research. The method is based on References D.1 and D.2.

D.2 DRAG BREAKDOWN

To simplified the analysis, the total aircraft drag coefficient is written as :

$$C_D = C_{D_0} + C_{D_L} \qquad (D.1)$$

where :

C_D = total aircraft drag coefficient
C_{D_0} = aircraft zero-lift drag coefficient
C_{D_L} = aircraft drag coefficient due to lift/induced drag

D.2.1 Aircraft Zero-Lift Drag

Parasite drag includes all drag terms that are independent of lift and Mach number. It is comprises friction, form, pressure and interference drag. Friction and form drag are Reynolds number dependent, whereas pressure and interference drag are not. Parasite drag is also sometimes called "minimum drag" or "zero lift drag" (C_{D_0}), and for an uncambered airfoil these terms are synonymous. For a cambered airfoil, they are not the same. For the purposes of this research, the term "zero lift drag" (C_{D_0}) is related to the sum of parasite drag and wave drag at zero-lift. The aircraft zero-lift drag coefficient is computed from :

$$C_{D_0} = C_{D_{0W}} + C_{D_{0NW}} \qquad (D.2)$$

where :

C_{D_0} = aircraft zero-lift drag coefficient
$C_{D_{0W}}$ = wing zero-lift drag coefficient
$C_{D_{0NW}}$ = zero-lift drag coefficient due to other aircraft components (fuselage, engine-nacelles, empenage, etc.)

Based on Reference D.1, for a typical transport aircraft $C_{D_{0W}} = 0.4\,C_{D_0}$ and $C_{D_{0NW}} = 0.6\,C_{D_0}$.

The transonic wing zero-lift drag coefficient is found from :

$$C_{D_{0W}} = C_{D_{0W.SUB.}} + C_{D_{WWAVE}} \qquad (D.3)$$

where :

$C_{D_{0W.SUB.}}$ = the drag coefficient due to friction. It is assumed to stay constant with Mach number in the entire transonic speed range.

$C_{D_{WWAVE}}$ = the wing wave drag coefficient which depends on the wing sweep angle, $\wedge_{c/4.}$

According to Reference D.1, the subsonic wing zero-lift drag coefficient may be computed from :

$$C_{D_{0W.SUB.}} = (R_{wf})(R_{LS})(C_f)\{1 + L'(t/c) + 100(t/c)^4\}S_{wet}/S \qquad (D.4)$$

where :

R_{wf} = wing/fuselage interference factor (see Reference D.2).
R_{LS} = lifting surface correction factor (see Reference D.2).
C_f = smooth flat plate skin friction coefficient, see equation D.5.
L' = airfoil thickness location parameter (see Figure 4.4 of Reference D.1).
t/c = thickness chord ratio defined at the mean geometric chord of the wing
S_{wet} = wetted area of the wing.
S = reference area

Based on Reference D.3, the mean skin friction on a smooth flat plate with some degree of laminar flow may be computed from :

$$C_f = (C_{f0})(1 - x_t/c + x_0/c)^{(5/6)} \qquad (D.5a)$$

$$x_0/c = (R_N)^{0.2}[\{0.664(x_t/c)^{0.5}\}/\{0.0225(R_N)^{0.5}\}]^{(6/5)} \qquad (D.5b)$$

where :

C_{f0} = turbulent smooth flat plate skin friction coefficient, see
x_t/c = transition position, expressed as a fraction of the chord
R_N = Reynolds number (based on geometric average chord)

D.2.2 Aircraft Drag Due To Lift

Induced Drag includes inviscid and viscous effects, but excludes trim drag. (Nicolai uses a somewhat more concise terminology, reserving the term "induced" drag for three-dimensional drag due to lift. Skin friction and separation drag due to lift are called "viscous" drag due to lift).

Induced drag is usually quantified as a factor on the theoretical induced drag of a wing with elliptical lift distribution. This factor is 1/e, where "e" is the Oswald efficiency factor. (Reference D.4, Nicolai uses the letter "e" to define the "wing planform efficiency factor", which is meant to include three-dimensional effect only). This research will uses "e" to refer to a factor which includes both three-dimensional and viscous effects.

The drag coefficient pretty much has a parabolic behavior with the lift coefficient (in the range of cruise lift), except at large angle of attack (Reference D.4). Sometimes, early in the design when very little is known about the aircraft configuration, the expression for induced drag (C_{D_L}) will be approximated by :

$$C_{D_L} = K(C_L)^2 \qquad \text{(D.6a)}$$

$$K = 1/(\pi Ae) \qquad \text{(D.6b)}$$

where :

A = wing aspect ratio

A simplified method of calculating the Oswald efficiency factor, suitable for parametric analysis, may be derived from Reference D.5 in which :

$$e = 1/\{(\pi Ak) + (1/us)\} \qquad \text{(D.7)}$$

where :

u = non-elliptic distribution factor (0.99 for a high aspect ratio wing.
s = fuselage correction factor.
k = sweep correction factor.

The graphical definition of s given in Reference D.5 may be approximated by the expression :

$$s = 1 - 1.556[d_f/b]^2 \qquad \text{(D.8)}$$

where :

d_f = fuselage diameter.
b = wing span.

The sweep correction factor, k, may be approximated by :

$$k = (0.38 + 0.000057 \wedge_{c/4}^{2}) C_{D_0} \qquad \text{(D.9)}$$

D.3 DRAG REDUCTIONS VERIFICATION

Where possible, it is important to compare the results from this study with those performed by other organisations, particularly as data from these has been extensively used within this study.

Boeing (Reference D.6).studied the implications of retro-fitting HLFC to the wing, fin and tailplane of a Boeing 757-200 aircraft. This does not closely match of the ATRA aircraft types included in this study, preventing any direct comparisons. However, the reduction in profile drag associated with the various HLFC applications are provided. These are compared with the corresponding drag reductions predicted by drag breakdown method described in the previous section.

Cruise conditions : Mach 0.8, 37,000 ft and $R_N = 5.9e^6/m$

a. Laminar, basic trapezoidal wing spanwise from root to tip on both of upper surface

(average : 0 - 0.5 chord) and lower surface (average : 0 - 0.38 chord) :
cruise drag reduction = 11.405 %, Reference D.6 quote 11 %.

b. Laminar, basic trapezoidal wing spanwise from root to tip on upper surface (average : 0 - 0.5 chord) only :
cruise drag reduction = 7.68 %, Reference D.6 quote 7 %.

D.4 DRAG REDUCTION FOR THE ATRA-100

Cruise conditions : Mach 0.8, 35,000 ft and $R_N = 6.28e^6/m$

Laminar, wing spanwise from kink to tip on upper surface (average : 0 - 0.65 chord) only :
cruise drag reduction = 7.675 %.